Ph.D. Viva-Voce Seminar

December 17, 2024

Nuclei Segmentation and Color Normalization of Histological Images:

Rough-Fuzzy Circular Clustering to Deep Generative Modeling

Suman Mahapatra

Senior Research Fellow

Supervisor: **Prof. Pradipta Maji**

Machine Intelligence Unit
Indian Statistical Institute, Kolkata, INDIA

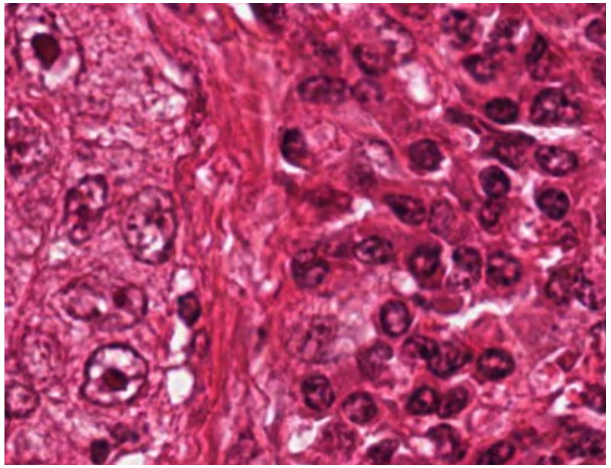
Histological Image Analysis

- In histology, microscopic images of tissue sections are examined to study the manifestation of diseases under consideration.

Histological Image Analysis - Importance

- In histology, microscopic images of tissue sections are examined to study the manifestation of diseases under consideration.

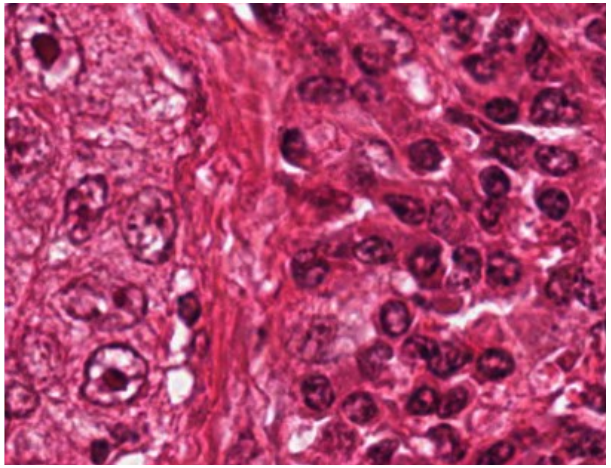
- Important properties of histological images, as compared to radiological, cytological and other imaging modalities, are
  - enormous density of data,
  - more cellular details.



Histological Image Analysis - Importance

- In histology, microscopic images of tissue sections are examined to study the manifestation of diseases under consideration.

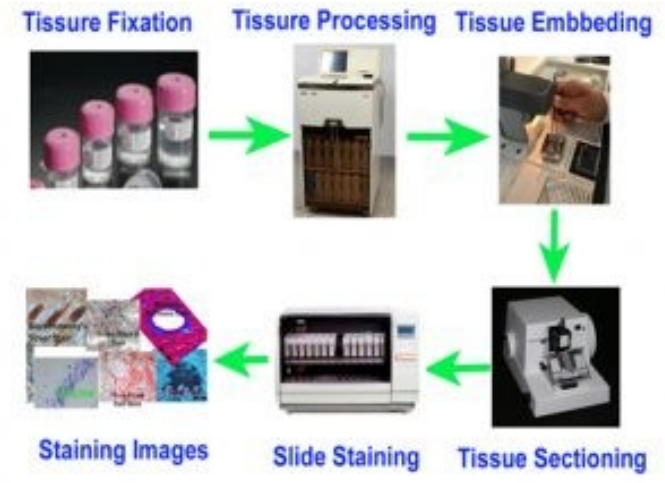
- Important properties of histological images, as compared to radiological, cytological and other imaging modalities, are
  - enormous density of data,
  - more cellular details.

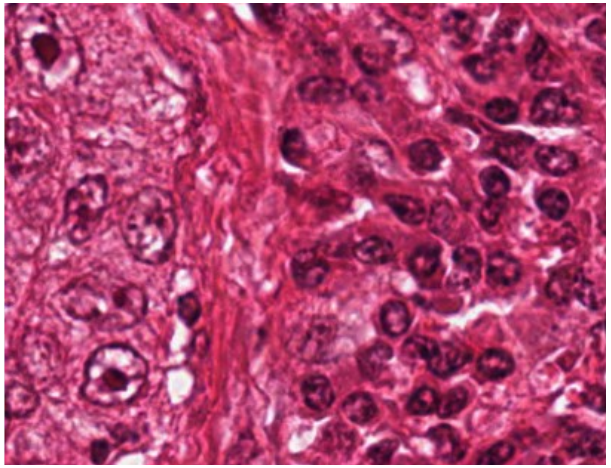


- It makes computer-aided diagnosis more accurate than other imaging modalities.

Histological Image Analysis - Staining

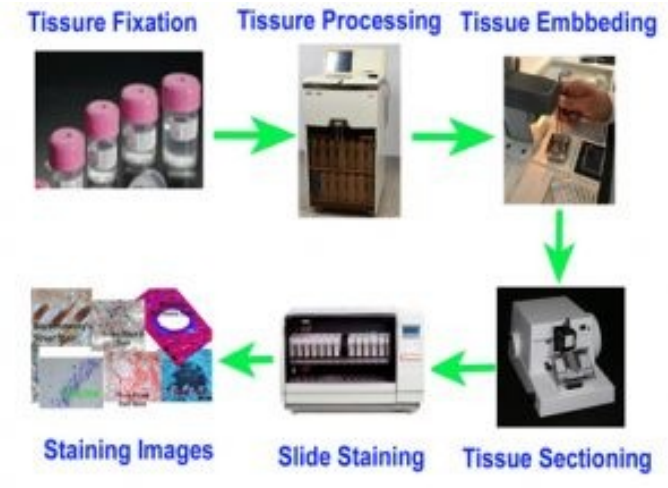
- To facilitate pathologists' examination, tissue samples are stained with multiple contrasting histochemical reagents, which in turn highlight different tissue structures and cellular features.

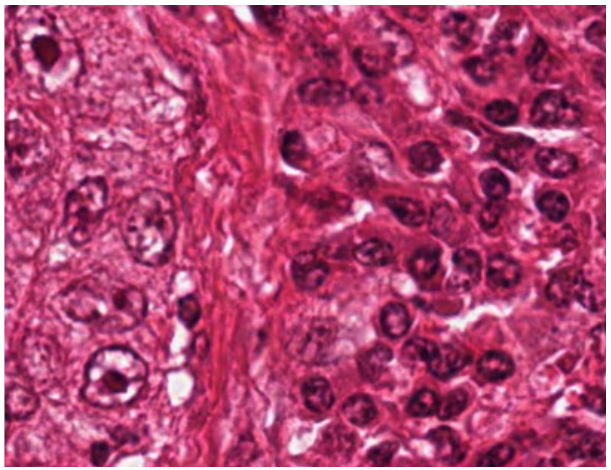




Histological Image Analysis - Staining

- To facilitate pathologists' examination, tissue samples are stained with multiple contrasting histochemical reagents, which in turn highlight different tissue structures and cellular features.





- Hence, color in pathology plays a pivotal role as a good indicator of histological components.

Histological Image Analysis- ROI Segmentation

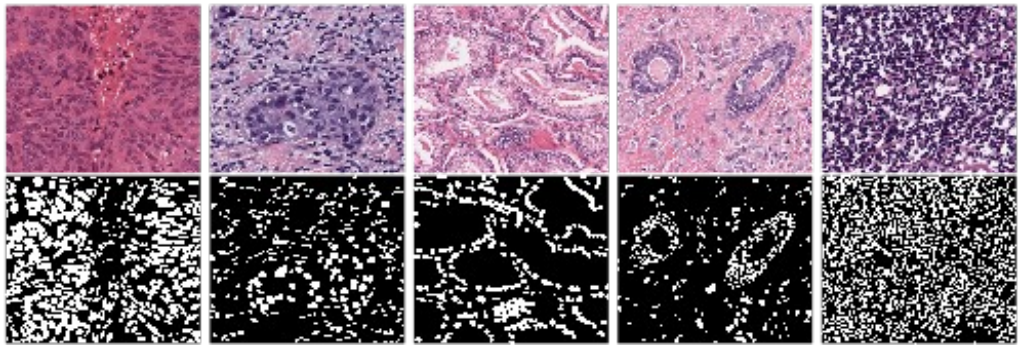
- Region-of-interests (ROI) segmentation is one of most important and significant tasks in medical image analysis.

Histological Image Analysis- Nuclei Segmentation

- The shape and distribution of cell nuclei in histological images are used to determine tissue and cancer types.
- Nuclei segmentation is very critical in cancer identification, grading and prognosis.

Tissue image →

Ground-truth map →



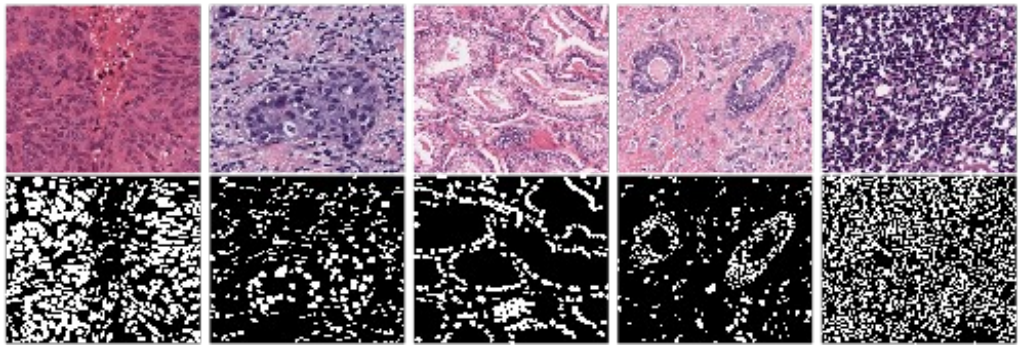
- Accurate segmentation of cell nuclei is a pivotal step to identify abnormalities and to aid in subsequent image analysis tasks.

Histological Image Analysis- Nuclei Segmentation

- The shape and distribution of cell nuclei in histological images are used to determine tissue and cancer types.
- Nuclei segmentation is very critical in cancer identification, grading and prognosis.

Tissue image →

Ground-truth map →



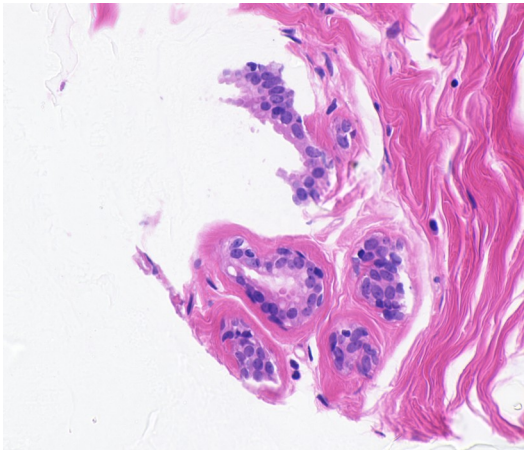
- Accurate segmentation of cell nuclei is a pivotal step to identify abnormalities and to aid in subsequent image analysis tasks.
- A number of challenges are associated with nuclei segmentation:
  (a) variation in stain color appearance,
  (b) differences in nuclear morphology,
  (c) nuclear overlapp and occlusion.

Variation in Stain Color Appearance

- One of the most common and primary problems of histological tissue analysis is the inadmissible inter and intra-specimen variation in the appearance of stained tissue color.

Variation in Stain Color Appearance

- One of the most common and primary problems of histological tissue analysis is the inadmissible inter and intra-specimen variation in the appearance of stained tissue color.



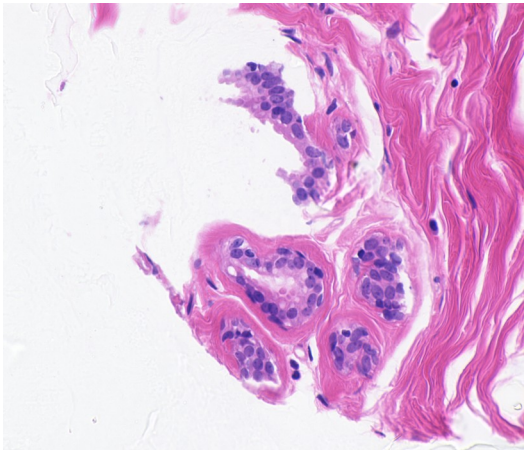
Biopsy 1

UCSB (University of California, Santa Barbara) Breast Cancer Cell Data: Total number of samples/images is 58; Hematoxylin and eosin (H&E) stained 10 biopsy sets.

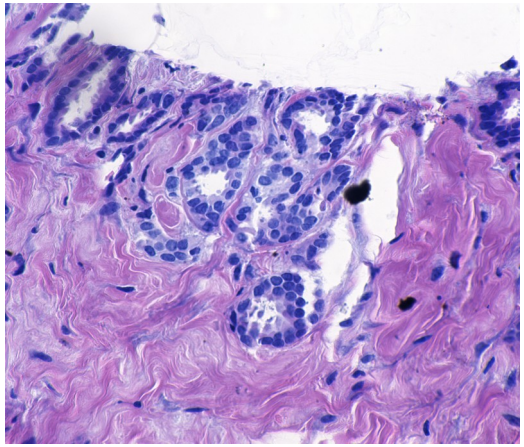
E. D. Gelasca *et al*., "Evaluation and benchmark for biological image segmentation", *IEEE International Conference on Image Processing*, 2008.

Variation in Stain Color Appearance

- One of the most common and primary problems of histological tissue analysis is the inadmissible inter and intra-specimen variation in the appearance of stained tissue color.



Biopsy 1



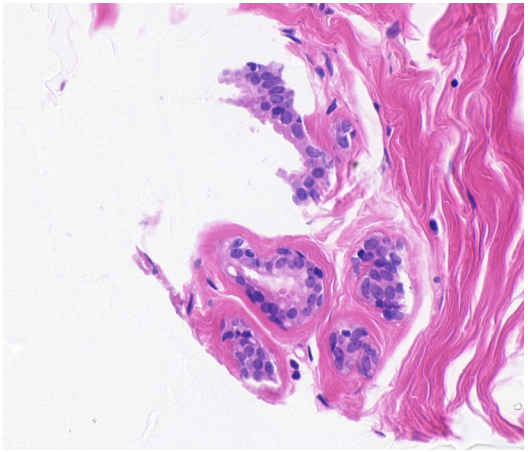
Biopsy 8

UCSB (University of California, Santa Barbara) Breast Cancer Cell Data: Total number of samples/images is 58; Hematoxylin and eosin (H&E) stained 10 biopsy sets.

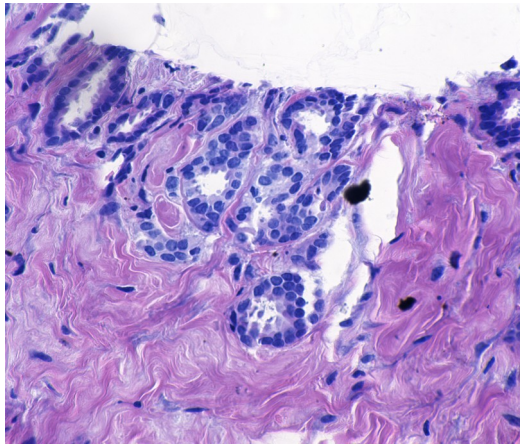
E. D. Gelasca *et al*., "Evaluation and benchmark for biological image segmentation", *IEEE International Conference on Image Processing*, 2008.

Variation in Stain Color Appearance

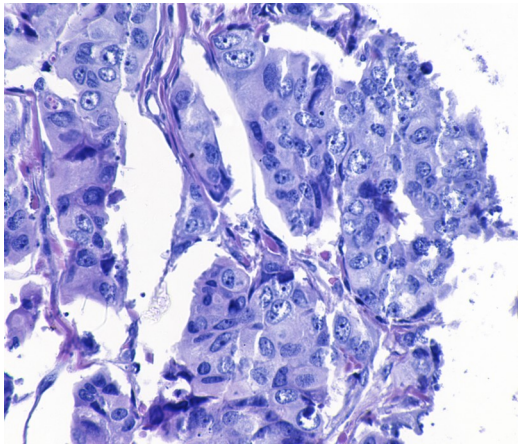
- One of the most common and primary problems of histological tissue analysis is the inadmissible inter and intra-specimen variation in the appearance of stained tissue color.



Biopsy 1



Biopsy 8



Biopsy 8

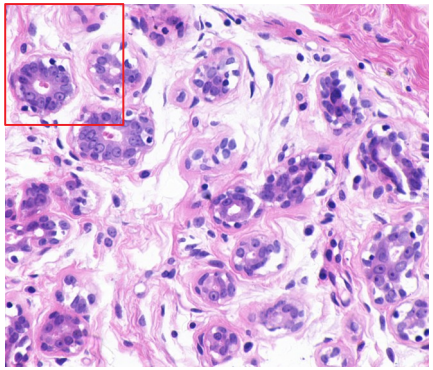
UCSB (University of California, Santa Barbara) Breast Cancer Cell Data: Total number of samples/images is 58; Hematoxylin and eosin (H&E) stained 10 biopsy sets.

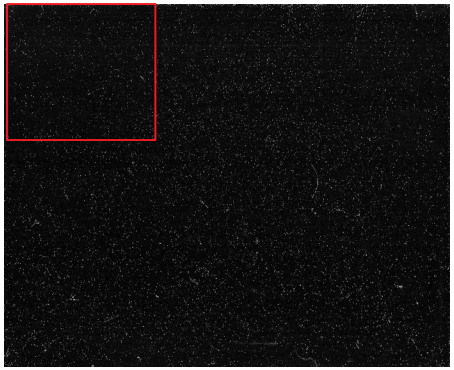
E. D. Gelasca *et al*., "Evaluation and benchmark for biological image segmentation", *IEEE International Conference on Image Processing*, 2008.

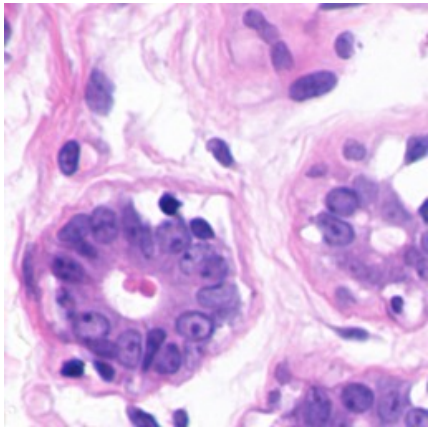
Factors Responsible for Color Inconsistency

- Manual sectioning of the tissue samples during specimen preparation
- Orientation of the lens aperture
- Inconsistency in staining procedure
- Variation in quality of stains obtained from different manufacturers
- Storage condition
- Inter-patient and inter-biopsy staining variations and so on.

Impact of Dust



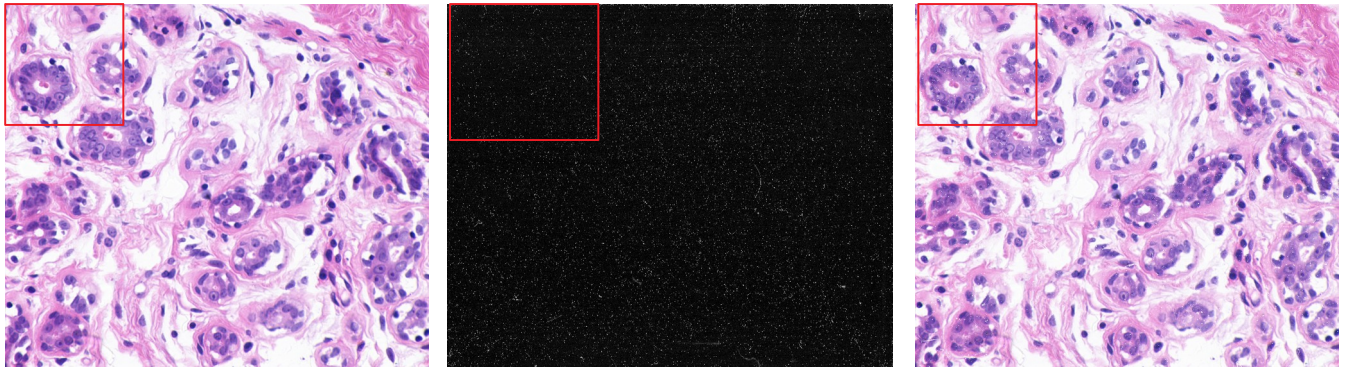


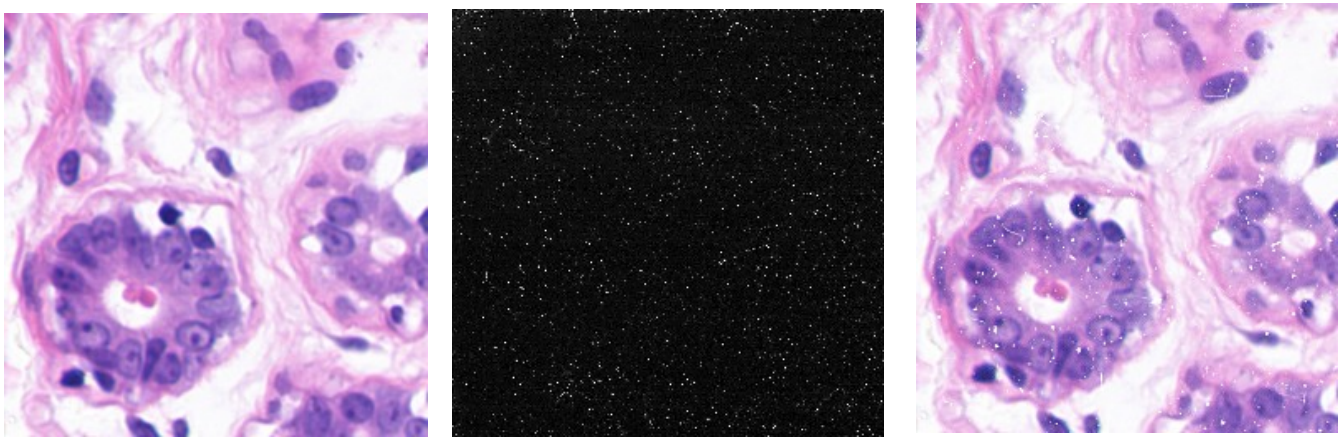




Original **Dust film**

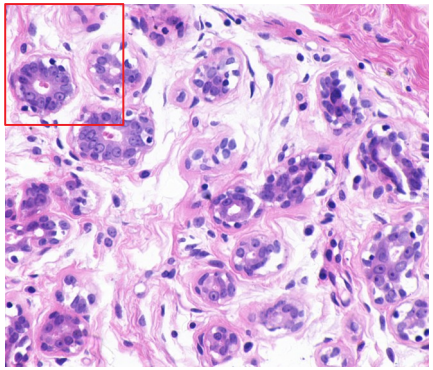
Impact of Dust

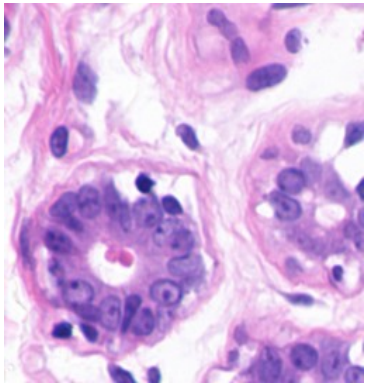




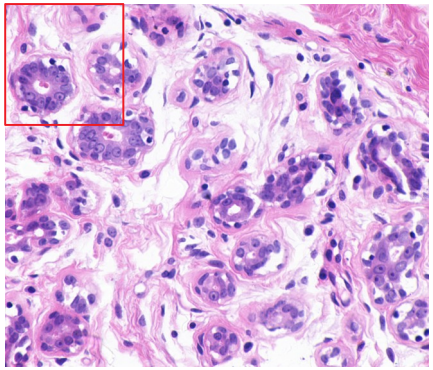
Original **Dust film** **Degraded by dust**

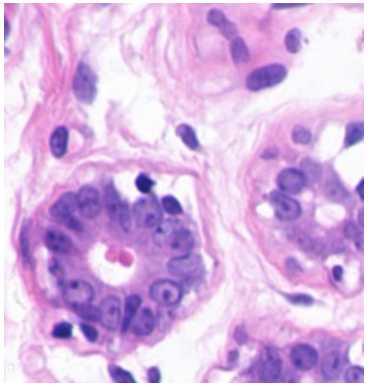
Effect of Fading

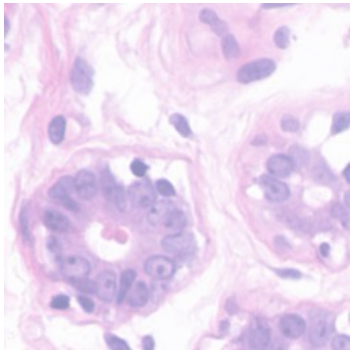


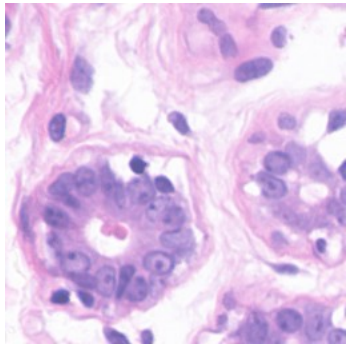


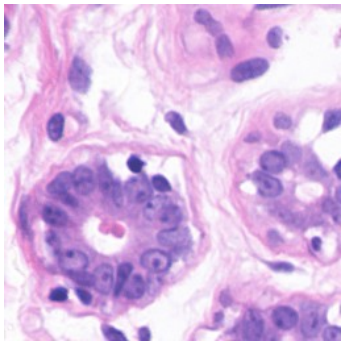
Effect of Fading







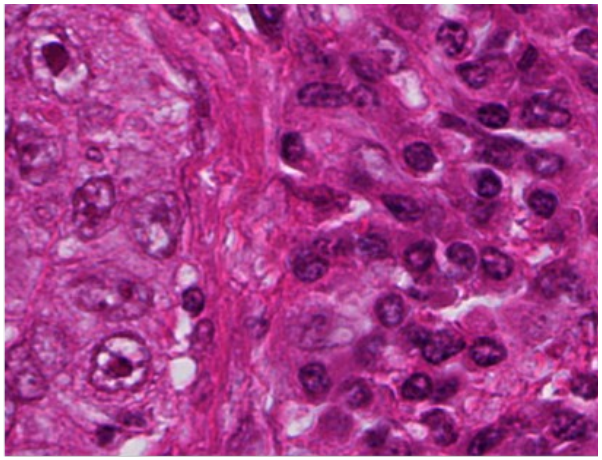




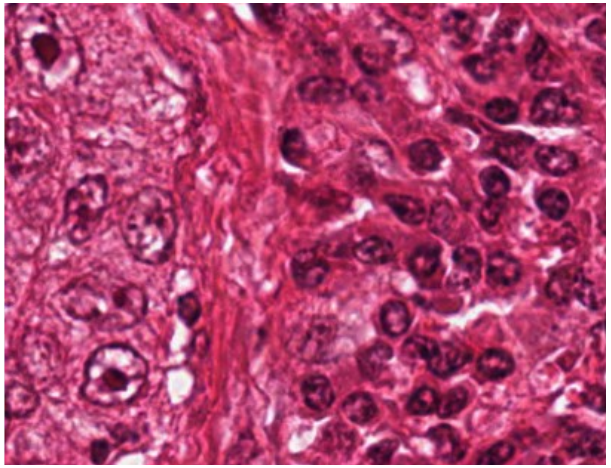
Opacity=10 **Opacity=25** **Opacity=50** **Opacity=75** **Opacity=90**

Why Color Normalization?

- Color inconsistency present among histological images, collected from different sources, may significantly affect the performance of computer-aided diagnosis.



Hamamatsu Nanozoomer

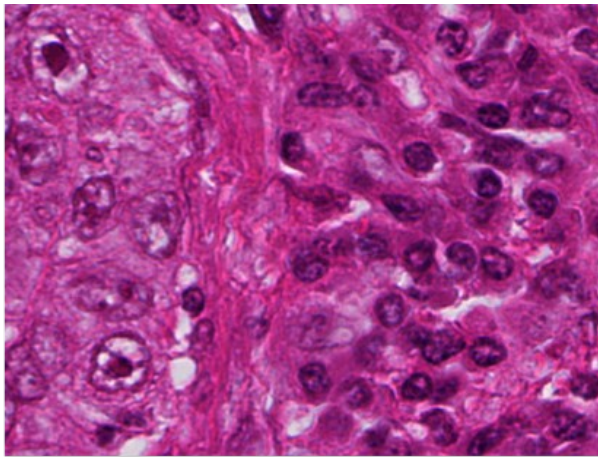


Aperio Scanscope

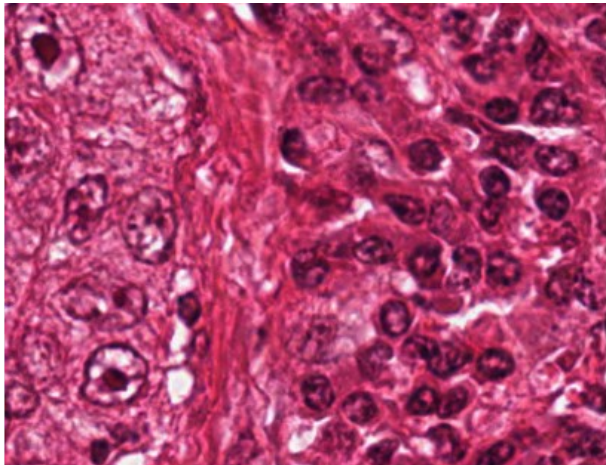
Image courtesy: http://camper.in.tum.de/Students/MaBaDaHistologyProcess

Why Color Normalization?

- Color inconsistency present among histological images, collected from different sources, may significantly affect the performance of computer-aided diagnosis.



Hamamatsu Nanozoomer



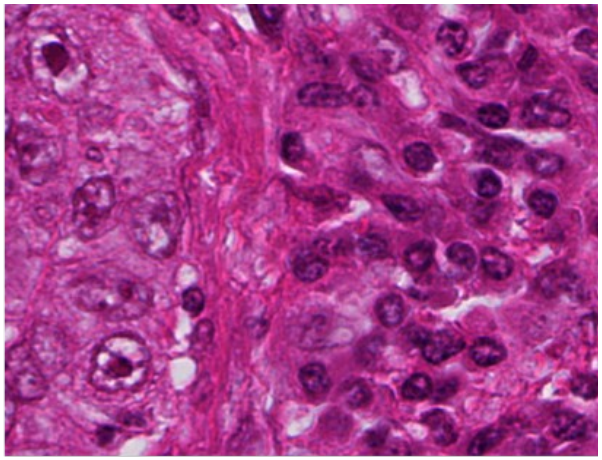
Aperio Scanscope

Challenge: How to reduce color variation among the images within particular biopsy set.

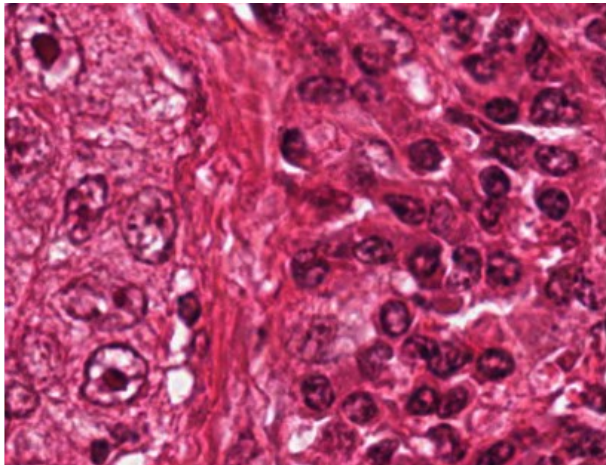
Image courtesy: http://camper.in.tum.de/Students/MaBaDaHistologyProcess

Why Color Normalization?

- Histological information consists of morphological information and details of in-situ molecular and cellular structures, which is very important in therapeutic diagnosis.



Hamamatsu Nanozoomer

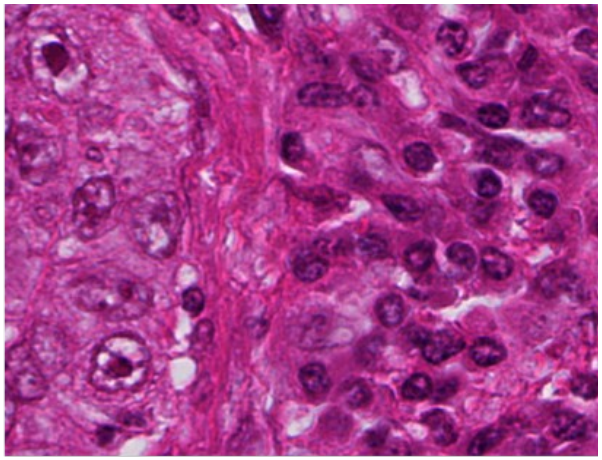


Aperio Scanscope

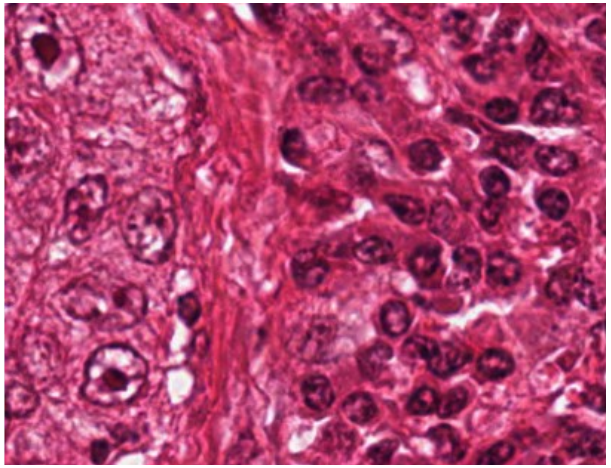
Image courtesy: http://camper.in.tum.de/Students/MaBaDaHistologyProcess

Why Color Normalization?

- Histological information consists of morphological information and details of in-situ molecular and cellular structures, which is very important in therapeutic diagnosis.



Hamamatsu Nanozoomer

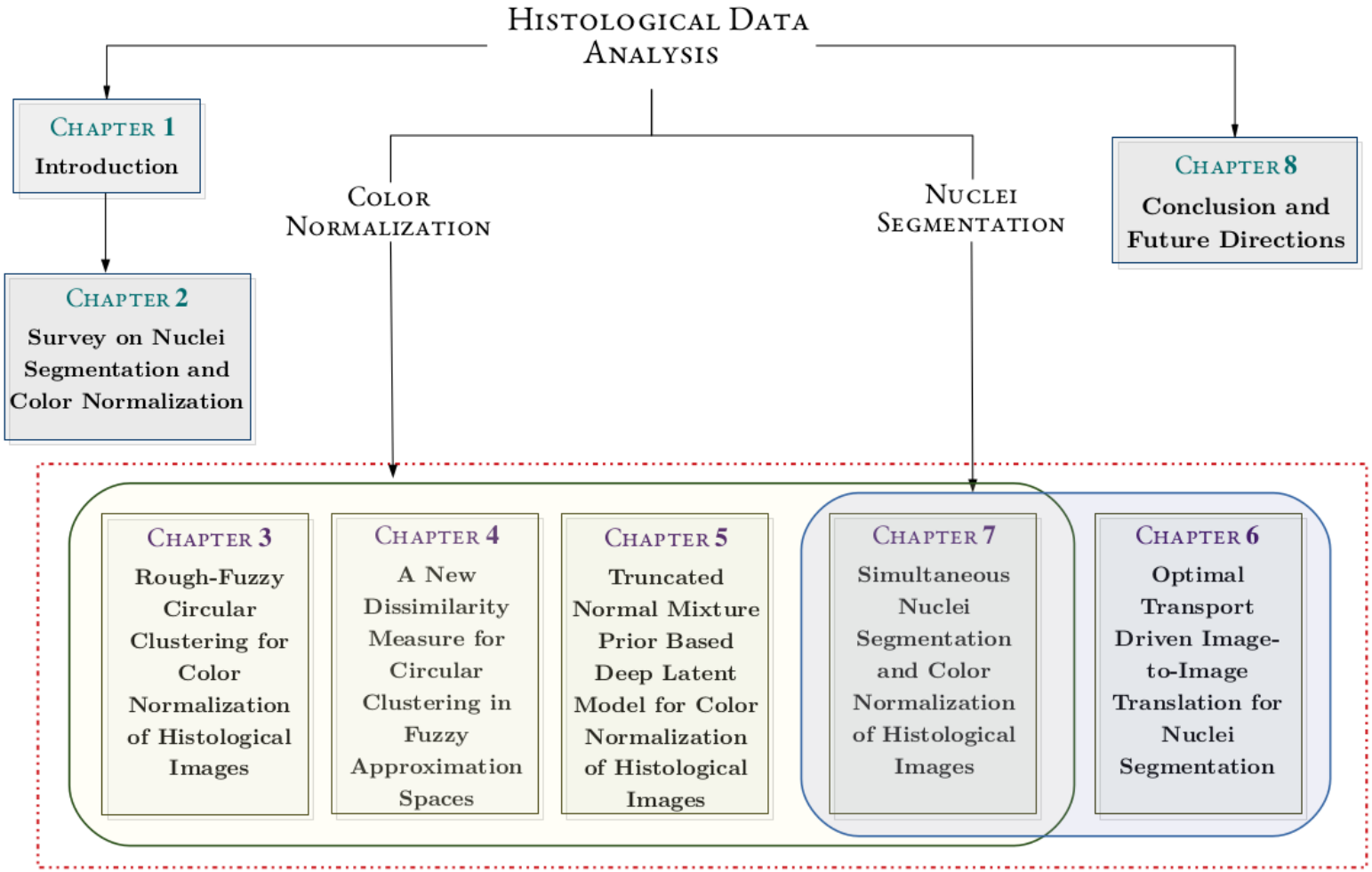


Aperio Scanscope

Challenge: Reduce color disagreement without hampering histological information in the images.

Image courtesy: http://camper.in.tum.de/Students/MaBaDaHistologyProcess

Outline of the Thesis



Chapter 3

Rough-Fuzzy Circular Clustering for Color Normalization of Histological Images

*P. Maji and **S. Mahapatra**, "Rough-Fuzzy Circular Clustering for Color Normalization of Histological Images", **Fundamenta Informaticae**, vol. 164, no. 1, pp. 103-117, 2019.*

Rough-Fuzzy Circular Clustering

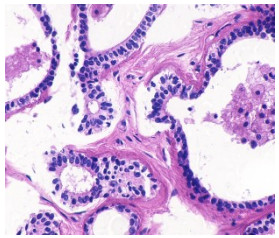
- HSI color space is taken into consideration.

why not
RGB color space?

Rough-Fuzzy Circular Clustering

- HSI color space is taken into consideration.

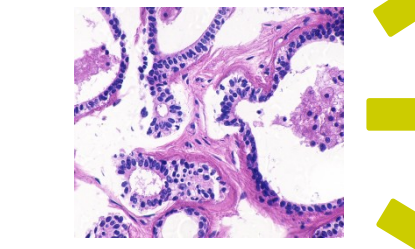
why not RGB color space?



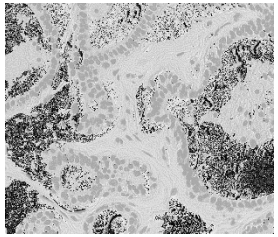
Histological image

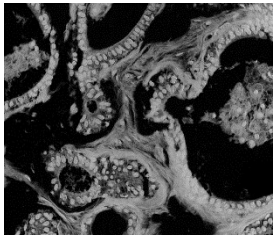
Rough-Fuzzy Circular Clustering

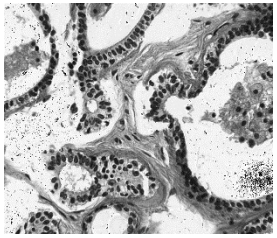
- HSI color space is taken into consideration.



Histological image







Hue: representative of color

range: $0 \leq \theta < 2\pi$, circular in nature

Saturation: contains stain bound information

Intensity: intensity/ value information

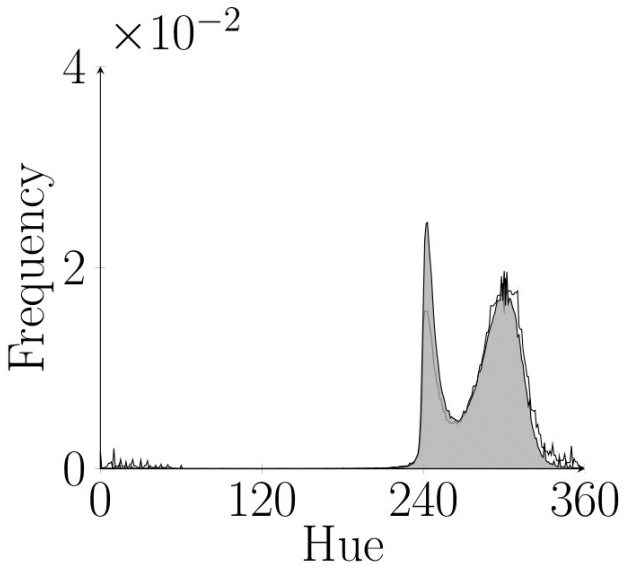
Rough-Fuzzy Circular Clustering

- Analysis is performed on saturation-weighted hue histogram.

why not standard hue histogram?

Rough-Fuzzy Circular Clustering

- Analysis is performed on saturation-weighted hue histogram.



Hue histogram

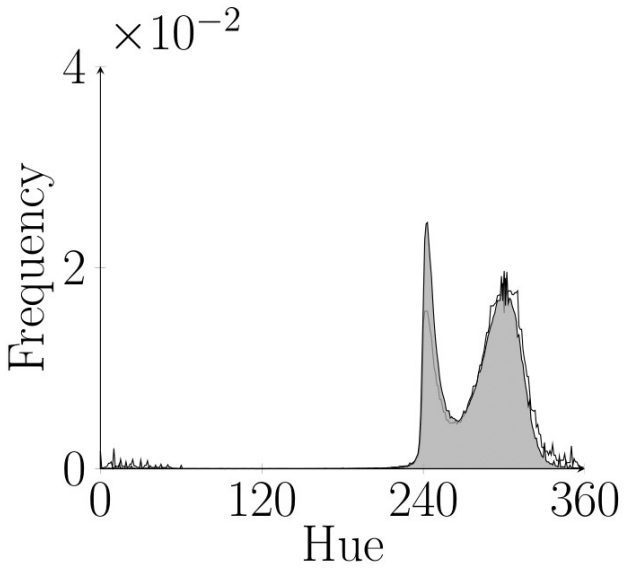
why not standard hue histogram?

a number of sharp ridges attributed by achromatic pixels

ill-defined: small or insignificant saturation values

Rough-Fuzzy Circular Clustering

- Analysis is performed on saturation-weighted hue histogram.



Hue histogram

why not standard hue histogram?

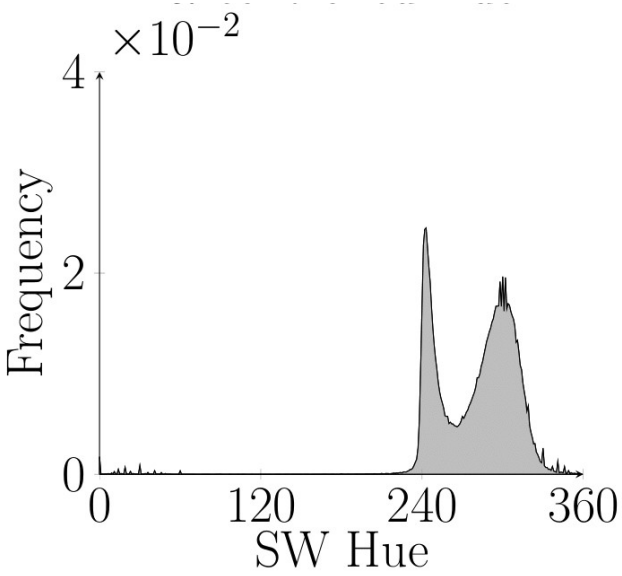
a number of sharp ridges attributed by achromatic pixels

ill-defined: small or insignificant saturation values

Solution??

Rough-Fuzzy Circular Clustering

- Analysis is performed on saturation-weighted hue histogram.



SW Hue histogram

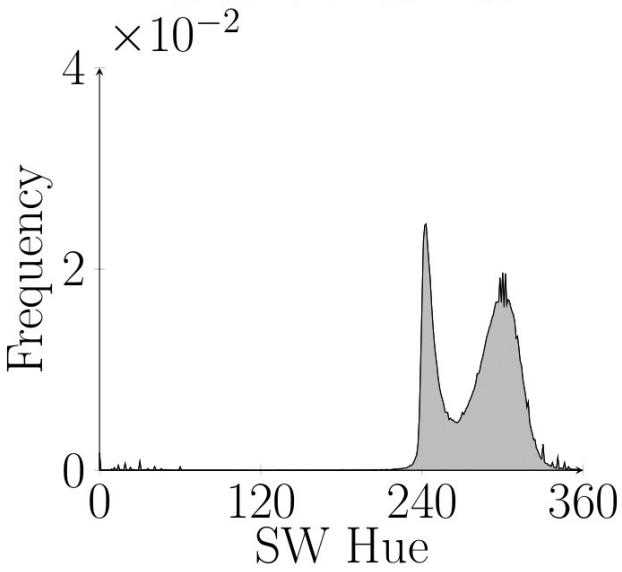
$$H^{SW}(\theta) = \sum_{k \in I} s_k \delta(\theta, h_k)$$

$$\text{where, } \delta(\theta, h_k) = \begin{cases} 1 & \text{if } \theta = h_k \\ 0 & \text{otherwise} \end{cases}$$

A. Hanbury, "Circular statistics applied to colour images", ***Computer Vision Winter Workshop***, 91(1-2), pp. 53-71, 2003.

Rough-Fuzzy Circular Clustering

- Analysis is performed on saturation-weighted hue histogram.



SW Hue histogram

$$H^{SW}(\theta) = \sum_{k \in I} s_k \delta(\theta, h_k)$$

$$\text{where, } \delta(\theta, h_k) = \begin{cases} 1 & \text{if } \theta = h_k \\ 0 & \text{otherwise} \end{cases}$$

reduces effects of achromatic pixels

A. Hanbury, "Circular statistics applied to colour images", ***Computer Vision Winter Workshop***, 91(1-2), pp. 53-71, 2003.

Rough-Fuzzy Circular Clustering

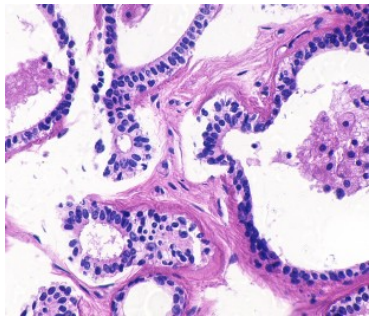
- A fuzzy clustering in circular domain

Why fuzzy clustering?

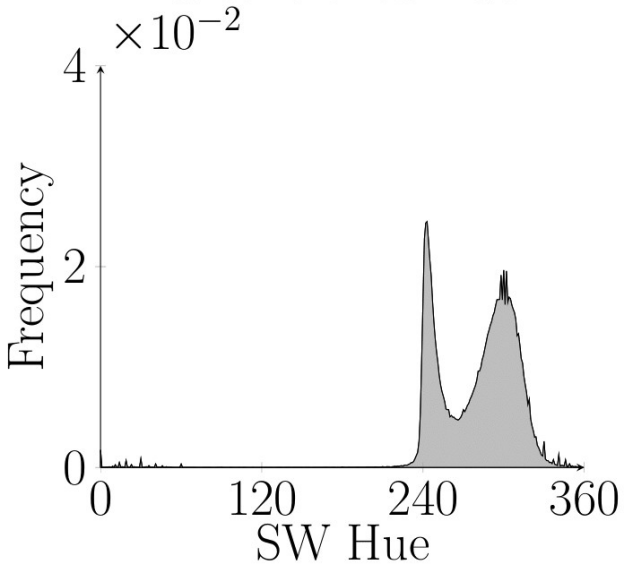
Rough-Fuzzy Circular Clustering

- A fuzzy clustering in circular domain

Why fuzzy clustering?



Histological image

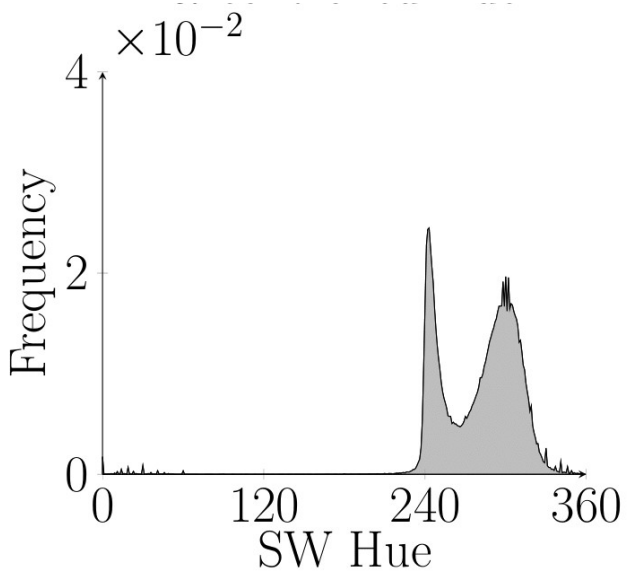


H-stain: representative hue value **260**

E-stain: representative hue value **320**

Rough-Fuzzy Circular Clustering

- A fuzzy clustering in circular domain



Why fuzzy clustering?

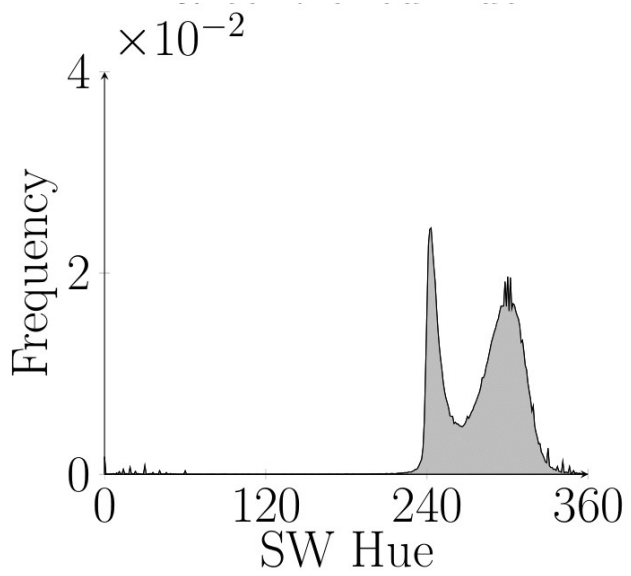
Due to staining routine and storage condition, stains become overlapped

Fuzzy set: to deal with overlapping nature of stains

L. A. Zadeh, "Fuzzy Sets: Information and Control", vol. 24, no. 3, pp. 338-353, 1965.

Rough-Fuzzy Circular Clustering

- A rough-fuzzy clustering in circular domain



Why fuzzy clustering?

Due to staining routine and storage condition, stains become overlapped

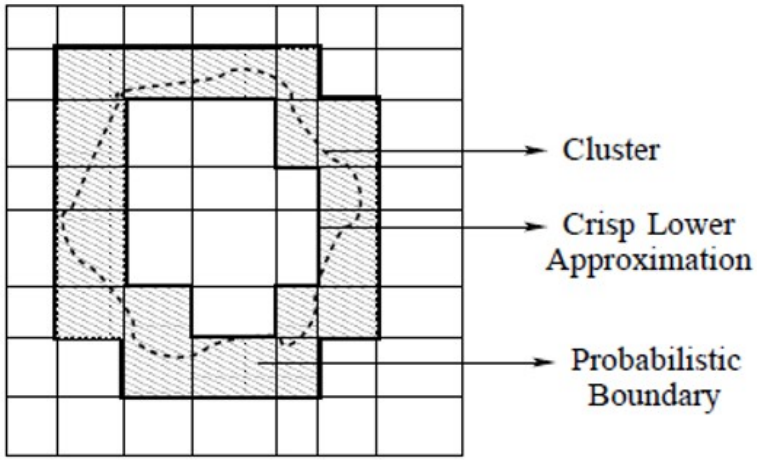
Fuzzy set: to deal with overlapping nature of stains

Why rough set?

L. A. Zadeh, "Fuzzy Sets: Information and Control", vol. 24, no. 3, pp. 338-353, 1965.

Rough-Fuzzy Circular Clustering

- A rough-fuzzy clustering in circular domain



Why fuzzy clustering?

Due to staining routine and storage condition, stains become overlapped

Fuzzy set: to deal with overlapping nature of stains

Why rough set?

Rough set: to deal with uncertainty and incompleteness in class definition

L. A. Zadeh, "Fuzzy Sets: Information and Control", vol. 24, no. 3, pp. 338-353, 1965.
Z. Pawlak, "Rough Sets: Theoretical Aspects of Reasoning About Data", Dordrecht, The Netherlands: Kluwer, 1991.

Objective Function

Minimization of objective function with respect to parameter set ψ:

$$J(\psi) = \sum_{i=1}^{c} \left[\omega \times J_i^L(\psi) + (1-\omega) \times J_i^B(\psi)\right]$$

Objective Function

Minimization of objective function with respect to parameter set ψ:

$$J(\psi) = \sum_{i=1}^{c} [\omega \times J_i^L(\psi) + (1-\omega) \times J_i^B(\psi)]$$

$$\psi = \{v_i, \mu_{ij}\}$$

corresponding to lower approximation region for *i*-th stain class:

$$J_i^L(\psi) = \sum_{x_j \in \underline{A}(\beta_i)} [1 - \cos(x_j - v_i)] H^{sw}(x_j)$$

corresponding to boundary region for *i*-th stain class:

$$J_i^B(\psi) = \sum_{x_j \in B(\beta_i)} \mu_{ij}^m [1 - \cos(x_j - v_i)] H^{sw}(x_j)$$

Estimation of Membership Function

Minimization of following Lagrangian based on $\sum_{i=1}^{c} \mu_{ij} = 1, \forall j$

$$\mathcal{J}^B(\psi) = \sum_{i=1}^{c} \sum_{x_j \in B(\beta_i)} \mu_{ij}^m \left[1 - \cos(x_j - v_i)\right] H^{sw}(x_j) + \lambda \sum_{x_j \in B(\beta_i)} \left[1 - \sum_{i=1}^{c} \mu_{ij}\right] H^{sw}(x_j)$$

$$\frac{\partial \mathcal{J}^B(\psi)}{\partial \mu_{ij}} = 0 \quad \Rightarrow \quad \mu_{ij} = \left(\sum_{k=1}^{c} \left(\frac{d_{ij}}{d_{kj}} \right)^{\frac{1}{m-1}} \right)^{-1}$$

$$d_{ij} = \left[1 - \cos(x_j - v_i)\right] \quad \textbf{Cosine distance}$$

Computation of Cluster Centroid

$$\frac{\partial J(\psi)}{\partial v_i} = 0$$

$$v_i = \arctan\left[\frac{\omega \times \mathcal{P}_1 + (1-\omega) \times \mathcal{P}_2}{\omega \times \mathcal{Q}_1 + (1-\omega) \times \mathcal{Q}_2}\right]$$

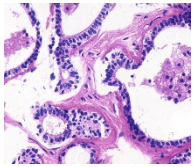
$$\mathcal{P}_1 = \sum_{x_j \in \underline{A}(\beta_i)} \sin(x_j) H^{sw}(x_j), \mathcal{P}_2 = \sum_{x_j \in B(\beta_i)} \mu_{ij}^m \sin(x_j) H^{sw}(x_j)$$

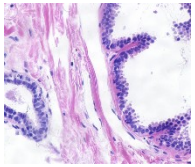
$$\mathcal{Q}_1 = \sum_{x_j \in \underline{A}(\beta_i)} \cos(x_j) H^{sw}(x_j), \text{and} \quad \mathcal{Q}_2 = \sum_{x_j \in B(\beta_i)} \mu_{ij}^m \cos(x_j) H^{sw}(x_j)$$

depends on the choice of relative importance parameter ω

Color Normalization Method - RFCC$_{cosine}$

Template

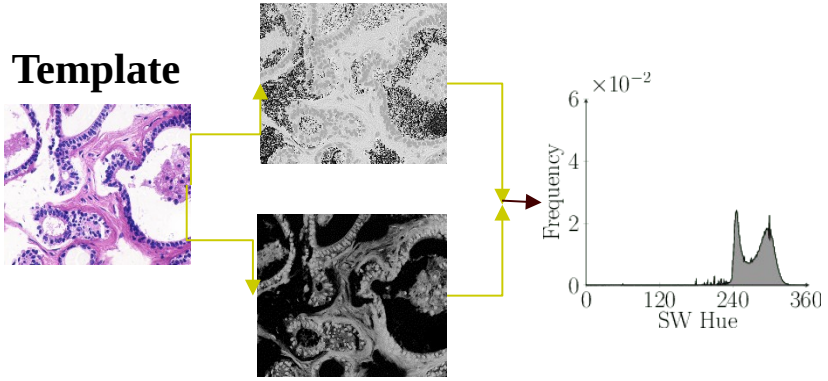


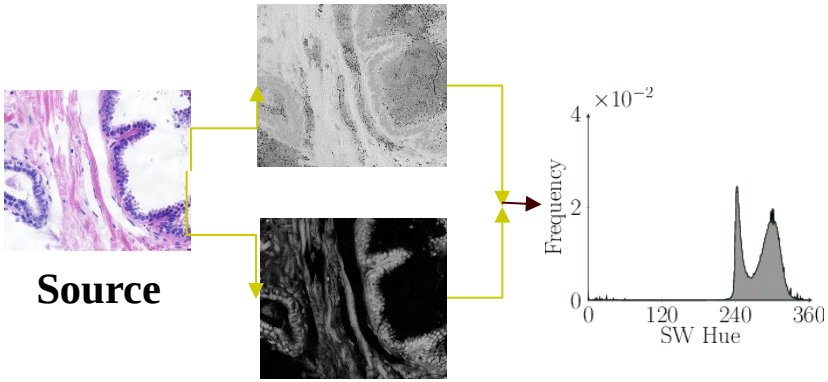


Source

Color Normalization Method - RFCC$_{cosine}$

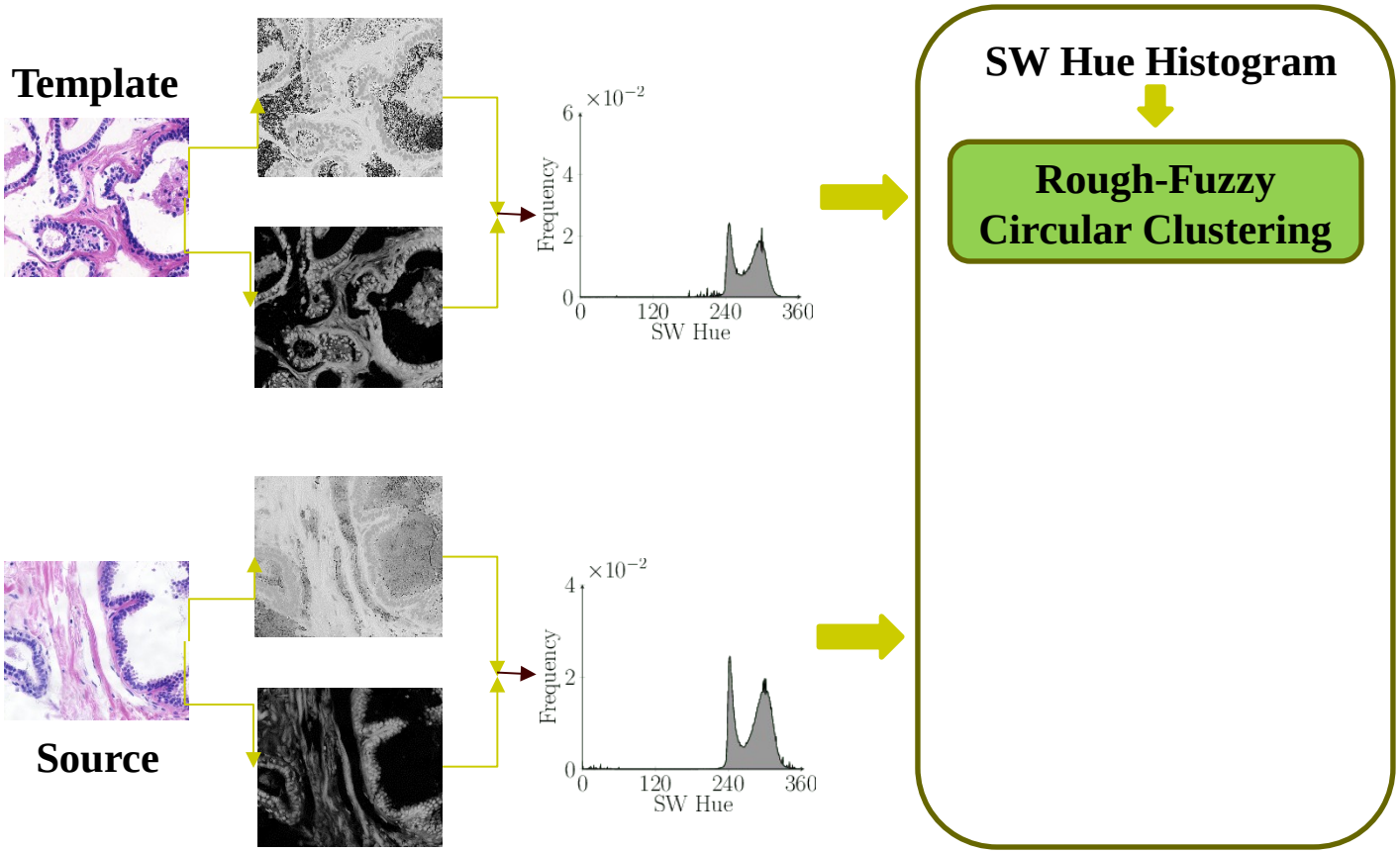
Template



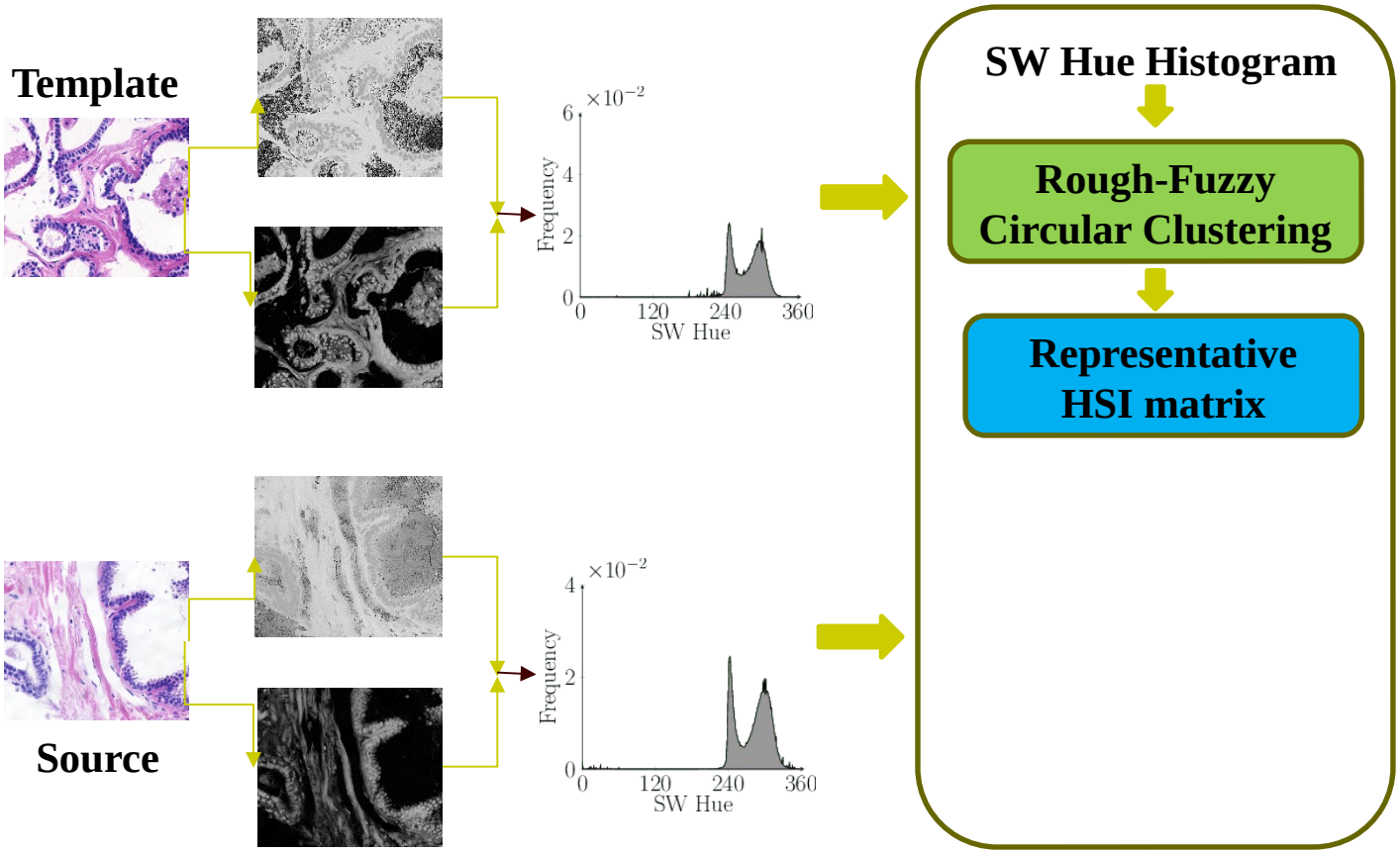


Source

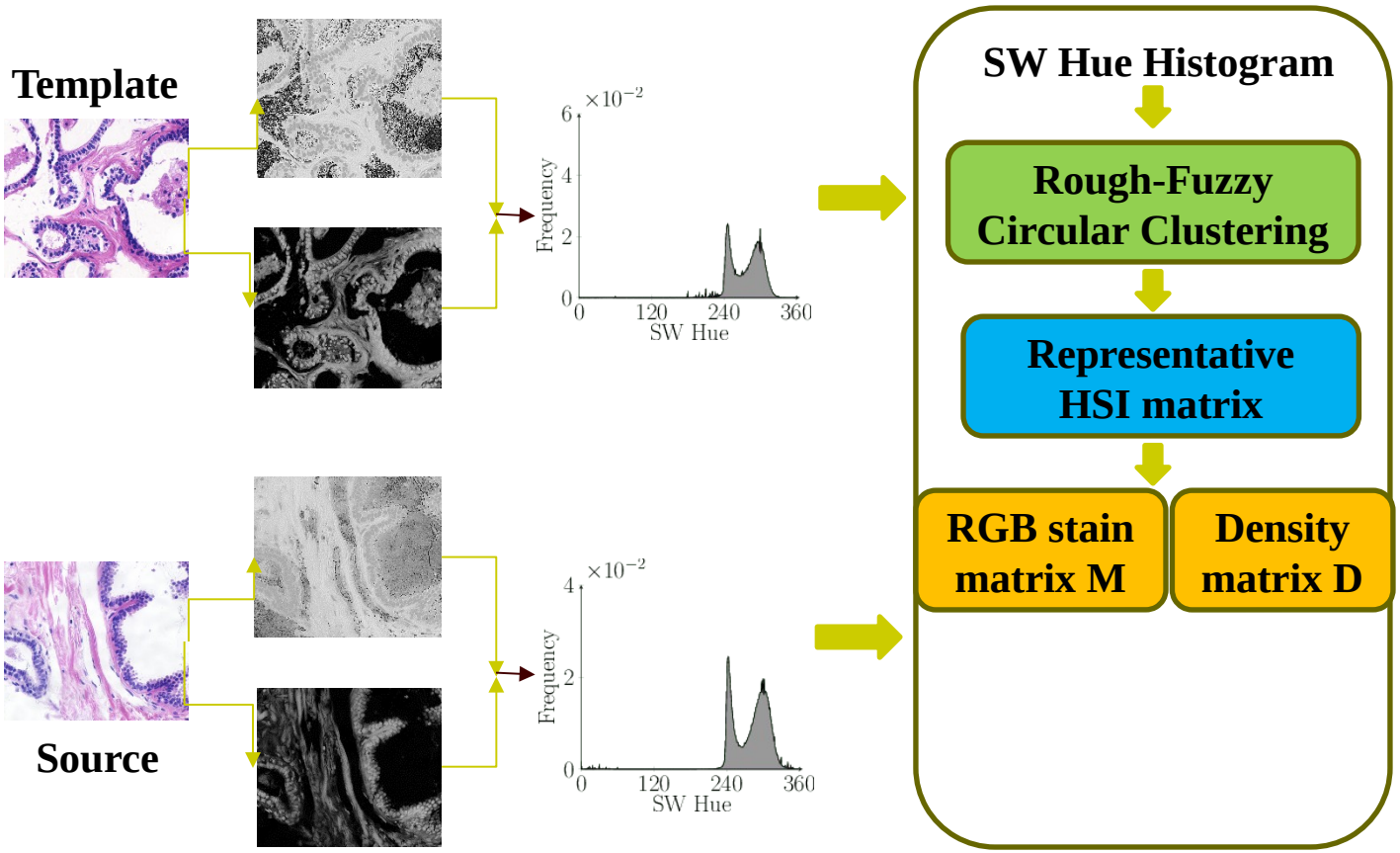
Color Normalization Method - RFCC$_{cosine}$



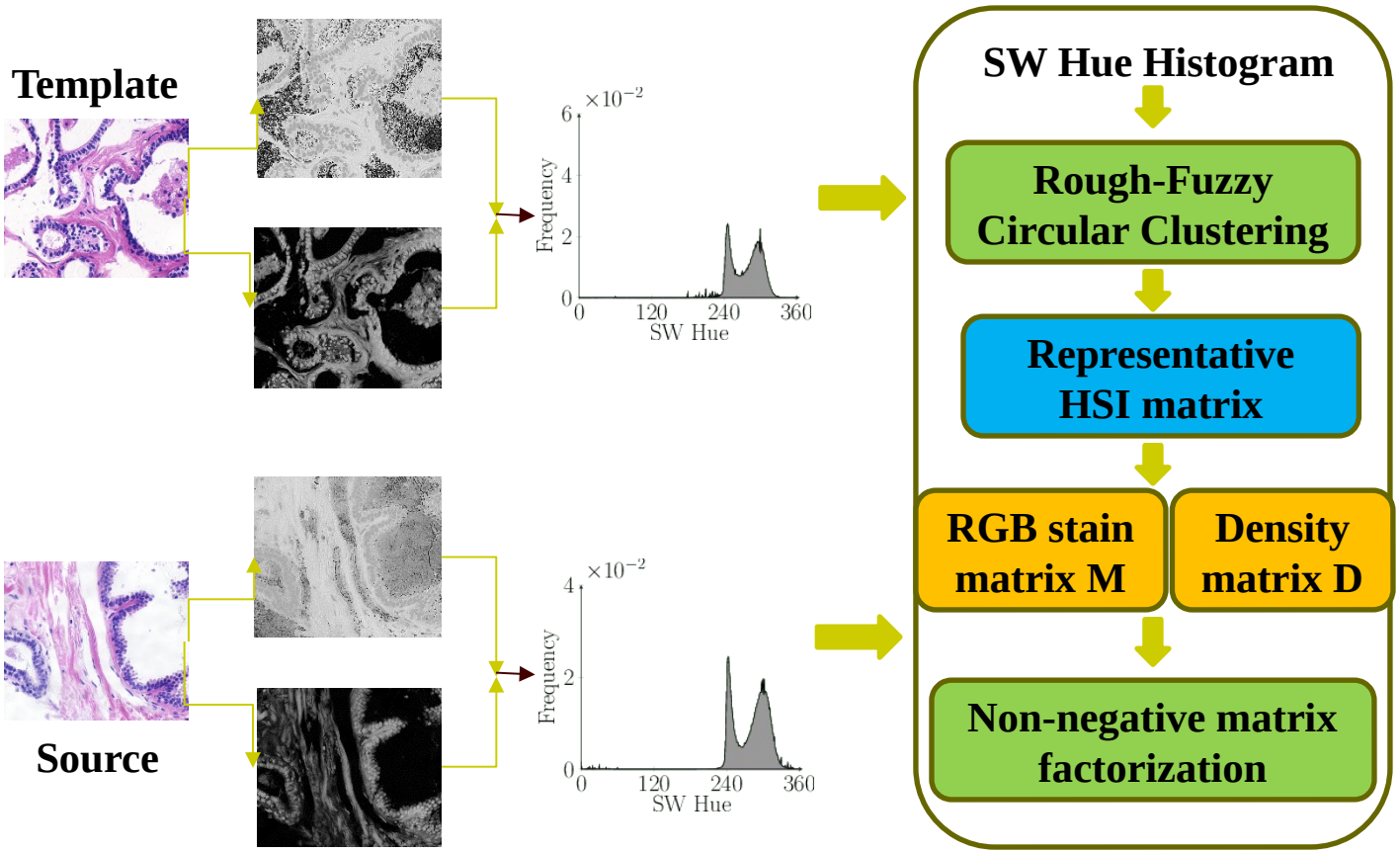
Color Normalization Method - RFCC$_{cosine}$



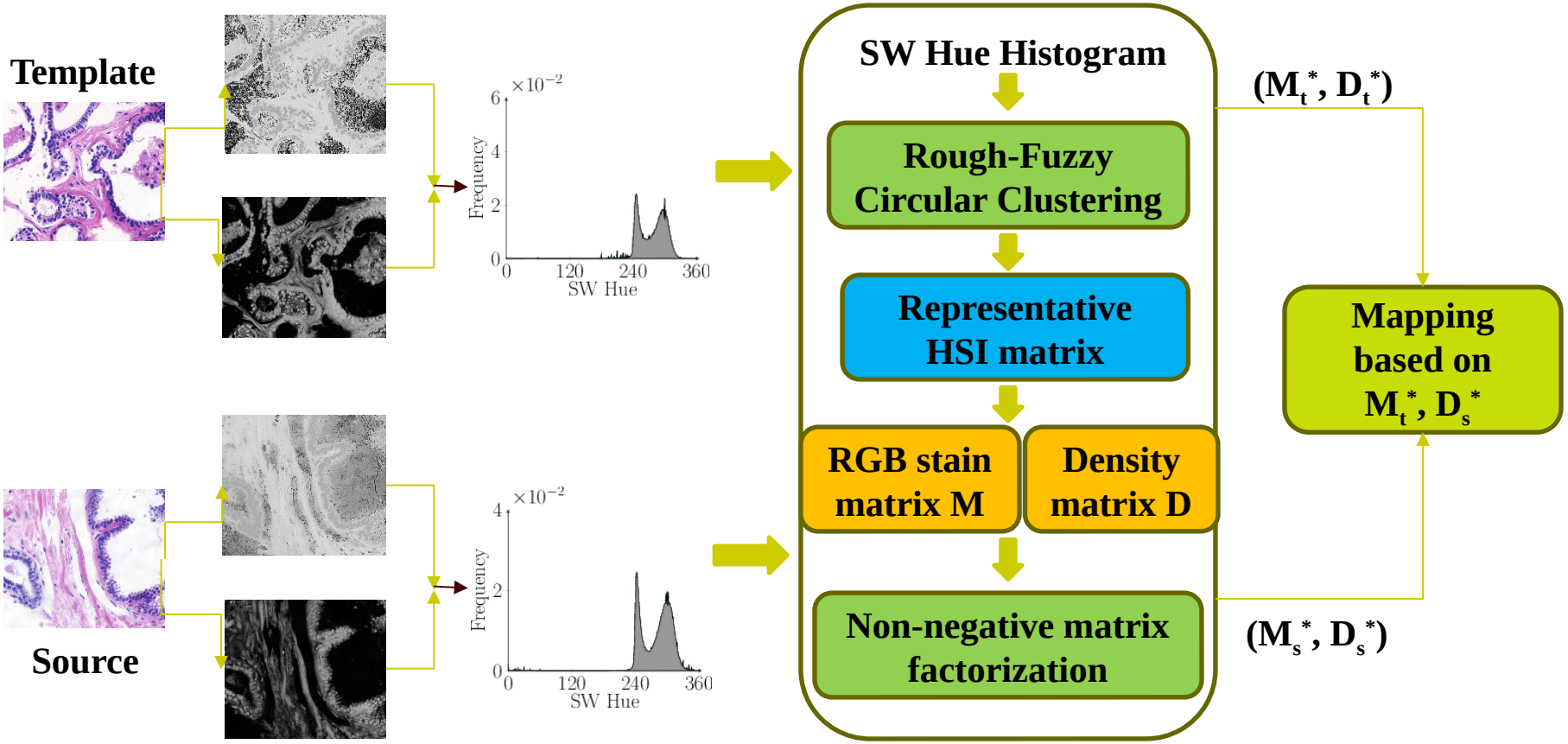
Color Normalization Method - RFCC$_{cosine}$



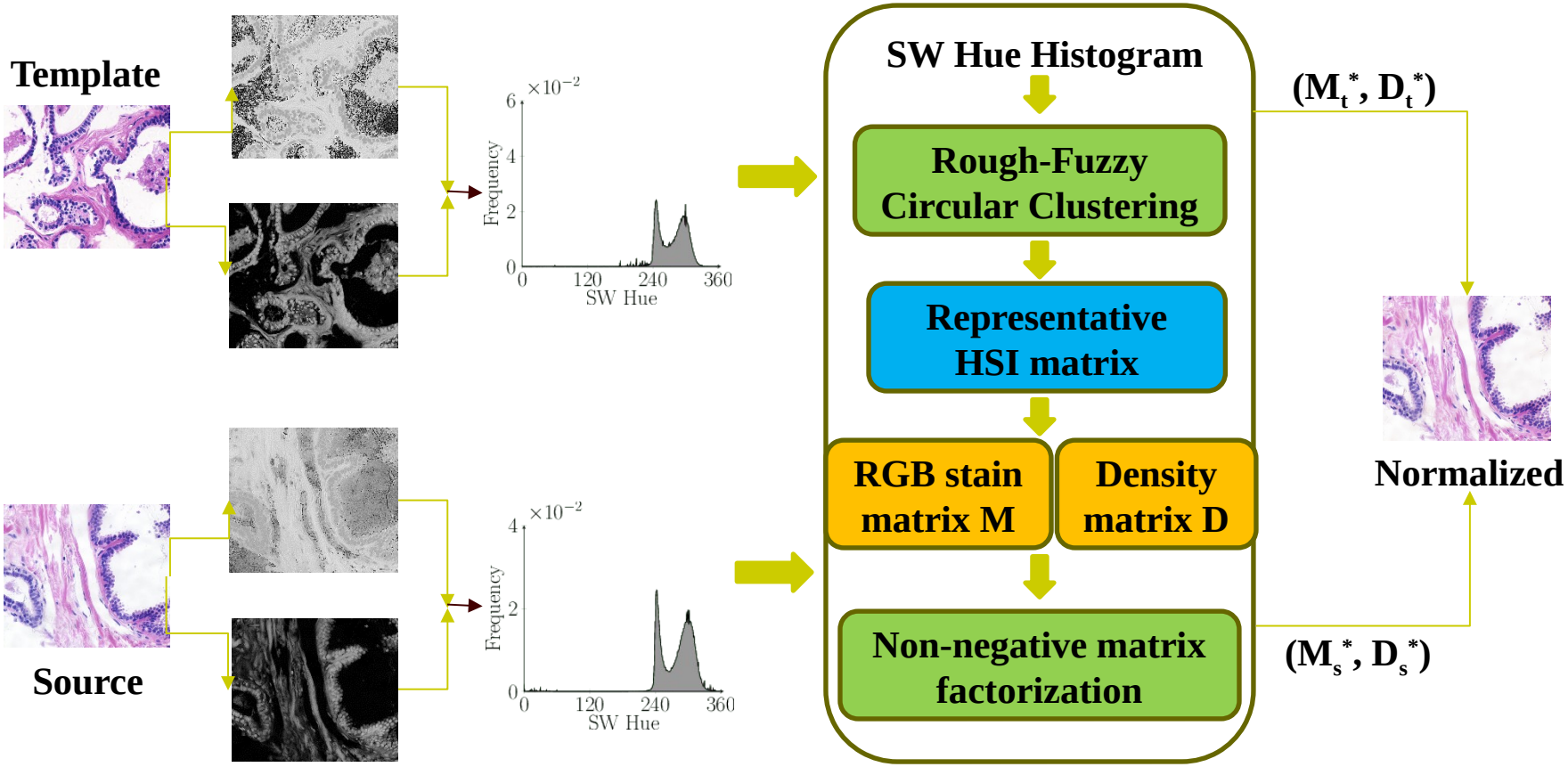
Color Normalization Method - RFCC$_{cosine}$



Color Normalization Method - RFCC$_{cosine}$



Color Normalization Method - RFCC$_{cosine}$



Description of Data Sets

- **UCSB** (University of California, Santa Barbara) Breast Cancer Cell Data : Total number of images = **58**
- Data specifications: hematoxylin and eosin (H&E) stained biopsy images (**10 biopsy sets**: 9 sets × 6 + 1 set × 4).
- Each image has a resolution of 896 × 768.
- Associated ground-truth annotation with nuclei considered as ROI.
- Images are stored in 24-bit nonlinear RGB format.
- Number of classes : Non-cancerous benign cell (32 images) and Cancerous malignant cell (26 images).

E. D. Gelasca *et al*., "Evaluation and benchmark for biological image segmentation", *IEEE International Conference on Image Processing*, 2008.

Performance on UCSB Data: Histogram

Different Biopsy Sets	Different Channels	Standard Histogram		SW Histogram	
		σ_H	σ_E	σ_H	σ_E
ytma10_010704	Red	6.31	**2.68**	**2.39**	3.65
	Green	3.80	1.08	**1.39**	**1.03**
	Blue	2.22	**2.20**	**1.59**	2.55
ytma12_010804	Red	3.99	**5.26**	**1.89**	5.73
	Green	3.16	**1.63**	**1.17**	2.03
	Blue	1.25	1.46	**0.94**	**1.19**
ytma23_022103	Red	**1.61**	**5.12**	1.67	5.31
	Green	1.33	**1.53**	**1.24**	1.80
	Blue	0.69	1.49	**0.64**	**1.38**
ytma49_042003	Red	3.98	3.07	**3.28**	**2.36**
	Green	2.41	**0.45**	**1.99**	0.54
	Blue	1.02	1.51	**0.69**	**0.94**
ytma49_042203	Red	7.53	5.77	**2.24**	**3.07**
	Green	4.09	5.90	**1.49**	**0.87**
	Blue	1.65	12.86	**0.64**	**1.89**

Note: σ_X represents the standard deviation of the estimated stain vectors of X-stain, corresponding to all images of the same biopsy set; $X \in \{H, E\}$

Performance on UCSB Data: Histogram

Different Biopsy Sets	Different Channels	Standard Histogram		SW Histogram	
		σ_H	σ_E	σ_H	σ_E
ytma10_010704	Red	6.31	**2.68**	**2.39**	3.65
	Green	3.80	1.08	**1.39**	**1.03**
	Blue	2.22	**2.20**	**1.59**	2.55
ytma12_010804	Red	3.99	**5.26**	**1.89**	5.73
	Green	3.16	**1.63**	**1.17**	2.03
	Blue	1.25	1.46	**0.94**	**1.19**
ytma23_022103	Red	**1.61**	**5.12**	1.67	5.31
	Green	1.33	**1.53**	**1.24**	1.80
	Blue	0.69	1.49	**0.64**	**1.38**
ytma49_042003	Red	3.98	3.07	**3.28**	**2.36**
	Green	2.41	**0.45**	**1.99**	0.54
	Blue	1.02	1.51	**0.69**	**0.94**
ytma49_042203	Red	7.53	5.77	**2.24**	**3.07**
	Green	4.09	5.90	**1.49**	**0.87**
	Blue	1.65	12.86	**0.64**	**1.89**

H-stain: minimum value in **14/15 cases**

E-stain: minimum value in **8/15 cases**

Performance on UCSB Data: Histogram

Different Biopsy Sets	Different Channels	Standard Histogram		SW Histogram	
		σ_H	σ_E	σ_H	σ_E
ytma49_042403	Red	2.28	**3.29**	**1.72**	3.80
	Green	1.38	**0.91**	**0.94**	1.10
	Blue	**0.71**	1.28	0.76	**0.72**
ytma49_072303	Red	1.45	4.24	**1.41**	**2.86**
	Green	**1.14**	1.19	**1.14**	**1.09**
	Blue	**0.29**	1.08	0.30	**0.67**
ytma49_111003	Red	**1.89**	**3.24**	2.79	5.34
	Green	**1.51**	**1.31**	2.39	2.69
	Blue	**1.01**	**1.44**	1.08	1.93
ytma49_111303	Red	**1.70**	6.29	2.29	**6.09**
	Green	**1.43**	**2.44**	2.06	2.54
	Blue	**0.79**	1.82	0.80	**1.80**
ytma55_030603	Red	4.18	6.46	**1.91**	**3.84**
	Green	3.21	3.57	**1.52**	**1.62**
	Blue	0.80	10.41	**0.77**	**1.67**

H-stain: minimum value in **21/30 cases**

E-stain: minimum value in **17/30 cases**

Performance on UCSB Data: Clustering

Different Biopsy Sets	Different Channels	Hard		Fuzzy		$RFCC_{cosine}$	
		σ_H	σ_E	σ_H	σ_E	σ_H	σ_E
ytma10_010704	Red	**2.37**	3.69	2.51	3.79	2.39	**3.65**
	Green	**1.25**	1.04	1.35	1.09	1.39	**1.03**
	Blue	1.26	2.52	**1.21**	**2.49**	1.59	2.55
ytma12_010804	Red	2.00	5.78	**1.89**	5.85	**1.89**	**5.73**
	Green	1.24	2.06	1.18	2.08	**1.17**	**2.03**
	Blue	0.95	1.20	**0.91**	1.21	0.94	**1.19**
ytma23_022103	Red	1.70	**5.30**	**1.67**	5.42	**1.67**	5.31
	Green	1.26	1.81	1.27	1.83	**1.24**	**1.80**
	Blue	**0.63**	**1.36**	0.66	1.39	0.64	1.38
ytma49_042003	Red	3.29	**2.36**	3.45	2.37	**3.28**	**2.36**
	Green	**1.99**	0.55	2.11	**0.54**	**1.99**	**0.54**
	Blue	**0.66**	**0.94**	0.94	0.95	0.69	**0.94**
ytma49_042203	Red	2.25	3.09	2.39	3.07	**2.24**	**3.07**
	Green	**1.44**	0.90	1.65	**0.87**	1.49	**0.87**
	Blue	0.72	**1.80**	**0.64**	1.90	**0.64**	1.89

H-stain: minimum value in **8/15 cases**

E-stain: minimum value in **11/15 cases**

Performance on UCSB Data: Clustering

Different Biopsy Sets	Different Channels	Hard		Fuzzy		$RFCC_{cosine}$	
		σ_H	σ_E	σ_H	σ_E	σ_H	σ_E
ytma49_042403	Red	1.73	3.93	1.73	4.08	**1.72**	**3.80**
	Green	0.96	1.13	**0.94**	1.17	**0.94**	**1.10**
	Blue	0.76	0.77	**0.70**	0.87	0.76	**0.72**
ytma49_072303	Red	**1.41**	**2.83**	**1.41**	2.89	**1.41**	2.86
	Green	**1.13**	**1.08**	1.15	1.11	1.14	1.09
	Blue	0.31	0.69	0.32	0.73	**0.30**	**0.67**
ytma49_111003	Red	2.81	**5.26**	**2.67**	5.53	2.79	5.34
	Green	2.37	**2.64**	**2.32**	2.82	2.39	2.69
	Blue	1.13	**1.92**	1.10	1.97	**1.08**	1.93
ytma49_111303	Red	2.28	**5.96**	**2.25**	6.17	2.29	6.09
	Green	**2.04**	**2.50**	2.05	2.59	2.06	2.54
	Blue	**0.78**	**1.79**	0.84	1.82	0.80	1.80
ytma55_030603	Red	1.94	3.86	**1.85**	4.08	**1.91**	**3.84**
	Green	1.54	**1.62**	**1.51**	1.72	1.52	**1.62**
	Blue	0.78	1.71	0.78	1.73	**0.77**	**1.67**

H-stain: minimum value in **15/30 cases**

E-stain: minimum value in **18/30 cases**

Performance on UCSB Data: Existing

Different Biopsy Sets	Different Channels	PF		HTN		SPCN		EM		$RFCC_{cosine}$	
		σ_H	σ_E	σ_H	σ_E	σ_H	σ_E	σ_H	σ_E	σ_H	σ_E
ytma10_010704	Red	3.04	**2.72**	2.67	3.25	2.42	3.93	2.45	4.10	**2.39**	3.65
	Green	2.23	2.01	1.68	0.97	1.66	0.73	1.61	**0.69**	**1.39**	1.03
	Blue	2.67	5.79	1.14	**2.43**	1.01	2.55	**0.92**	2.51	1.59	2.55
ytma12_010804	Red	1.99	**3.79**	**1.37**	5.79	2.20	6.26	2.08	7.73	1.89	5.73
	Green	2.16	2.82	**1.07**	**1.82**	1.80	2.14	1.66	2.54	1.17	2.03
	Blue	1.72	6.81	**0.55**	1.30	0.79	1.36	0.83	1.56	0.94	**1.19**
ytma23_022103	Red	1.77	**3.43**	2.39	5.36	**1.07**	5.75	1.18	7.27	1.67	5.31
	Green	1.95	**0.46**	2.25	1.59	**1.10**	1.81	1.16	2.21	1.24	1.80
	Blue	1.31	3.34	0.70	1.57	0.86	1.71	0.89	1.86	**0.64**	**1.38**
ytma49_042003	Red	**3.11**	2.11	3.17	**1.86**	3.14	2.98	4.56	4.53	3.28	2.36
	Green	2.98	2.02	2.35	**0.45**	2.44	0.74	3.40	0.96	**1.99**	0.54
	Blue	1.09	3.67	**0.55**	0.98	0.79	1.18	1.21	1.42	0.69	**0.94**
ytma49_042203	Red	2.29	**2.18**	4.04	3.13	1.99	3.36	**1.93**	3.88	2.24	3.07
	Green	2.95	1.40	3.81	0.92	2.02	**0.84**	2.06	1.18	**1.49**	0.87
	Blue	1.88	3.72	1.15	2.12	**0.60**	2.03	0.69	2.02	0.64	**1.89**

H-stain: minimum value in **5/15 cases**

E-stain: minimum value in **4/15 cases**

Performance on UCSB Data: Existing

Different Biopsy Sets	Different Channels	PF		HTN		SPCN		EM		$RFCC_{cosine}$	
		σ_H	σ_E	σ_H	σ_E	σ_H	σ_E	σ_H	σ_E	σ_H	σ_E
ytma49_042403	Red	3.08	**3.13**	3.42	3.67	2.99	4.89	3.39	6.66	**1.72**	3.80
	Green	3.16	3.18	2.55	**0.96**	2.38	1.38	2.72	1.67	**0.94**	1.10
	Blue	1.04	5.38	**0.63**	**0.47**	0.93	0.64	0.92	0.80	0.76	0.72
ytma49_072303	Red	2.09	2.63	2.49	2.82	1.99	**1.57**	2.52	1.99	**1.41**	2.86
	Green	2.48	1.22	2.55	0.95	2.15	**0.66**	2.67	0.95	**1.14**	1.09
	Blue	0.57	1.43	0.38	0.80	0.46	0.79	0.36	0.98	**0.30**	**0.67**
ytma49_111003	Red	1.90	13.17	1.64	6.94	4.00	9.65	**1.62**	8.12	2.79	**5.34**
	Green	2.60	11.29	1.61	3.49	1.69	5.79	**1.45**	4.63	2.39	**2.69**
	Blue	3.62	10.73	1.23	2.79	9.77	4.17	1.29	2.62	**1.08**	**1.93**
ytma49_111303	Red	2.15	6.12	**1.20**	6.71	1.44	6.85	1.63	8.87	2.29	**6.09**
	Green	2.52	**1.75**	**1.30**	2.46	1.56	2.85	1.75	3.27	2.06	2.54
	Blue	1.50	4.30	**0.24**	2.34	0.34	2.31	0.55	2.70	0.80	**1.80**
ytma55_030603	Red	2.18	7.85	1.88	16.56	1.35	5.22	**1.25**	7.60	1.91	**3.84**
	Green	3.39	3.90	1.81	2.09	1.48	2.36	**1.37**	3.19	1.52	**1.62**
	Blue	2.73	8.20	0.67	8.32	0.70	**1.62**	**0.67**	2.28	0.77	1.67

H-stain: minimum value in **11/30 cases**

E-stain: minimum value in **12/30 cases**

Performance on UCSB Data:

Normalized median intensity

$$\mathrm{NMI}(I) = \frac{\underset{i \in \mathrm{ROI}(I)}{\mathrm{med}} \{W(i)\}}{\underset{i \in \mathrm{ROI}(I)}{\max} \{W(i)\}}$$

It evaluates color consistency of a specific ROI within an image

L. G. Nyuel *et al.*, "New variants of a method of MRI scale standardization", *IEEE Transactions on Medical Imaging*, 19(2), pp. 143-150, 2000.

Performance on UCSB Data:

Normalized median intensity

$$\mathrm{NMI}(I) = \frac{\underset{i \in \mathrm{ROI}(I)}{\mathrm{med}} \{W(i)\}}{\underset{i \in \mathrm{ROI}(I)}{\max} \{W(i)\}}$$

It evaluates color consistency of a specific ROI within an image

Different Histograms /Clustering Methods	Normalized Median Intensity (NMI)			
	Mean	Median	Wilcoxon Test	Paired-t Test
Standard Histogram	0.700852	0.697148	9.29E-09	2.42E-06
Hard Clustering	0.701822	0.696991	3.49E-09	1.22E-07
Fuzzy Clustering	0.702271	0.696991	9.48E-09	2.18E-07
$\mathrm{RFCC}_{\mathrm{cosine}}$	**0.710847**	**0.707624**		

L. G. Nyuel *et al.*, "New variants of a method of MRI scale standardization", *IEEE Transactions on Medical Imaging*, 19(2), pp. 143-150, 2000.

Performance on UCSB Data:

Normalized median intensity

$$\mathrm{NMI}(I) = \frac{\underset{i \in \mathrm{ROI}(I)}{\mathrm{med}} \{W(i)\}}{\underset{i \in \mathrm{ROI}(I)}{\max} \{W(i)\}}$$

It evaluates color consistency of a specific ROI within an image

Different Histograms /Clustering Methods	Normalized Median Intensity (NMI)			
	Mean	Median	Wilcoxon Test	Paired-t Test
Standard Histogram	0.700852	0.697148	9.29E-09	2.42E-06
Hard Clustering	0.701822	0.696991	3.49E-09	1.22E-07
Fuzzy Clustering	0.702271	0.696991	9.48E-09	2.18E-07
$\mathrm{RFCC}_{\mathrm{cosine}}$	**0.710847**	**0.707624**		

sufficient??

L. G. Nyuel *et al.*, "New variants of a method of MRI scale standardization", *IEEE Transactions on Medical Imaging*, 19(2), pp. 143-150, 2000.

Performance on UCSB Data:

Normalized median intensity

$$\mathrm{NMI}(I) = \frac{\underset{i \in \mathrm{ROI}(I)}{\mathrm{med}} \{W(i)\}}{\underset{i \in \mathrm{ROI}(I)}{\max} \{W(i)\}}$$

It evaluates color consistency of a specific ROI within an image

Different Histograms /Clustering Methods	Normalized Median Intensity (NMI)			
	Mean	Median	Wilcoxon Test	Paired-t Test
Standard Histogram	0.700852	0.697148	9.29E-09	2.42E-06
Hard Clustering	0.701822	0.696991	3.49E-09	1.22E-07
Fuzzy Clustering	0.702271	0.696991	9.48E-09	2.18E-07
$\mathrm{RFCC}_{\mathrm{cosine}}$	**0.710847**	**0.707624**		

sufficient??

NMI fails to capture within-biopsy color constancy information

L. G. Nyuel *et al.*, "New variants of a method of MRI scale standardization", *IEEE Transactions on Medical Imaging*, 19(2), pp. 143-150, 2000.

Proposed Quantitative Indices

Between-Image Color Constancy Index

$$\mathrm{BiCC}(I) = \frac{1}{2(|S|-1)} \times \sum_{J \neq I} \frac{\underset{i \in \mathrm{ROI}(I)}{\mathrm{med}} \{W(i)\} + \underset{j \in \mathrm{ROI}(J)}{\mathrm{med}} \{W(j)\}}{\max\{\underset{i \in \mathrm{ROI}(I)}{\max} \{W(i)\}, \underset{j \in \mathrm{ROI}(J)}{\max} \{W(j)\}\}}$$

It evaluates color consistency of ROI among images within a particular biopsy set

Within-Set Color Constancy Index

$$\mathrm{WsCC}(S) = \frac{1}{|S|} \sum_{I \in S} \mathrm{NMI}(I) \times \mathrm{BiCC}(I);$$

Overall representation of within-image and within-biopsy color consistency

Performance on UCSB Data:

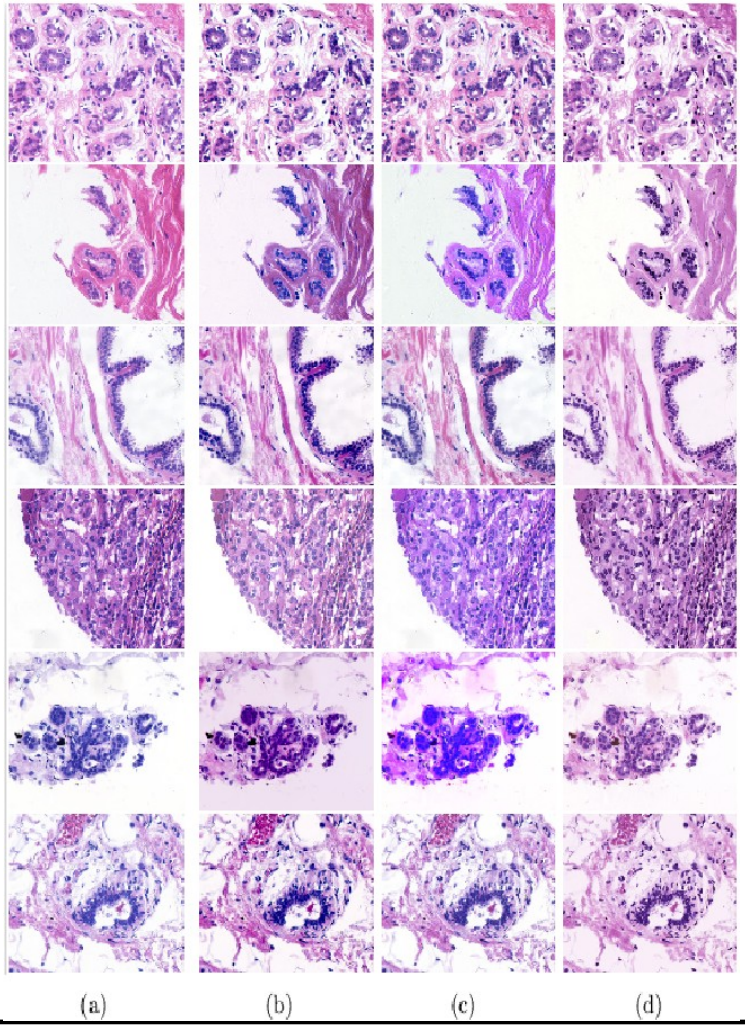
Between-image Color Constancy (BiCC) Index

Different Histograms /Clustering Methods	Between-image Color Constancy (BiCC) index			
	Mean	Median	Wilcoxon Test	Paired-t Test
Standard Histogram	0.670558	0.657639	1.75E-11	2.19E-17
Hard Clustering	0.670490	0.658078	1.75E-11	2.28E-19
Fuzzy Clustering	0.671444	0.658307	1.75E-11	2.13E-18
$\text{RFCC}_{\text{cosine}}$	**0.692504**	**0.681332**		

Within-set Color Constancy (WsCC) Index

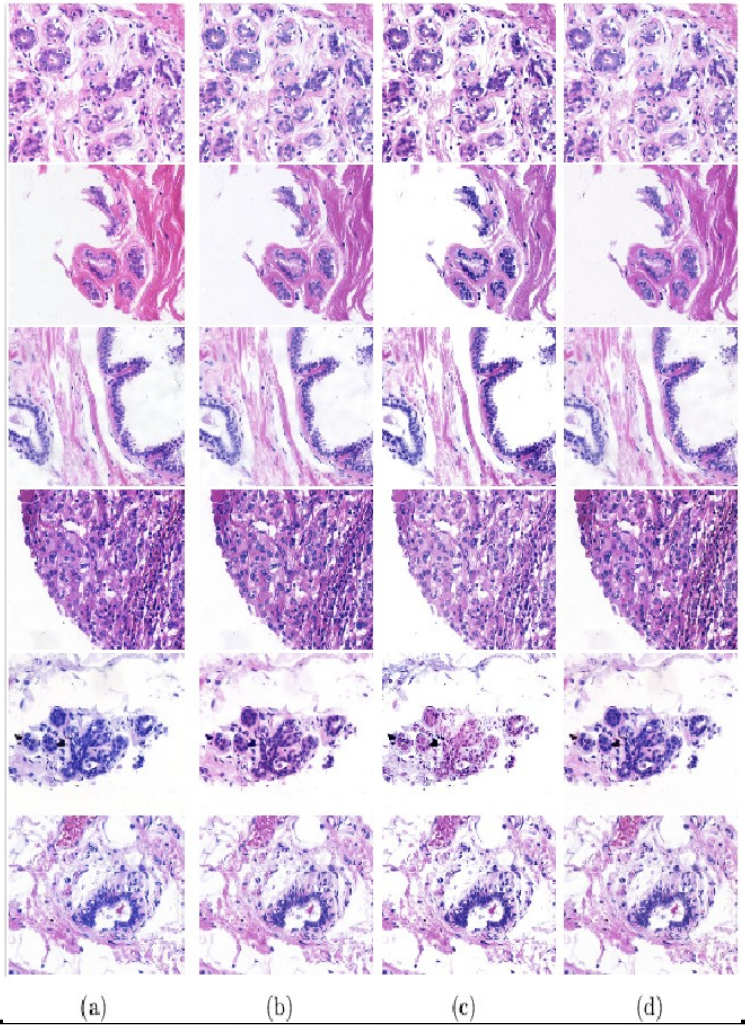
Different Histograms /Clustering Methods	Within-set Color Constancy (WsCC) index			
	Mean	Median	Wilcoxon Test	Paired-t Test
Standard Histogram	0.474186	0.465024	1.75E-11	2.40E-16
Hard Clustering	0.473908	0.464562	1.75E-11	3.54E-18
Fuzzy Clustering	0.475167	0.465122	1.75E-11	3.44E-17
$\text{RFCC}_{\text{cosine}}$	**0.494584**	**0.475552**		

Performance on UCSB Data: Qualitative



Original and color normalized images of UCSB data set obtained using different methods : (a) Original, (b) ColTrans, (c) PF, (d) SCD.

Performance on UCSB Data: Qualitative



Original and color normalized images of UCSB data set obtained using different methods : (a) Original, (b) HTN, (c) SPCN and (d) $RFCC_{cosine}$.

Performance on UCSB Data: vs Existing

Normalized Median Intensity (NMI)

Different Methods	Normalized Median Intensity (NMI)			
	Mean	Median	Wilcoxon Test	Paired-t Test
CT	0.661974	0.680989	4.83E-06	3.40E-06
PF	0.689482	0.689037	8.24E-04	2.05E-04
SCD	0.602906	0.586130	2.47E-10	3.81E-14
HTN	0.706873	0.701627	2.58E-04	1.65E-03
SPCN	0.680182	0.679416	4.49E-06	5.92E-07
$\text{RFCC}_{\text{cosine}}$	**0.710847**	**0.707624**		

L. G. Nyuel *et al.*, "New variants of a method of MRI scale standardization", *IEEE Transactions on Medical Imaging*, 19(2), pp. 143-150, 2000.

Performance on UCSB Data: vs Existing

Between-image Color Constancy (BiCC) Index

Different Methods	Between-image Color Constanc (BiCC) Index			
	Mean	Median	Wilcoxon Test	Paired-t Test
CT	0.613403	0.625624	4.94E-11	1.09E-13
PF	0.657836	0.660921	8.73E-07	3.49E-08
SCD	0.566423	0.563674	1.75E-11	3.22E-22
HTN	0.674506	0.661148	2.16E-11	2.24E-14
SPCN	0.647584	0.646141	1.81E-08	1.76E-10
$\text{RFCC}_{\text{cosine}}$	**0.692504**	**0.681332**		

Within-set Color Constancy (WsCC) Index

Different Methods	Within-set Color Constanc (WsCC) Index			
	Mean	Median	Wilcoxon Test	Paired-t Test
CT	0.409771	0.424711	5.91E-09	3.18E-10
PF	0.455051	0.455632	2.29E-05	2.50E-06
SCD	0.350092	0.329816	1.85E-11	6.50E-20
HTN	0.479276	0.470083	1.36E-10	4.90E-12
SPCN	0.441564	0.439264	1.52E-07	9.00E-09
$\text{RFCC}_{\text{cosine}}$	**0.494584**	**0.475552**		

Key Takeaways - RFCC$_{cosine}$

- Unsupervised method: a rough-fuzzy clustering is performed on SW hue histogram.
- Quantitative indices are proposed to assess inter-biopsy color consistency.
- Cosine distance is utilized to deal with the circular nature of hue values.

Key Takeaways - $RFCC_{cosine}$

- Unsupervised method: a rough-fuzzy clustering is performed on SW hue histogram.
- Quantitative indices are proposed to assess inter-biopsy color consistency.
- Cosine distance is utilized to deal with the circular nature of hue values.
- Cosine distance is not flexible: cannot capture concentration of hue values around the mean of each stain class.

Key Takeaways - RFCC$_{cosine}$

- Unsupervised method: a rough-fuzzy clustering is performed on SW hue histogram.
- Quantitative indices are proposed to assess inter-biopsy color consistency.
- Cosine distance is utilized to deal with the circular nature of hue values.
- Cosine distance is not flexible: cannot capture concentration of hue values around the mean of each stain class.
- Next chapter tries to utilize cosine distance in a more flexible way to capture underlying data distribution.

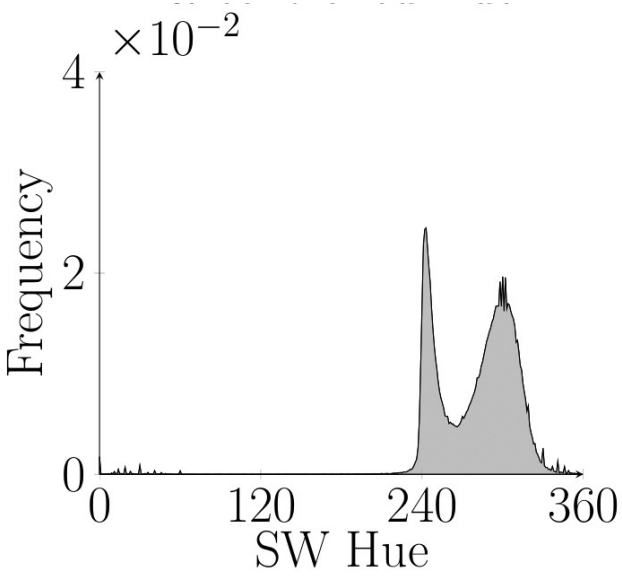
Chapter 4

A New Dissimilarity Measure for Circular Clustering in Fuzzy Approximation Spaces

P. Maji and **S. Mahapatra**, "Circular Clustering in Fuzzy Approximation Spaces for Color Normalization of Histological Images", **IEEE Transactions on Medical Imaging**, vol. 39, no. 5, pp. 1735-1745, 2020.

Rough-Fuzzy Circular Clustering

- Clustering is performed on weighted hue histogram.



SW Hue histogram

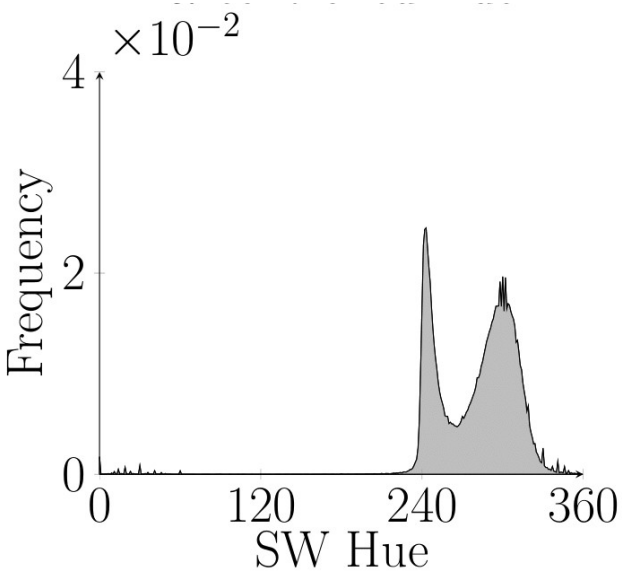
$$H^{SW}(\theta) = \sum_{k \in I} s_k \delta(\theta, h_k)$$

$$\text{where, } \delta(\theta, h_k) = \begin{cases} 1 & \text{if } \theta = h_k \\ 0 & \text{otherwise} \end{cases}$$

A. Hanbury, "Circular statistics applied to colour images", ***Computer Vision Winter Workshop***, 91(1-2), pp. 53-71, 2003.

Rough-Fuzzy Circular Clustering

- Clustering is performed on weighted hue histogram.



SW Hue histogram

$$H^{SW}(\theta) = \sum_{k \in I} s_k \delta(\theta, h_k)$$

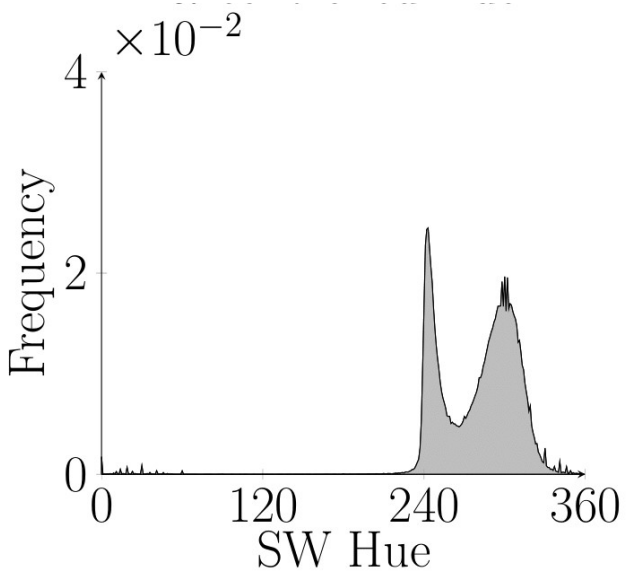
$$\text{where, } \delta(\theta, h_k) = \begin{cases} 1 & \text{if } \theta = h_k \\ 0 & \text{otherwise} \end{cases}$$

why not SW hue histogram?

A. Hanbury, "Circular statistics applied to colour images", ***Computer Vision Winter Workshop***, 91(1-2), pp. 53-71, 2003.

Rough-Fuzzy Circular Clustering

- Clustering is performed on weighted hue histogram.



SW Hue histogram

$$H^{SW}(\theta) = \sum_{k \in I} s_k \delta(\theta, h_k)$$

$$\text{where, } \delta(\theta, h_k) = \begin{cases} 1 & \text{if } \theta = h_k \\ 0 & \text{otherwise} \end{cases}$$

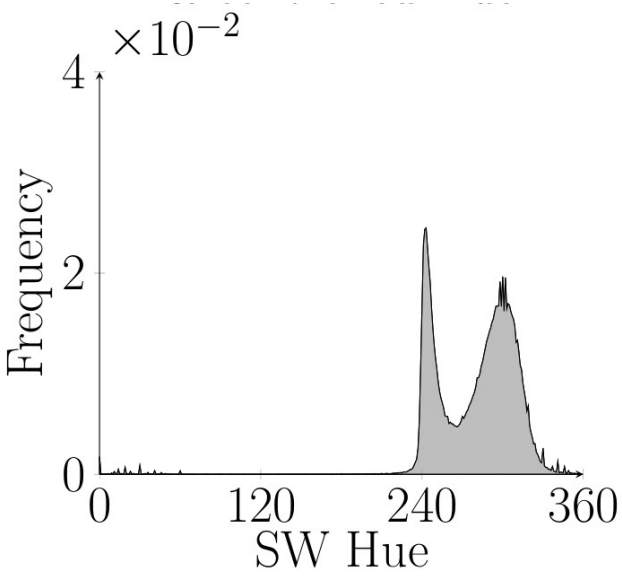
why not SW hue histogram?

no local neighborhood information

A. Hanbury, "Circular statistics applied to colour images", ***Computer Vision Winter Workshop***, 91(1-2), pp. 53-71, 2003

Rough-Fuzzy Circular Clustering

- Clustering is performed on weighted hue histogram.



SW Hue histogram

$$H^{SW}(\theta) = \sum_{k \in I} s_k \delta(\theta, h_k)$$

$$\text{where, } \delta(\theta, h_k) = \begin{cases} 1 & \text{if } \theta = h_k \\ 0 & \text{otherwise} \end{cases}$$

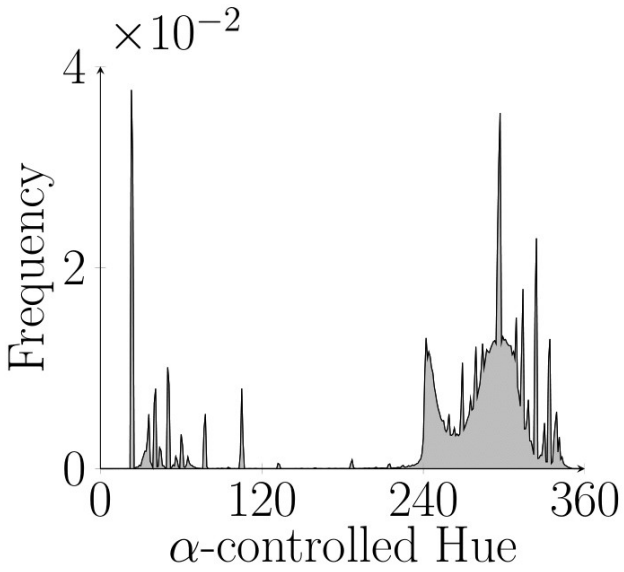
why not SW hue histogram?

Solution??

A. Hanbury, "Circular statistics applied to colour images", ***Computer Vision Winter Workshop***, 91(1-2), pp. 53-71, 2003.

Rough-Fuzzy Circular Clustering

- Clustering is performed on weighted hue histogram.



α-controlled hue histogram

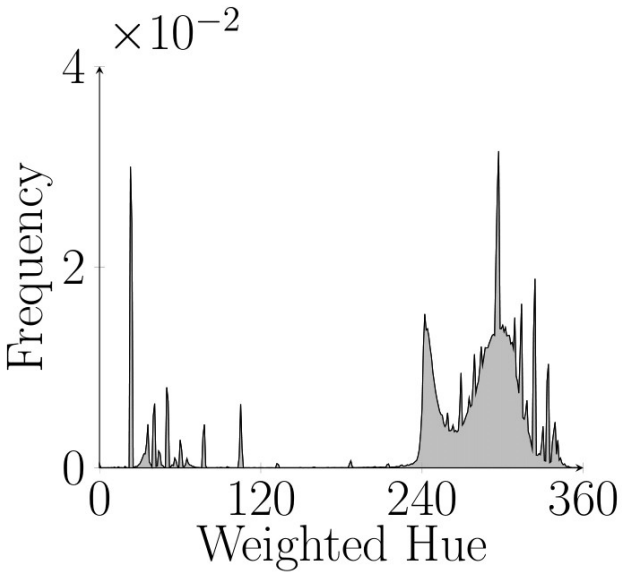
like linear space, local neighborhood information is computed as follows:

$$\xi_k = \frac{1}{1+\alpha}\left(h_k + \frac{\alpha}{|N_k|}\sum_{h_j \in N_k} h_j\right)$$

S. Szilagyi et al. , "MR Brain Image Segmentation Using An Enhanced Fuzzy C-Means Algorithm", ***Proceedings of 25th Annual International Conference of IEEE Engineering in Medicine and Biology Society***, pp. 724-726, 2003.

Rough-Fuzzy Circular Clustering

- Clustering is performed on weighted hue histogram.



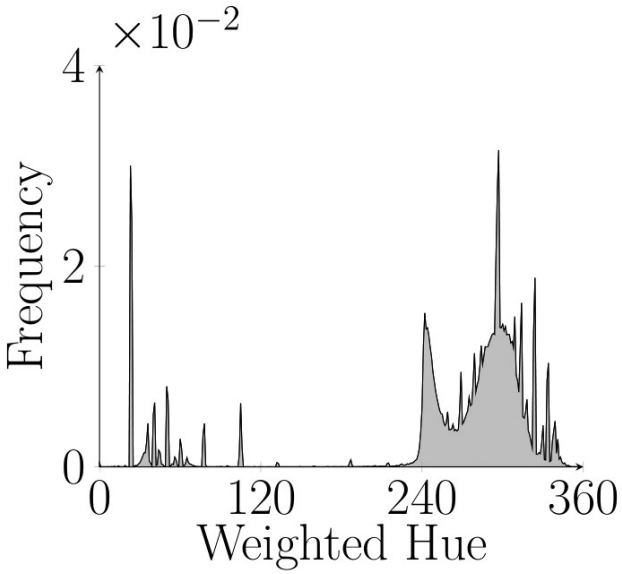
Weighted Hue histogram

Combing both, Weighted Hue histogram *H* is defined as:

$$H(\theta) = \frac{1}{2}\left[H^{SW}(\theta) + H^{\alpha}(\theta)\right]$$

Rough-Fuzzy Circular Clustering

- Clustering is performed on weighted hue histogram.



Weighted Hue histogram

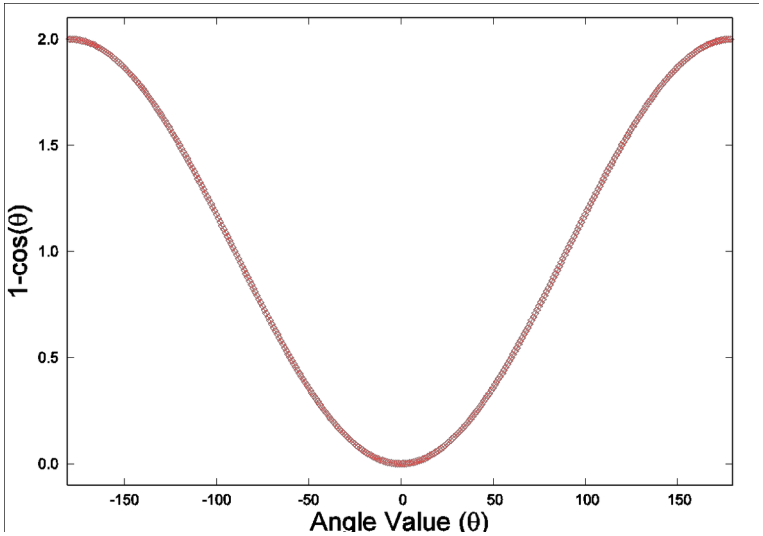
Combing both, Weighted Hue histogram *H* is defined as:

$$H(\theta) = \frac{1}{2}\left[H^{SW}(\theta) + H^{\alpha}(\theta)\right]$$

incorporates both saturation weighted hue information and local neighbourhood information

New Dissimilarity Measure

- Clustering is performed based on a new dissimilarity measure.

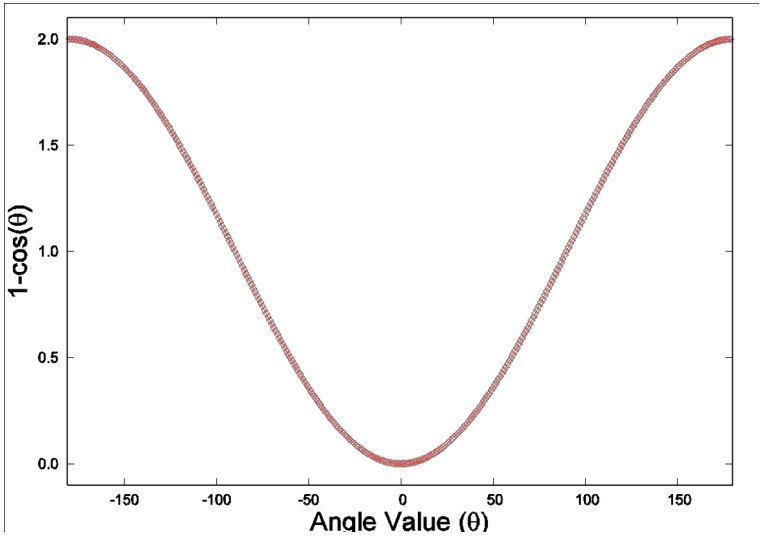


why not cosine distance?

Cosine distance

New Dissimilarity Measure

- Clustering is performed based on a new dissimilarity measure.



why not cosine distance?

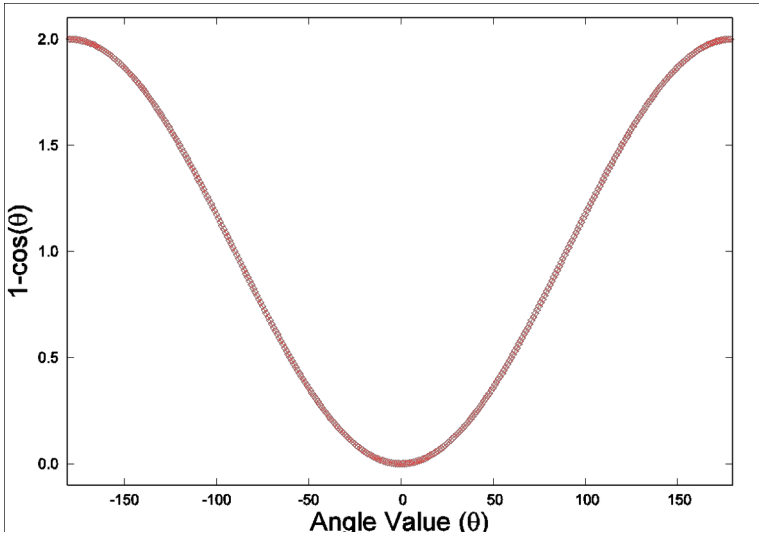
fails to model concentration of hue values near its peak

cannot capture inherent data distribution

Cosine distance

New Dissimilarity Measure

- Clustering is performed based on a new dissimilarity measure.



Cosine distance

why not cosine distance?

fails to model concentration of hue values near its peak

cannot capture inherent data distribution

Solution??

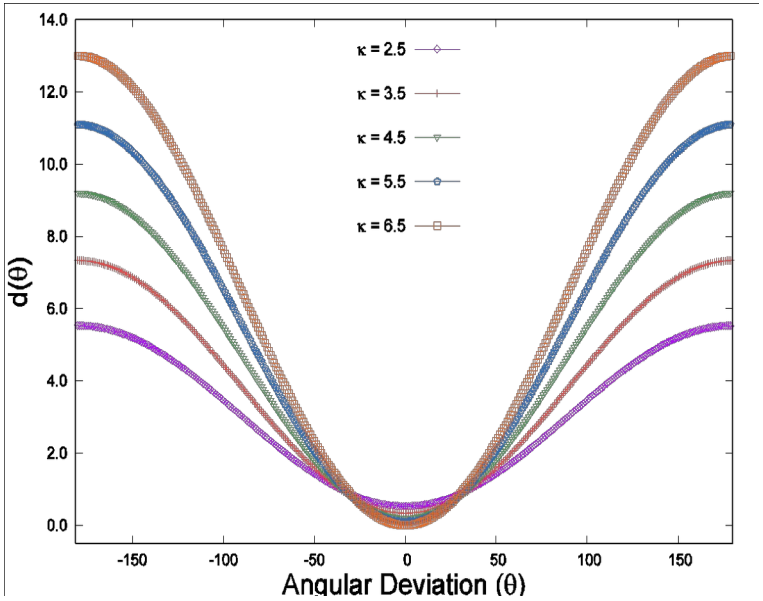
New Dissimilarity Measure

- Clustering is performed based on a new dissimilarity measure.

New dissimilarity measure:

$$d(\theta_i,\theta_j) = \log\left(2\pi I_0(\kappa)\right) - \kappa\cos\left(\theta_i - \theta_j\right)$$

$$I_0(\kappa) = \frac{1}{2\pi}\int_0^{2\pi}\exp\left(\kappa\cos\theta\right)d\theta$$



***I_0(.)* is the modified Bessel function of first kind and order zero.**

$$1)\; d(\theta_i,\theta_j) = d(\theta_j,\theta_i)$$

$$2)\; d(\theta_i,\theta_i) < d(\theta_i,\theta_j)\forall j \neq i$$

$$3)\; d(\theta_i,\theta_k) \leq d(\theta_i,\theta_j) + d(\theta_j,\theta_k)\forall\,\theta_i,\theta_j,\theta_k \in [0,2\pi)$$

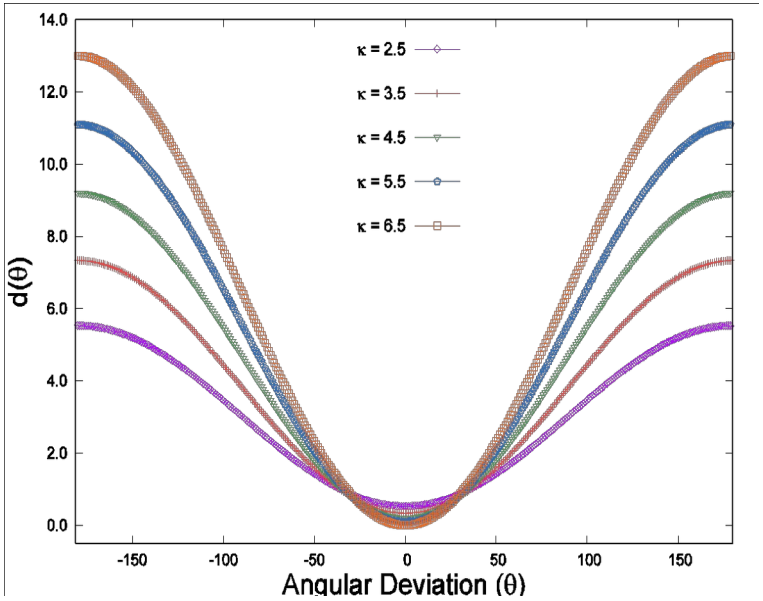
New Dissimilarity Measure

- Clustering is performed based on a new dissimilarity measure.

New dissimilarity measure:

$$d(\theta_i, \theta_j) = \log\left(2\pi I_0(\kappa)\right) - \kappa \cos\left(\theta_i - \theta_j\right)$$

area under the curve is varied using κ without affecting periodicity



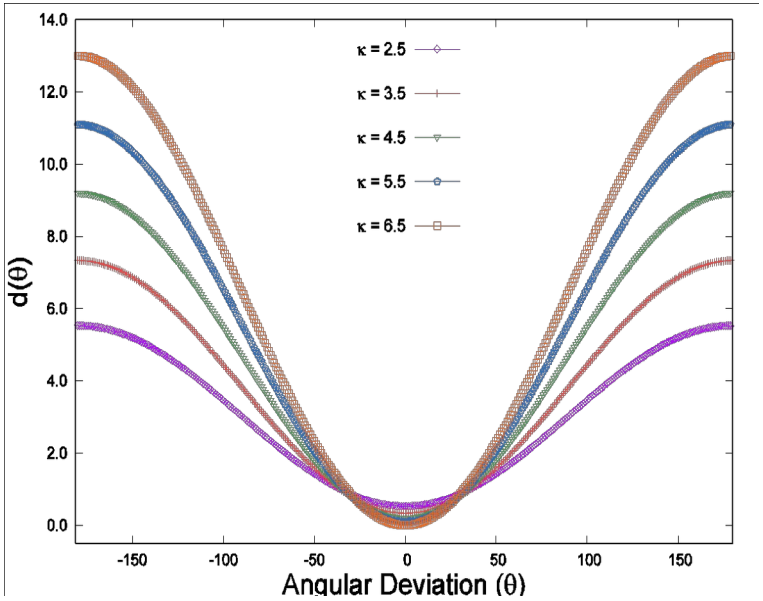
New Dissimilarity Measure

- Clustering is performed on based on a new dissimilarity measure.

New dissimilarity measure:

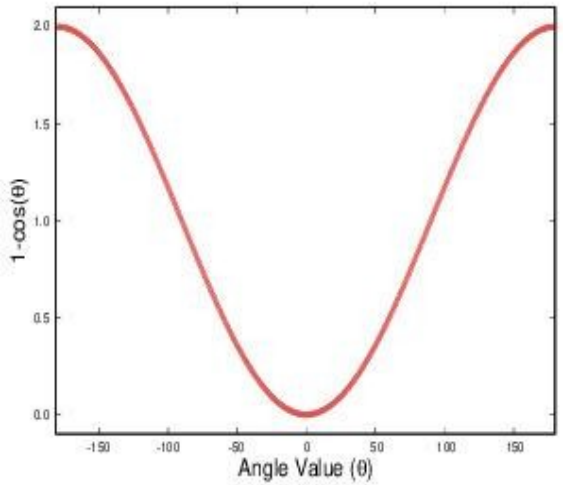
$$d(\theta_i, \theta_j) = \log\left(2\pi I_0(\kappa)\right) - \kappa \cos\left(\theta_i - \theta_j\right)$$

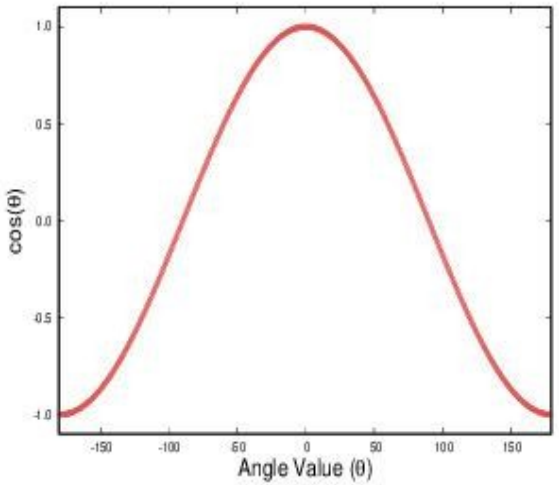
area under the curve is varied using κ without affecting periodicity

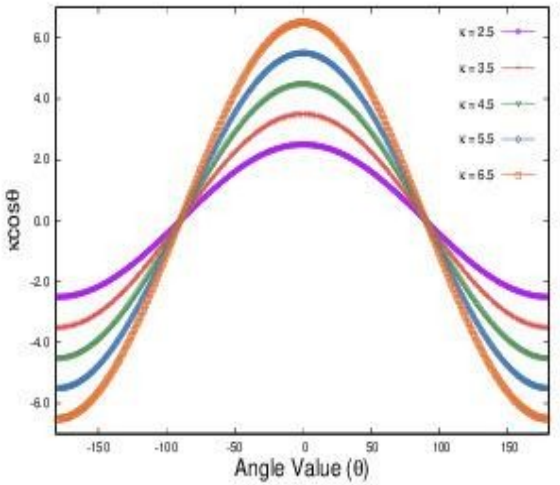


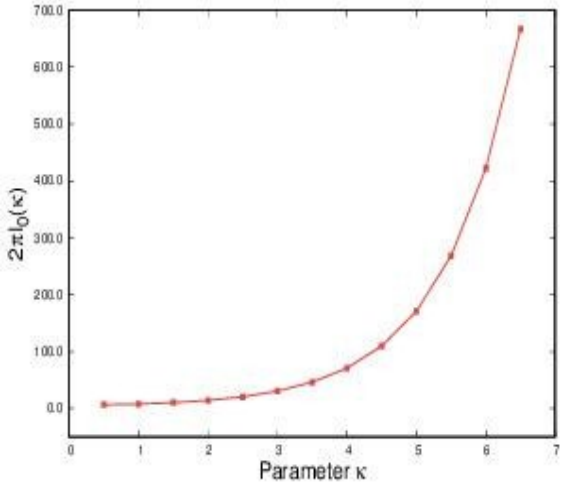
can capture intrinsic data distribution

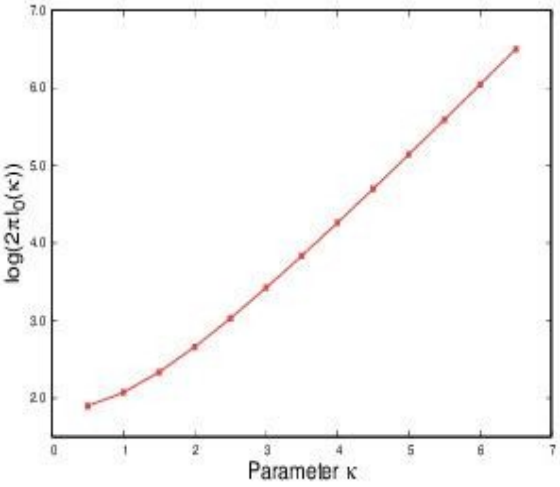
New Dissimilarity Measure

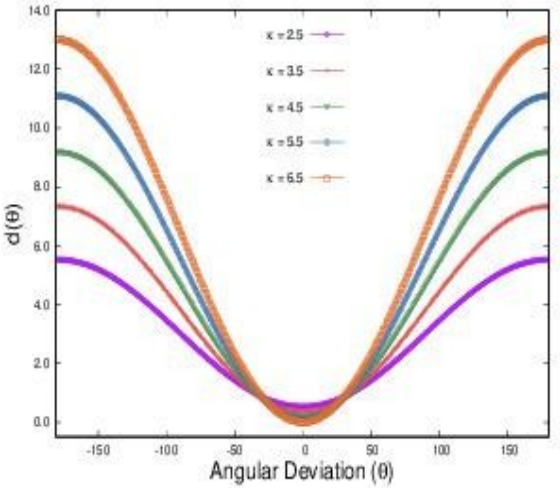












Objective Function

Minimization of objective function with respect to parameter set ψ:

$$J_{RF}(\psi) = \sum_{i=1}^{c} \left[\omega \times J_i^L(\psi) + (1-\omega) \times J_i^B(\psi) \right]$$

Objective Function

Minimization of objective function with respect to parameter set ψ:

$$J_{RF}(\psi) = \sum_{i=1}^{c} \left[\omega \times J_i^L(\psi) + (1-\omega) \times J_i^B(\psi) \right]$$

$$\psi = \{ \nu_{ij}, \mu_i, \kappa_i \}$$

corresponding to lower approximation region for *i*-th class:

$$J_i^L(\psi) = \sum_{\theta_j \in \underline{A}(\beta_i)} \left[\log(2\pi I_0(\kappa_i)) - \kappa_i \cos(\theta_j - \mu_i) \right] H(\theta_j)$$

corresponding to boundary region for *i*-th class:

$$J_i^B(\psi) = \sum_{\theta_j \in B(\beta_i)} \nu_{ij}^m \left[\log(2\pi I_0(\kappa_i)) - \kappa_i \cos(\theta_j - \mu_i) \right] H(\theta_j) + \sum_{\theta_j \in B(\beta_i)} \left[\nu_{ij}^m \log(\nu_{ij}^m) - \nu_{ij}^m \right] H(\theta_j)$$

Estimation of Membership Function

$$\frac{\partial J_{RF}(\psi)}{\partial \nu_{ij}} = 0 \quad \Rightarrow \quad \nu_{ij} = \left[\frac{\exp\{\kappa_i \cos(\theta_j - \mu_i)\}}{2\pi I_0(\kappa_i)} \right]^{\frac{1}{m}}$$

Fuzzy membership function follows von Mises distribution

N. I. Fisher, "Statistical Analysis of Circular Data", *Cambridge University Press*, Cambridge, U.K., 1995.

Estimation of Membership Function

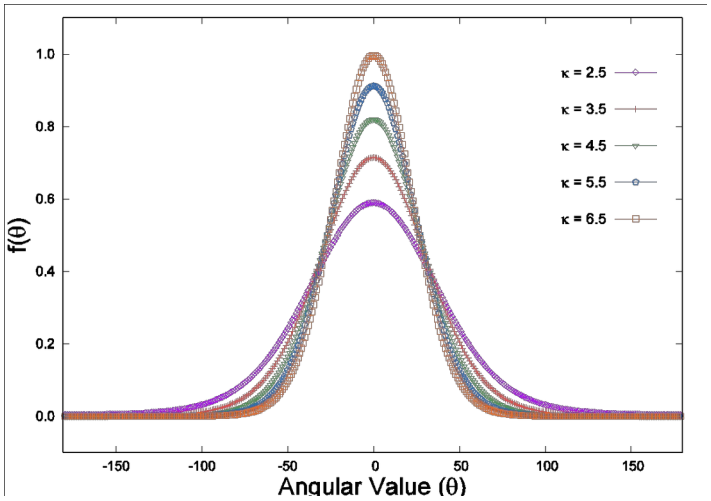
$$\frac{\partial J_{RF}(\psi)}{\partial \nu_{ij}} = 0 \quad \Rightarrow \quad \nu_{ij} = \left[\frac{\exp\{\kappa_i \cos(\theta_j - \mu_i)\}}{2\pi I_0(\kappa_i)} \right]^{\frac{1}{m}}$$

Fuzzy membership function follows von Mises distribution

Von Mises probability distribution:

$$vM(\mu,\kappa) = \frac{1}{2\pi I_0(\kappa)} \exp\{\kappa \cos(\theta - \mu)\}$$

$$\mu \in [0, 2\pi) \qquad \kappa > 0$$



N. I. Fisher, "Statistical Analysis of Circular Data", *Cambridge University Press*, Cambridge, U.K., 1995.

Estimation of Cluster Prototype

$$\frac{\partial J_{RF}(\psi)}{\partial \mu_i} = 0$$

$$\mu_i = \arctan\left[\frac{\omega \times \sum_{\theta_j \in \underline{A}(\beta_i)} \sin(\theta_j) H(\theta_j) + (1-\omega) \times \sum_{\theta_j \in B(\beta_i)} \nu_{ij}^m \sin(\theta_j) H(\theta_j)}{\omega \times \sum_{\theta_j \in \underline{A}(\beta_i)} \cos(\theta_j) H(\theta_j) + (1-\omega) \times \sum_{\theta_j \in B(\beta_i)} \nu_{ij}^m \cos(\theta_j) H(\theta_j)}\right]$$

Estimation of Cluster Prototype

$$\frac{\partial J_{RF}(\psi)}{\partial \mu_i} = 0$$

$$\mu_i = \arctan\left[\frac{\omega \times \sum_{\theta_j \in \underline{A}(\beta_i)} \sin(\theta_j) H(\theta_j) + (1-\omega) \times \sum_{\theta_j \in B(\beta_i)} \nu_{ij}^m \sin(\theta_j) H(\theta_j)}{\omega \times \sum_{\theta_j \in \underline{A}(\beta_i)} \cos(\theta_j) H(\theta_j) + (1-\omega) \times \sum_{\theta_j \in B(\beta_i)} \nu_{ij}^m \cos(\theta_j) H(\theta_j)}\right]$$

depends on the choice of relative importance parameter ω

Estimation of Concentration Parameter

$$\frac{\partial J_{RF}(\psi)}{\partial \kappa_i} = 0$$

$$\kappa_i = \mathrm{T}^{-1}\left[\frac{\omega \times \sum_{\theta_j \in \underline{A}(\beta_i)} \cos(\theta_j - \mu_i) H(\theta_j) + (1-\omega) \times \sum_{\theta_j \in B(\beta_i)} \nu_{ij}^m \cos(\theta_j - \mu_i) H(\theta_j)}{\omega \times \sum_{\theta_j \in \underline{A}(\beta_i)} H(\theta_j) + (1-\omega) \times \sum_{\theta_j \in B(\beta_i)} \nu_{ij}^m H(\theta_j)}\right]$$

$$\mathrm{T}(\kappa_i) = \frac{I_1(\kappa_i)}{I_0(\kappa_i)}$$

Estimation of Concentration Parameter

$$\frac{\partial J_{RF}(\psi)}{\partial \kappa_i} = 0$$

$$\kappa_i = \mathrm{T}^{-1}\left[\frac{\omega \times \sum_{\theta_j \in \underline{A}(\beta_i)} \cos(\theta_j - \mu_i) H(\theta_j) + (1-\omega) \times \sum_{\theta_j \in B(\beta_i)} \nu_{ij}^m \cos(\theta_j - \mu_i) H(\theta_j)}{\omega \times \sum_{\theta_j \in \underline{A}(\beta_i)} H(\theta_j) + (1-\omega) \times \sum_{\theta_j \in B(\beta_i)} \nu_{ij}^m H(\theta_j)}\right]$$

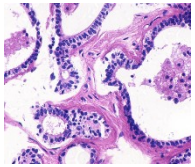
$$\mathrm{T}(\kappa_i) = \frac{I_1(\kappa_i)}{I_0(\kappa_i)}$$

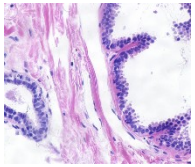
T^{-1}(.) is approximated using numerical methods

N. I. Fisher, "Statistical Analysis of Circular Data", *Cambridge University Press*, Cambridge, U.K., 1995.

Color Normalization Method - RFCC$_{vM}$

Template

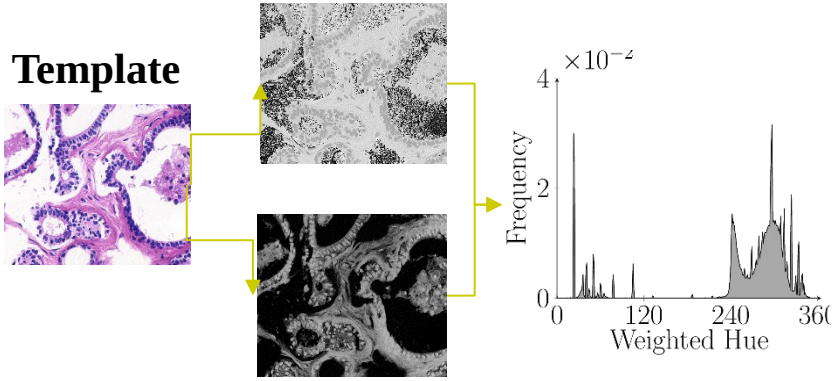


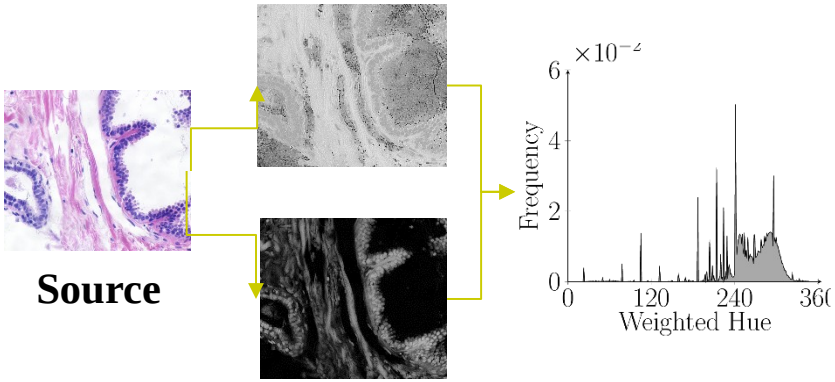


Source

Color Normalization Method - RFCCvM

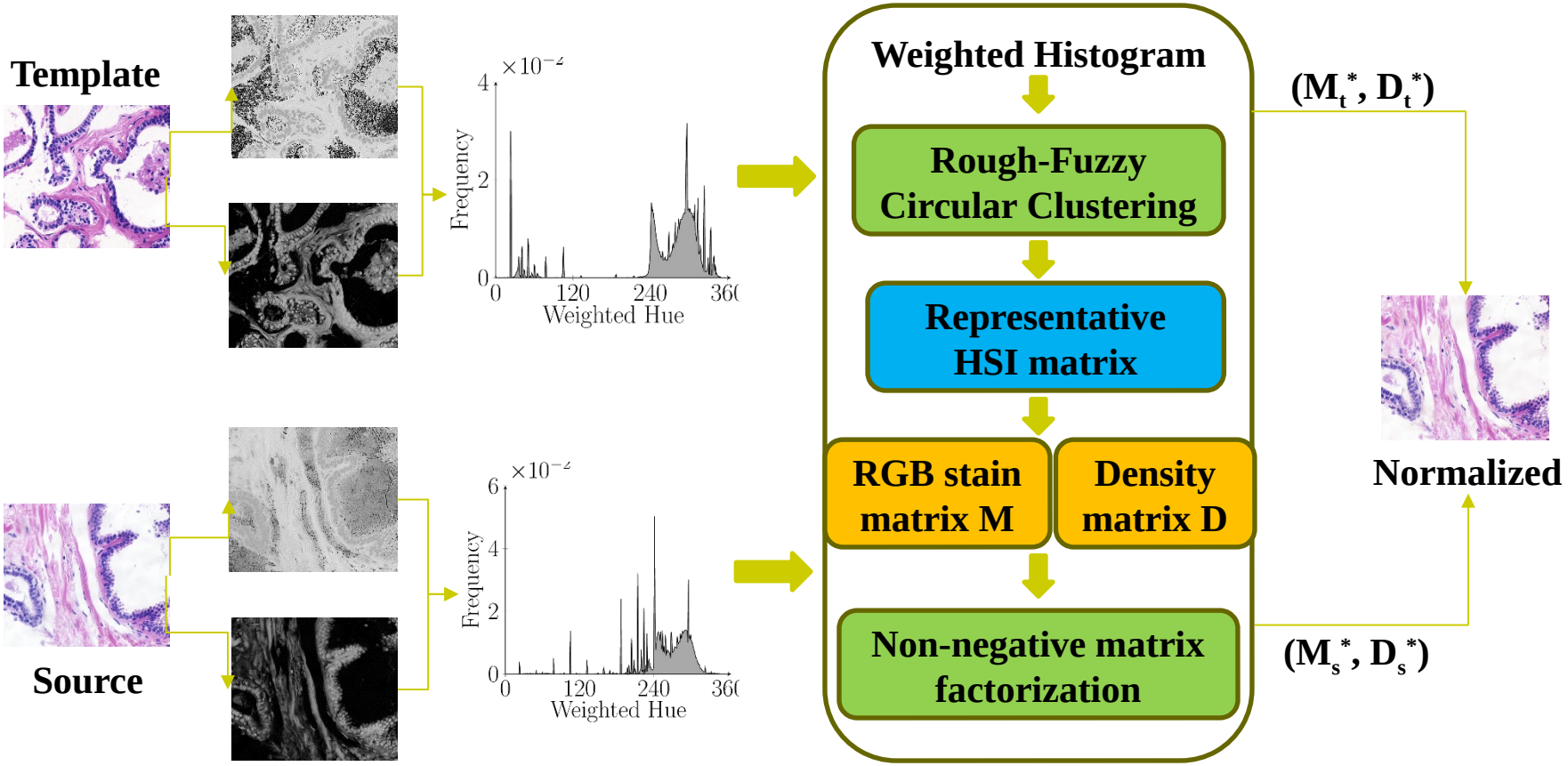
Template





Source

Color Normalization Method - RFCCvM



Description of Data Sets

- **CMU** Data (published by the bimagicLab in Carnegie Mellon University)
- Total number of images = **3**
- Data specifications: H & E stained biopsy images.
- Each image has a resolution of 1280 × 1024.
- Associated stain decomposition ground-truth, **separate H-stained and E-stained images**.
- Images are stored in 48-bit linear RGB format.

M. T. McCann *et al*., "Algorithm and benchmark dataset for stain separation in histology images", *IEEE International Conference on Image Processing*, 2014.

Performance on UCSB Data: Histogram

Different Biopsy Sets	Different Channels	Standard		SW		α-controlled		$RFCC_{vM}$	
		σ_H	σ_E	σ_H	σ_E	σ_H	σ_E	σ_H	σ_E
ytma10_010704	Red	10.41	2.86	3.54	4.10	9.55	**1.91**	**2.84**	2.35
	Green	6.71	1.02	2.02	1.08	7.47	0.99	**1.27**	**0.89**
	Blue	6.71	2.49	**1.25**	2.71	1.50	2.56	1.64	**1.86**
ytma12_010804	Red	7.36	5.54	**2.08**	6.00	19.53	8.63	3.59	**4.14**
	Green	5.97	1.71	**1.36**	2.10	6.16	11.68	2.67	**1.60**
	Blue	2.96	1.43	**0.93**	1.19	22.98	18.45	0.96	**1.06**
ytma23_022103	Red	2.80	5.44	1.73	5.35	12.69	4.95	**1.37**	**4.00**
	Green	2.16	1.52	1.34	1.80	5.42	12.44	**1.07**	**1.51**
	Blue	0.67	1.76	0.73	1.38	21.09	18.08	**0.58**	**0.77**
ytma49_042003	Red	3.20	3.19	3.34	2.94	18.85	4.46	**2.66**	**2.94**
	Green	1.81	**0.49**	2.17	0.57	5.65	11.14	**1.72**	0.61
	Blue	0.91	1.50	0.60	1.26	23.14	18.93	**0.55**	**0.83**
ytma49_042203	Red	9.36	4.16	**2.38**	3.20	7.32	7.01	2.80	**2.77**
	Green	4.98	9.62	**1.85**	0.79	4.81	3.14	2.24	**0.58**
	Blue	16.37	13.66	**0.47**	2.07	0.99	9.39	0.54	**2.06**

H-stain: minimum value in **8/15 cases**

E-stain: minimum value in **13/15 cases**

Performance on UCSB Data: Histogram

Different Biopsy Sets	Different Channels	Standard		SW		α-controlled		$RFCC_{vM}$	
		σ_H	σ_E	σ_H	σ_E	σ_H	σ_E	σ_H	σ_E
ytma49_042403	Red	3.48	3.53	**1.23**	3.74	17.89	4.91	2.22	**2.30**
	Green	2.37	**0.92**	**0.72**	1.06	5.92	11.39	1.16	0.93
	Blue	0.76	1.53	0.62	0.94	22.68	19.31	**0.49**	**0.87**
ytma49_072303	Red	2.11	5.00	1.15	3.71	1.04	1.90	**1.04**	**1.73**
	Green	1.66	1.39	0.95	1.38	0.84	**0.68**	**0.73**	0.76
	Blue	0.34	1.55	0.31	1.04	0.27	0.63	**0.20**	**0.40**
ytma49_111003	Red	**1.99**	**3.53**	2.68	5.62	19.34	6.61	2.74	3.60
	Green	**1.56**	**1.36**	2.44	2.91	2.24	9.68	2.61	1.58
	Blue	1.07	1.82	0.83	2.00	23.70	18.82	**0.77**	**1.20**
ytma49_111303	Red	2.22	4.96	2.01	6.55	19.98	6.91	**1.38**	**3.35**
	Green	2.15	1.95	1.91	2.64	4.96	12.02	**1.31**	**1.69**
	Blue	0.65	1.53	0.79	2.02	25.99	19.91	**0.59**	**1.17**
ytma55_030603	Red	7.08	6.75	**2.08**	4.58	2.36	8.33	2.99	**3.60**
	Green	6.01	3.19	**1.75**	1.78	2.04	1.62	2.78	**1.46**
	Blue	1.15	9.99	1.01	2.06	0.86	4.09	**0.85**	**1.63**

H-stain: minimum value in **17/30 cases**

E-stain: minimum value in **24/30 cases**

Performance on UCSB Data: Dissimilarity

Different Biopsy Sets	Different Channels	Cosine Distance		Proposed Dissimilarity	
		σ_H	σ_E	σ_H	σ_E
ytma10_010704	Red	3.19	3.03	**2.84**	**2.35**
	Green	1.69	1.07	**1.27**	**0.89**
	Blue	**1.35**	2.30	1.64	**1.86**
ytma12_010804	Red	**3.38**	5.69	3.59	**4.14**
	Green	2.71	2.06	**2.67**	**1.60**
	Blue	**0.96**	1.10	**0.96**	**1.06**
ytma23_022103	Red	1.57	5.36	**1.37**	**4.00**
	Green	1.30	1.79	**1.07**	**1.51**
	Blue	0.67	1.36	**0.58**	**0.77**
ytma49_042003	Red	3.31	**2.53**	**2.66**	2.94
	Green	2.05	**0.55**	**1.72**	0.61
	Blue	0.98	1.07	**0.55**	**0.83**
ytma49_042203	Red	**2.64**	3.28	2.80	**2.77**
	Green	**2.07**	0.91	2.24	**0.58**
	Blue	**0.31**	**1.95**	0.54	2.06

H-stain: minimum value in **10/15 cases**

E-stain: minimum value in **12/15 cases**

Performance on UCSB Data: Dissimilarity

Different Biopsy Sets	Different Channels	Cosine Distance		Proposed Dissimilarity	
		σ_H	σ_E	σ_H	σ_E
ytma49_042403	Red	**1.78**	3.79	2.22	**2.30**
	Green	**1.07**	1.07	1.16	**0.93**
	Blue	0.66	0.88	**0.49**	**0.87**
ytma49_072303	Red	1.86	3.40	**1.04**	**1.73**
	Green	1.53	1.20	**0.73**	**0.76**
	Blue	0.30	0.83	**0.20**	**0.40**
ytma49_111003	Red	**2.34**	4.65	2.74	**3.60**
	Green	**2.07**	2.19	2.61	**1.58**
	Blue	0.99	1.85	**0.77**	**1.20**
ytma49_111303	Red	1.83	5.85	**1.38**	**3.35**
	Green	1.66	2.47	**1.31**	**1.69**
	Blue	0.92	1.72	**0.59**	**1.17**
ytma55_030603	Red	**2.65**	4.03	2.99	**3.60**
	Green	**2.29**	1.65	2.78	**1.46**
	Blue	1.16	1.76	**0.85**	**1.63**

H-stain: minimum value in **19/30 cases**

E-stain: minimum value in **27/30 cases**

Performance on UCSB Data: Clustering

Different Biopsy Sets	Different Channels	Hard		Fuzzy		Rough-Fuzzy	
		σ_H	σ_E	σ_H	σ_E	σ_H	σ_E
ytma10_010704	Red	13.44	4.68	4.05	2.72	**2.84**	**2.35**
	Green	5.54	8.69	2.00	1.03	**1.27**	**0.89**
	Blue	17.29	15.85	**1.47**	1.87	1.64	**1.86**
ytma12_010804	Red	13.24	5.93	**3.45**	4.26	3.59	**4.14**
	Green	5.67	10.92	2.75	1.90	**2.67**	**1.60**
	Blue	21.17	18.49	**0.87**	**0.97**	0.96	1.06
ytma23_022103	Red	1.89	5.21	1.54	4.38	**1.37**	**4.00**
	Green	1.39	1.86	1.09	1.76	**1.07**	**1.51**
	Blue	0.65	1.23	0.65	0.86	**0.58**	**0.77**
ytma49_042003	Red	15.30	5.79	3.13	**2.58**	**2.66**	2.94
	Green	5.02	8.47	1.93	**0.59**	**1.72**	0.61
	Blue	18.37	15.92	0.70	0.96	**0.55**	**0.83**
ytma49_042203	Red	**2.68**	3.24	2.78	3.17	2.80	**2.77**
	Green	**1.85**	0.77	2.08	0.73	2.24	**0.58**
	Blue	0.63	1.99	0.43	**1.84**	**0.54**	2.06

H-stain: minimum value in **10/15 cases**

E-stain: minimum value in **11/15 cases**

Performance on UCSB Data: Clustering

Different Biopsy Sets	Different Channels	Hard		Fuzzy		Rough-Fuzzy	
		σ_H	σ_E	σ_H	σ_E	σ_H	σ_E
ytma49_042403	Red	2.89	3.38	**2.02**	2.67	2.22	**2.30**
	Green	1.72	1.07	**1.14**	0.96	1.16	**0.93**
	Blue	0.77	1.00	0.70	**0.83**	**0.49**	0.87
ytma49_072303	Red	1.70	3.19	1.09	1.97	**1.04**	**1.73**
	Green	1.29	1.18	0.85	0.84	**0.73**	**0.76**
	Blue	0.36	0.72	0.28	0.63	**0.20**	**0.40**
ytma49_111003	Red	3.05	3.87	2.97	4.58	**2.74**	**3.60**
	Green	2.61	1.85	**2.60**	2.23	2.61	**1.58**
	Blue	1.16	1.59	1.09	1.70	**0.77**	**1.20**
ytma49_111303	Red	1.73	5.44	1.43	3.71	**1.38**	**3.35**
	Green	1.55	2.41	**1.30**	2.03	1.31	**1.69**
	Blue	0.84	1.68	0.88	**1.17**	**0.59**	**1.17**
ytma55_030603	Red	2.69	4.32	**2.66**	4.61	2.99	**3.60**
	Green	**2.26**	1.89	2.31	1.86	2.78	**1.46**
	Blue	1.04	2.06	**0.77**	1.96	0.85	**1.63**

H-stain: minimum value in **18/30 cases**

E-stain: minimum value in **25/30 cases**

Performance on UCSB Data: Existing

Biopsy Sets	Ch.	PF		HTN		EPF		SPCN		EM		$RFCC_c$		$RFCC_{vM}$	
		σ_H	σ_E	σ_H	σ_E	σ_H	σ_E	σ_H	σ_E	σ_H	σ_E	σ_H	σ_E	σ_H	σ_E
ytma10_010704	R	3.04	2.72	2.67	3.25	2.49	**2.10**	2.42	3.93	2.45	4.10	**2.39**	3.65	2.84	2.35
	G	2.23	2.01	1.68	0.97	2.17	1.03	1.66	0.73	1.61	**0.69**	1.39	1.03	**1.27**	0.89
	B	2.67	5.79	1.14	2.43	**0.78**	2.90	1.01	2.55	0.92	2.51	1.59	2.55	1.64	**1.86**
ytma12_010804	R	1.99	**3.79**	**1.37**	5.79	2.02	8.31	2.20	6.26	2.08	7.73	1.89	5.73	3.59	4.14
	G	2.16	2.82	**1.07**	1.82	2.20	**1.13**	1.80	2.14	1.66	2.54	1.17	2.03	2.67	1.60
	B	1.72	6.81	**0.55**	1.30	0.72	1.58	0.79	1.36	0.83	1.56	0.94	1.19	0.96	**1.06**
ytma23_022103	R	1.77	**3.43**	2.39	5.36	2.33	6.73	**1.07**	5.75	1.18	7.27	1.67	5.31	1.37	4.00
	G	1.95	**0.46**	2.25	1.59	2.62	0.64	1.10	1.81	1.16	2.21	1.24	1.80	**1.07**	1.51
	B	1.31	3.34	0.70	1.57	0.92	1.50	0.86	1.71	0.89	1.86	0.64	1.38	**0.58**	**0.77**
ytma49_042003	R	3.11	2.11	3.17	1.86	3.67	**0.55**	3.14	2.98	4.56	4.53	3.28	2.36	**2.66**	2.94
	G	2.98	2.02	2.35	**0.45**	3.50	0.45	2.44	0.74	3.40	0.96	1.99	0.54	**1.72**	0.61
	B	1.09	3.67	0.55	0.98	1.42	1.39	0.79	1.18	1.21	1.42	0.69	0.94	**0.55**	**0.83**
ytma49_042203	R	2.29	**2.18**	4.04	3.13	2.13	5.97	1.99	3.36	**1.93**	3.88	2.24	3.07	2.80	2.77
	G	2.95	1.40	3.81	0.92	2.43	1.21	2.02	0.84	2.06	1.18	**1.49**	0.87	2.24	**0.58**
	B	1.88	3.72	1.15	2.12	0.97	2.99	0.60	2.03	0.69	2.02	0.64	**1.89**	**0.54**	2.06

H-stain: minimum value in **7/15 cases**

E-stain: minimum value in **5/15 cases**

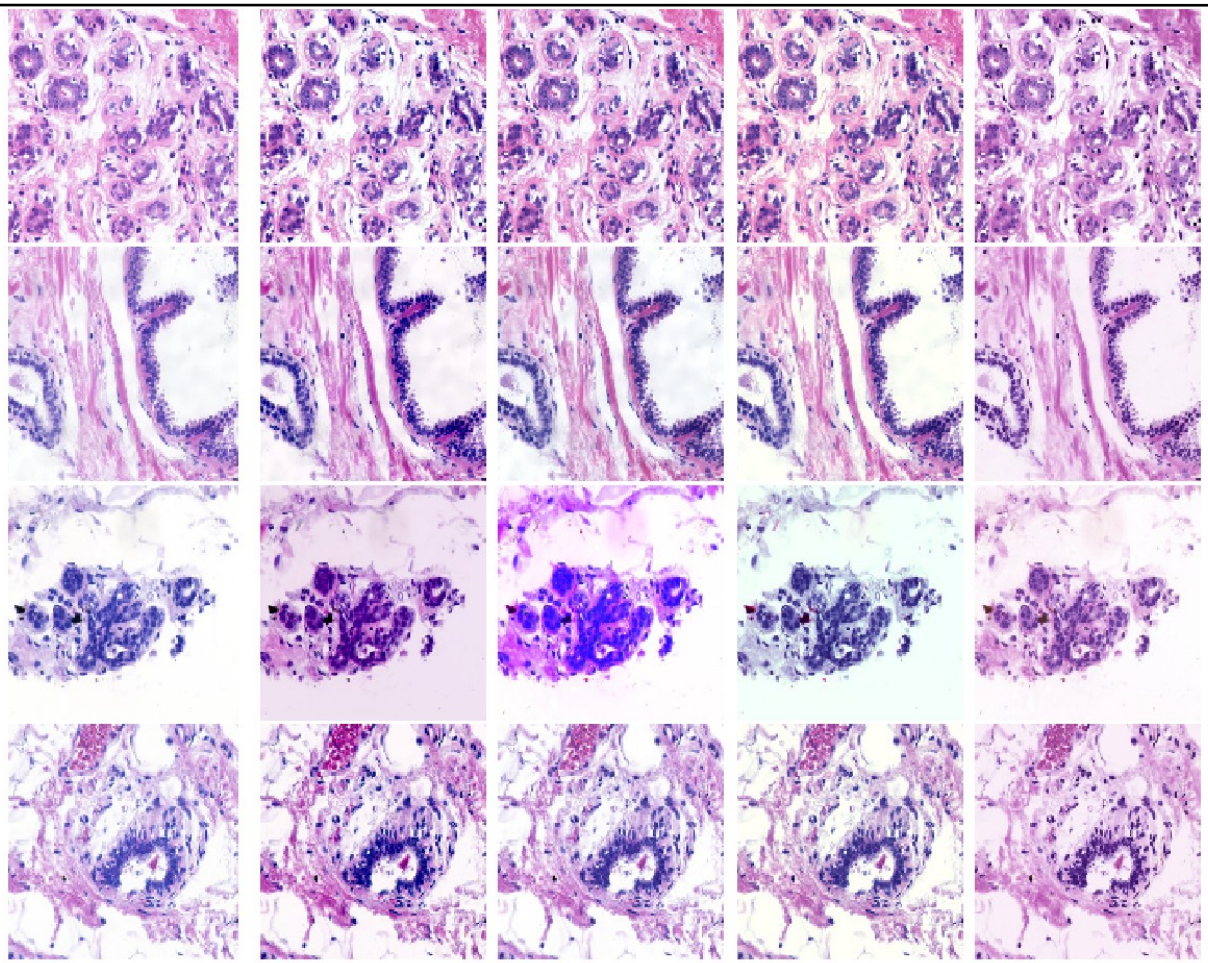
Performance on UCSB Data: Existing

Biopsy Sets	Ch.	PF		HTN		EPF		SPCN		EM		$RFCC_c$		$RFCC_{vM}$	
		σ_H	σ_E	σ_H	σ_E	σ_H	σ_E	σ_H	σ_E	σ_H	σ_E	σ_H	σ_E	σ_H	σ_E
ytma49_042403	R	3.08	3.13	3.42	3.67	3.03	**0.49**	2.99	4.89	3.39	6.66	**1.72**	3.80	2.22	2.30
	G	3.16	3.18	2.55	0.96	3.09	**0.35**	2.38	1.38	2.72	1.67	**0.94**	1.10	1.16	0.93
	B	1.04	5.38	0.63	**0.47**	0.79	1.09	0.93	0.64	0.92	0.80	0.76	0.72	**0.49**	0.87
ytma49_072303	R	2.09	2.63	2.49	2.82	2.73	2.60	1.99	**1.57**	2.52	1.99	1.41	2.86	**1.04**	1.73
	G	2.48	1.22	2.55	0.95	3.39	**0.14**	2.15	0.66	2.67	0.95	1.14	1.09	**0.73**	0.76
	B	0.57	1.43	0.38	0.80	0.64	0.79	0.46	0.79	0.36	0.98	0.30	0.67	**0.20**	**0.40**
ytma49_111003	R	1.90	13.17	1.64	6.94	5.66	14.97	4.00	9.65	**1.62**	8.12	2.79	5.34	2.74	**3.60**
	G	2.60	11.29	1.61	3.49	7.44	14.24	1.69	5.79	**1.45**	4.63	2.39	2.69	2.61	**1.58**
	B	3.62	10.73	1.23	2.79	4.37	12.09	9.77	4.17	1.29	2.62	1.08	1.93	**0.77**	**1.20**
ytma49_111303	R	2.15	6.12	**1.20**	6.71	3.39	10.67	1.44	6.85	1.63	8.87	2.29	6.09	1.38	**3.35**
	G	2.52	1.75	**1.30**	2.46	4.45	1.78	1.56	2.85	1.75	3.27	2.06	2.54	1.31	**1.69**
	B	1.50	4.30	**0.24**	2.34	1.37	2.49	0.34	2.31	0.55	2.70	0.80	1.80	0.59	**1.17**
ytma55_030603	R	2.18	7.85	1.88	16.56	2.41	5.76	1.35	5.22	**1.25**	7.60	1.91	3.84	2.99	**3.6**
	G	3.39	3.90	1.81	2.09	3.34	**1.34**	1.48	2.36	**1.37**	3.19	1.52	1.62	2.78	1.46
	B	2.73	8.20	0.67	8.32	**0.53**	**1.57**	0.70	1.62	0.67	2.28	0.77	1.67	0.85	1.63

H-stain: minimum value in **12/30 cases**

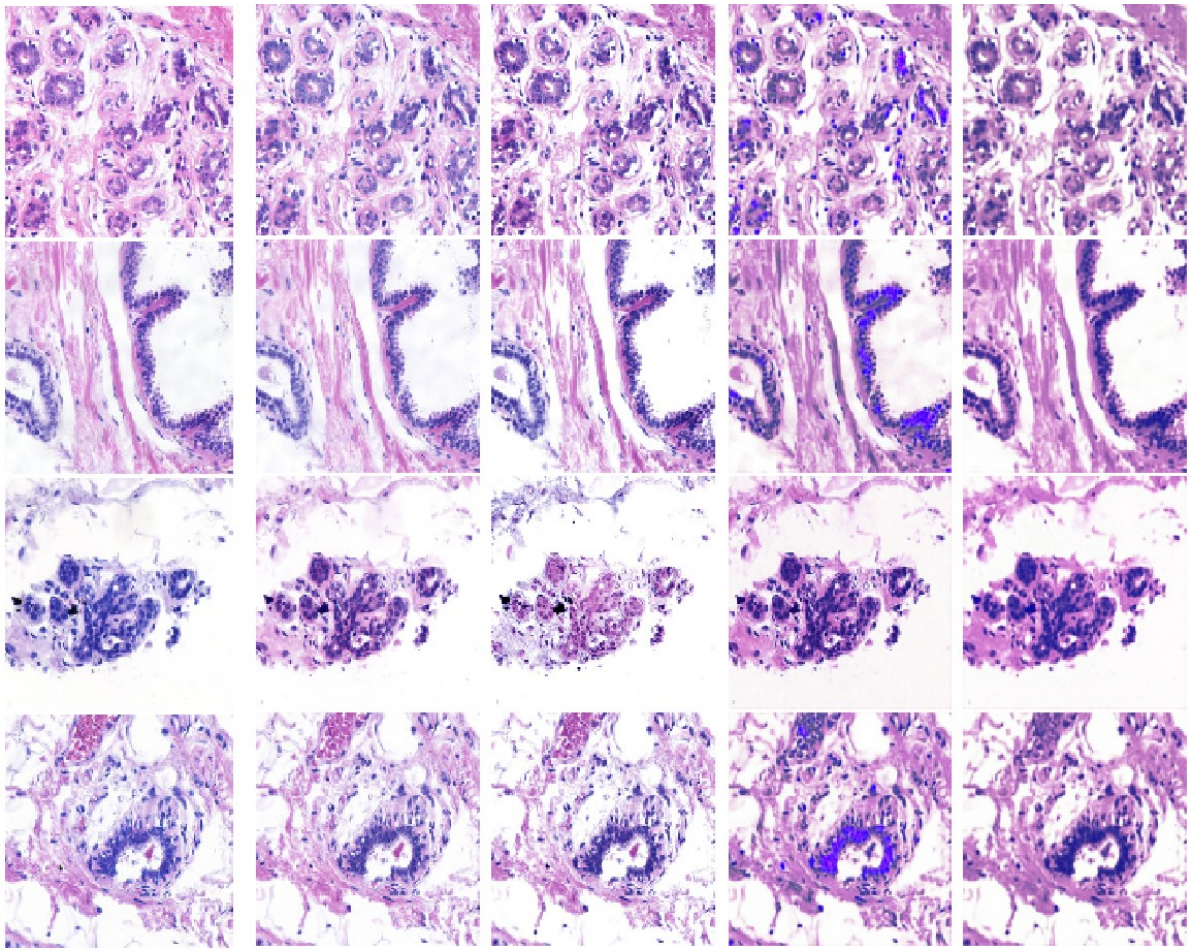
E-stain: minimum value in **13/30 cases**

Qualitative Analysis on UCSB Data



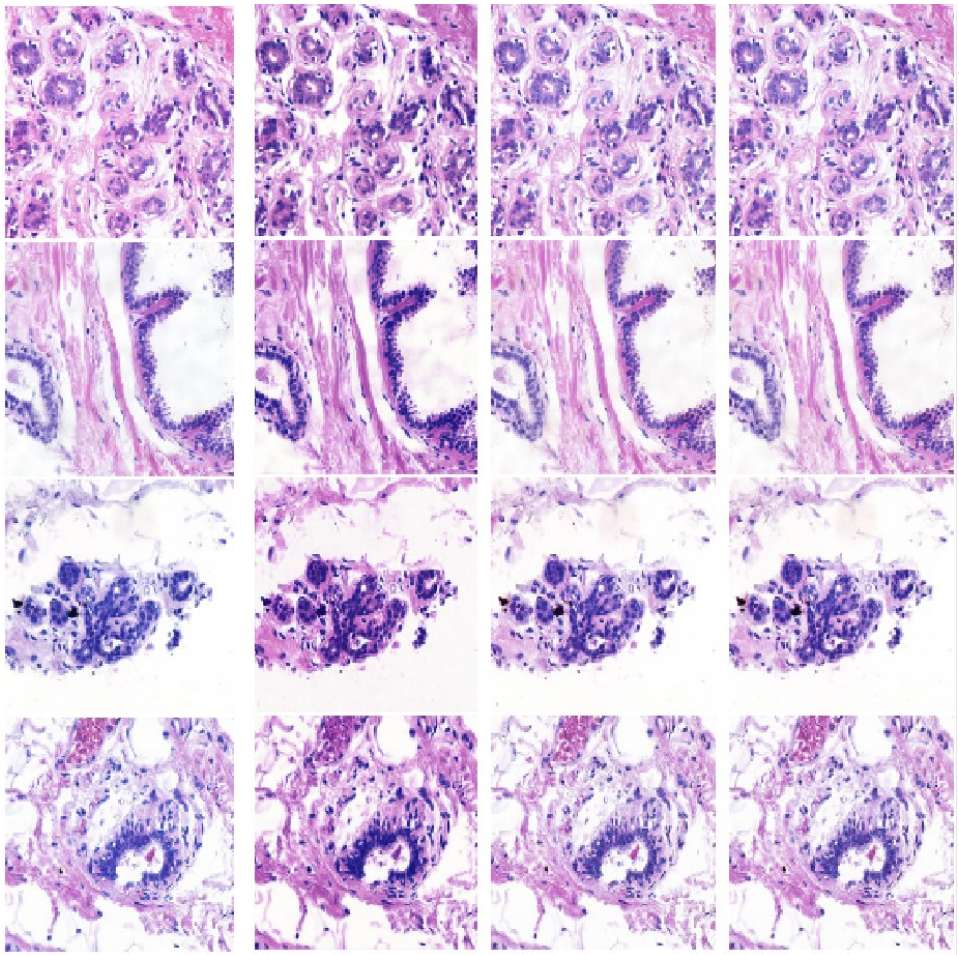
Qualitative performance analysis of different color normalization methods: (a) original, (b) ColTrans, (c) PF, (d) EPF, (e) SCD

Qualitative Analysis on UCSB Data



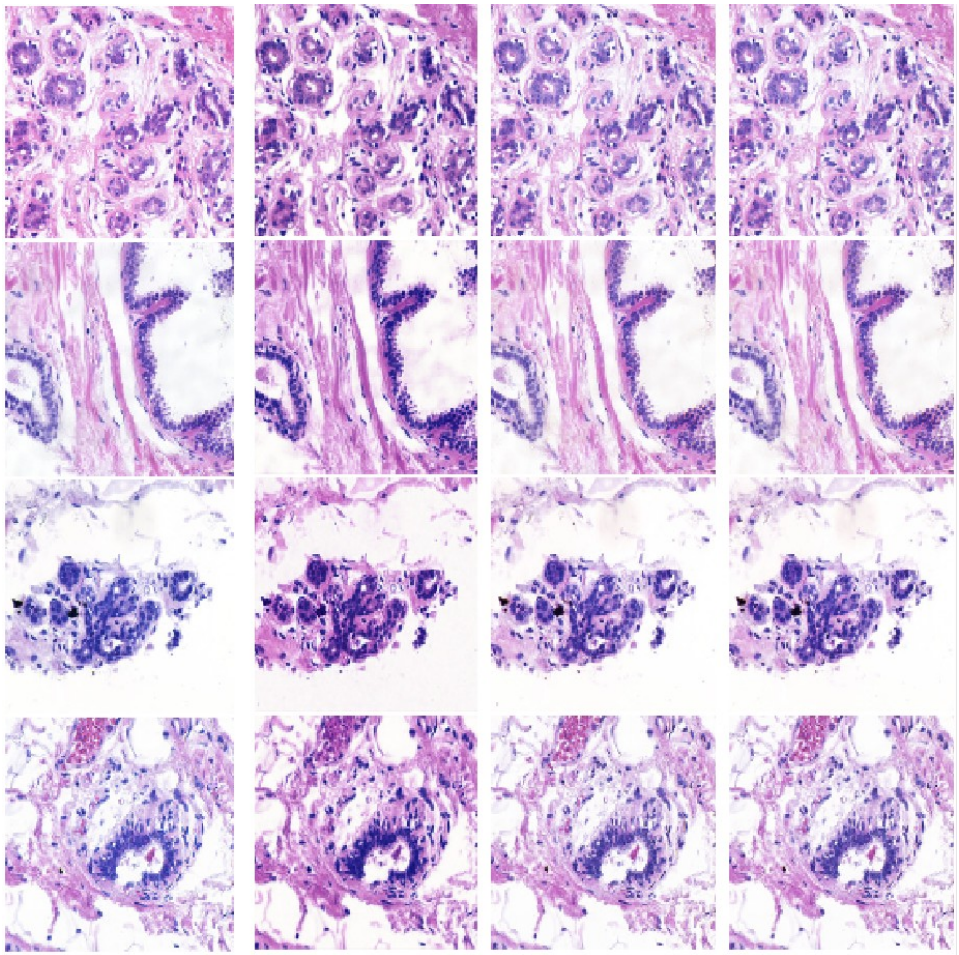
Qualitative performance analysis of different color normalization methods: (a) original, (b) HTN, (c) SPCN, (d) SN-GAN, (e) StainGAN

Qualitative Analysis on UCSB Data



Qualitative performance analysis of different color normalization methods: (a) original, (b) AST, (c) $RFCC_{cosine}$, (d) $RFCC_{vM}$

Qualitative Analysis on UCSB Data

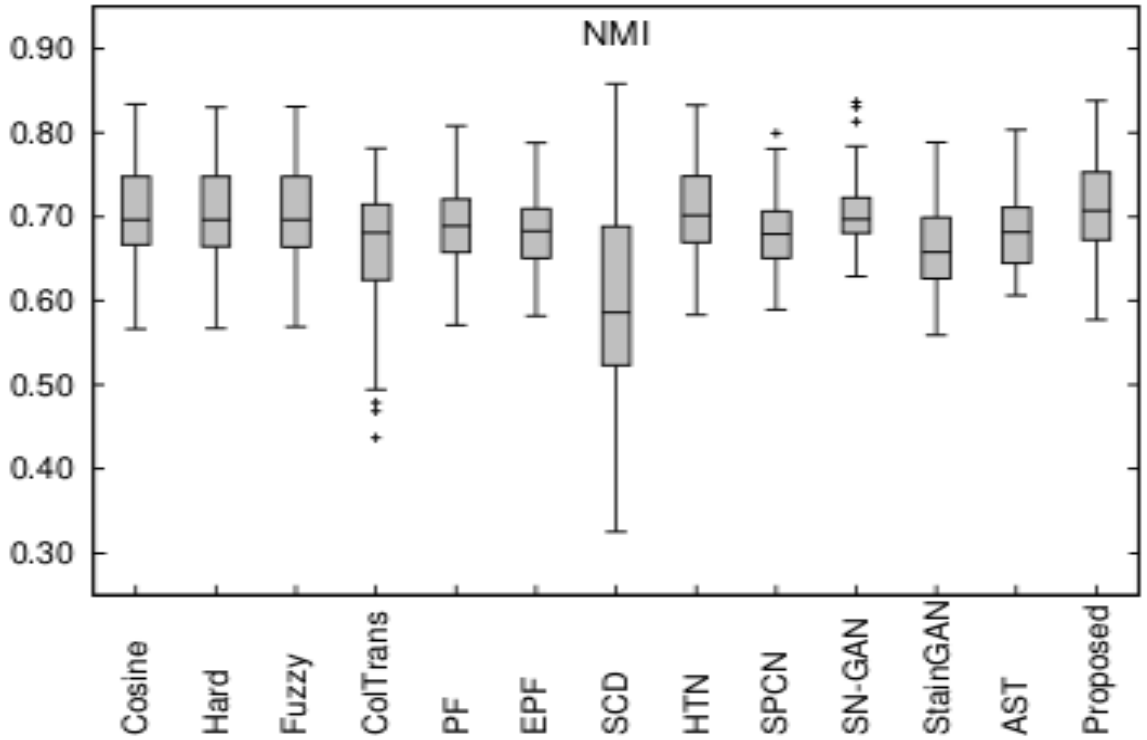


Qualitative performance analysis of different color normalization methods: (a) original, (b) AST, (c) $RFCC_{cosine}$, (d) $RFCC_{vM}$

The $RFCC_{vM}$ method outperforms other existing color normalization methods as per color consistency after normalization is concerned.

Performance on UCSB Data: vs Existing

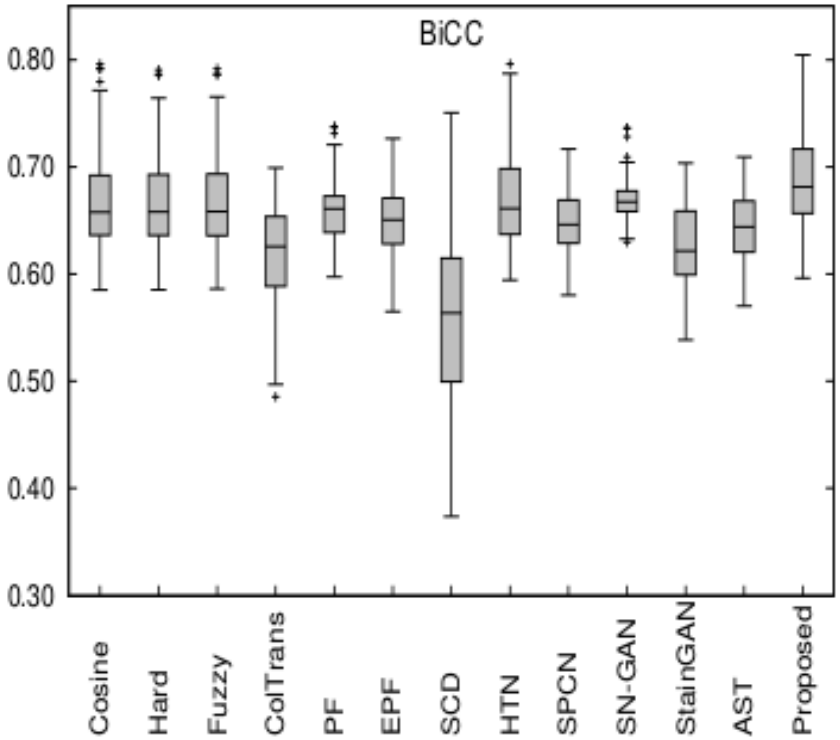
Normalized Median Intensity (NMI)



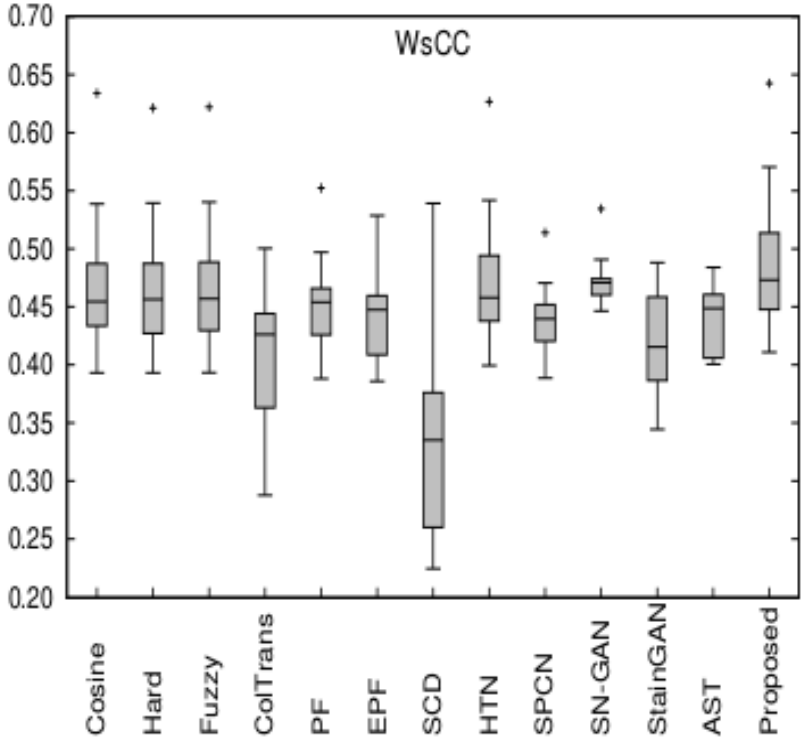
L. G. Nyuel *et al.*, "New variants of a method of MRI scale standardization", *IEEE Transactions on Medical Imaging*, 19(2), pp. 143-150, 2000.

Performance on UCSB Data: vs Existing

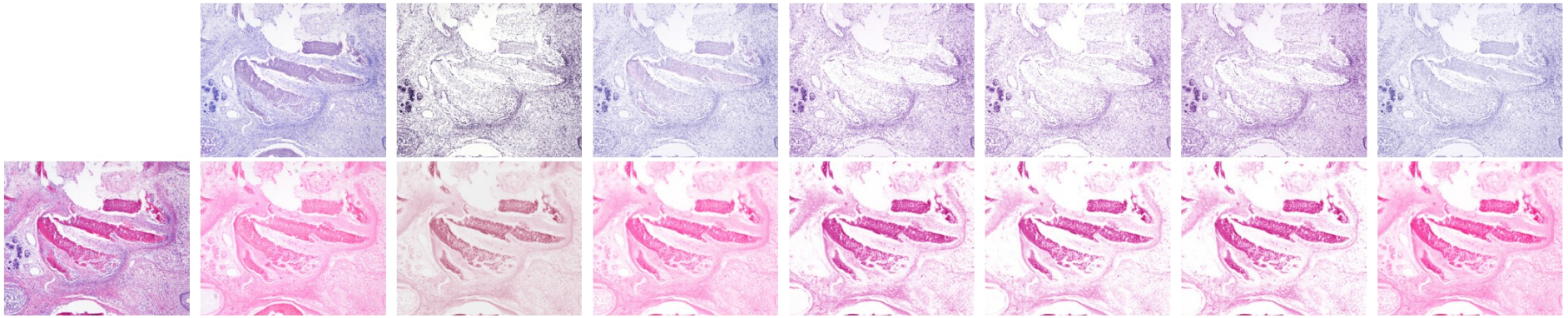
BiCC Index



WsCC Index



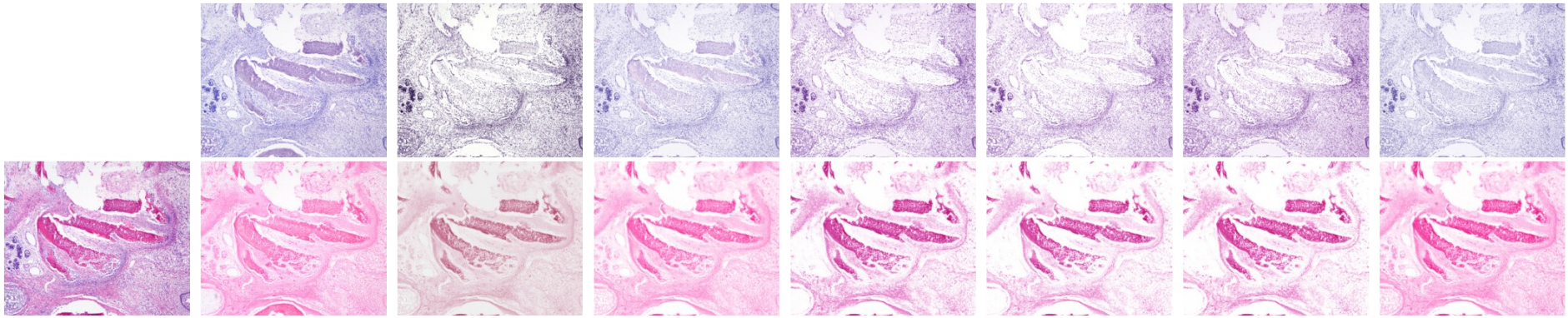
Performance on CMU Data



(a) CMU image (b) GT (c) PF (d) EPF (e) HTN (f) SPCN (g) EM (h) Proposed

Qualitative comparison of stain separation by different methods w.r.t. H-stain and E-stain

Performance on CMU Data

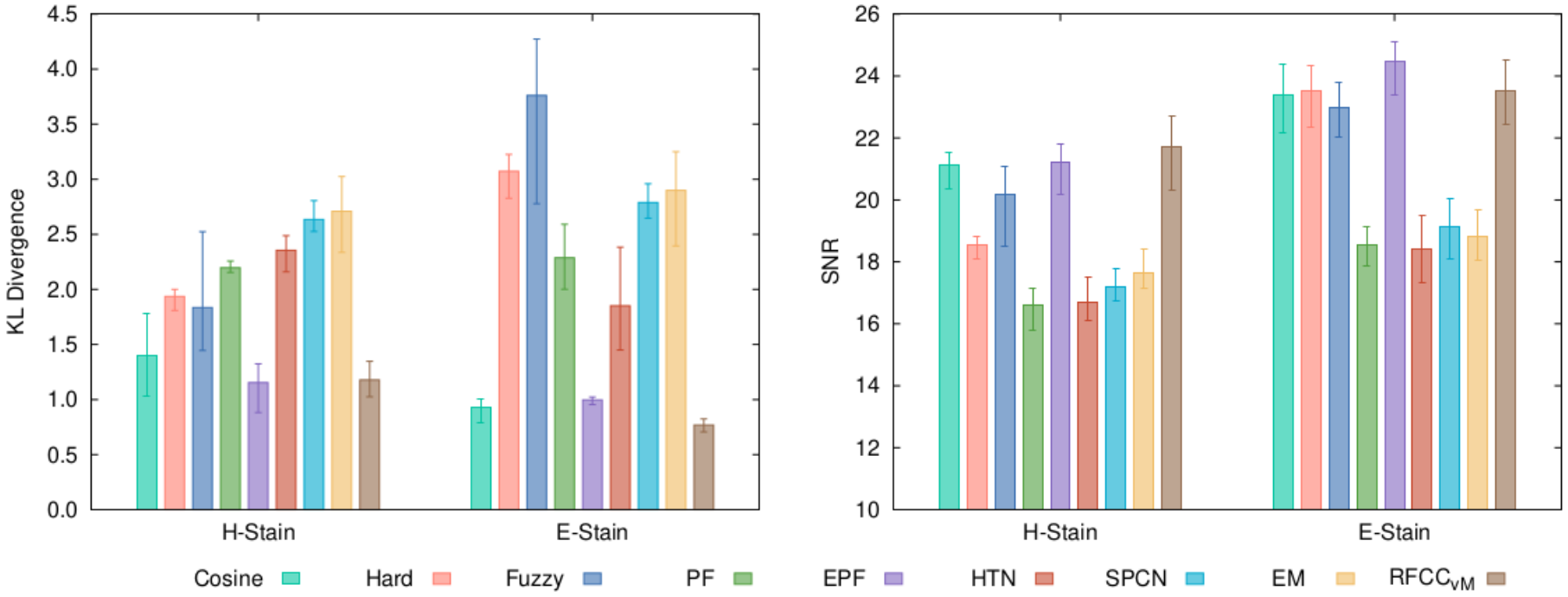


(a) CMU image (b) GT (c) PF (d) EPF (e) HTN (f) SPCN (g) EM (h) Proposed

Qualitative comparison of stain separation by different methods w.r.t. H-stain and E-stain

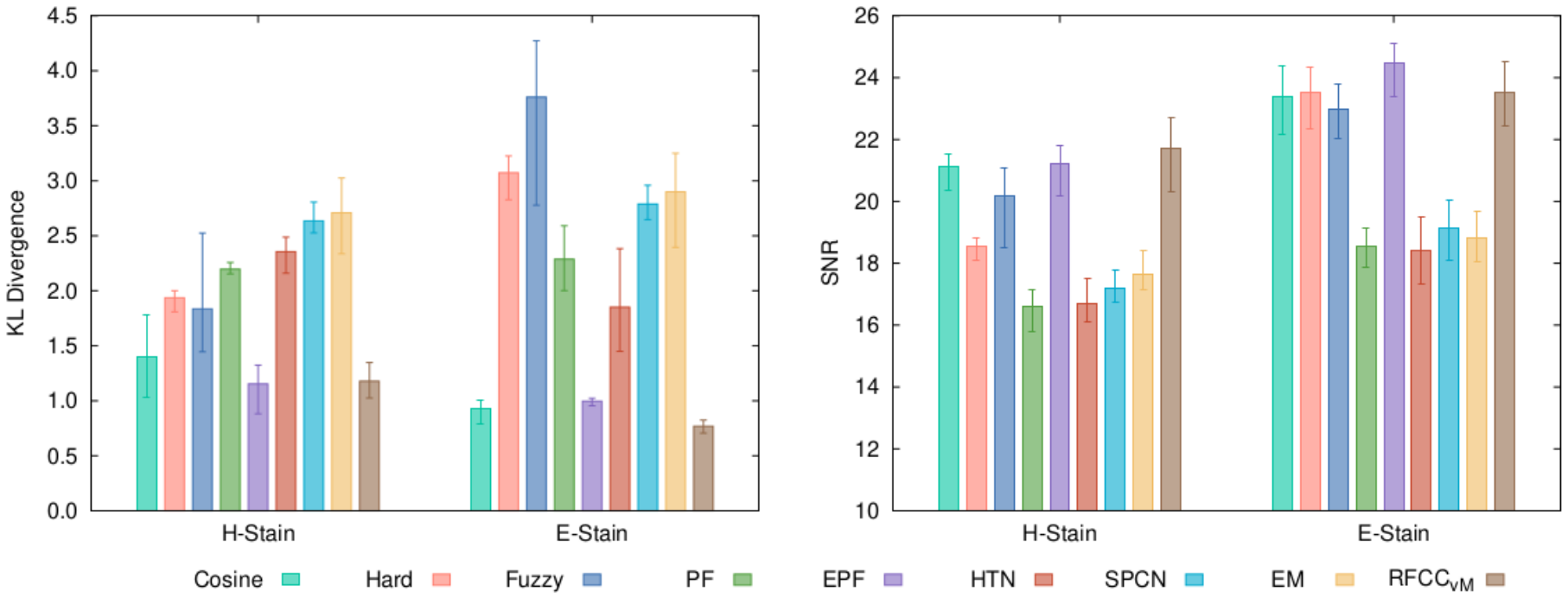
Only $RFCC_{vM}$ (proposed) method and EPF can extract intrinsic structures of biological components, highlighted by H-stain and E-stain

Performance on CMU Data



Quantitative comparison of stain separation by different methods w.r.t. H-stain and E-stain

Performance on CMU Data



Quantitative comparison of stain separation by different methods w.r.t. H-stain and E-stain

But, unlike EPF, the RFCC$_{vM}$ method is applicable to cases with more than 2 stains

EPF applies deconvolution: non-invertible stain matrix problem

Key Takeaways - $RFCC_{vM}$

- Unsupervised method: a rough-fuzzy clustering is performed on weighted hue histogram. Both $RFCC_{cosine}$ and $RFCC_{vM}$ are unsupervised methods.

- A circular dissimilarity measure is proposed to deal with the circular nature of hue values.

Key Takeaways - $RFCC_{vM}$

- Unsupervised method: a rough-fuzzy clustering is performed on weighted hue histogram. Both $RFCC_{cosine}$ and $RFCC_{vM}$ are unsupervised methods.
- A circular dissimilarity measure is proposed to deal with the circular nature of hue values.
- Correlation between color appearance information and stain density information is not explored.

Key Takeaways - $RFCC_{vM}$

- Unsupervised method: a rough-fuzzy clustering is performed on weighted hue histogram. Both $RFCC_{cosine}$ and $RFCC_{vM}$ are unsupervised methods.
- A circular dissimilarity measure is proposed to deal with the circular nature of hue values.
- Correlation between color appearance information and stain density information is not explored.
- Next chapter tries to utilize supervised deep generative model to increase the accuracy of stain estimation as well as color normalization.
- Tries to disentangle color appearance and stain density information so that loss or modification in one information does not affect other.

Chapter 5

Truncated Normal Mixture Prior Based Deep Latent Model for Color Normalization of Histological Images

S. Mahapatra *and P. Maji, "Truncated Normal Mixture Prior Based Deep Latent Model for Color Normalization of Histological Images",* ***IEEE Transactions on Medical Imaging****, vol. 42, no. 6, pp. 1746-1757, 2023.*

TredMiL: Truncated Normal Mixture Prior Based Deep Latent Model

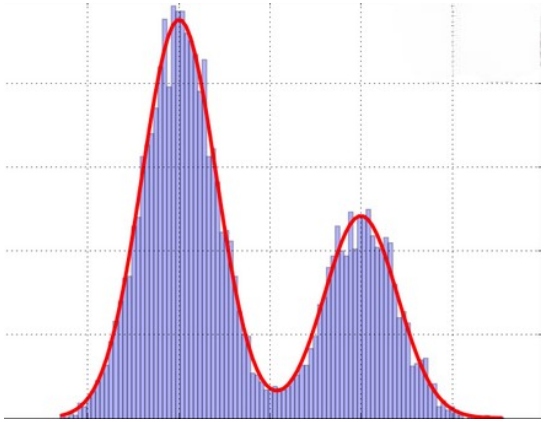
- It consists of four deep networks:
  - a color appearance encoder $\boldsymbol{E}_c$, which extracts the color appearance information,
  - a stain density encoder $\boldsymbol{E}_s$, which captures the information regarding amount of stains bound to biological components,
  - a decoder/generator $\boldsymbol{G}$, and
  - a discriminator $\boldsymbol{D}$.

- The networks ($\boldsymbol{E}_c$, $\boldsymbol{E}_s$, $\boldsymbol{G}$, $\boldsymbol{D}$) should be any differentiable functions.

- The networks $\boldsymbol{E}_c$, $\boldsymbol{E}_s$, $\boldsymbol{G}$, and $\boldsymbol{D}$ are chosen to be convolutional neural networks considering their tremendous success in different image analysis tasks.

TredMiL: Truncated Normal Mixture Prior Based Deep Latent Model

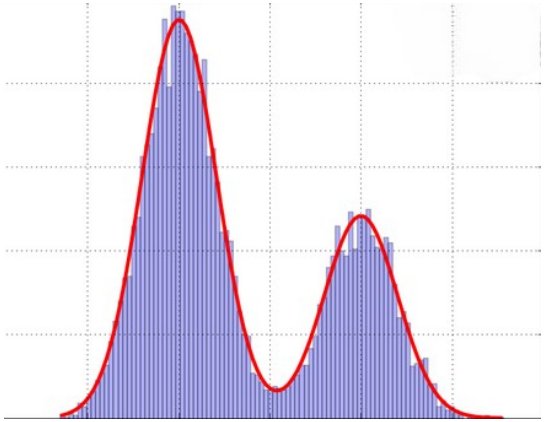
- The model assumes that the latent color appearance code (z_c) and stain density code (z_s) are independent of each other.
- A generative module and a reconstructive module are designed to capture disentangled color appearance and stain density information.
- The disentangled representation enhances the generalizability and adaptability of the model.
- Latent color appearance code is assumed to be sampled from a mixture of probability distributions.



TredMiL: Truncated Normal Mixture Prior Based Deep Latent Model

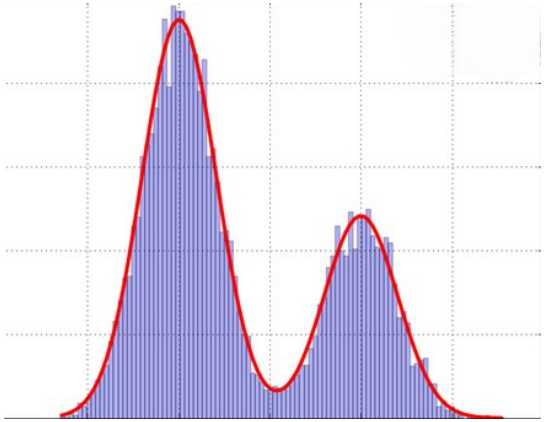
- The model assumes that the latent color appearance code (z_c) and stain density code (z_s) are independent of each other.
- A generative module and a reconstructive module are designed to capture disentangled color appearance and stain density information.
- The disentangled representation enhances the generalizability and adaptability of the model.
- Latent color appearance code is assumed to be sampled from a mixture of probability distributions.

Why?



TredMiL: Truncated Normal Mixture Prior Based Deep Latent Model

- The model assumes that the latent color appearance code (z_c) and stain density code (z_s) are independent of each other.
- A generative module and a reconstructive module are designed to capture disentangled color appearance and stain density information.
- The disentangled representation enhances the generalizability and adaptability of the model.
- Outer tails of mixture model are prone to outliers and do not contribute adequately in handling overlapping information.

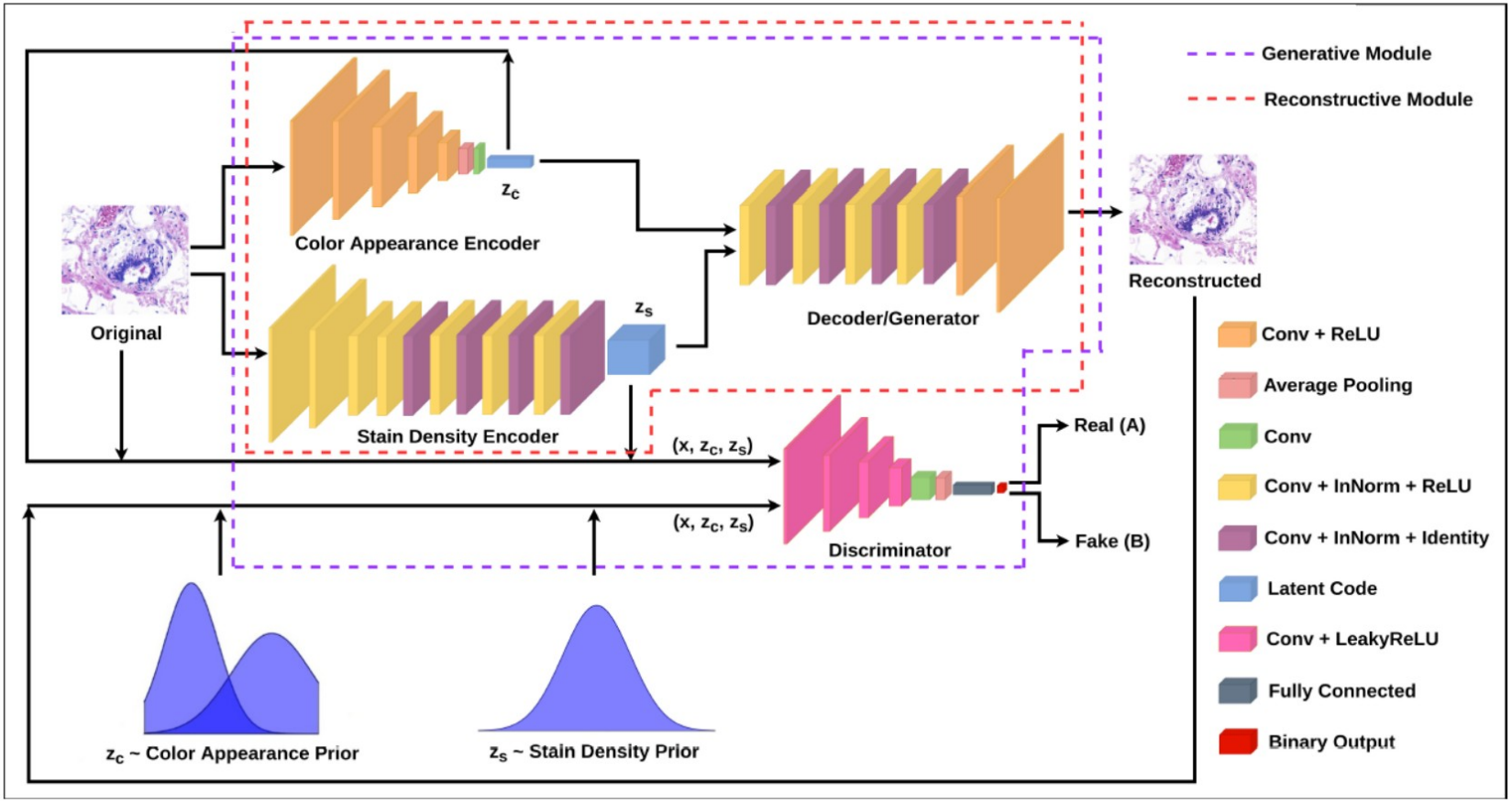


TredMiL: Truncated Normal Mixture Prior Based Deep Latent Model

- The model assumes that the latent color appearance code (z_c) and stain density code (z_s) are independent of each other.
- A generative module and a reconstructive module are designed to capture disentangled color appearance and stain density information.
- The disentangled representation enhances the generalizability and adaptability of the model.
- TredMiL assumes that the latent color appearance code, extracted through the color appearance encoder, is sampled from a mixture of truncated normal distributions.



Block Diagram: TredMiL



'Conv' means convolutional layer, 'ReLU' denotes rectified linear unit, 'InNorm' represents instance normalization, 'Identity' means identity function, i.e., $f(x) = x$, 'LeakyReLU' denotes leaky rectified linear unit.

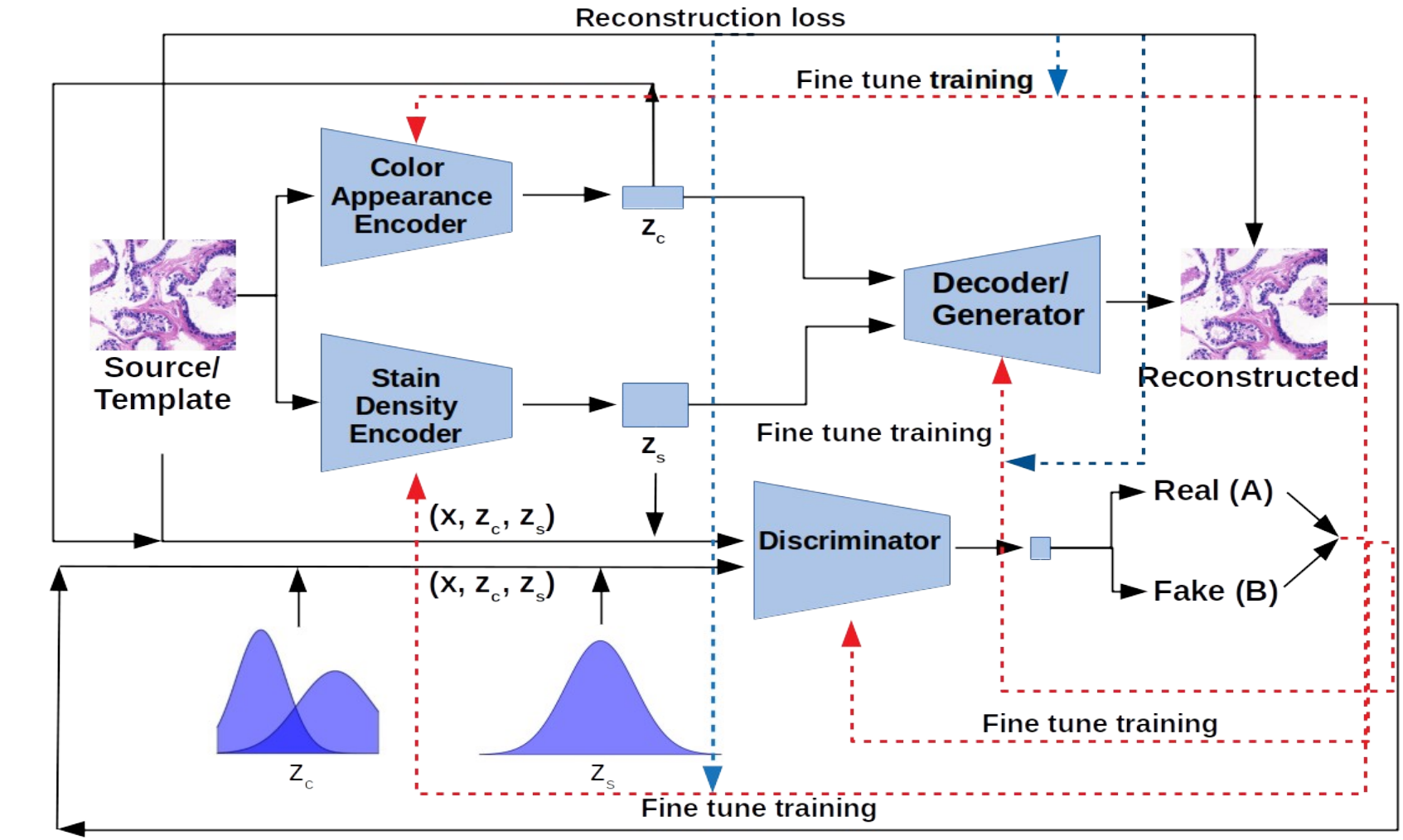
TredMiL: Truncated Normal Mixture Prior Based Deep Latent Model

- Each training set image $\boldsymbol{x}$ is fed simultaneously into both the color appearance encoder $\boldsymbol{E_c(x;\ \theta_{Ec})}$ and the stain density encoder $\boldsymbol{E_s(x;\ \theta_{Es})}$, which eventually output the latent color appearance code $\boldsymbol{z_c}$ and latent stain density representation $\boldsymbol{z_s}$, respectively.

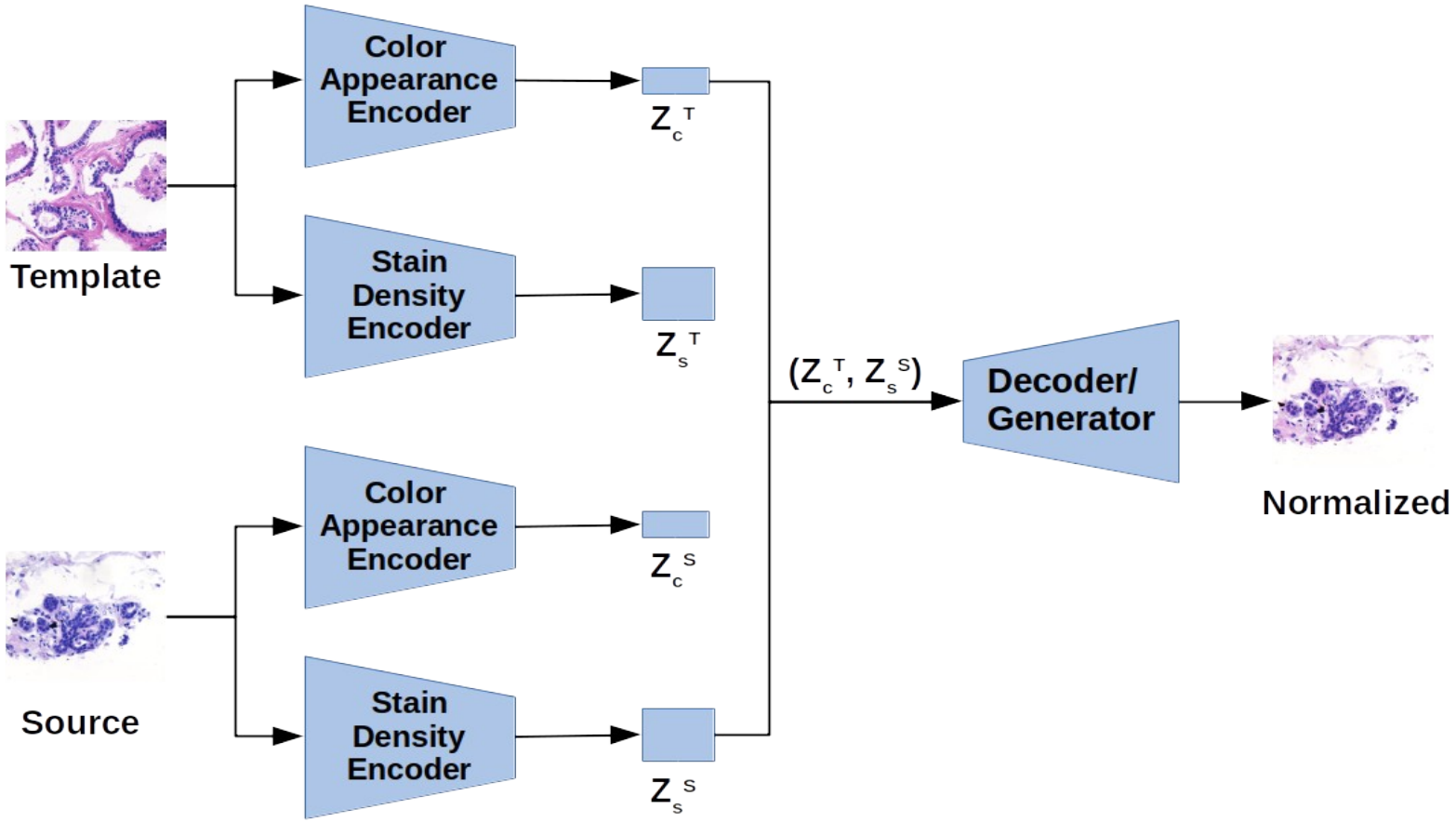
- Both the latent representations $\boldsymbol{z_c}$ and $\boldsymbol{z_s}$ are fed into the decoder /generator $\boldsymbol{G}$ as inputs, which generates the reconstructed image.

- The discriminator $\boldsymbol{D}$ takes inputs in the form of triplets ($\boldsymbol{x}$, $\boldsymbol{z_c}$, $\boldsymbol{z_s}$) and discriminates real encoding from the generated/fake encoding.

TredMiL: Training Scheme



TredMiL: Mapping Scheme



TredMiL: Objective Function

- The adversarial objective term, attributed by the generative module, is framed as follows:

$$J_{\text{adv}} = J_{\text{G}}(\mathcal{D}) + J_{\text{G}}(\mathcal{G})$$

- The objective functions, corresponding to the generative module, are given as follows:

$$J_{\text{G}}(\mathcal{D}) = \min_{\mathcal{D}} J_1(\mathcal{E}_c, \mathcal{E}_s, \mathcal{G}, \mathcal{D}),$$

$$J_1(\mathcal{E}_c, \mathcal{E}_s, \mathcal{G}, \mathcal{D}) = \underbrace{E_{x\sim P_X(x)} E_{z_c\sim P_{\mathcal{E}_c}(z_c|x)} E_{z_s\sim P_{\mathcal{E}_s}(z_s|x)} (A - \mathcal{D}[x, z_c, z_s])^2}_{R}$$
$$+ \underbrace{E_{z_c\sim P_{Z_c}(z_c)} E_{z_s\sim P_{Z_s}(z_s)} E_{x\sim P_{\mathcal{G}}(x|z_c,z_s)} (B - \mathcal{D}[x, z_c, z_s])^2}_{G}$$

- A and B denote the labels, assigned by discriminator D, to designate real and generated/fake encoding, respectively.

TredMiL: Objective Function

- The adversarial objective term, attributed by the generative module, is framed as follows:

$$J_{\text{adv}} = J_{\text{G}}(\mathcal{D}) + J_{\text{G}}(\mathcal{G})$$

- The objective functions, corresponding to the generative module, are given as follows:

Discriminator perspective ➡ $J_{\text{G}}(\mathcal{D}) = \min_{\mathcal{D}} J_1(\mathcal{E}_c, \mathcal{E}_s, \mathcal{G}, \mathcal{D}),$

$$J_1(\mathcal{E}_c, \mathcal{E}_s, \mathcal{G}, \mathcal{D}) = \underbrace{E_{x\sim P_X(x)} E_{z_c\sim P_{\mathcal{E}_c}(z_c|x)} E_{z_s\sim P_{\mathcal{E}_s}(z_s|x)} (A - \mathcal{D}[x, z_c, z_s])^2}_{R}$$
$$+ \underbrace{E_{z_c\sim P_{Z_c}(z_c)} E_{z_s\sim P_{Z_s}(z_s)} E_{x\sim P_{\mathcal{G}}(x|z_c,z_s)} (B - \mathcal{D}[x, z_c, z_s])^2}_{G}$$

- A and B denote the labels, assigned by discriminator D, to designate real and generated/fake encoding, respectively.

TredMiL: Objective Function

- The adversarial objective term, attributed by the generative module, is framed as follows:

$$J_{\text{adv}} = J_{\text{G}}(\mathcal{D}) + J_{\text{G}}(\mathcal{G})$$

- The objective functions, corresponding to the generative module, are given as follows:

$$J_{\text{G}}(\mathcal{D}) = \min_{\mathcal{D}} J_1(\mathcal{E}_c, \mathcal{E}_s, \mathcal{G}, \mathcal{D}),$$

Real encoding

$$J_1(\mathcal{E}_c, \mathcal{E}_s, \mathcal{G}, \mathcal{D}) = \underbrace{E_{x\sim P_X(x)} E_{z_c\sim P_{\mathcal{E}_c}(z_c|x)} E_{z_s\sim P_{\mathcal{E}_s}(z_s|x)} (A - \mathcal{D}[x, z_c, z_s])^2}_{R}$$
$$+ \underbrace{E_{z_c\sim P_{z_c}(z_c)} E_{z_s\sim P_{z_s}(z_s)} E_{x\sim P_{\mathcal{G}}(x|z_c,z_s)} (B - \mathcal{D}[x, z_c, z_s])^2}_{G}$$

- A and B denote the labels, assigned by discriminator D, to designate real and generated/fake encoding, respectively.

TredMiL: Objective Function

- The adversarial objective term, attributed by the generative module, is framed as follows:

$$J_{\text{adv}} = J_{\text{G}}(\mathcal{D}) + J_{\text{G}}(\mathcal{G})$$

- The objective functions, corresponding to the generative module, are given as follows:

$$J_{\text{G}}(\mathcal{D}) = \min_{\mathcal{D}} J_1(\mathcal{E}_c, \mathcal{E}_s, \mathcal{G}, \mathcal{D}),$$

$$J_1(\mathcal{E}_c, \mathcal{E}_s, \mathcal{G}, \mathcal{D}) = \underbrace{E_{x\sim P_X(x)} E_{z_c\sim P_{\mathcal{E}_c}(z_c|x)} E_{z_s\sim P_{\mathcal{E}_s}(z_s|x)} (A - \mathcal{D}[x, z_c, z_s])^2}_{R}$$

$$+ \underbrace{E_{z_c\sim P_{Z_c}(z_c)} E_{z_s\sim P_{Z_s}(z_s)} E_{x\sim P_{\mathcal{G}}(x|z_c,z_s)} (B - \mathcal{D}[x, z_c, z_s])^2}_{G}$$

Fake encoding

- A and B denote the labels, assigned by discriminator D, to designate real and generated/fake encoding, respectively.

TredMiL: Objective Function

- Similarly, $J_{\mathrm{G}}(\mathcal{G}) = \min_{\mathcal{G}} J_2(\mathcal{E}_c, \mathcal{E}_s, \mathcal{G}, \mathcal{D}),$ **Generator perspective**

$$J_2(\mathcal{E}_c, \mathcal{E}_s, \mathcal{G}, \mathcal{D}) = E_{z_c \sim P_{z_c}(z_c)} E_{z_s \sim P_{z_s}(z_s)} E_{x \sim P_{\mathcal{G}}(x|z_c, z_s)} (C - \mathcal{D}[x, z_c, z_s])^2$$

- C represents the label, assigned by discriminator ***D*** to designate generated/fake encoding, as desired by generator ***G***.

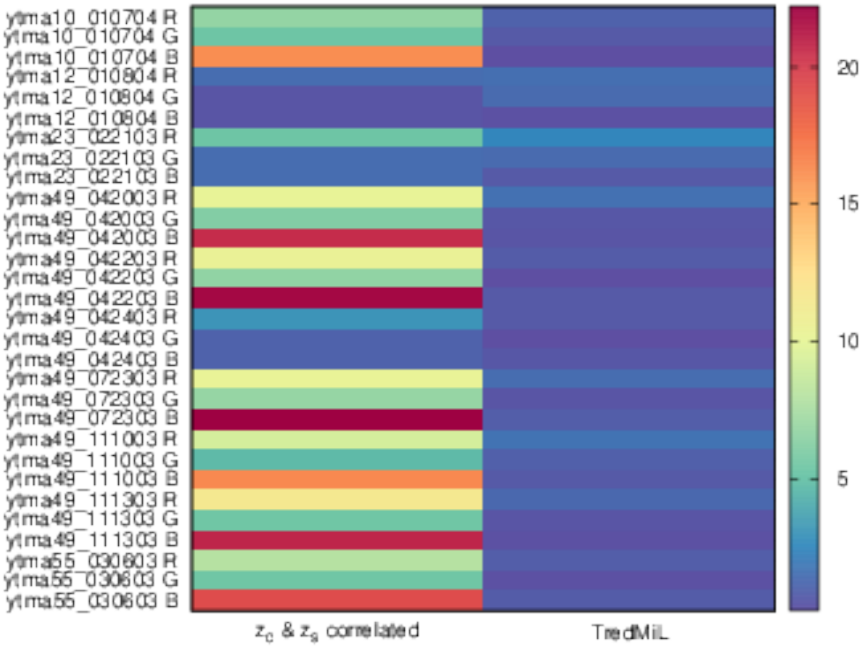
- The reconstruction objective to be minimized is as follows:

$$J_{\text{rec}} = \underbrace{-E_{Q(z_c,z_s)}[\log P_{\mathcal{G}}(x \mid z_c, z_s)]}_{L_R} - E_{Q(z_c,z_s)}[\log Q(z_c, z_s)] + \underbrace{D_{KL}[Q(z_c) \mid\mid P_{z_c}(z_c)]}_{R_1} + \underbrace{D_{KL}[Q(z_s) \mid\mid P_{z_s}(z_s)]}_{R_2},$$

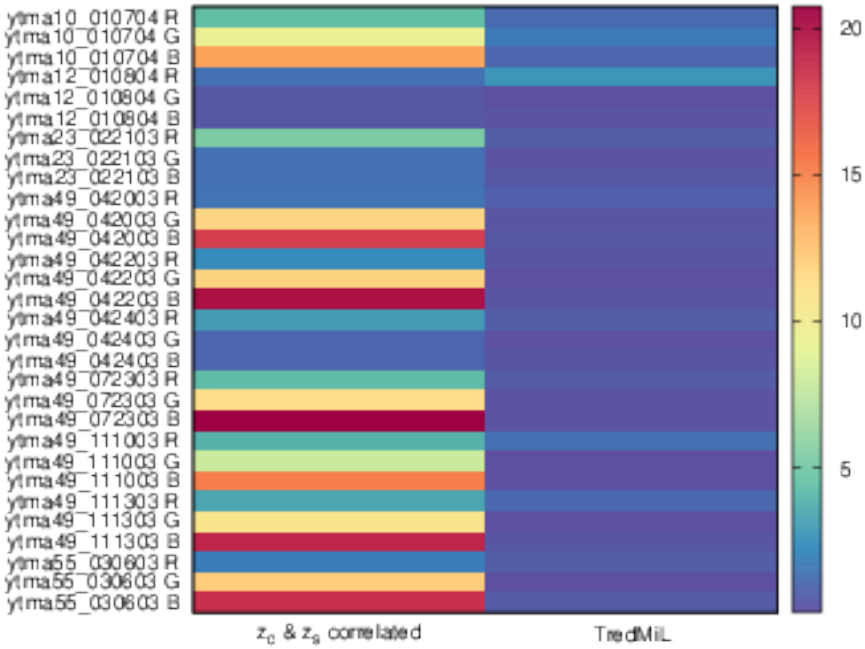
- where L_R is reconstruction loss, R_1 and R_2 denote the regularization terms corresponding to color appearance code z_c and stain density code z_s, respectively, and D_{KL} is the KL divergence.

Correlation Between Color Appearance Encoder and Stain Density Encoder

Hematoxylin

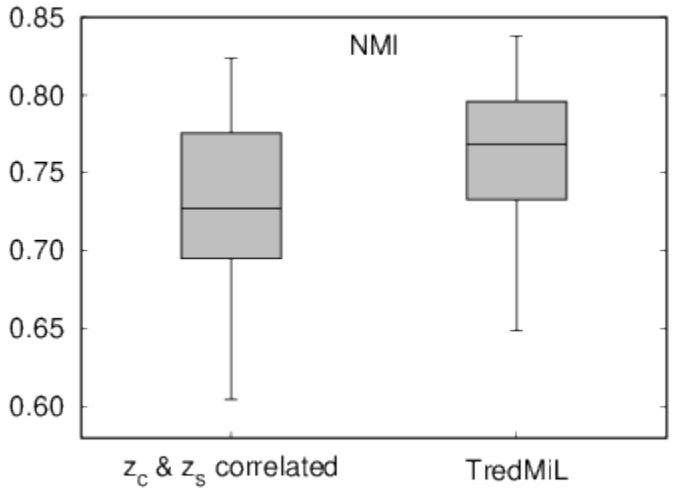


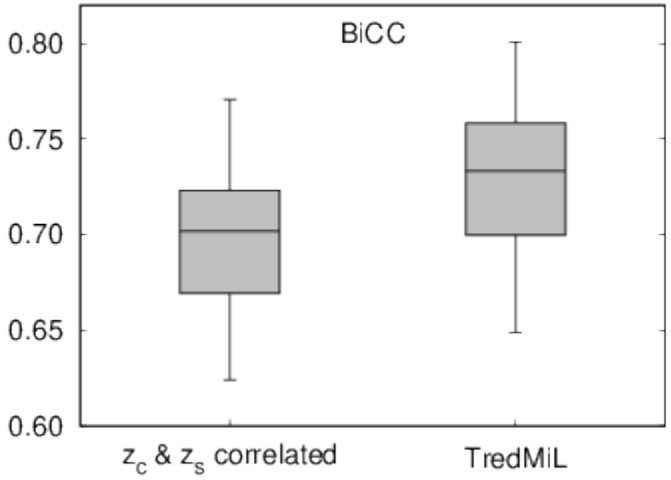
Eosin



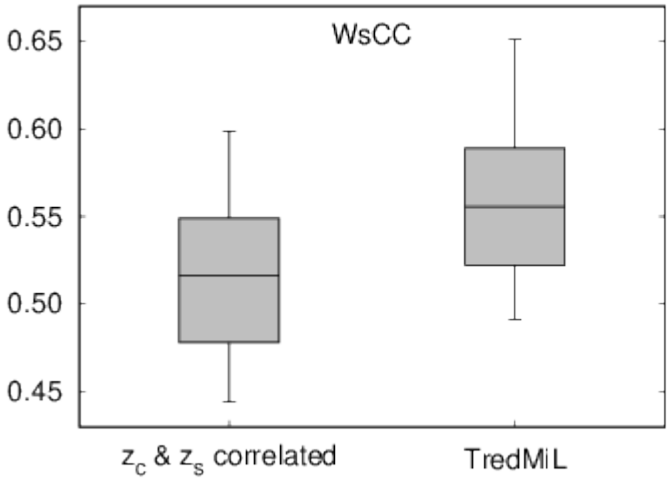
Stain Estimation

Correlation Between Color Appearance Encoder and Stain Density Encoder

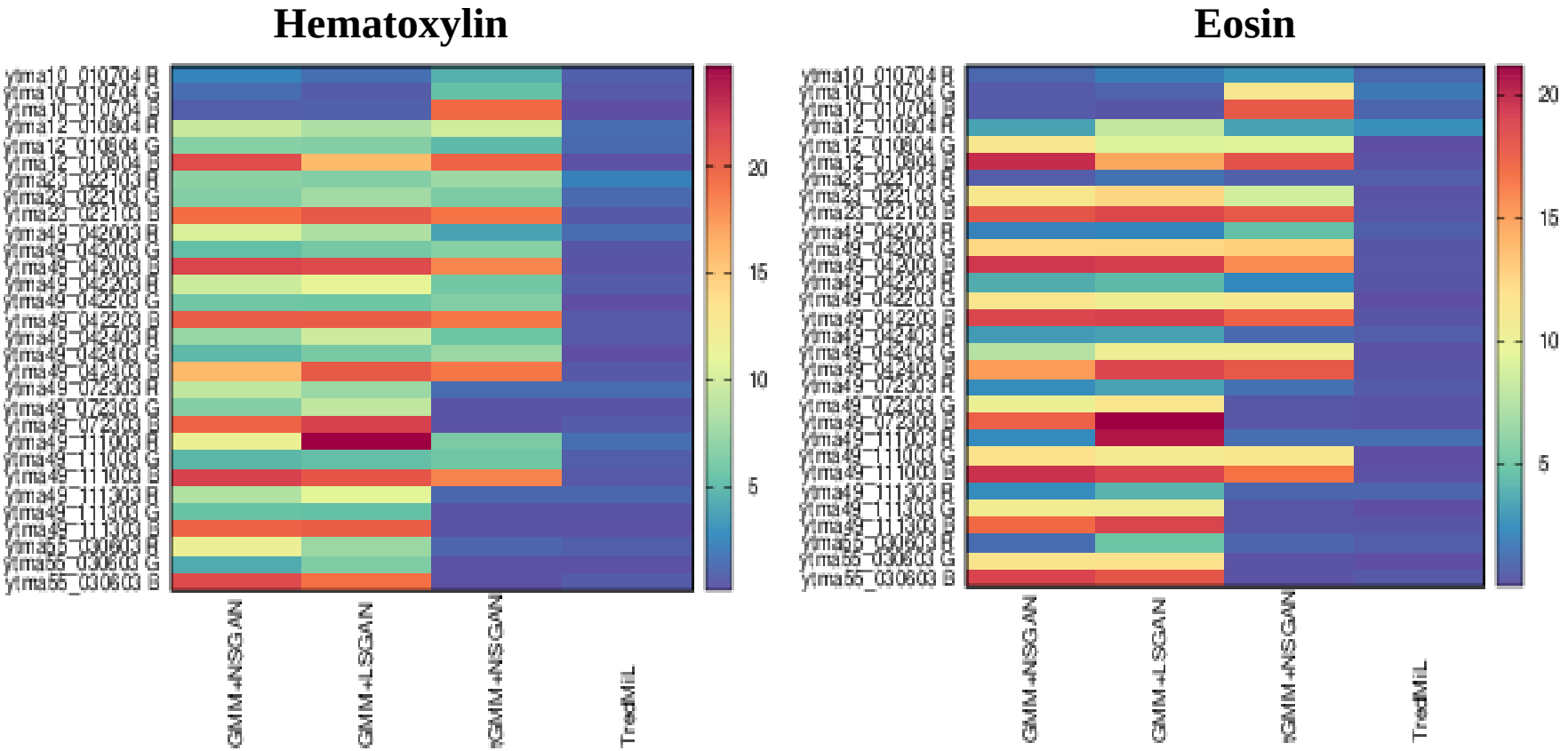




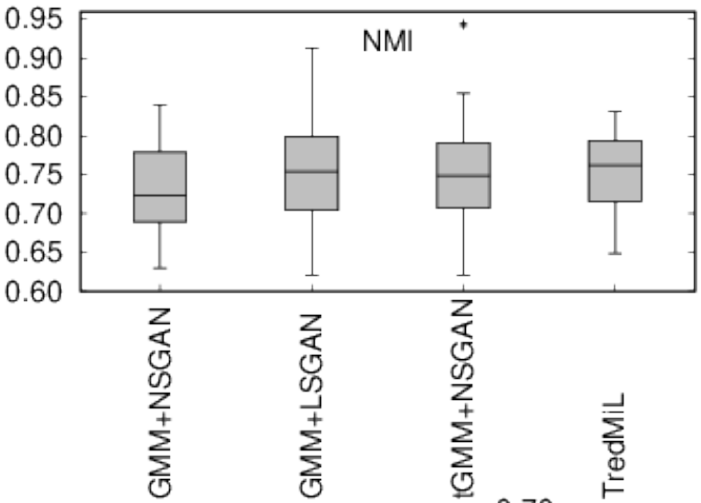
Color Normalization

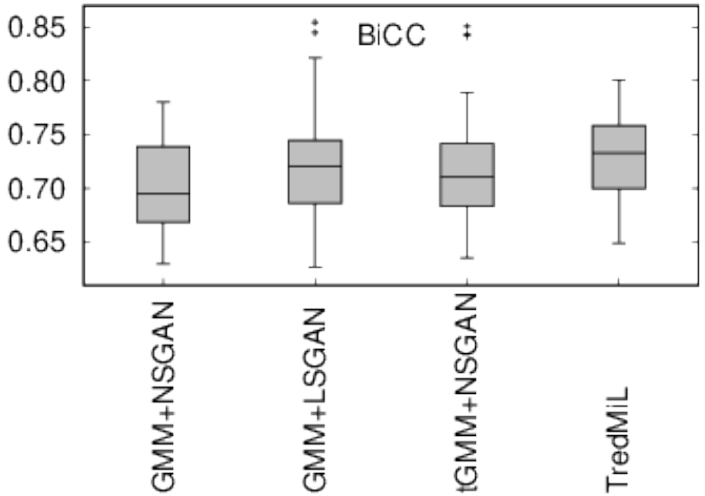


Mixture Models and GAN Formulations

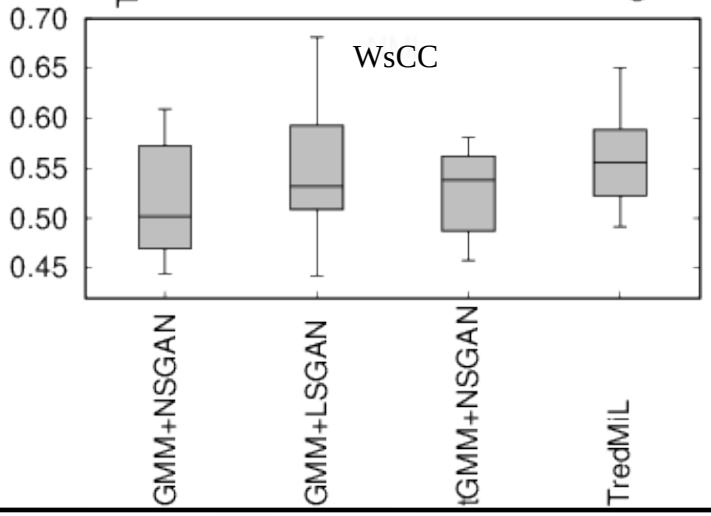


Mixture Models and GAN Formulations

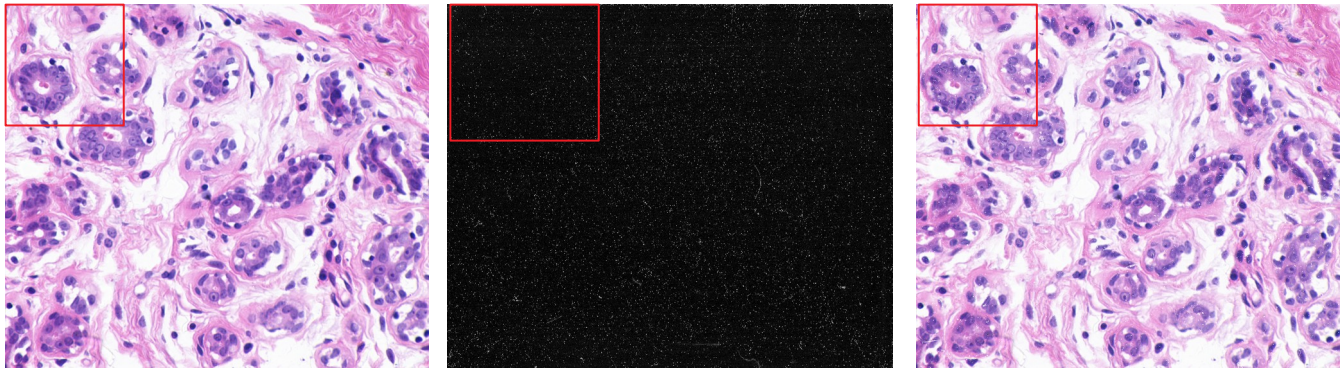


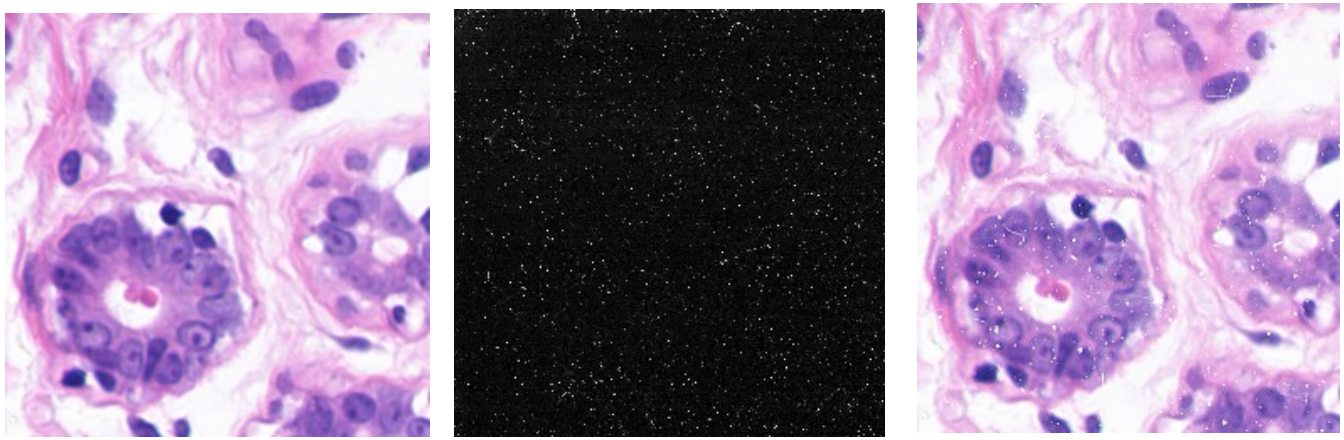


Color Normalization



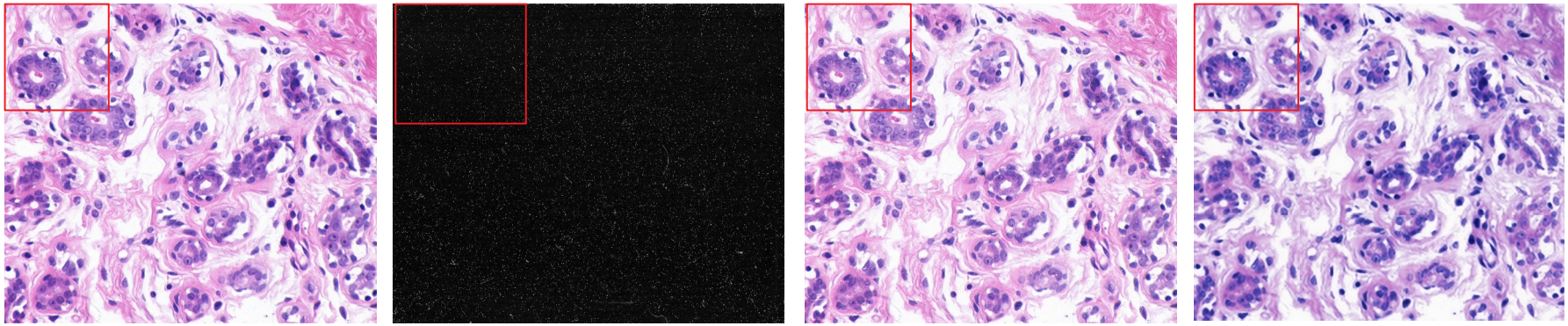
TredMiL in Presence of Dust

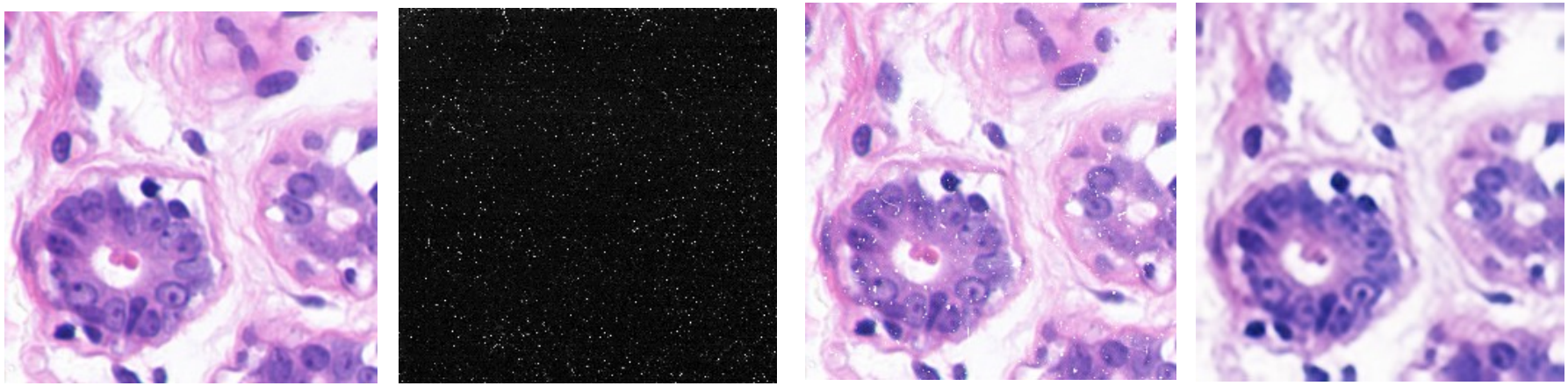




Original **Dust film** **Dust added**

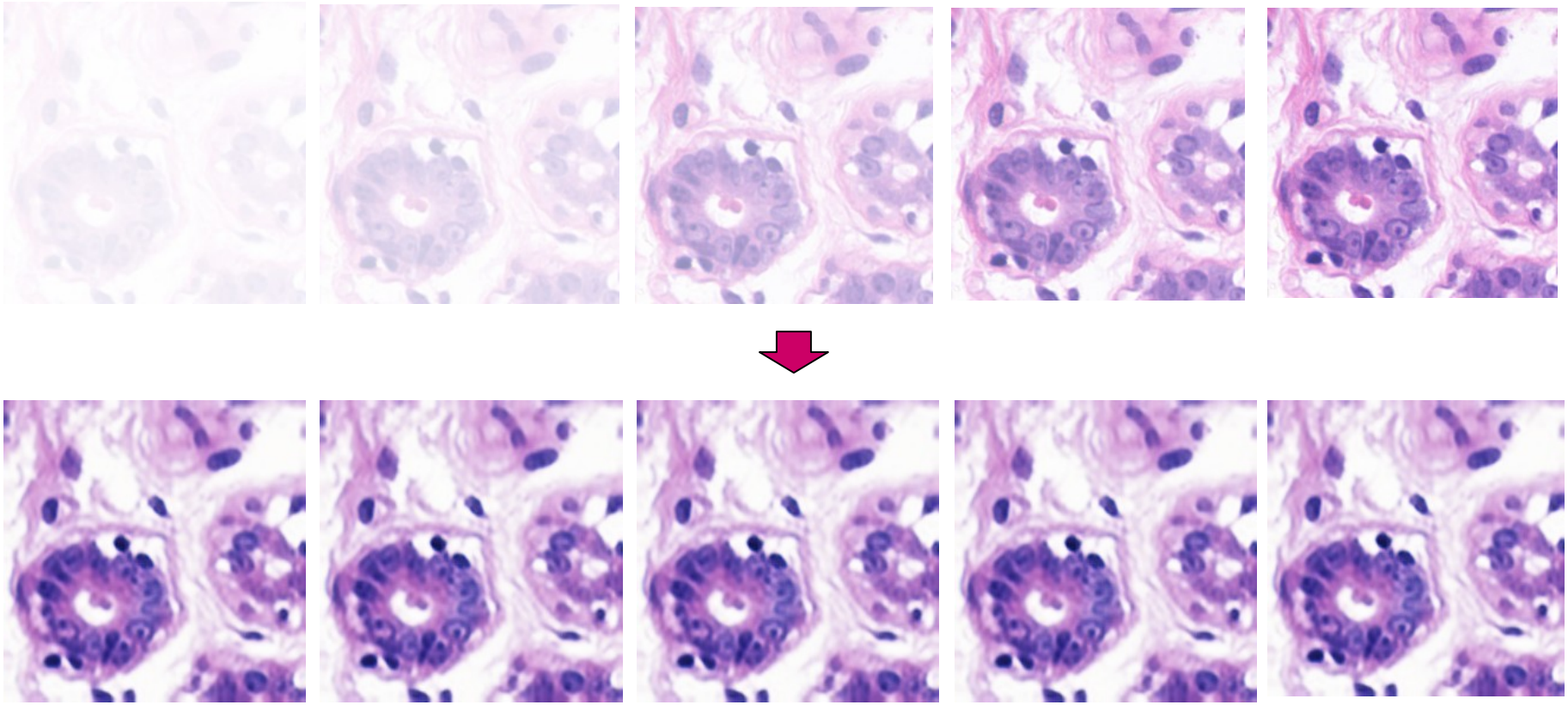
TredMiL in Presence of Dust





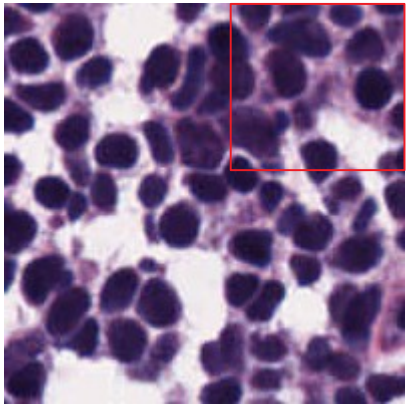
Original **Dust film** **Dust added** **Reconstructed**

TredMiL: Effect of Fading

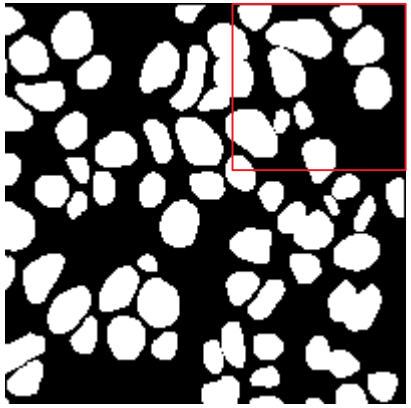


Opacity=10 **Opacity=25** **Opacity=50** **Opacity=75** **Opacity=90**

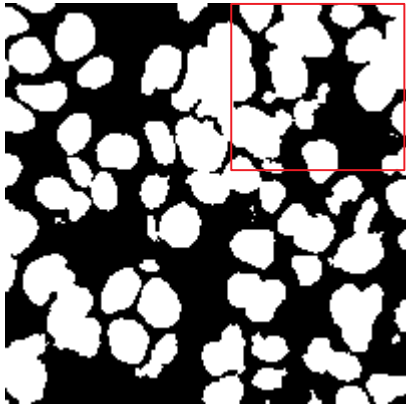
Color Normalization on Nuclei Segmentation



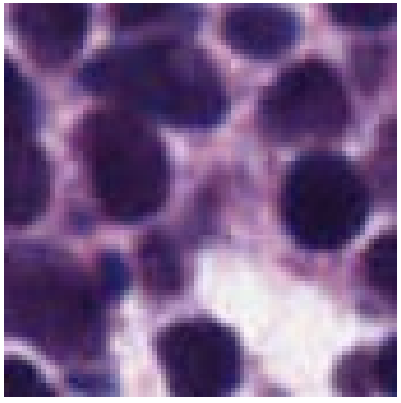
Original

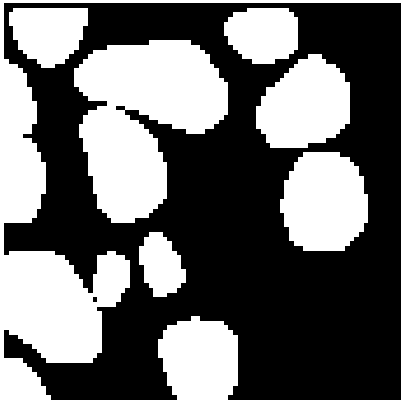


Ground-truth



Before normalization

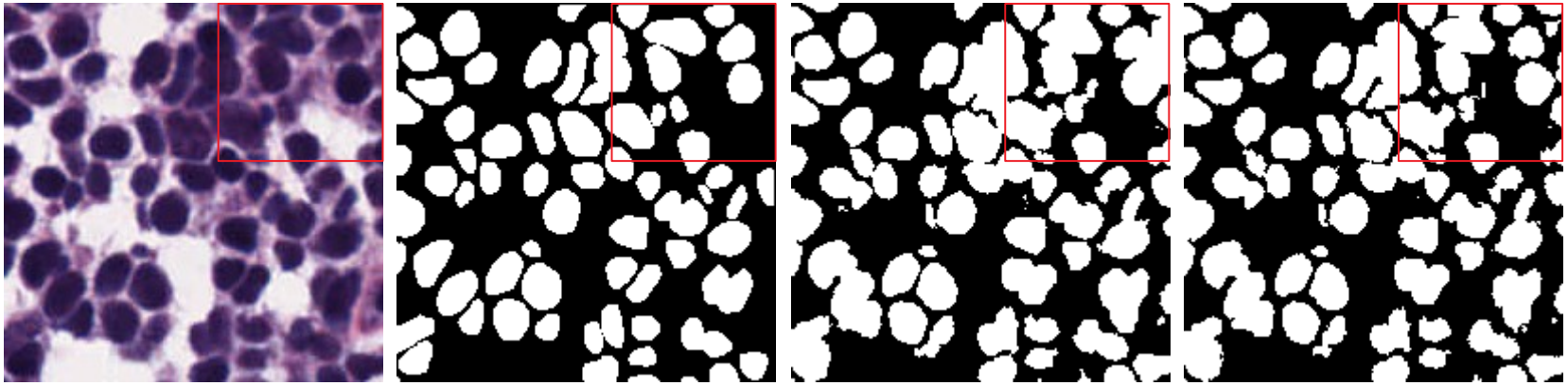




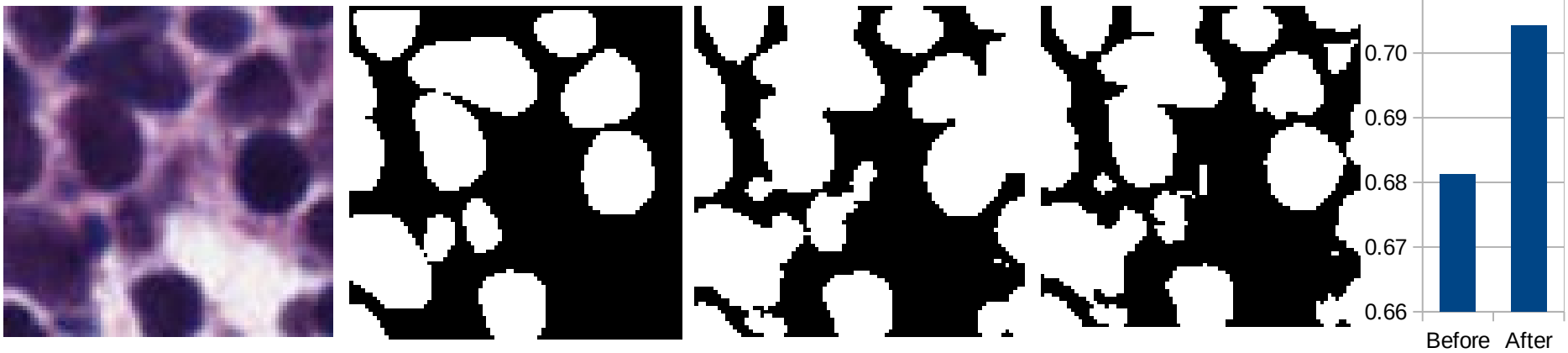


N. Kumar et al., "A Dataset and a Technique for Generalized Nuclear Segmentation for Computational Pathology", ***IEEE Transactions on Medical Imaging***, 36(7), pp. 1550-1560, 2017.

Color Normalization on Nuclei Segmentation



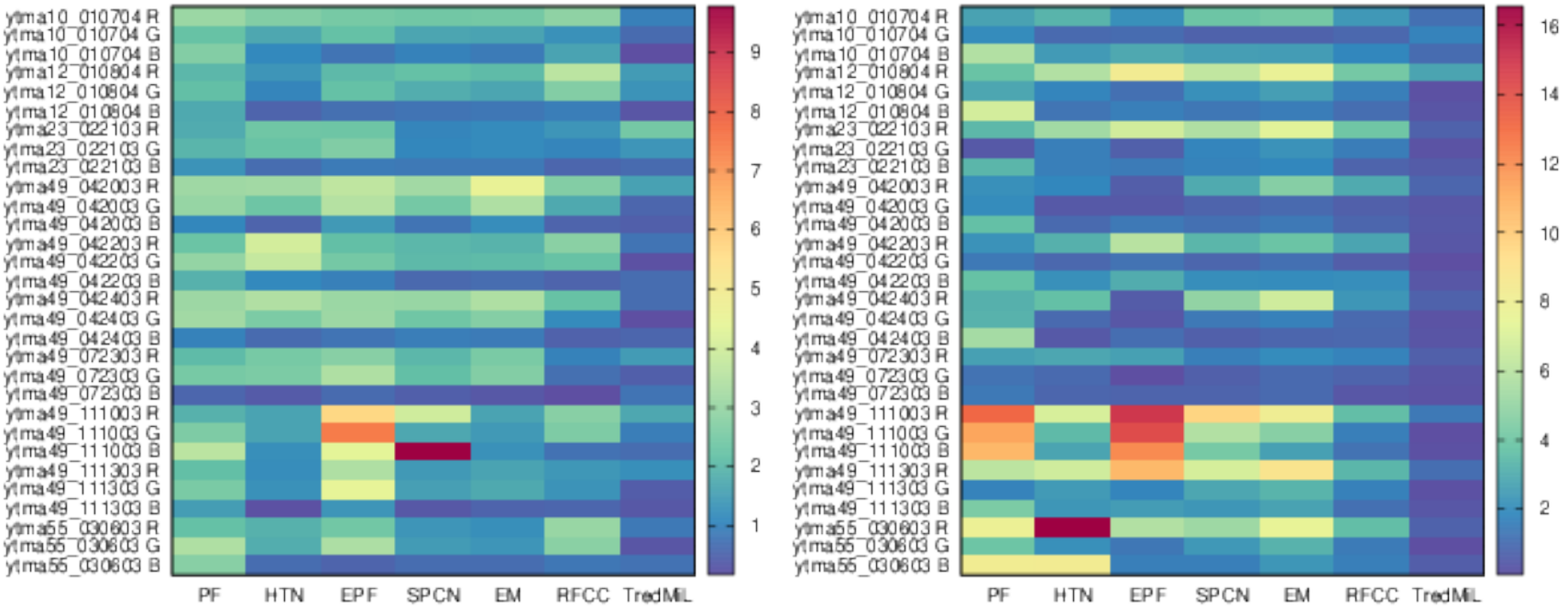
Original | Ground-truth | Before normalization | After normalization



N. Kumar et al., "A Dataset and a Technique for Generalized Nuclear Segmentation for Computational Pathology", ***IEEE Transactions on Medical Imaging***, 36(7), pp. 1550-1560, 2017.

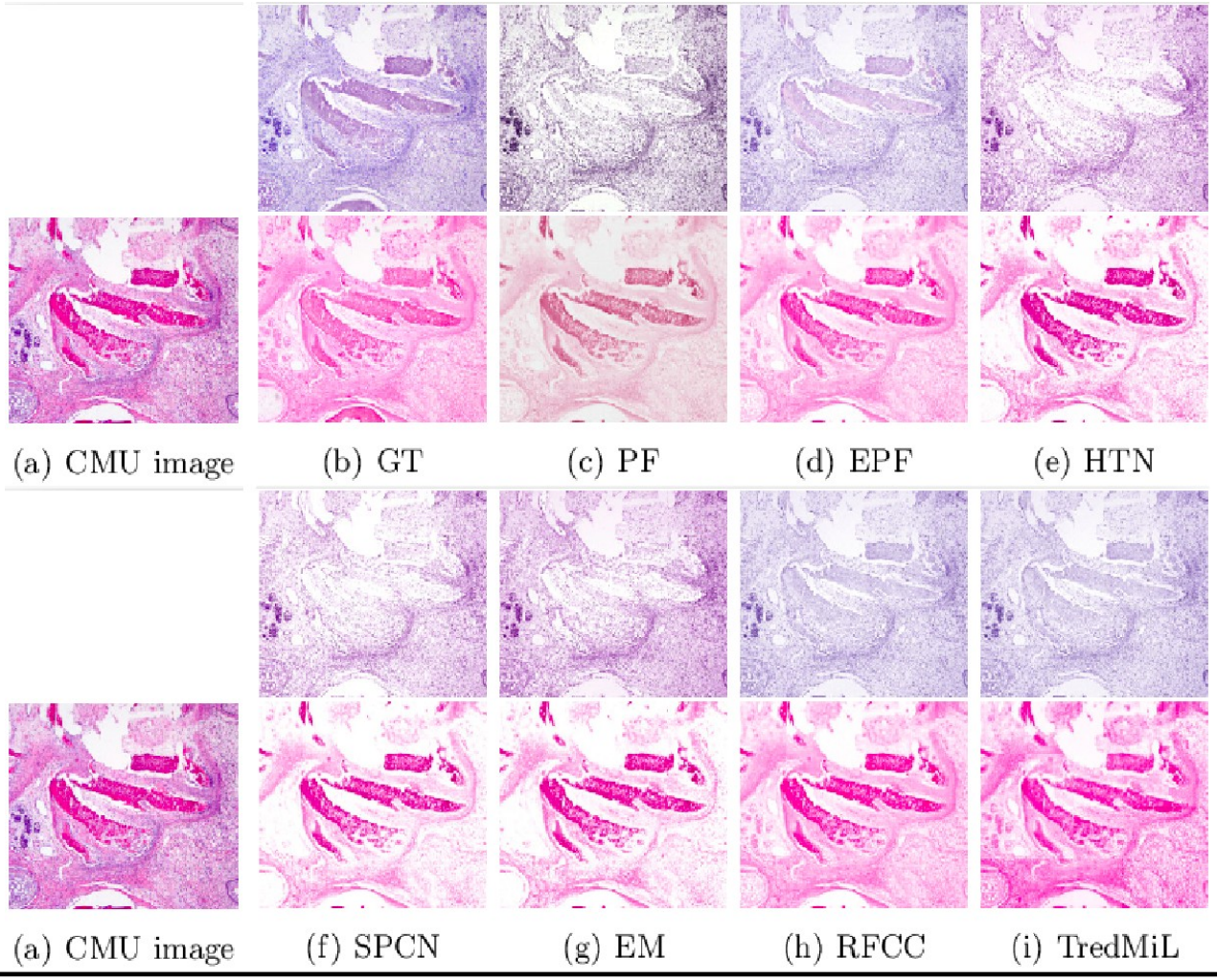
Performance Analysis: Stain separation

Hematoxylin **Eosin**



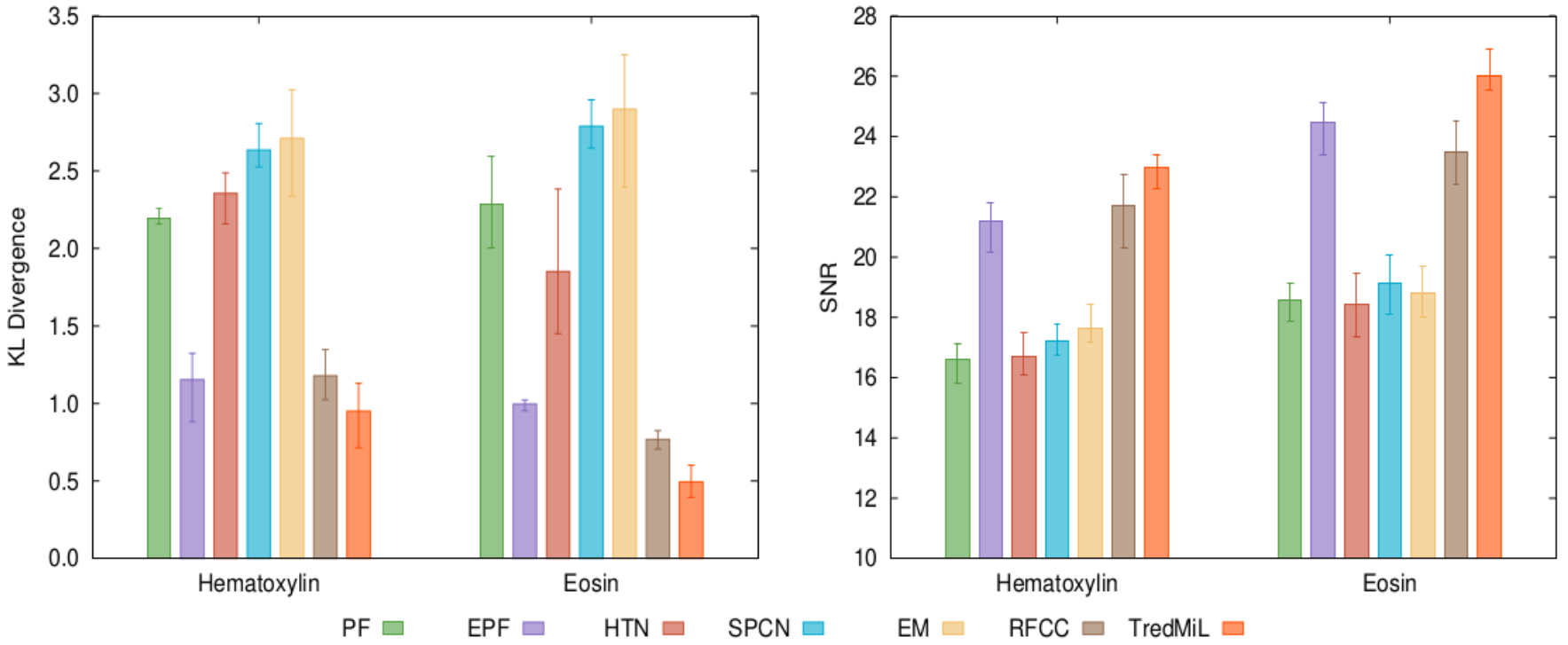
Quantitative Comparison of Stain Separation vs existing methods: PF, HTN, EPF, SPCN, EM and $RFCC_{vM}$

Performance in Stain Separation



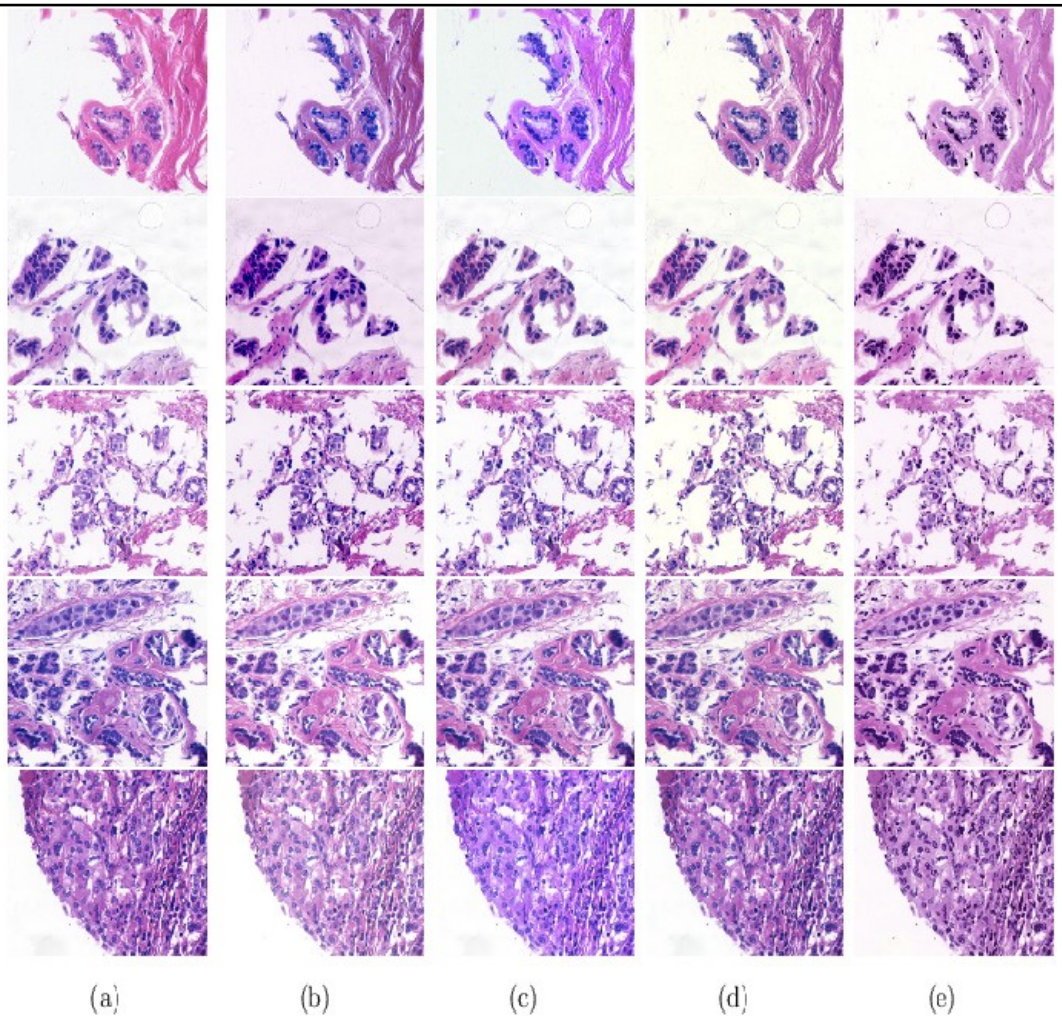
Qualitative comparison of stain separation by different methods w.r.t. H-stain and E-stain

Performance in Stain Separation



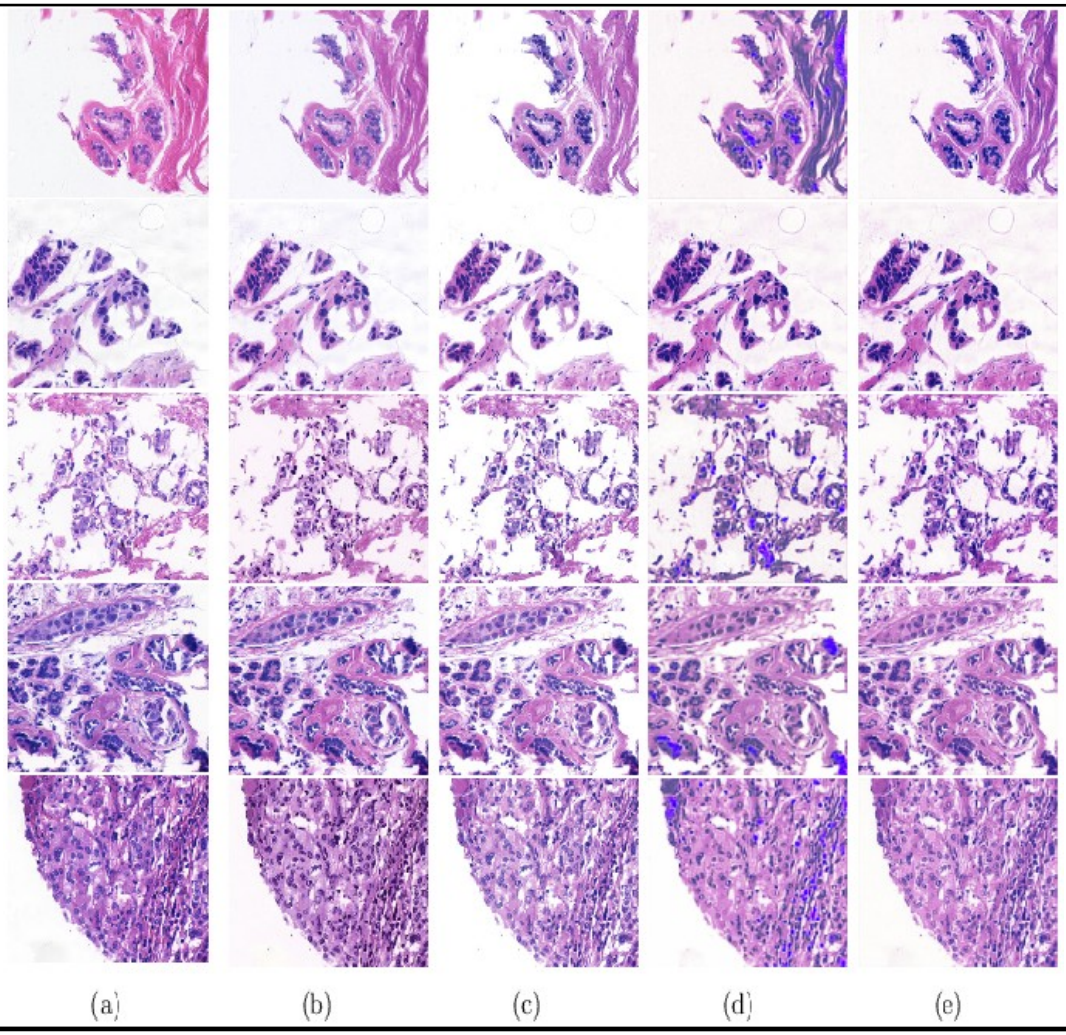
Quantitative comparison of stain separation by different methods w.r.t. H-stain and E-stain

Qualitative Analysis: Color Normalization



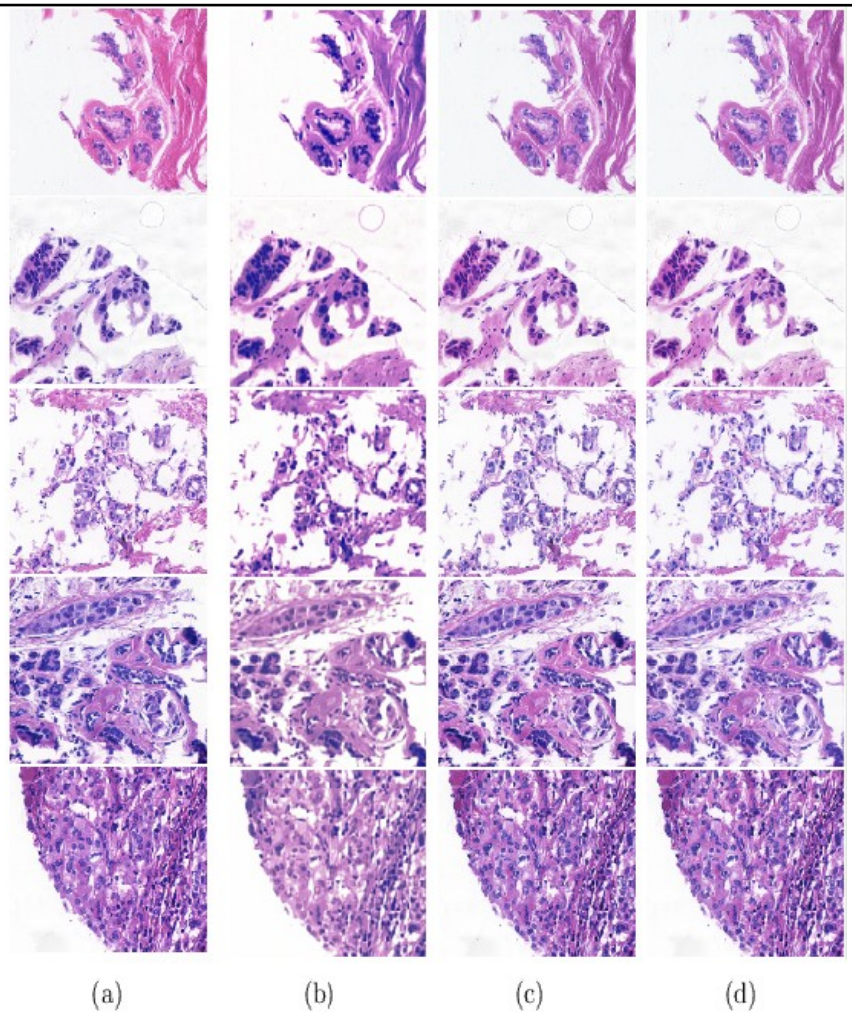
Qualitative performance analysis of different color normalization methods: (a) original, (b) ColTrans, (c) PF, (d) EPF, (e) SCD

Qualitative Analysis: Color Normalization



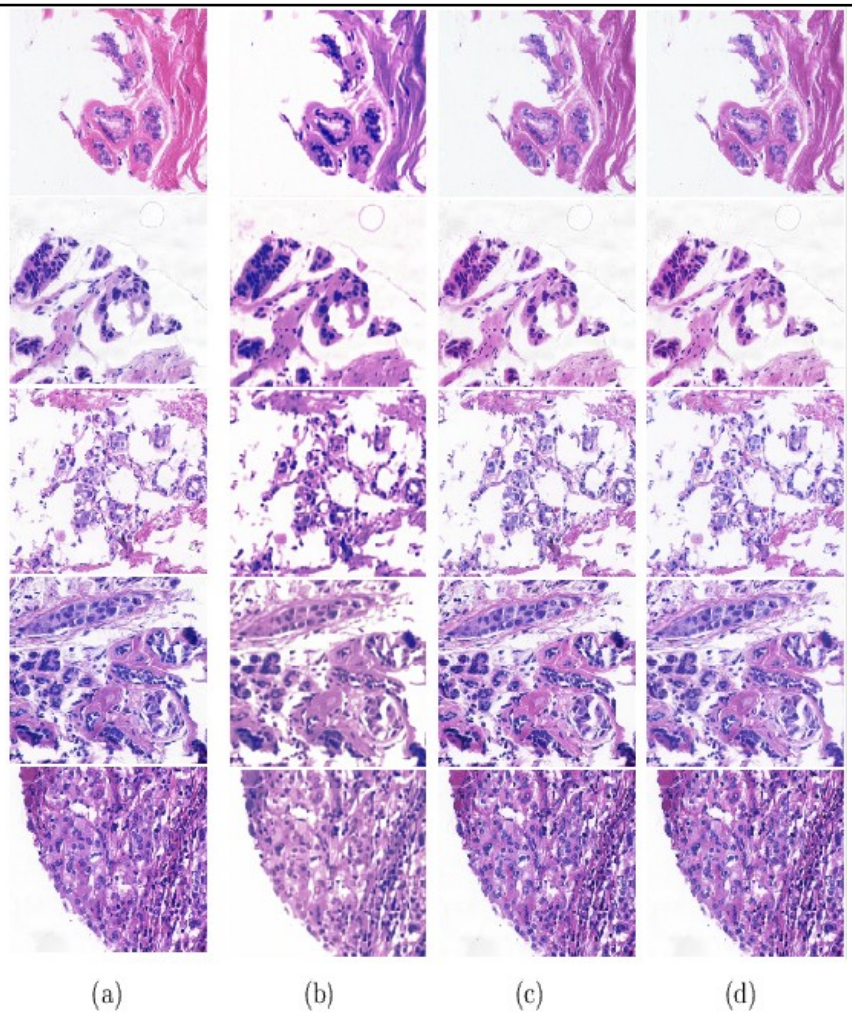
Qualitative performance analysis of different color normalization methods: (a) original, (b) HTN, (c) SPCN, (d) SN-GAN, (e) StainGAN

Qualitative Analysis: Color Normalization



Qualitative performance analysis of different color normalization methods: (a) original, (b) AST, (c) $RFCC_{vM,}$ (d) TredMiL

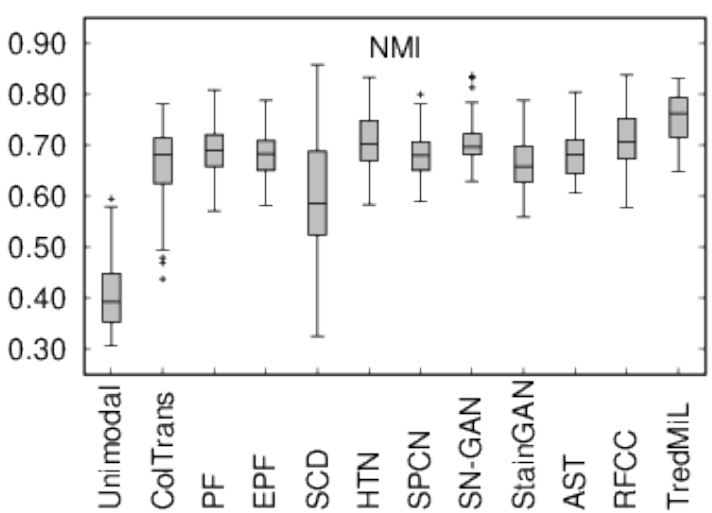
Qualitative Analysis: Color Normalization

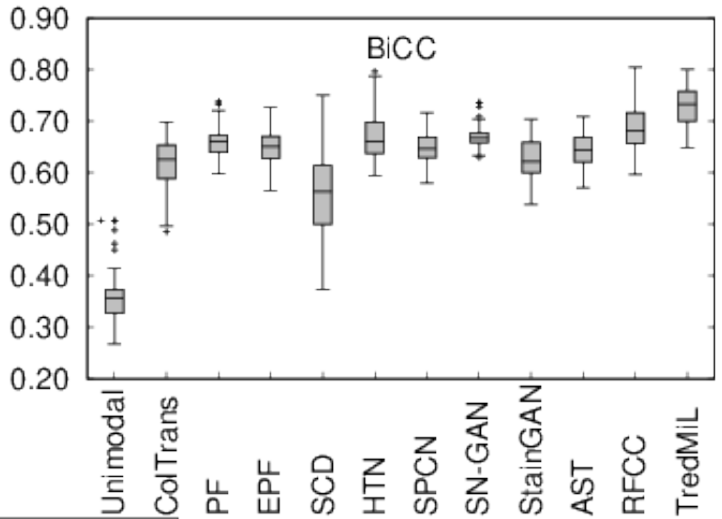


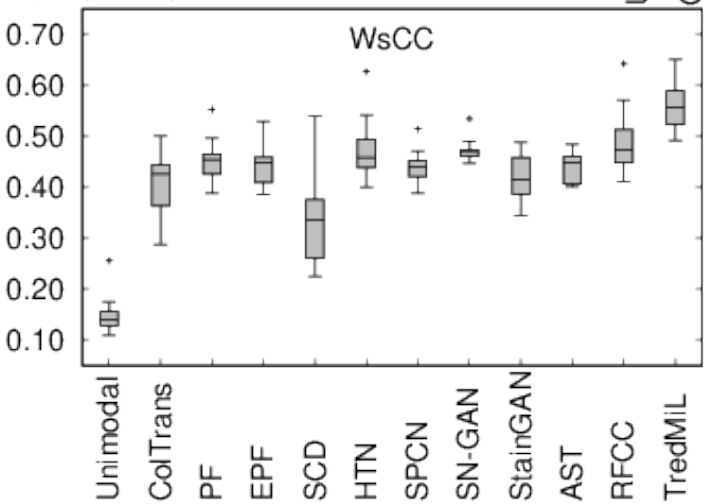
Qualitative performance analysis of different color normalization methods: (a) original, (b) AST, (c) $RFCC_{vM}$, (d) TredMiL

The TredMiL method outperforms other existing color normalization methods as per color consistency after normalization is concerned.

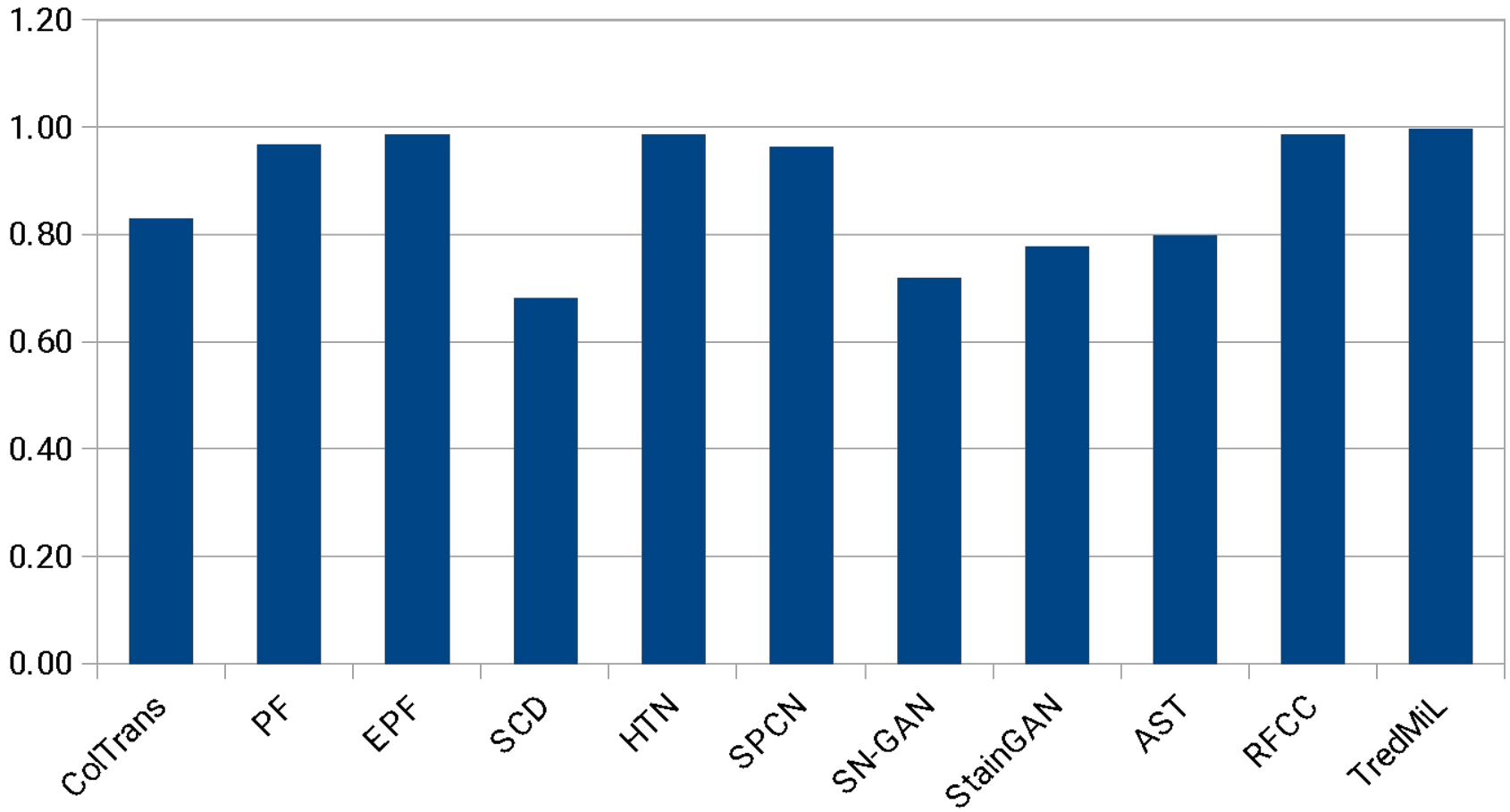
Performance Analysis: Color Normalization







Structural Similarity w.r.t. SSIM Index

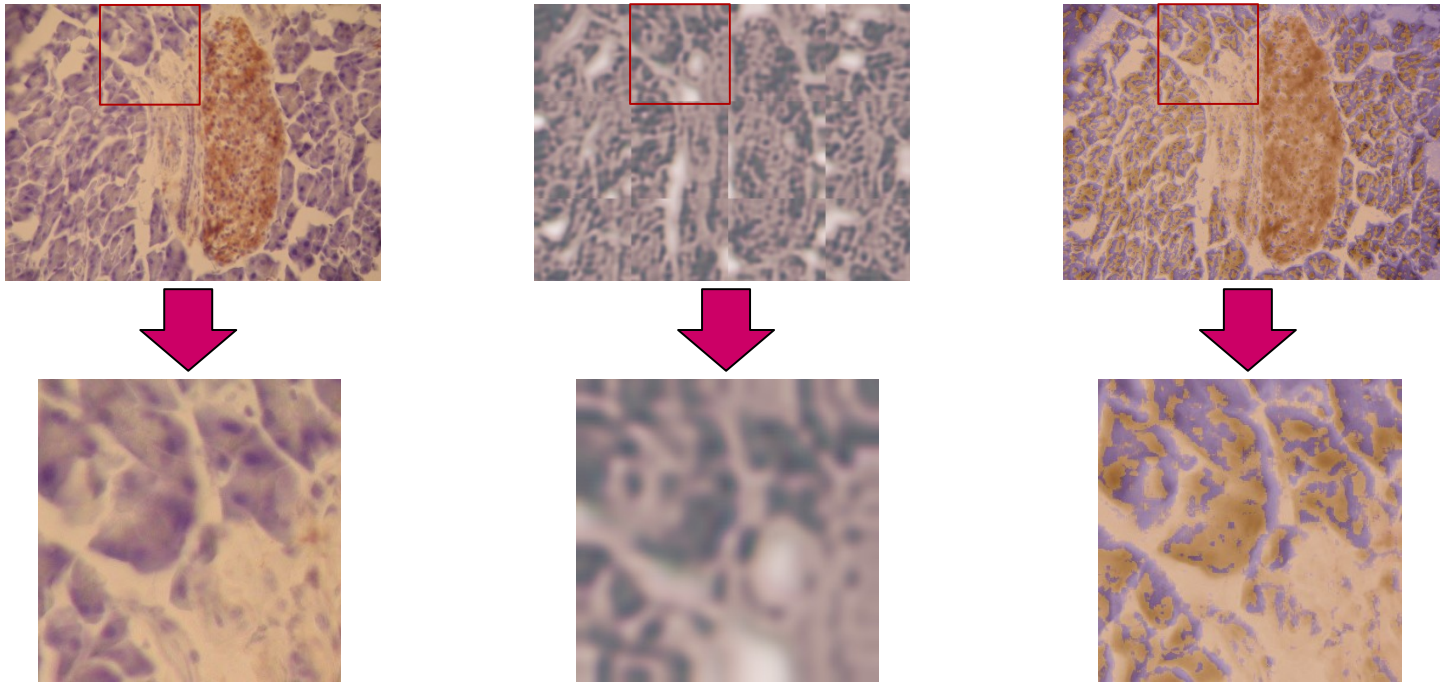


Z. Wang et al., "Image Quality Assessment: From Error Visibility to Structural Similarity", ***IEEE Transactions on Image Processing***, 13(4), pp. 600-612, 2004.

Application to Other Staining (H&DAB Stain)

Model trained on H&E stained samples:

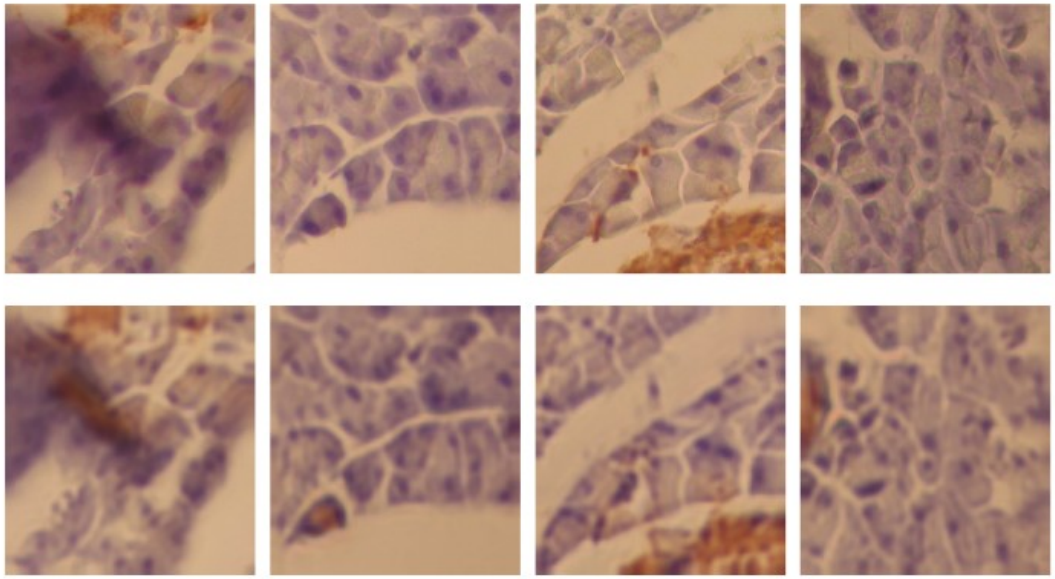
Source | TredMiL | $RFCC_{vM}$



M. Kuse et al., "Local Isotropic Phase Symmetry Measure for Detection of Beta Cells and Lymphocytes", ***Journal of Pathology Informatics***, 2(2), pp. 2, 2012.

Application to Other Staining (H&DAB Stain)

Model trained on H&DAB stained samples:



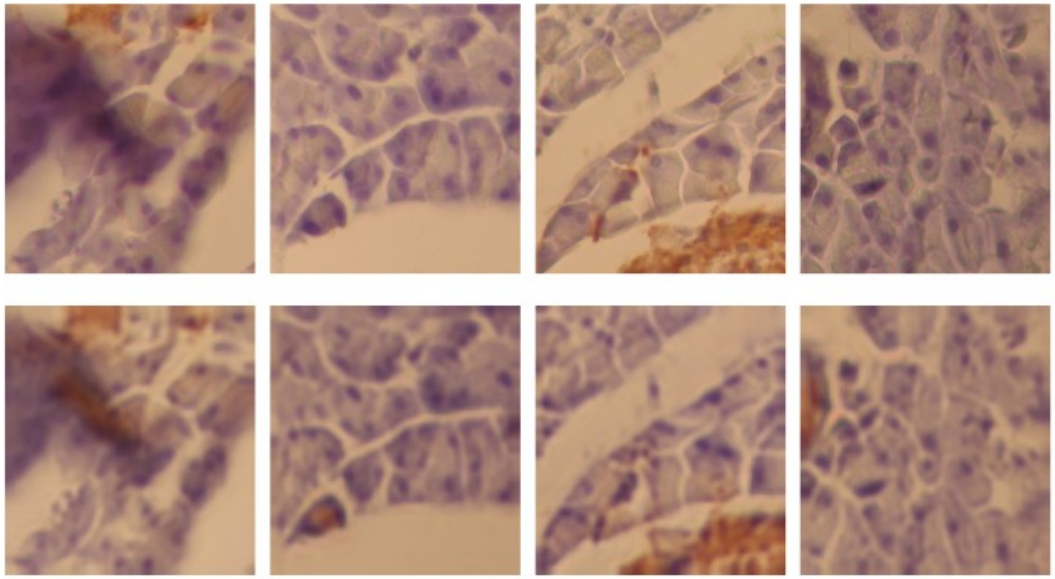
(a) patch 1 (b) patch 2 (c) patch 3 (d) patch 4

Column 1: original image patches, Column 2: color normalized images

M. Kuse et al., "Local Isotropic Phase Symmetry Measure for Detection of Beta Cells and Lymphocytes", ***Journal of Pathology Informatics***, 2(2), pp. 2, 2012.

Application to Other Staining (H&DAB Stain)

Model trained on H&DAB stained samples:



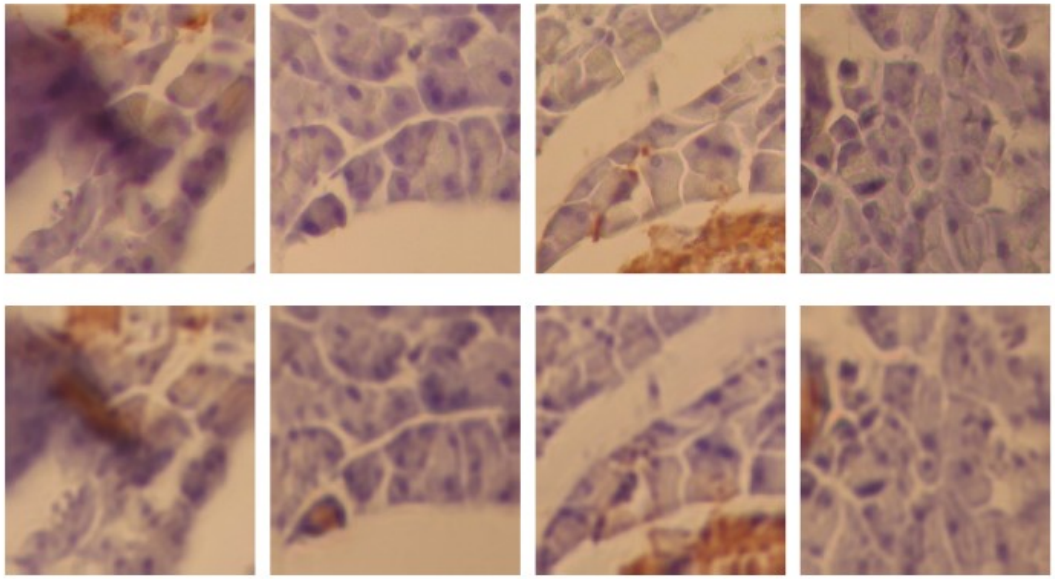
(a) patch 1 (b) patch 2 (c) patch 3 (d) patch 4

Brown DAB in H&DAB staining is not a light absorber, it scatters light

M. Kuse et al., "Local Isotropic Phase Symmetry Measure for Detection of Beta Cells and Lymphocytes", ***Journal of Pathology Informatics***, 2(2), pp. 2, 2012.

Application to Other Staining (H&DAB)

Model trained on H&DAB stained samples:



(a) patch 1 (b) patch 2 (c) patch 3 (d) patch 4

Thorough understanding of immunohistochemical staining is required

M. Kuse et al., "Local Isotropic Phase Symmetry Measure for Detection of Beta Cells and Lymphocytes", ***Journal of Pathology Informatics***, 2(2), pp. 2, 2012.

Key Takeaways - TredMiL

- Truncated normal mixture prior based latent color appearance code to design a deep generative model to solve color deviation problem.
- This chapter demonstrates that color normalization has huge impact on subsequent nuclei segmentation task.
- Mitigating disagreement in stained tissue color appearance improves quality of ROI segmentation.

Key Takeaways - TredMiL

- Truncated normal mixture prior based latent color appearance code to design a deep generative model to solve color deviation problem.
- This chapter demonstrates that color normalization has huge impact on subsequent nuclei segmentation task.
- Mitigating disagreement in stained tissue color appearance improves quality of ROI segmentation.
- Next chapter tries to devise a nuclei segmentation algorithm, generalizable to segmentation problems with different types of target domain image representations.

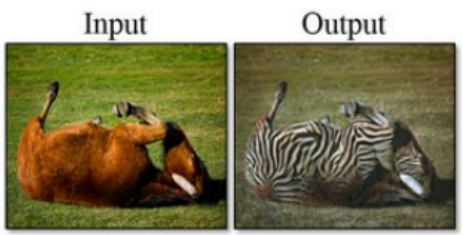
Chapter 6

Optimal Transport Driven Asymmetric Image-to-Image Translation for Nuclei Segmentation

S. Mahapatra *and P. Maji, "Optimal Transport Driven Asymmetric Image-to-Image Translation for Nuclei Segmentation of Histological Images",* ***IEEE Transactions on Artificial Intelligence (under review)****, pp. 1-12, Manuscript ID: TAI-2024-Nov-A-01785.*

Motivation

- Image-to-image (I2I) translation network aims to transfer images from a source domain to a target domain while preserving the content representations.
- I2I networks have been applied in computer vision and image processing problems, viz., image synthesis, segmentation, style transfer, object transfiguration etc.

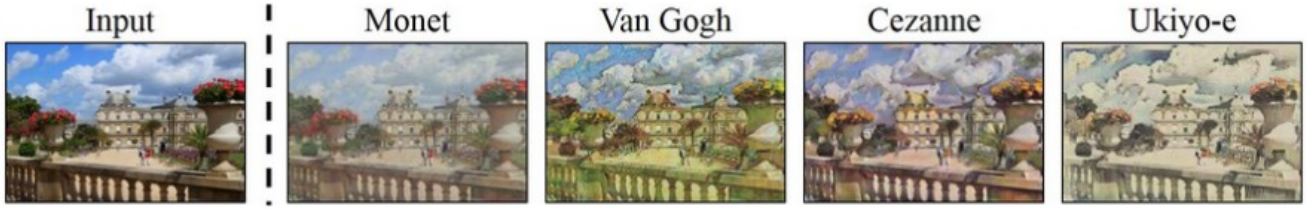




Season transfer



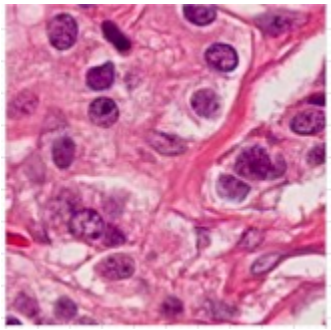
Object transfiguration



Collection Style transfer

- I2I networks can be broadly categorized into two groups: paired networks, such as Pix2Pix and unpaired networks, such as, CycleGAN.

Motivation: Information-disparity

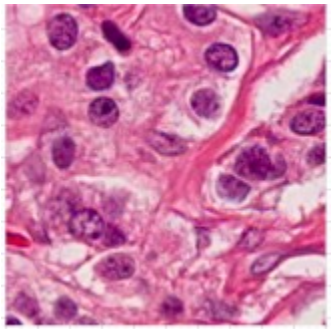


information-rich histological image space $\mathcal{X}$



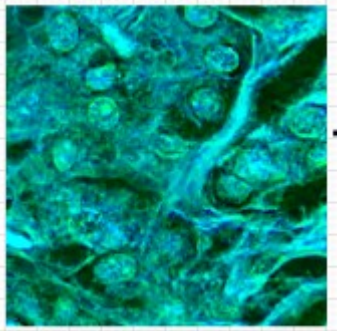
information-poor segmentation map domain $\mathcal{Y}$

Motivation: Information-disparity



information-rich histological image space $\mathcal{X}$

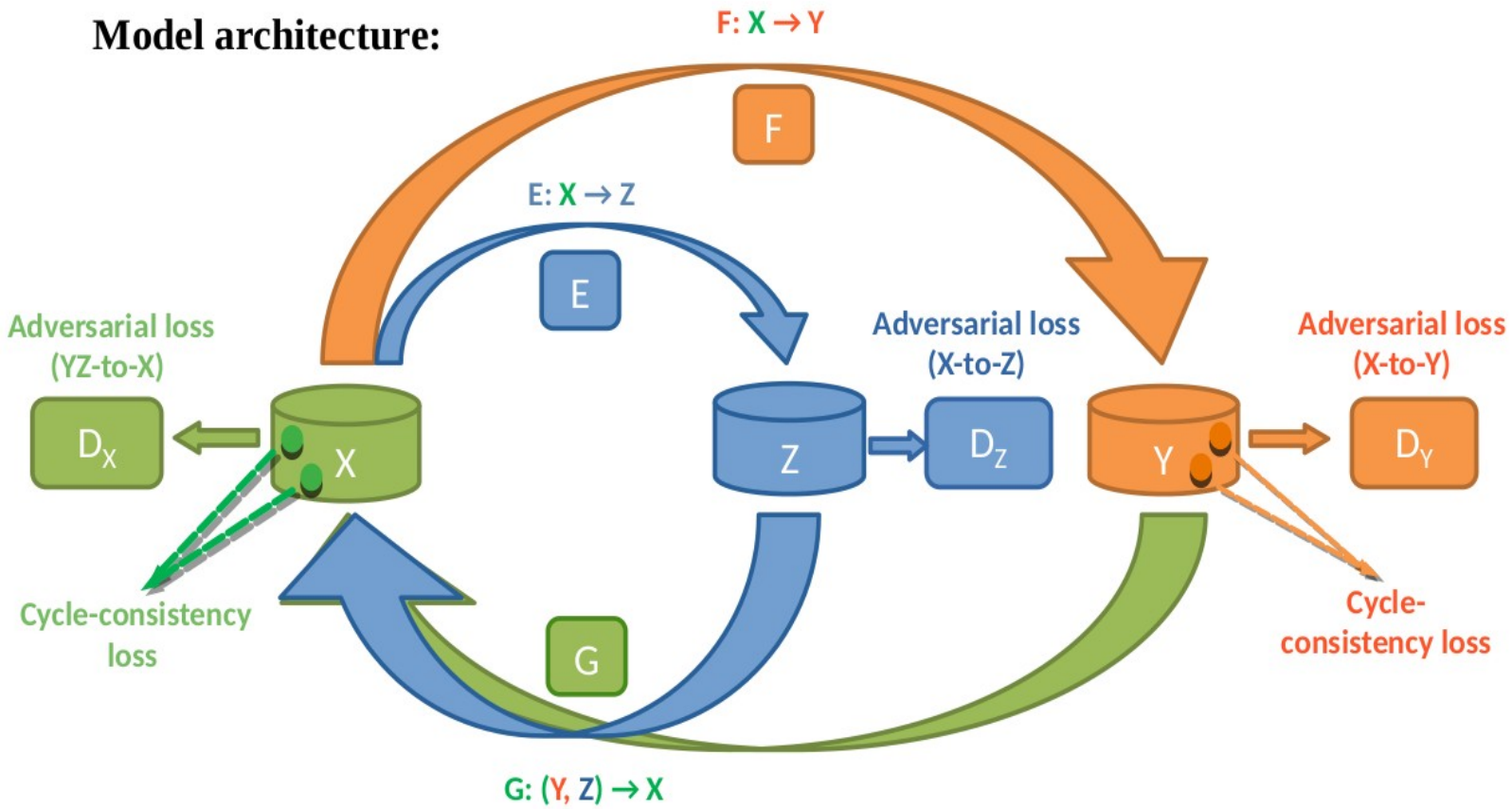
$\mathcal{Z}$ embedding space



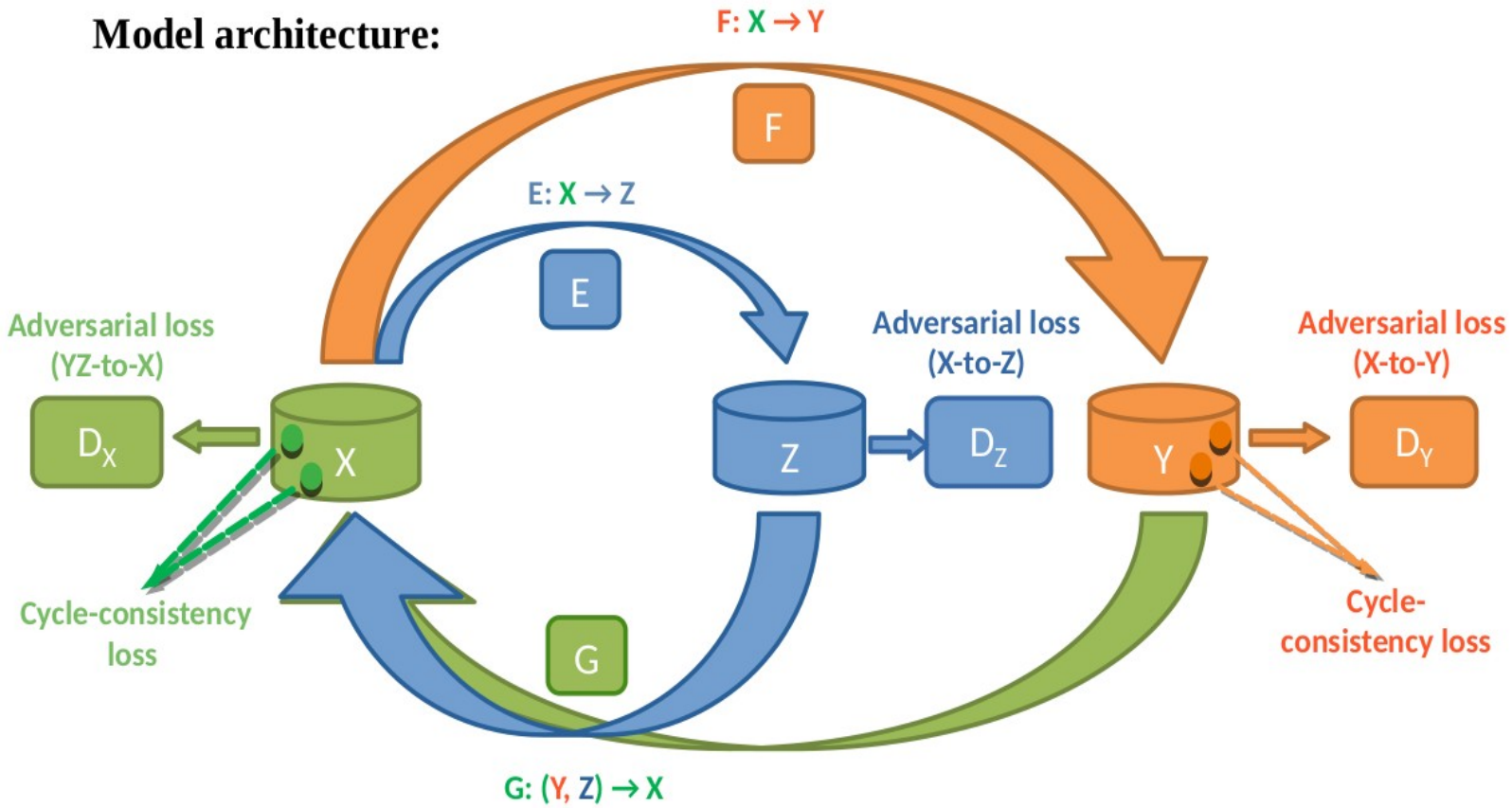


information-poor segmentation map domain $\mathcal{Y}$

Motivation

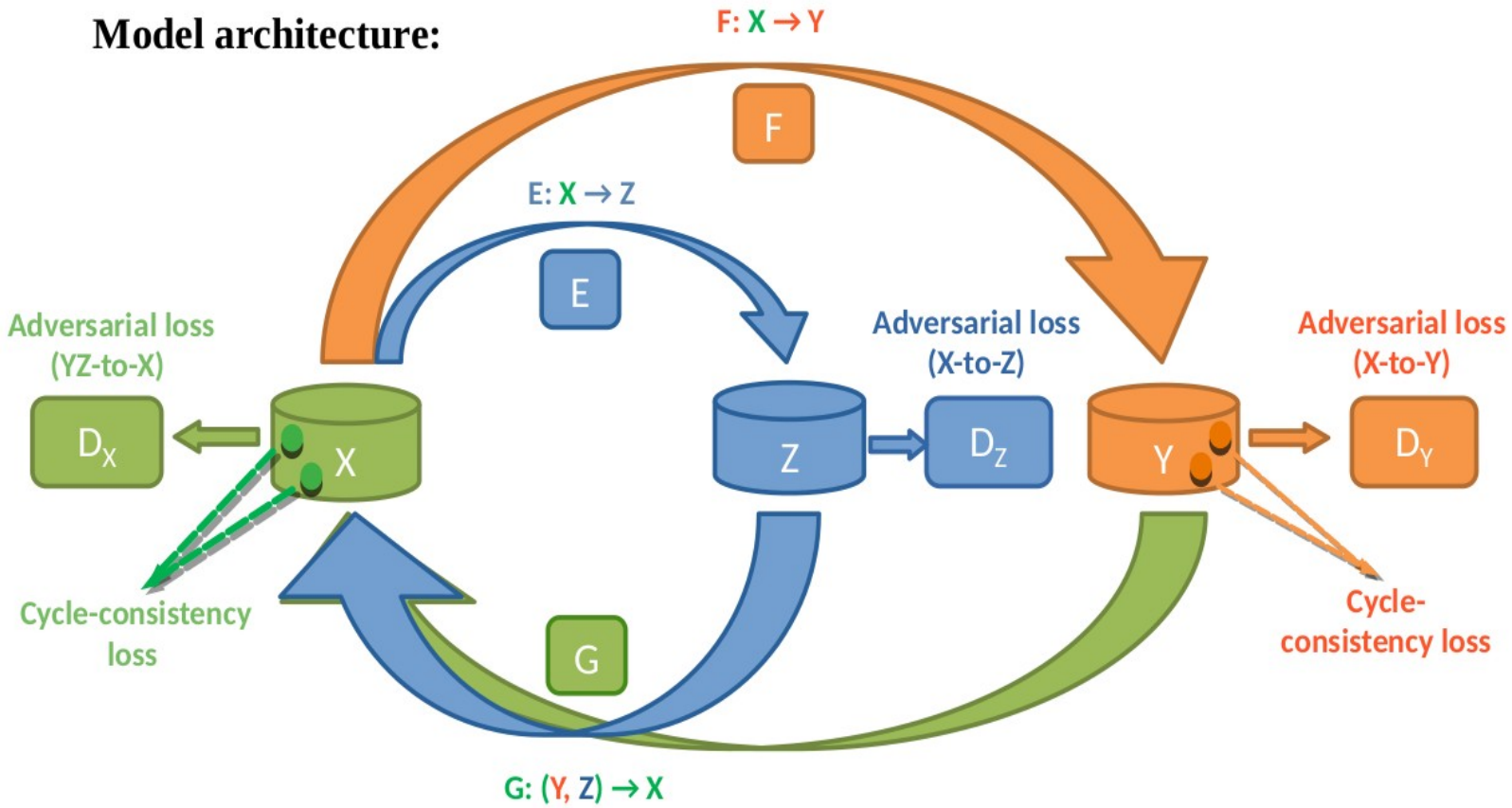

Model architecture:
F: X → Y
F
E: X → Z
E
Adversarial loss
(YZ-to-X)
Adversarial loss
(X-to-Z)
Adversarial loss
(X-to-Y)
D_X
X
Z
D_Z
Y
D_Y
Cycle-consistency
loss
Cycle-
consistency loss
G
G: (Y, Z) → X

Motivation



Inefficient architecture

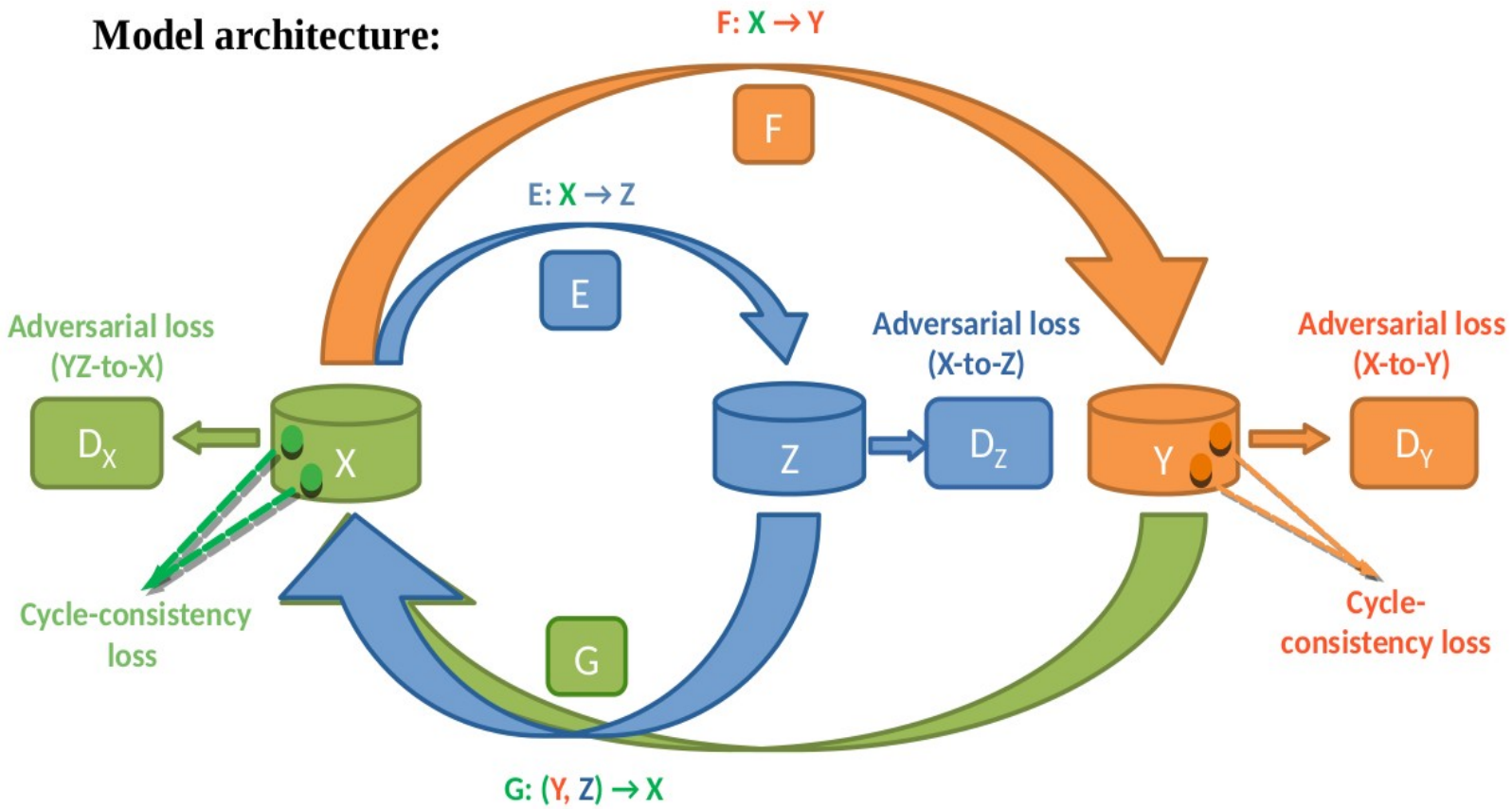
Motivation



Inefficient architecture

Large number of parameters

Motivation

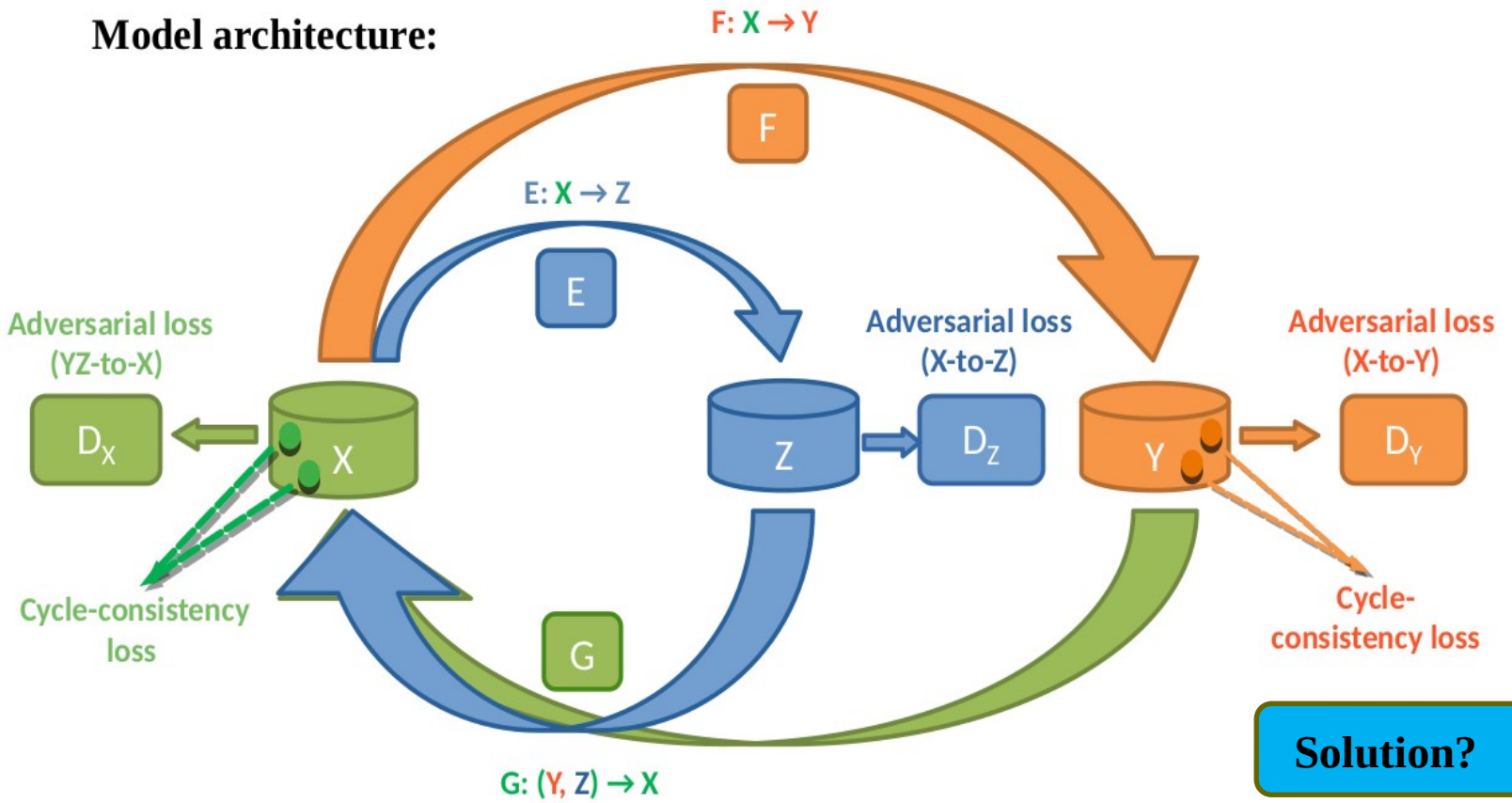


Inefficient architecture

Large number of parameters

Huge training complexity

Motivation



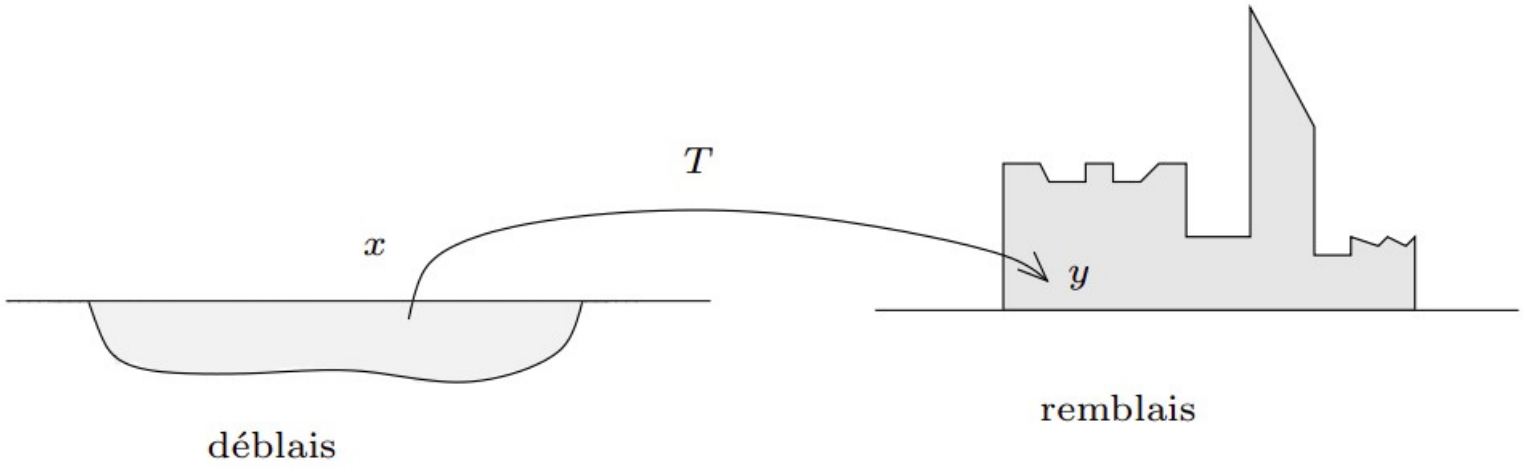
Solution?

Inefficient architecture

Large number of parameters

Huge training complexity

Optimal Transport



déblai : amount of material extracted from earth or mine

remblai : material input into a new construction

moving one distribution of mass to another as efficiently as possible

C. Villani, "Optimal Transport: Old and New", ***Springer Berlin Heidelberg***, 2008.

Ostrich: Optimal Transport Driven Asymmetric Image-to-Image Translation Approach

Total cost

$$K(G_\theta, F_\phi, E_\omega) = \int_{\mathcal{X}\times\mathcal{Y}\times\mathcal{Z}} \{\|x - G_\theta(y,z)\| + \|F_\phi(x) - y\| + \|E_\omega(x) - z\|\} d\pi^*(x,y,z)$$

$$= \frac{1}{3}\{\max_{\varphi}[\int_{\mathcal{X}} \varphi(x) d\mu(x) + \int_{\mathcal{Y}\times\mathcal{Z}} \inf_{x}[\|x - G_\theta(y,z)\| + \|F_\phi(x) - y\| + \|E_\omega(x) - z\| - \varphi(x)]$$

$$d(\nu \times \eta)(y,z)]$$

$$+ \max_{\psi}[\int_{\mathcal{Y}} \psi(y) d\nu(y) + \int_{\mathcal{X}} \inf_{y}[\|x - G_\theta(y,z)\| + \|F_\phi(x) - y\|\|E_\omega(x) - z\| - \psi(y)] d\mu(x)]$$

$$+ \max_{\xi}[\int_{\mathcal{Z}} \xi(z) d\eta(z) + \int_{\mathcal{X}} \inf_{z}[\|x - G_\theta(y,z)\| + \|F_\phi(x) - y\| + \|E_\omega(x) - z\| - \xi(z)] d\mu(x)]\}.$$

Primal form

Ostrich: Optimal Transport Driven Asymmetric Image-to-Image Translation Approach

Total cost

$$l(G_\theta, F_\phi, E_\omega; \varphi, \psi, \xi) = l_{GAN}(G_\theta, F_\phi, E_\omega; \varphi, \psi, \xi) + \lambda_2 l_{cycle}(G_\theta, F_\phi, E_\omega) + \lambda_1 l_{ssim}(F_\phi)$$

Ostrich: Optimal Transport Driven Asymmetric Image-to-Image Translation Approach

Total cost

$$l(G_\theta, F_\phi, E_\omega; \varphi, \psi, \xi) = l_{GAN}(G_\theta, F_\phi, E_\omega; \varphi, \psi, \xi) + \lambda_2 l_{cycle}(G_\theta, F_\phi, E_\omega) + \lambda_1 l_{ssim}(F_\phi)$$

Dual form of the primal formulation in previous slide

Ostrich: Optimal Transport Driven Asymmetric Image-to-Image Translation Approach

Total cost

$$l(G_\theta, F_\phi, E_\omega; \varphi, \psi, \xi) = l_{GAN}(G_\theta, F_\phi, E_\omega; \varphi, \psi, \xi) + \lambda_2 l_{cycle}(G_\theta, F_\phi, E_\omega) + \lambda_1 l_{ssim}(F_\phi)$$

Regularizer

Dual form

Ostrich: Optimal Transport Driven Asymmetric Image-to-Image Translation Approach

Total cost

$$l(G_\theta, F_\phi, E_\omega; \varphi, \psi, \xi) = l_{GAN}(G_\theta, F_\phi, E_\omega; \varphi, \psi, \xi) + \lambda_2 l_{cycle}(G_\theta, F_\phi, E_\omega) + \lambda_1 l_{ssim}(F_\phi)$$

GAN loss

Dual form

Ostrich: Optimal Transport Driven Asymmetric Image-to-Image Translation Approach

Total cost

$$l(G_\theta, F_\phi, E_\omega; \varphi, \psi, \xi) = l_{GAN}(G_\theta, F_\phi, E_\omega; \varphi, \psi, \xi) + \lambda_2 l_{cycle}(G_\theta, F_\phi, E_\omega) + \lambda_1 l_{ssim}(F_\phi)$$

GAN loss

$$l_{GAN}(G_\theta, F_\phi, E_\omega; \varphi, \psi, \xi) = \max_{\varphi \in Lip_1(\mathcal{X})} \left[\int_{\mathcal{X}} \varphi(x) d\mu(x) - \int_{\mathcal{Y}\times\mathcal{Z}} \varphi(G_\theta(y,z)) d(\nu \times \eta)(y,z) \right]$$

$$\max_{\psi \in Lip_1(\mathcal{Y})} \left[\int_{\mathcal{Y}} \psi(y) d\nu(y) - \int_{\mathcal{X}} \psi(F_\phi(x)) d\mu(x) \right] + \max_{\xi \in Lip_1(\mathcal{Z})} \left[\int_{\mathcal{Z}} \xi(z) d\eta(z) - \int_{\mathcal{X}} \xi(E_\omega(x)) d\mu(x) \right]$$

Dual form

Ostrich: Optimal Transport Driven Asymmetric Image-to-Image Translation Approach

Total cost

$$l(G_\theta, F_\phi, E_\omega; \varphi, \psi, \xi) = l_{GAN}(G_\theta, F_\phi, E_\omega; \varphi, \psi, \xi) + \lambda_2 l_{cycle}(G_\theta, F_\phi, E_\omega) + \lambda_1 l_{ssim}(F_\phi)$$

Cycle-consistency loss

Dual form

Ostrich: Optimal Transport Driven Asymmetric Image-to-Image Translation Approach

Total cost

$$l(G_\theta, F_\phi, E_\omega; \varphi, \psi, \xi) = l_{GAN}(G_\theta, F_\phi, E_\omega; \varphi, \psi, \xi) + \lambda_2 l_{cycle}(G_\theta, F_\phi, E_\omega) + \lambda_1 l_{ssim}(F_\phi)$$

Cycle-consistency loss

$$l_{cycle}(G_\theta, F_\phi, E_\omega) = \int_{\mathcal{X}} \|x - G_\theta{}^z(F_\phi(x))\| d\mu(x) + \int_{\mathcal{X}} \|x - G_{\theta_y}(E_\omega(x))\| d\mu(x)$$

$$+ \int_{\mathcal{Y}} \|y - F_\phi(G_\theta{}^z(y))\| d\nu(y) + \int_{\mathcal{Z}} \|z - E_\omega(G_{\theta_y}(z))\| d\eta(z)$$

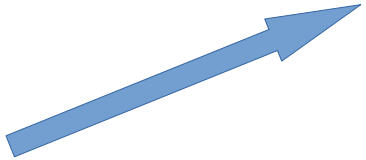
Dual form

Ostrich: Optimal Transport Driven Asymmetric Image-to-Image Translation Approach

Total cost

$$l(G_\theta, F_\phi, E_\omega; \varphi, \psi, \xi) = l_{GAN}(G_\theta, F_\phi, E_\omega; \varphi, \psi, \xi) + \lambda_2 l_{cycle}(G_\theta, F_\phi, E_\omega) + \lambda_1 l_{ssim}(F_\phi)$$

SSIM loss



Dual form

Ostrich: Optimal Transport Driven Asymmetric Image-to-Image Translation Approach

Total cost

$$l(G_\theta, F_\phi, E_\omega; \varphi, \psi, \xi) = l_{GAN}(G_\theta, F_\phi, E_\omega; \varphi, \psi, \xi) + \lambda_2 l_{cycle}(G_\theta, F_\phi, E_\omega) + \lambda_1 l_{ssim}(F_\phi)$$

SSIM loss

$$l_{ssim}(F_\phi) = \|1 - SSIM(F_\phi(x), VO(f_{rgb}^{hed}(x)[:, :, 0]))\|$$

Dual form

Ostrich: Optimal Transport Driven Asymmetric Image-to-Image Translation Approach

Theorem 6.1. *If the sections of generator G_θ, that is, G_{θ_y} and $G_\theta{}^z$, are considered to be the inverse operators of forward operators E_ω and F_ϕ, respectively, that is, $G_{\theta_y} = E_\omega{}^{-1}$ and $G_\theta{}^z = F_\phi{}^{-1}$ and $G_\theta{}^z$ is a p-Lipschitz functions in domain $\mathcal{Y}$, then the problem with $p = 1$, can be represented by the following equivalent problem:*

$$\min_{\phi,\omega} \max_{\psi,\xi} l(F_\phi, E_\omega; \psi, \xi)$$

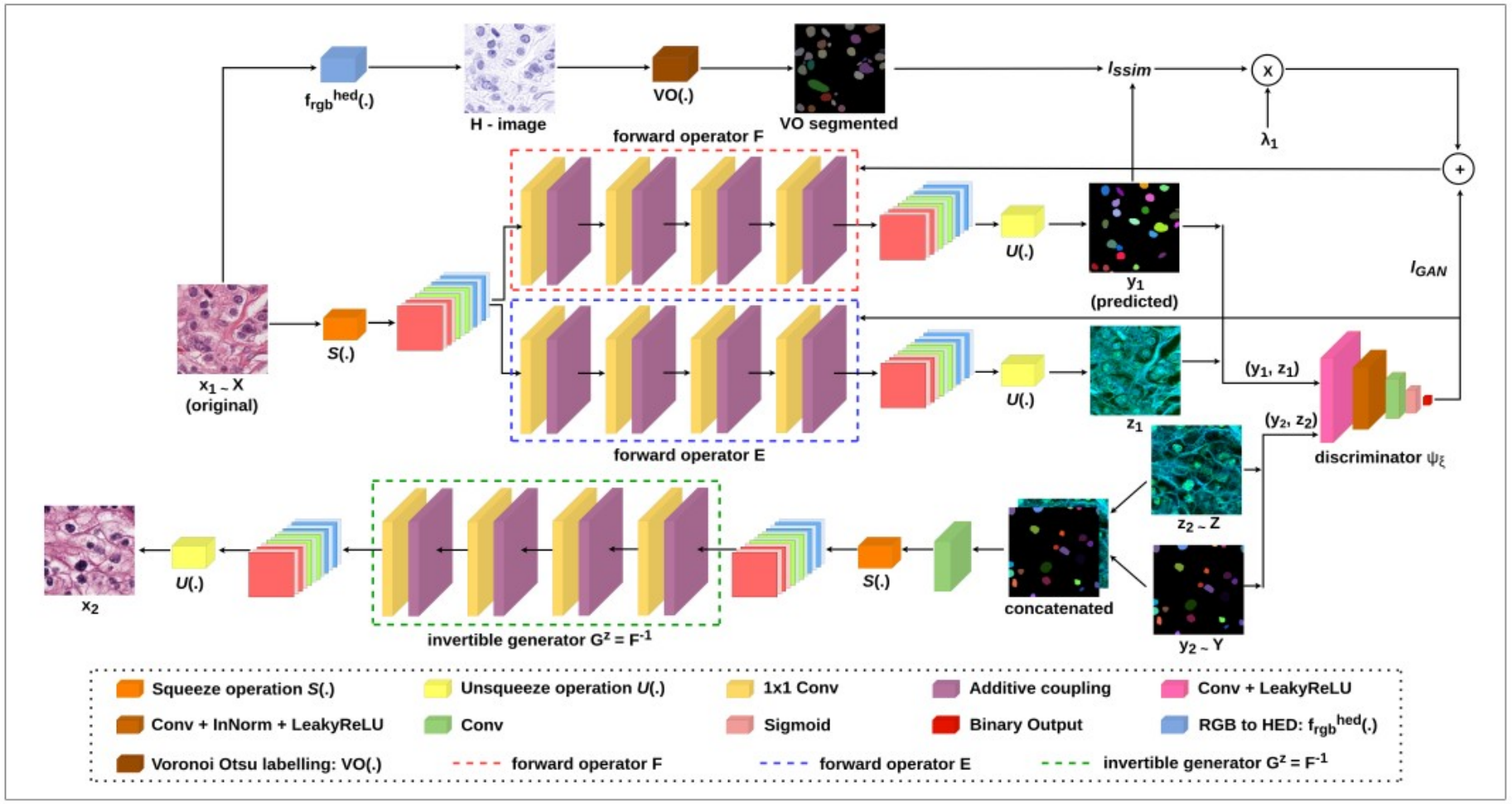
$$\textit{where} \quad l(F_\phi, E_\omega; \psi, \xi) = 2l_{GAN}(F_\phi; \psi) + l_{GAN}(E_\omega; \xi) + \lambda_1 l_{ssim}(F_\phi)$$

and

$$l_{GAN}(F_\phi; \psi) = \max_{\psi \in Lip_1(\mathcal{Y})} \int_{\mathcal{Y}} \psi(y) d\nu(y) - \int_{\mathcal{X}} \psi(F_\phi(x)) d\mu(x),$$

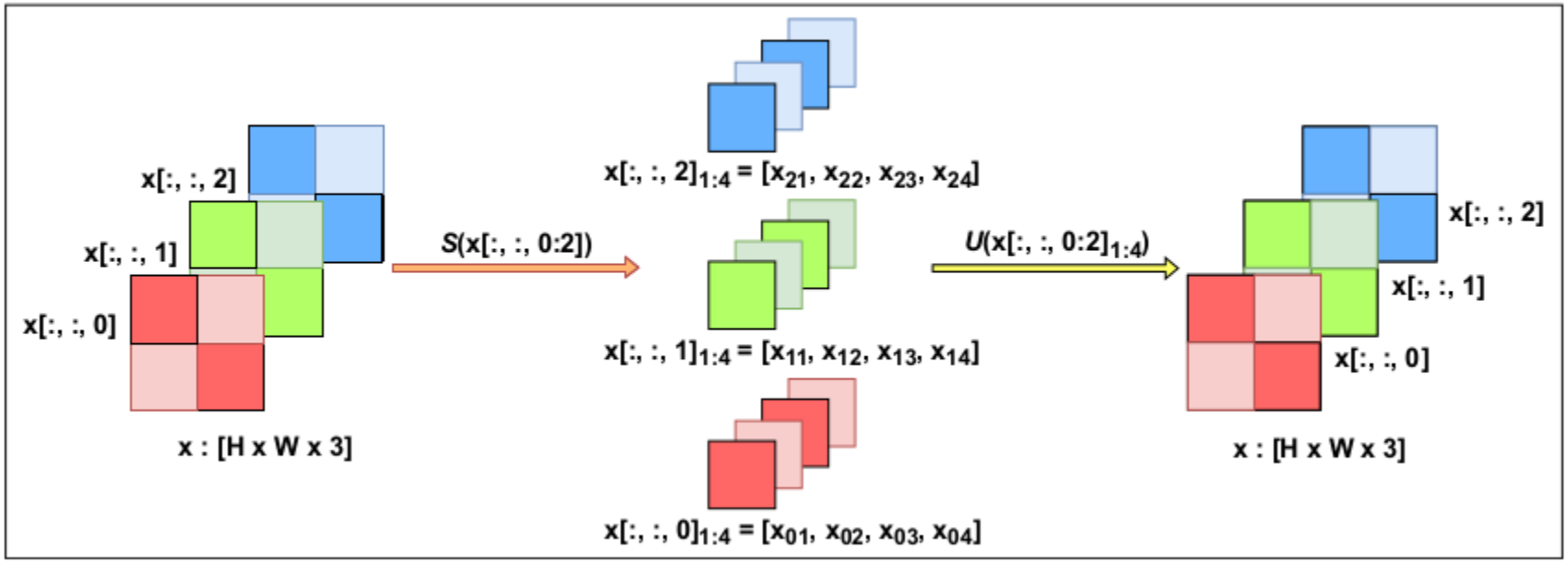
$$l_{GAN}(E_\omega; \xi) = \max_{\xi \in Lip_1(\mathcal{Z})} \int_{\mathcal{Z}} \xi(z) d\eta(z) - \int_{\mathcal{X}} \xi(E_\omega(x)) d\mu(x).$$

Block Diagram: Ostrich



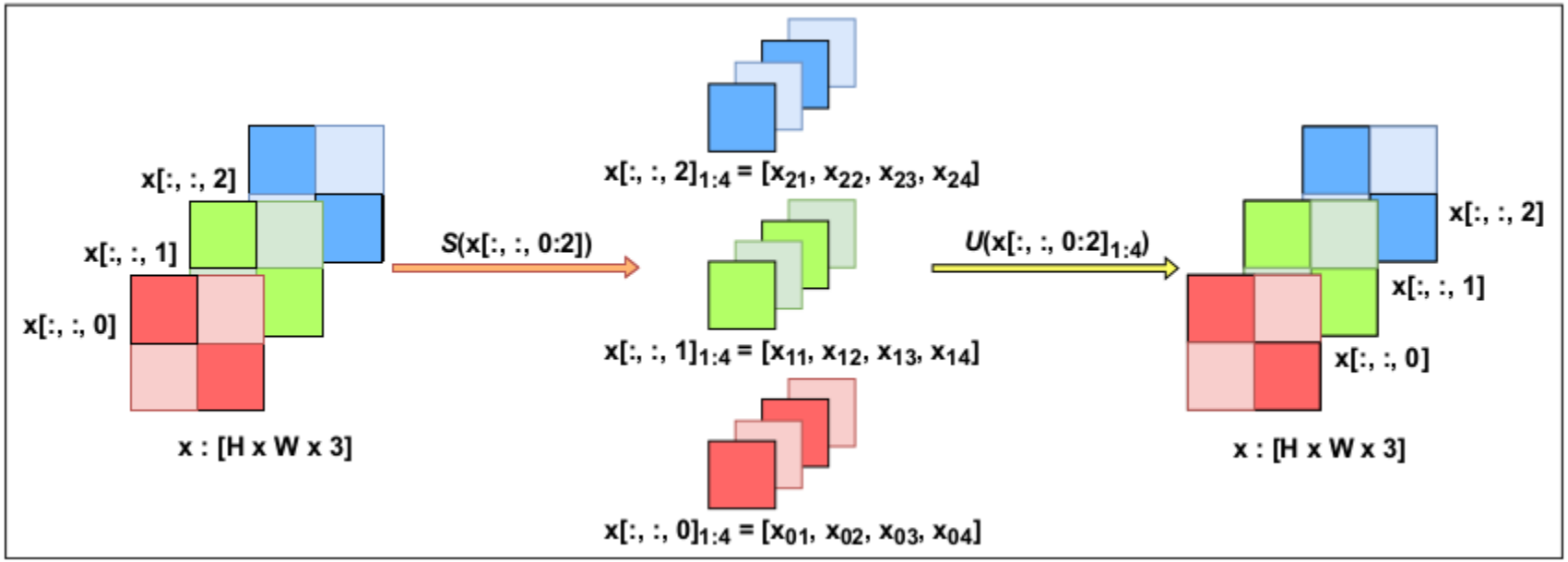
Ostrich: Optimal Transport Driven Asymmetric Image-to-Image Translation Approach

Spatially constrained squeeze operation



Ostrich: Optimal Transport Driven Asymmetric Image-to-Image Translation Approach

Spatially constrained squeeze operation



Squeeze operation

$$[x[:,:,0]_{1:4}, x[:,:,1]_{1:4}, x[:,:,2]_{1:4}] = S(x[:,:,0:2]) = S(x)$$

Unsqueeze operation

$$x = U([x[:,:,0:2]_{1:4}]).$$

Description of Data Sets

- **TCGA** (The Cancer Genome Atlas) - cropped from nuclei-dense regions of WSIs : Total number of images = **30**
- Data specifications: hematoxylin and eosin (H&E) stained images.
- Each image has a resolution of 1000 × 1000.
- Associated nuclei instance segmentation and binary semantic segmentation maps.
- Multi-organ data : images correspond to different organs, such as, kidney, lung, liver, prostate etc.

N. Kumar *et al*., "A dataset and a technique for generalized nuclear segmentation for computational pathology", *IEEE Transactions on Medical Imaging*, 36(7), pp. 1550-1560, 2017.

Description of Data Sets

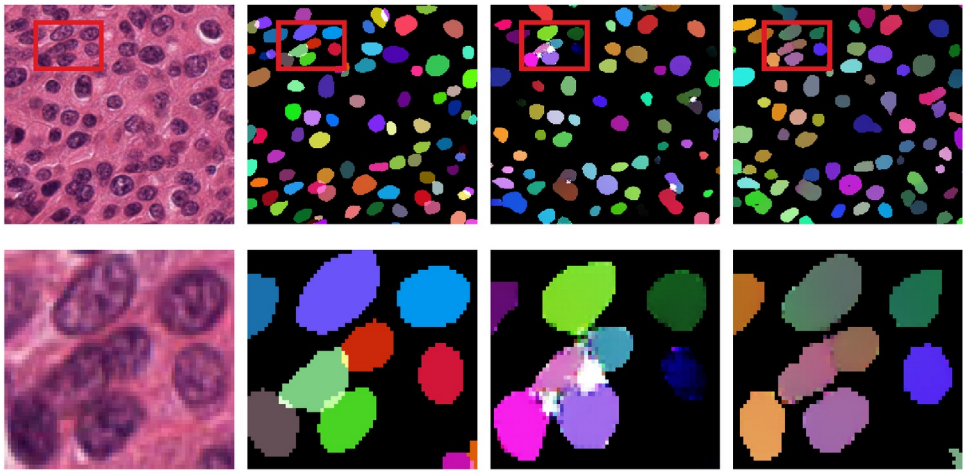
- **CoNIC** (Colon Nuclei Identification and Counting Challenge, 2022) – published as a challenge data set : Total number of image patch samples = **4981**
- Data specifications: hematoxylin and eosin (H&E) stained images.
- Each image has a resolution of 256 × 256.
- Associated nuclei instance segmentation maps in grayscale.
- Colon cancer data : images correspond to colon.

S. Graham *et al*., "Conic: colon nuclei identification and counting challenge, 2022", *arXiv preprint arXiv: 2111.14485*, 2021.

Performance on TCGA Data

Ablation study

Qualitative performance analysis in nuclei instance segmentation : (a) Original image, (b) Ground-truth; Segmentation performance of (c) "Ostrich \ R" and (d) Ostrich



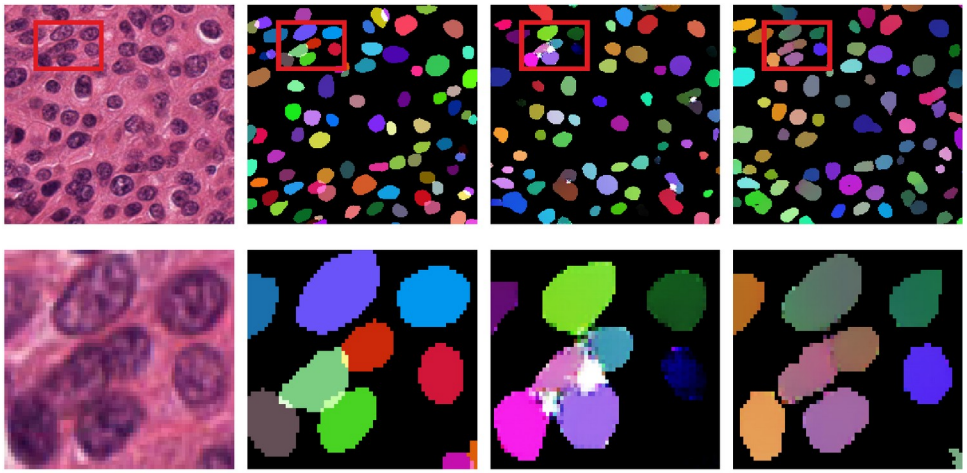
(a) (b) (c) (d)

R = $l_{ssim}(F_\phi)$

Performance on TCGA Data

Ablation study

Qualitative performance analysis in nuclei instance segmentation : (a) Original image, (b) Ground-truth; Segmentation performance of (c) "Ostrich \ R" and (d) Ostrich



(a) (b) (c) (d)

R = $l_{ssim}(F_\phi)$

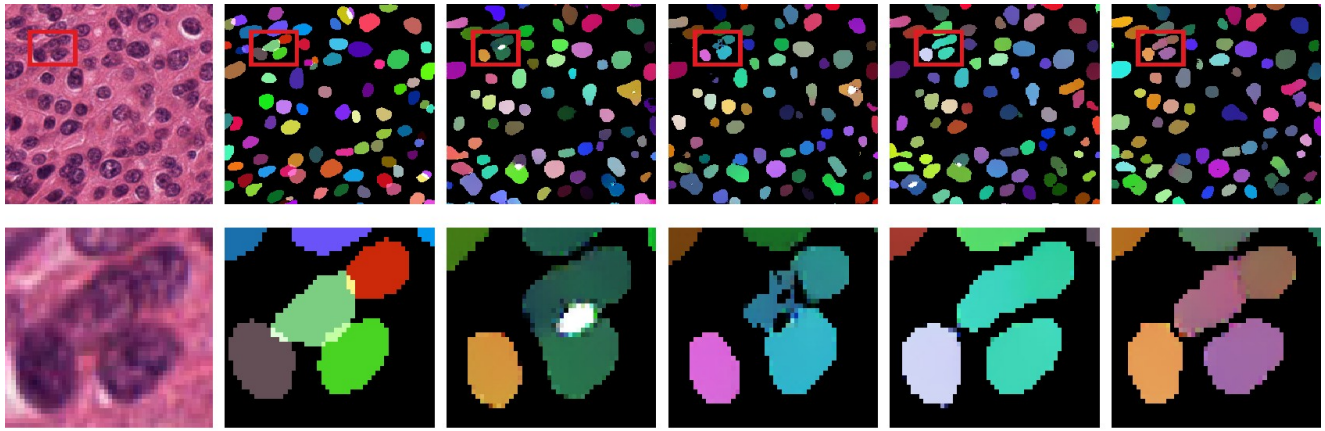
Quantitative performance analysis of "Ostrich \ R" and Ostrich in nuclei instance segmentation

Methods	Dice	Jaccard	Precision	Recall
Ostrich $\setminus R$	0.761814	0.606573	0.791683	0.734116
Ostrich	**0.788035**	**0.641520**	**0.813523**	**0.764096**

Performance on TCGA Data

Comparison with Baseline Methods

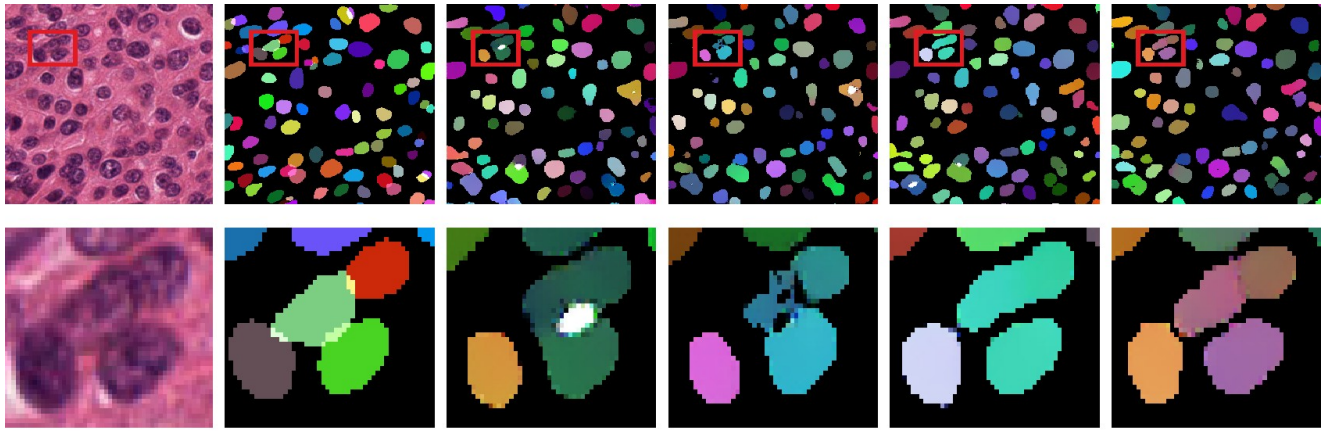
Qualitative performance analysis in nuclei instance segmentation : (a) Original image, (b) Ground-truth; Segmentation performance of (c) CycleGAN, (d) OT-CycleGAN, (e) Asym-CycleGAN and (f) Ostrich



Performance on TCGA Data

Comparison with Baseline Methods

Qualitative performance analysis in nuclei instance segmentation : (a) Original image, (b) Ground-truth; Segmentation performance of (c) CycleGAN, (d) OT-CycleGAN, (e) Asym-CycleGAN and (f) Ostrich



(a) (b) (c) (d) (e) (f)

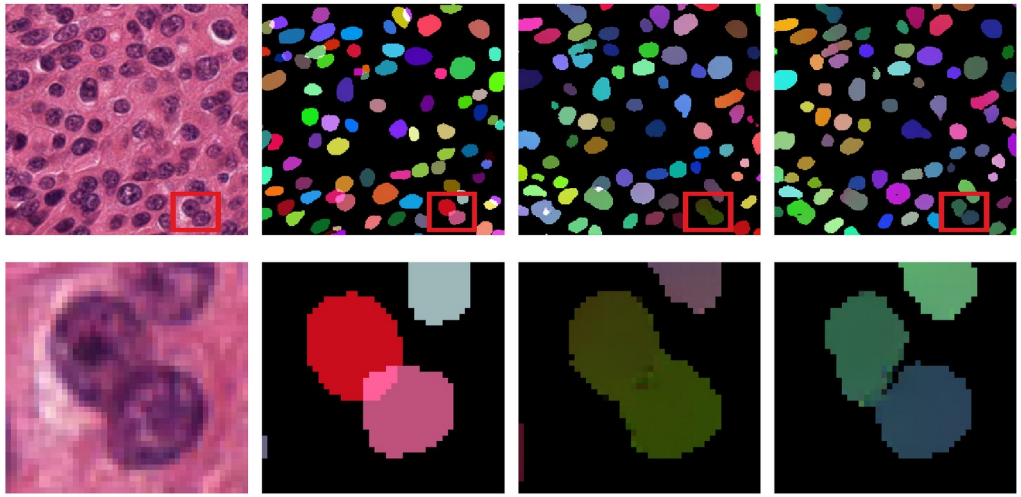
Quantitative performance analysis of CycleGAN, OT-CycleGAN, Asym-CycleGAN and Ostrich in nuclei instance segmentation

Methods	No. of params (M)	Dice	Jaccard	Precision	Recall
CycleGAN	18.035	0.754221	0.598782	0.764761	0.743967
OT-CycleGAN	4.353	0.766668	0.614903	0.804106	0.732561
Asym-CycleGAN	27.053	0.783812	0.638815	0.806971	0.761945
Ostrich	7.271	**0.788035**	**0.641520**	**0.813523**	**0.764096**

Performance on TCGA Data

Importance of Spatially-Constrained Squeeze Operation

Qualitative performance analysis in nuclei instance segmentation : (a) Original image, (b) Ground-truth; Segmentation performance of (c) Checkerboard masking and (d) Ostrich

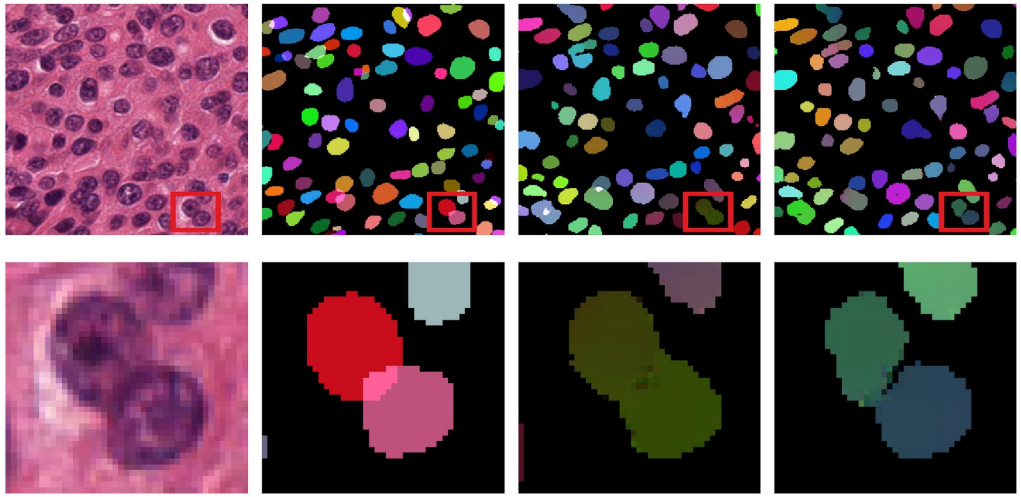


(a) (b) (c) (d)

Performance on TCGA Data

Importance of Spatially-Constrained Squeeze Operation

Qualitative performance analysis in nuclei instance segmentation : (a) Original image, (b) Ground-truth; Segmentation performance of (c) Checkerboard masking and (d) Ostrich



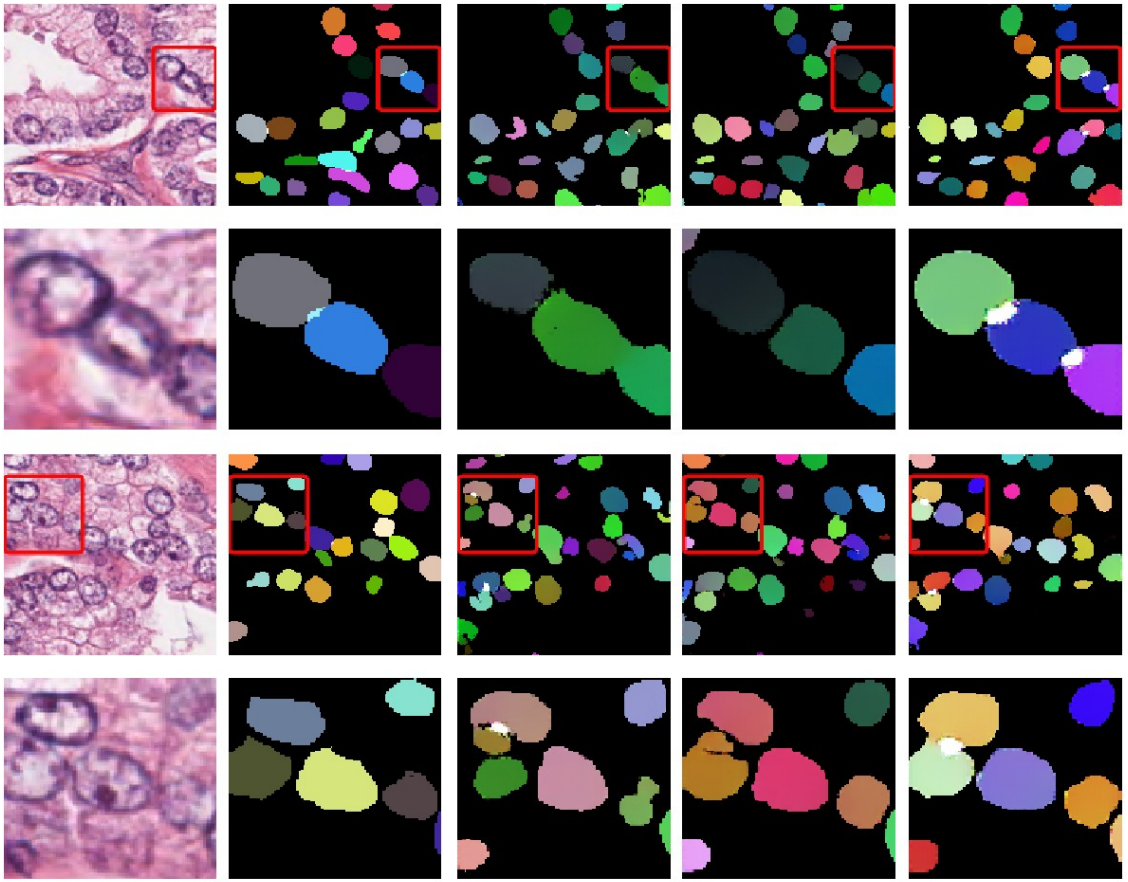
(a) (b) (c) (d)

Quantitative performance analysis of checkerboard masking and Ostrich in nuclei instance segmentation

Method	Dice	Jaccard	Precision	Recall
Checkerboard	0.772020	0.629522	0.785028	0.759437
Ostrich	**0.788035**	**0.641520**	**0.813523**	**0.764096**

Performance on TCGA Data

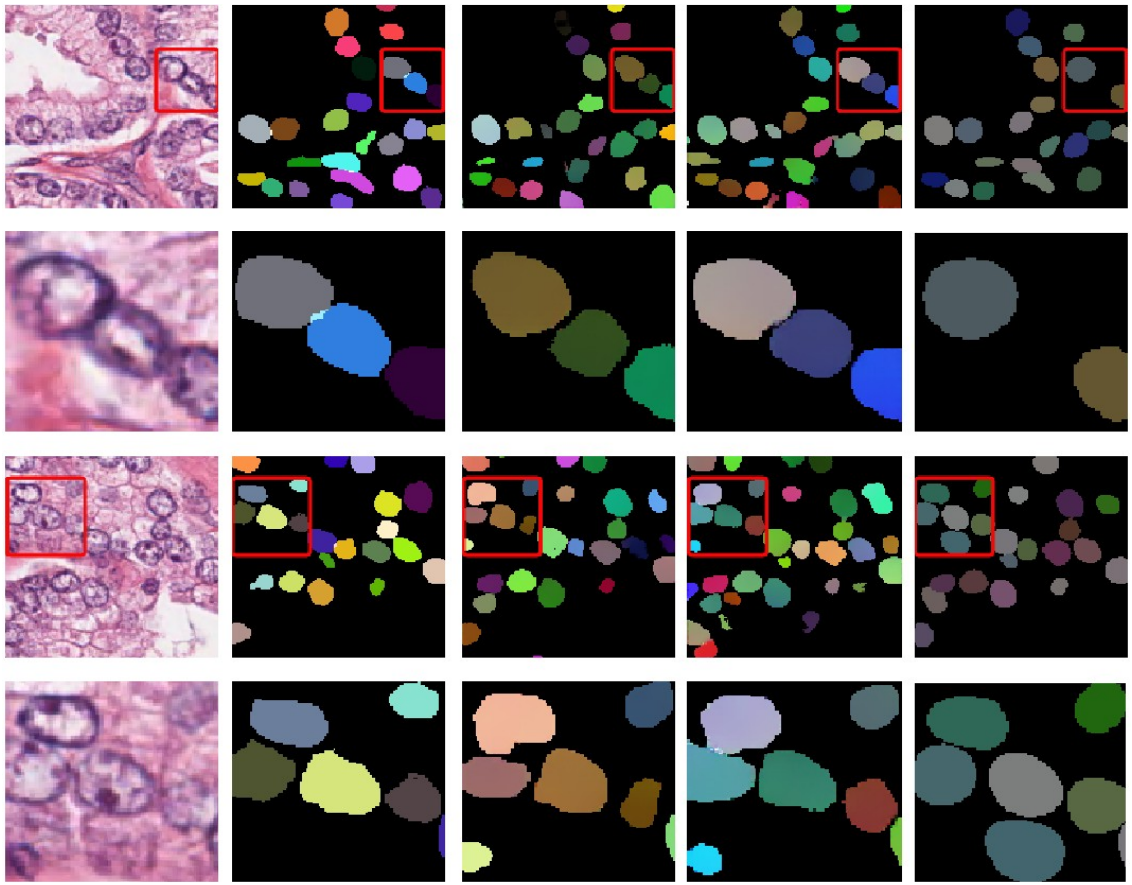
Comparison with Existing Methods



Qualitative performance analysis in nuclei instance segmentation : (a) Original image, (b) Ground-truth; Segmentation performance of (c) U-Net, (d) Mask-R-CNN, (e) U-Net++

Performance on TCGA Data

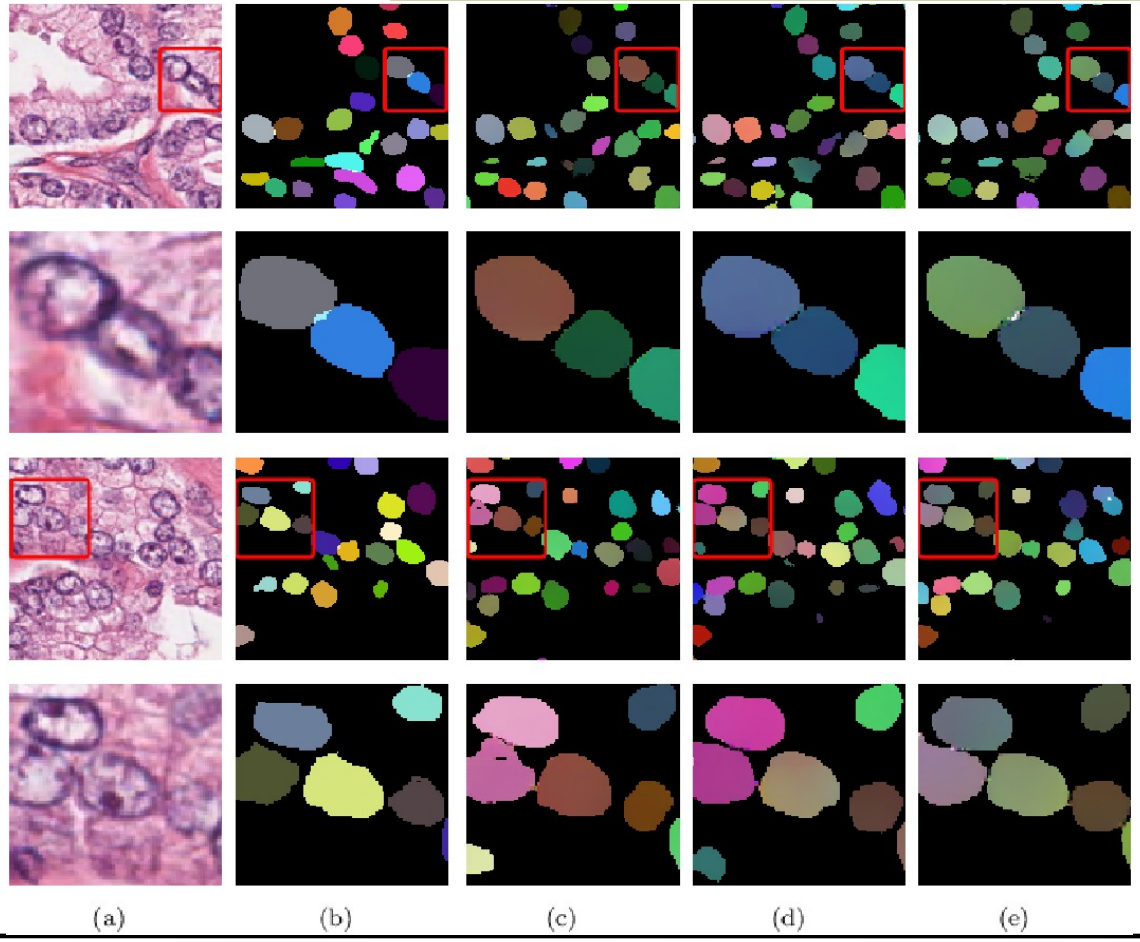
Comparison with Existing Methods



Qualitative performance analysis in nuclei instance segmentation : (a) Original image, (b) Ground-truth; Segmentation performance of (c) HoVer-Net, (d) MoNS, (e) Stardist

Performance on TCGA Data

Comparison with Existing Methods



Qualitative performance analysis in nuclei instance segmentation : (a) Original image, (b) Ground-truth; Segmentation performance of (c) Swin-MIL, (d) BoNuS, (e) Ostrich

Performance on TCGA Data

Comparison with Existing Methods

Quantitative performance analysis of different formulations, U-Net, Mask-R-CNN, U-Net++, HoVer-Net, MoNS, Stardist, Swin-MIL, BoNuS and Ostrich in nuclei instance segmentation

Methods	Dice	Jaccard	Precision	Recall
Ostrich	**0.788035**	**0.641520**	**0.813523**	0.764096
Ostrich $\setminus R$	0.761814	0.606573	0.791683	0.734116
CycleGAN	0.754221	0.598782	0.764761	0.743967
OT-CycleGAN	0.766668	0.614903	0.804106	0.732561
Asym-CycleGAN	0.783812	0.638815	0.806971	0.761945
Checkerboard	0.772020	0.629522	0.785028	0.759437
U-Net	0.645650	0.446128	0.624558	0.668216
Mask-R-CNN	0.747086	0.585659	0.799975	0.700757
U-Net++	0.773155	0.620294	0.796708	0.750955
HoVer-Net	0.744516	0.586780	0.811804	0.687529
MoNS	0.755509	0.614706	0.748012	0.763157
Stardist	0.743228	0.585713	0.811579	0.685495
Swin-MIL	0.749044	0.593266	0.801989	0.702656
BoNuS	0.784740	0.639496	0.806351	**0.764257**

BoNuS performs slightly better than Ostrich with respect to **recall**

Performance on TCGA Data

Comparison with Existing Methods

Quantitative performance analysis of different formulations, U-Net, Mask-R-CNN, U-Net++, HoVer-Net, MoNS, Stardist, Swin-MIL, BoNuS and Ostrich in nuclei instance segmentation

Methods	Dice	Jaccard	Precision	Recall
Ostrich	**0.788035**	**0.641520**	**0.813523**	0.764096
Ostrich $\setminus R$	0.761814	0.606573	0.791683	0.734116
CycleGAN	0.754221	0.598782	0.764761	0.743967
OT-CycleGAN	0.766668	0.614903	0.804106	0.732561
Asym-CycleGAN	0.783812	0.638815	0.806971	0.761945
Checkerboard	0.772020	0.629522	0.785028	0.759437
U-Net	0.645650	0.446128	0.624558	0.668216
Mask-R-CNN	0.747086	0.585659	0.799975	0.700757
U-Net++	0.773155	0.620294	0.796708	0.750955
HoVer-Net	0.744516	0.586780	0.811804	0.687529
MoNS	0.755509	0.614706	0.748012	0.763157
Stardist	0.743228	0.585713	0.811579	0.685495
Swin-MIL	0.749044	0.593266	0.801989	0.702656
BoNuS	0.784740	0.639496	0.806351	**0.764257**

Ostrich outperforms state-of-the-art methods w.r.t. **Dice**, **Jaccard** and **Precision**

Performance on TCGA Data

Statistical Significance test: paired-*t*

Methods	Dice	Jaccard	Precision	Recall
Ostrich \R	9.88E-30	3.41E-30	1.44E-09	1.30E-10
CycleGAN	4.88E-32	3.39E-34	3.69E-32	8.40E-10
OT-CycleGAN	2.90E-33	2.26E-33	1.04E-05	6.73E-21
Asym-CycleGAN	*6.49E-02*	*5.42E-02*	5.43E-05	*8.31E-02*
Checkerboard	4.66E-13	5.70E-14	1.83E-61	1.10E-02
U-Net	6.67E-30	4.18E-36	1.25E-76	6.68E-06
Mask-R-CNN	1.17E-37	4.55E-39	3.77E-05	1.28E-25
U-Net++	1.08E-17	3.86E-18	5.03E-09	7.46E-03
HoVer-Net	1.77E-41	7.41E-45	*2.37E-01*	7.65E-54
MoNS	1.10E-14	1.84E-15	3.34E-48	*1.21E-01*
Stardist	1.46E-24	8.26E-26	*3.09E-01*	9.93E-27
Swin-MIL	1.95E-37	1.64E-41	1.74E-03	3.25E-49
BoNuS	*1.42E-01*	*1.05E-01*	9.20E-07	*9.43E-01*

Out of 52 cases, performs significantly better in 42 cases, better but not significantly in 9 cases

Performance on TCGA Data

Statistical Significance test: Wilcoxon

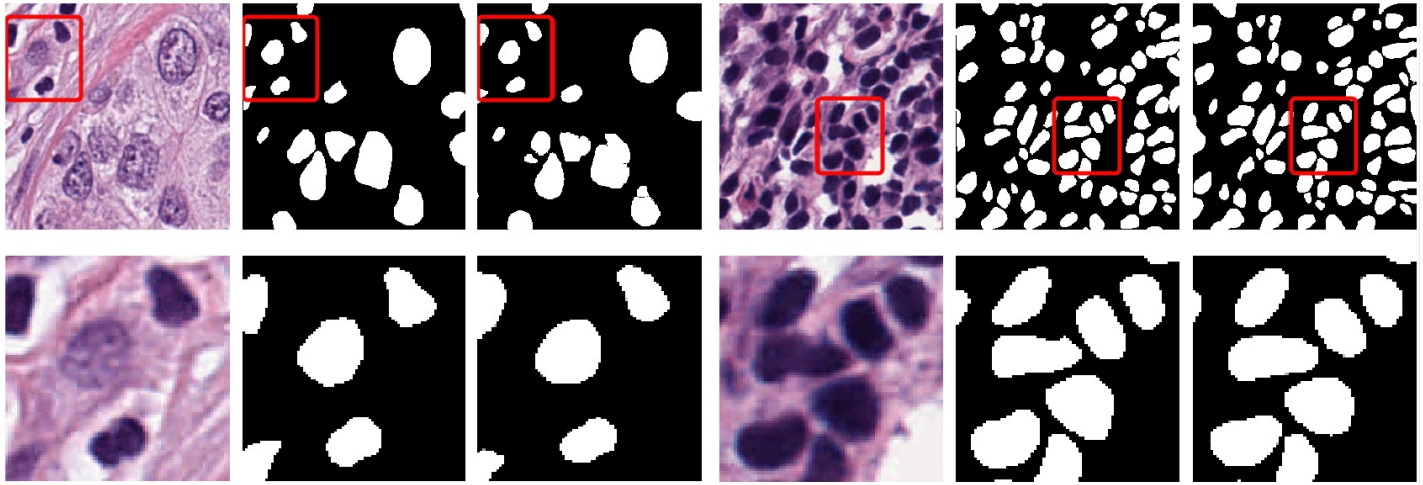
Methods	Dice	Jaccard	Precision	Recall
Ostrich \R	2.37E-23	2.34E-23	5.57E-07	2.01E-09
CycleGAN	9.05E-27	6.08E-27	1.66E-30	7.70E-10
OT-CycleGAN	8.58E-25	6.83E-25	7.49E-04	6.37E-18
Asym-CycleGAN	*8.56E-02*	*7.80E-02*	1.13E-03	*7.67E-02*
Checkerboard	7.74E-13	2.49E-13	8.57E-33	1.21E-02
U-Net	8.61E-32	7.06E-32	1.89E-33	4.45E-02
Mask-R-CNN	2.74E-28	3.20E-28	1.55E-03	1.41E-20
U-Net++	9.70E-17	6.71E-17	2.86E-07	1.88E-03
HoVer-Net	1.63E-30	1.23E-30	*6.85E-02*	4.13E-32
MoNS	1.46E-13	3.65E-14	2.11E-33	*1.10E-01*
Stardist	7.73E-22	6.91E-22	*3.40E-01*	3.03E-23
Swin-MIL	9.15E-32	8.48E-32	3.83E-02	1.47E-32
BoNuS	*8.18E-02*	*5.86E-02*	7.36E-06	*9.00E-01*

Out of 52 cases, performs significantly better in 42 cases, better but not significantly in 9 cases

Performance on TCGA Data

Performance in Binary Semantic Segmentation

Qualitative performance analysis in binary semantic segmentation :
(a) Original image 1, (b) Ground-truth 1, Segmentation performance of (c) Ostrich on image 1;
(d) Original image 2, (e) Ground-truth 2, Segmentation performance of (f) Ostrich on image 2;



(a) (b) (c) (d) (e) (f)

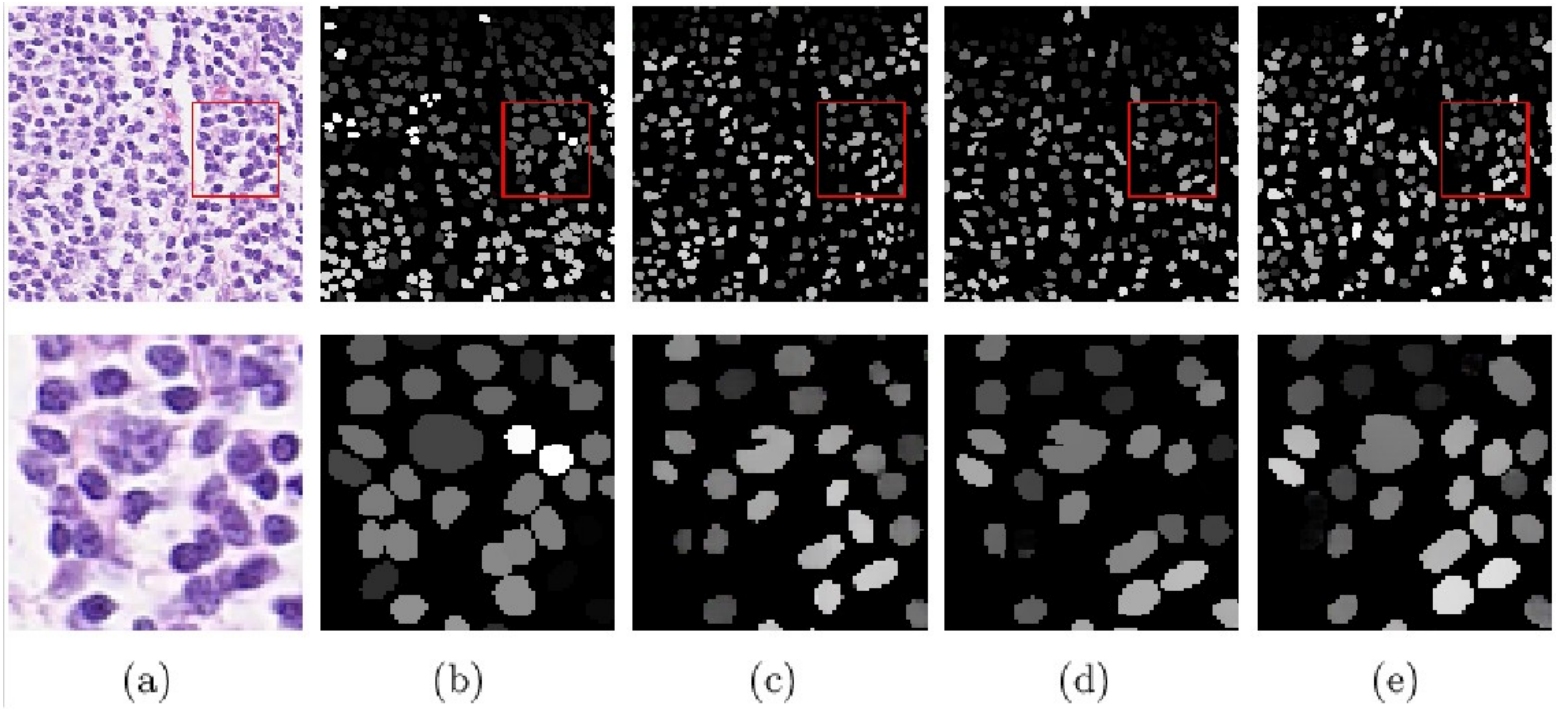
Quantitative performance analysis of Ostrich in binary semantic segmentation

Model	Dice	Jaccard	Precision	Recall
Ostrich	0.810099	0.746830	0.817761	0.802580

Performance on CoNIC Data

Comparison with Existing Methods

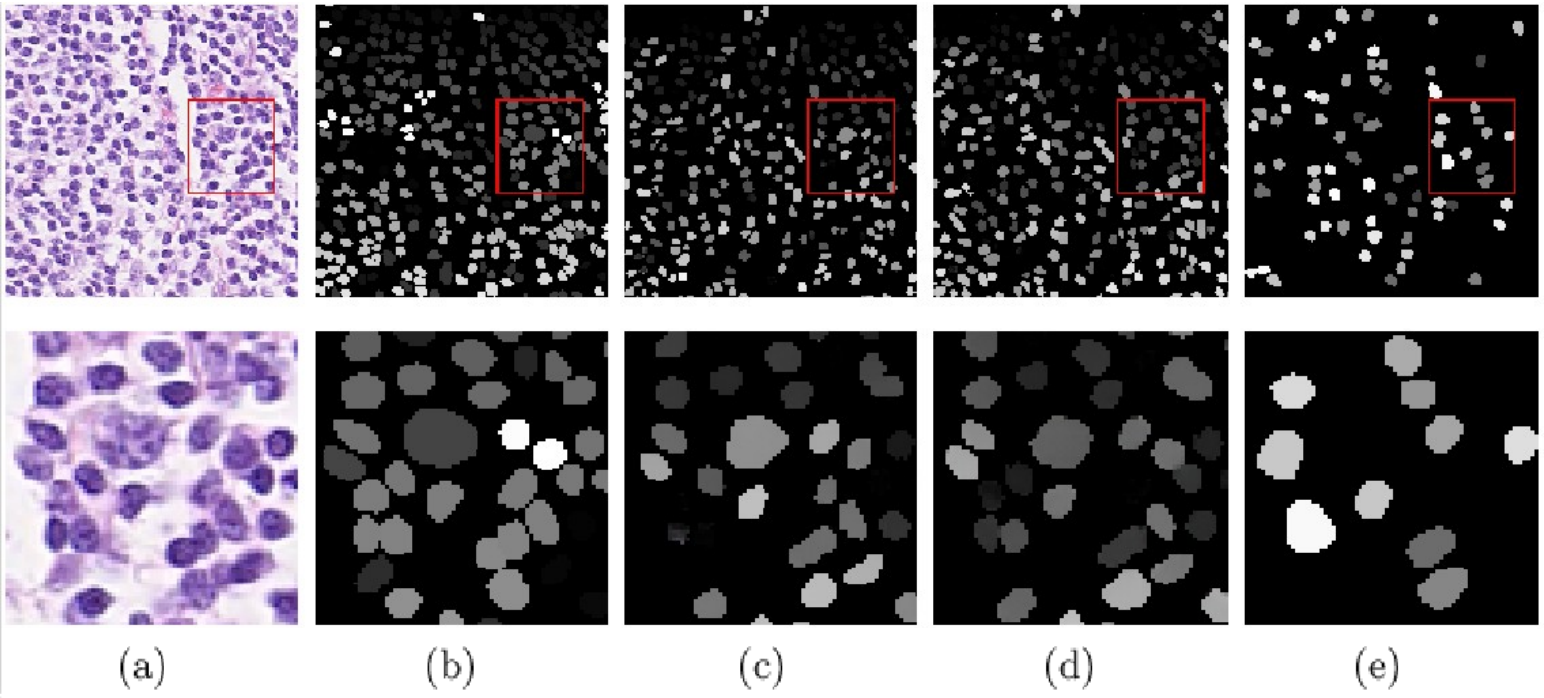
Qualitative performance analysis in nuclei instance segmentation : (a) Original image, (b) Ground-truth; Segmentation performance of (c) U-Net, (d) Mask-R-CNN, (e) U-Net++



Performance on CoNIC Data

Comparison with Existing Methods

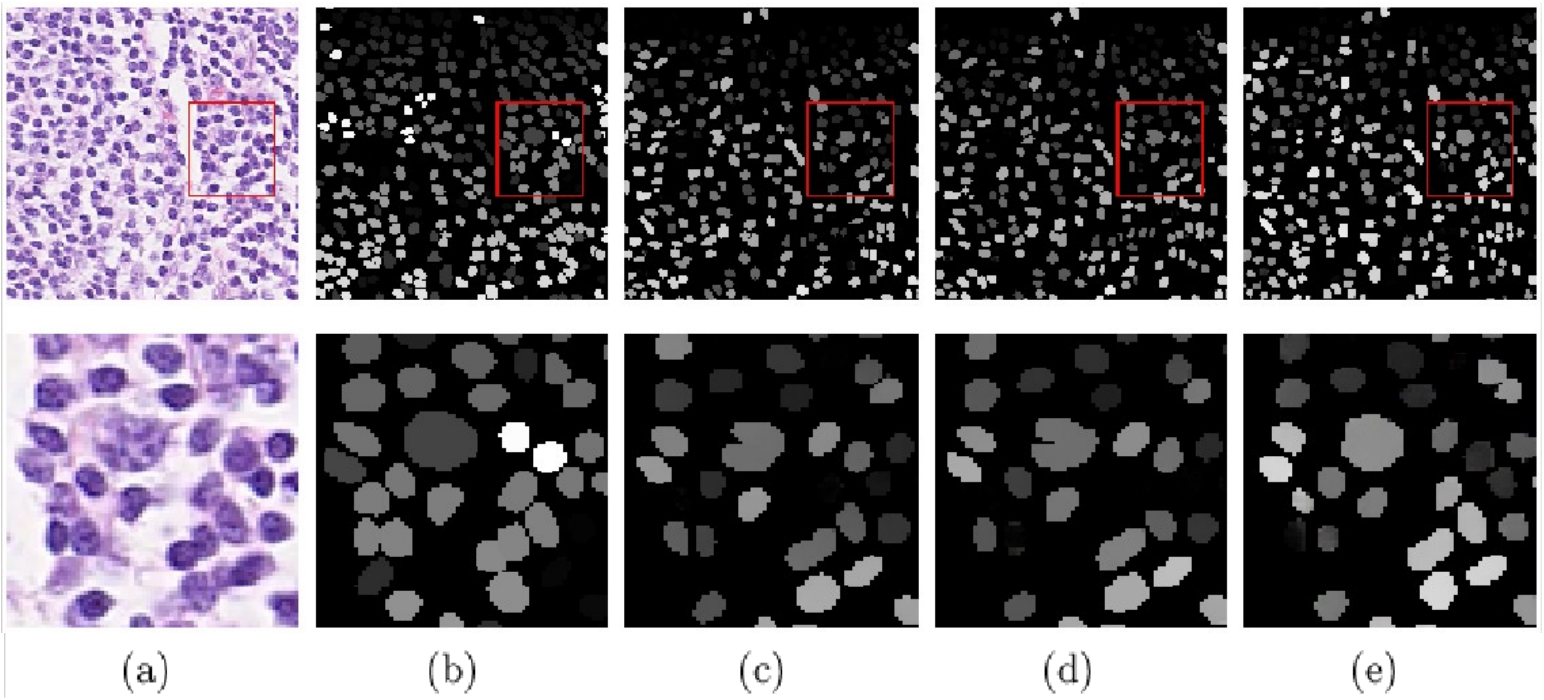
Qualitative performance analysis in nuclei instance segmentation : (a) Original image, (b) Ground-truth; Segmentation performance of (c) HoVer-Net, (d) MoNS, (e) Stardist



Performance on CoNIC Data

Comparison with Existing Methods

Qualitative performance analysis in nuclei instance segmentation : (a) Original image, (b) Ground-truth; Segmentation performance of (c) Swin-MIL, (d) BoNuS, (e) Ostrich



Performance on CoNIC Data

Comparison with Existing Methods

Quantitative performance analysis of U-Net, Mask-R-CNN, U-Net++, HoVer-Net, MoNS, Stardist, Swin-MIL, BoNuS and Ostrich in nuclei instance segmentation

Methods	Dice	Jaccard	Precision	Recall
Ostrich	**0.741107**	**0.591310**	**0.769381**	**0.793093**
U-Net	0.715636	0.561178	0.704462	0.681140
Mask-R-CNN	0.717821	0.562671	0.725431	0.706849
U-Net++	0.721316	0.568022	0.721591	0.706789
HoVer-Net	0.740318	0.590560	0.747550	0.698034
MoNS	0.722989	0.568692	0.722632	0.733005
Stardist	0.374534	0.240549	0.716413	0.275528
Swin-MIL	0.715991	0.560825	0.764054	0.682995
BoNuS	0.724678	0.571128	0.753906	0.768233

Ostrich outperforms state-of-the-art methods w.r.t. all evaluation indices

Performance on CoNIC Data

Statistical Significance test: paired-*t*

Methods	Dice	Jaccard	Precision	Recall
U-Net	1.21E-85	1.27E-86	9.99E-99	9.99E-99
Mask-R-CNN	9.99E-99	1.11E-99	9.99E-99	9.99E-99
U-Net++	1.02E-63	2.46E-87	9.99E-99	9.99E-99
HoVer-Net	*8.81E-02*	*1.44E-01*	4.57E-98	9.99E-99
MoNS	9.99E-99	9.99E-99	9.99E-99	9.99E-99
Stardist	9.99E-99	1.11E-99	1.24E-82	9.99E-99
Swin-MIL	9.99E-99	9.99E-99	5.75E-20	9.99E-99
BoNuS	4.28E-78	1.12E-93	9.99E-99	9.99E-99

Out of 32 cases, performs significantly better in 30 cases, better but not significantly in 2 cases

Performance on CoNIC Data

Statistical Significance test: Wilcoxon

Methods	Dice	Jaccard	Precision	Recall
U-Net	1.17E-71	2.67E-71	9.99E-99	9.99E-99
Mask-R-CNN	9.99E-99	9.99E-99	9.99E-99	9.99E-99
U-Net++	9.99E-99	9.99E-99	9.99E-99	9.99E-99
HoVer-Net	*1.93E-01*	*2.56E-01*	9.99E-99	9.99E-99
MoNS	9.99E-99	9.99E-99	9.99E-99	9.99E-99
Stardist	9.99E-99	1.11E-99	1.08E-83	9.99E-99
Swin-MIL	9.99E-99	9.99E-99	2.37E-31	9.99E-99
BoNuS	9.99E-99	9.99E-99	9.99E-99	9.99E-99

Out of 32 cases, performs significantly better in 30 cases, better but not significantly in 2 cases

Key Takeaways - Ostrich

- Optimal transport based nuclei segmentation method is proposed, which uses measure theoretic concept to perform image-to-image translation between two asymmetric image domains.

Key Takeaways - Ostrich

- Optimal transport based nuclei segmentation method is proposed, which uses measure theoretic concept to perform image-to-image translation between two asymmetric image domains.

- Stain color normalization enables better nuclei segmentation from histological images

- Accurate nuclei segmentation makes color normalization trivial

Key Takeaways - Ostrich

- Optimal transport based nuclei segmentation method is proposed, which uses measure theoretic concept to perform image-to-image translation between two asymmetric image domains.
- Stain color normalization enables better nuclei segmentation from histological images
- Accurate nuclei segmentation makes color normalization trivial
- Next chapter tries to integrate two intertwined procedures so that they take advantage from each other.
- May yield better nuclei segmentation as well as better color normalization performance.

Chapter 7

Simultaneous Nuclei Segmentation and Color Normalization of Histological Images

SNSCN: Simultaneous Nuclei Segmentation and Color Normalization of Histological Images

- It consists of five deep networks:
  - a color appearance encoder E_c, which extracts the color appearance information,
  - a segmentation map generator F, which generates segmentation map corresponding to each histological image
  - a embedding map generator E_w,
  - a decoder G
  - a discriminator D.

- The networks should be any differentiable functions.

- The networks are chosen to be convolutional neural networks considering their tremendous success in different image analysis tasks.

Proposed Model: SNSCN

$$J_{\text{adv}} = J_{\text{G}}(\mathcal{D}) + J_{\text{G}}(\mathcal{G}).$$

$$J_{\text{G}}(\mathcal{D}) = \min_{\mathcal{D}} J_1(\mathcal{E}_c, \mathcal{F}_\phi, \mathcal{E}_\omega, \mathcal{G}, \mathcal{D}),$$

$$J_1(\mathcal{E}_c, \mathcal{F}_\phi, \mathcal{E}_\omega, \mathcal{G}, \mathcal{D}) = \underbrace{E_{x\sim P_{\mathcal{X}}(x)} E_{z_c\sim P_{\mathcal{E}_c}(z_c|x)} E_{y\sim P_{\mathcal{F}_\phi}(y|x)} E_{z\sim P_{\mathcal{E}_\omega}(z|x)} (A - \mathcal{D}[x, z_c, y, z])^2}_{R} +$$

$$\underbrace{E_{z_c\sim P_{\mathcal{Z}_c}(z_c)} E_{y\sim P_{\mathcal{Y}}(y)} E_{y\sim P_{\mathcal{Y}}(y)} E_{x\sim P_{\mathcal{G}}(x|z_c,y,z)} (B - \mathcal{D}[x, z_c, y, z])^2}_{G},$$

- *A* and *B* denote the labels, assigned by discriminator *D*, to designate real and generated/fake encoding, respectively.

Proposed Model: SNSCN

$$J_{\text{adv}} = J_{\text{G}}(\mathcal{D}) + J_{\text{G}}(\mathcal{G}).$$

Discriminator perspective

$$J_{\text{G}}(\mathcal{D}) = \min_{\mathcal{D}} J_1(\mathcal{E}_c, \mathcal{F}_\phi, \mathcal{E}_\omega, \mathcal{G}, \mathcal{D}),$$

$$J_1(\mathcal{E}_c, \mathcal{F}_\phi, \mathcal{E}_\omega, \mathcal{G}, \mathcal{D}) = \underbrace{E_{x\sim P_{\mathcal{X}}(x)} E_{z_c\sim P_{\mathcal{E}_c}(z_c|x)} E_{y\sim P_{\mathcal{F}_\phi}(y|x)} E_{z\sim P_{\mathcal{E}_\omega}(z|x)} (A - \mathcal{D}[x, z_c, y, z])^2}_{R} +$$

$$\underbrace{E_{z_c\sim P_{\mathcal{Z}_c}(z_c)} E_{y\sim P_{\mathcal{Y}}(y)} E_{y\sim P_{\mathcal{Y}}(y)} E_{x\sim P_{\mathcal{G}}(x|z_c,y,z)} (B - \mathcal{D}[x, z_c, y, z])^2}_{G},$$

- A and B denote the labels, assigned by discriminator D, to designate real and generated/fake encoding, respectively.

Proposed Model: SNSCN

$$J_{\text{adv}} = J_{\text{G}}(\mathcal{D}) + J_{\text{G}}(\mathcal{G}).$$

$$J_{\text{G}}(\mathcal{D}) = \min_{\mathcal{D}} J_1(\mathcal{E}_c, \mathcal{F}_\phi, \mathcal{E}_\omega, \mathcal{G}, \mathcal{D}),$$

Real encoding

$$J_1(\mathcal{E}_c, \mathcal{F}_\phi, \mathcal{E}_\omega, \mathcal{G}, \mathcal{D}) = \underbrace{E_{x\sim P_{\mathcal{X}}(x)} E_{z_c\sim P_{\mathcal{E}_c}(z_c|x)} E_{y\sim P_{\mathcal{F}_\phi}(y|x)} E_{z\sim P_{\mathcal{E}_\omega}(z|x)} (A - \mathcal{D}[x, z_c, y, z])^2}_{R} +$$

$$\underbrace{E_{z_c\sim P_{\mathcal{Z}_c}(z_c)} E_{y\sim P_{\mathcal{Y}}(y)} E_{y\sim P_{\mathcal{Y}}(y)} E_{x\sim P_{\mathcal{G}}(x|z_c,y,z)} (B - \mathcal{D}[x, z_c, y, z])^2}_{G},$$

- A and B denote the labels, assigned by discriminator D, to designate real and generated/fake encoding, respectively.

Proposed Model: SNSCN

$$J_{\text{adv}} = J_{\text{G}}(\mathcal{D}) + J_{\text{G}}(\mathcal{G}).$$

$$J_{\text{G}}(\mathcal{D}) = \min_{\mathcal{D}} J_1(\mathcal{E}_c, \mathcal{F}_\phi, \mathcal{E}_\omega, \mathcal{G}, \mathcal{D}),$$

$$J_1(\mathcal{E}_c, \mathcal{F}_\phi, \mathcal{E}_\omega, \mathcal{G}, \mathcal{D}) = \underbrace{E_{x\sim P_{\mathcal{X}}(x)} E_{z_c\sim P_{\mathcal{E}_c}(z_c|x)} E_{y\sim P_{\mathcal{F}_\phi}(y|x)} E_{z\sim P_{\mathcal{E}_\omega}(z|x)} (A - \mathcal{D}[x, z_c, y, z])^2}_{R} +$$

$$\underbrace{E_{z_c\sim P_{\mathcal{Z}_c}(z_c)} E_{y\sim P_{\mathcal{Y}}(y)} E_{y\sim P_{\mathcal{Y}}(y)} E_{x\sim P_{\mathcal{G}}(x|z_c,y,z)} (B - \mathcal{D}[x, z_c, y, z])^2}_{G},$$

Fake encoding

- A and B denote the labels, assigned by discriminator D, to designate real and generated/fake encoding, respectively.

Proposed Model: SNSCN

$$J_{\text{adv}} = J_{\text{G}}(\mathcal{D}) + J_{\text{G}}(\mathcal{G}).$$

Generator perspective

$$J_{\text{G}}(\mathcal{G}) = \min_{\mathcal{G}} J_2(\mathcal{E}_c, \mathcal{F}_\phi, \mathcal{E}_\omega, \mathcal{G}, \mathcal{D}),$$

$$\mathbb{J}_{\text{rec}} = \underbrace{-E_{Q(z_c,y,z)}[\log P_{\mathcal{G}}(x \mid z_c, y, z)]}_{L_R} - E_{Q(z_c,y,z)}[\log Q(z_c, y, z)]$$

$$+ \underbrace{D_{KL}[Q(z_c) \parallel P_{\mathcal{Z}_c}(z_c)]}_{R_1} + \underbrace{D_{KL}[Q(y,z) \parallel P_{\mathcal{Y}\mathcal{Z}}(y,z)]}_{R_2},$$

$$l_{SSIM} = 1 - SSIM[x, \mathcal{G}(\mathcal{E}_c(x), \mathcal{F}_\phi(x), \mathcal{E}_\omega(x))]$$

Proposed Model: SNSCN

$$J_{\text{adv}} = J_{\text{G}}(\mathcal{D}) + J_{\text{G}}(\mathcal{G}).$$

$$J_{\text{G}}(\mathcal{G}) = \min_{\mathcal{G}} J_2(\mathcal{E}_c, \mathcal{F}_\phi, \mathcal{E}_\omega, \mathcal{G}, \mathcal{D}),$$

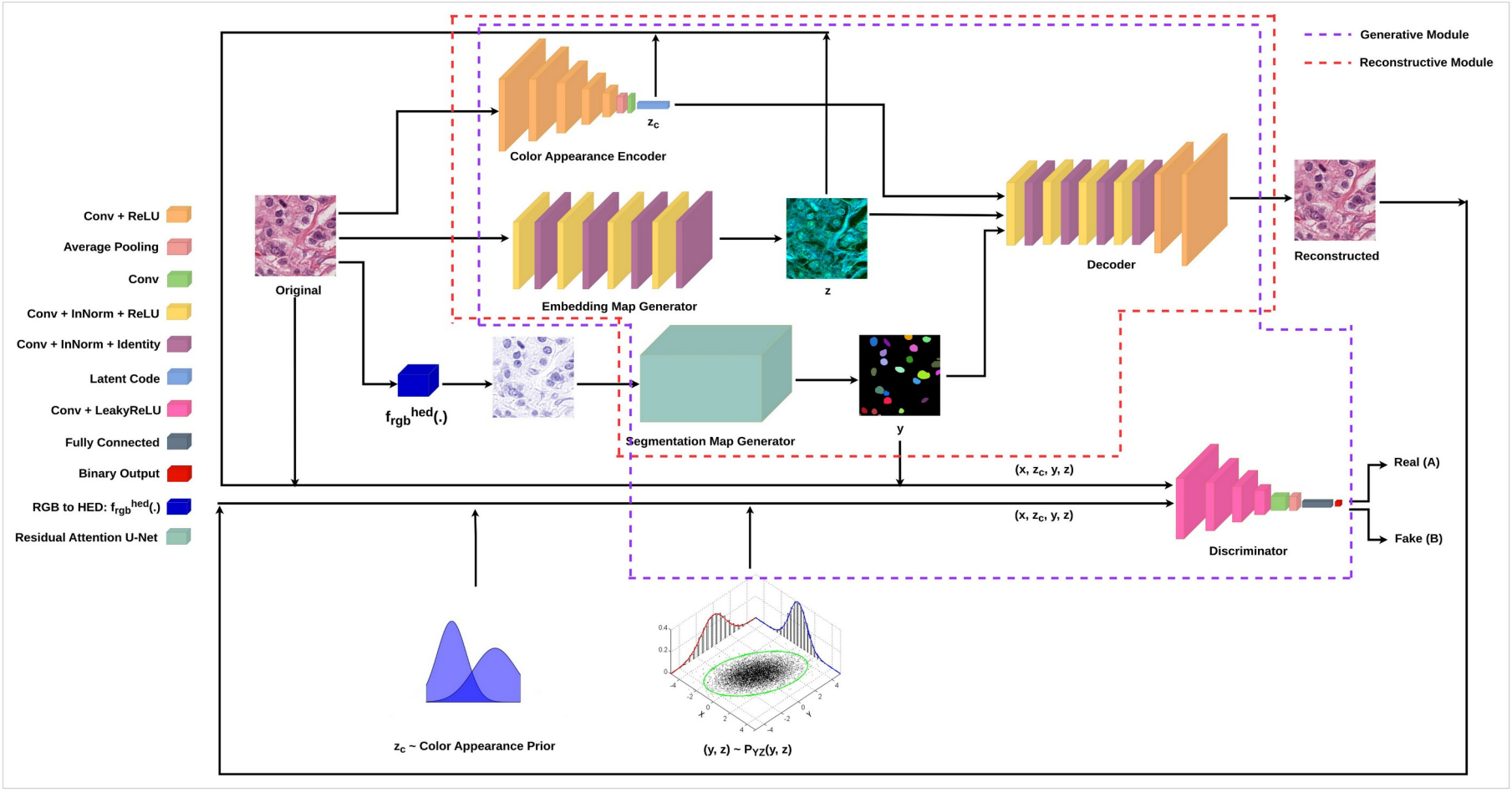
$$\mathbb{J}_{\text{rec}} = \underbrace{-E_{Q(z_c,y,z)}[\log P_{\mathcal{G}}(x \mid z_c, y, z)]}_{L_R} - E_{Q(z_c,y,z)}[\log Q(z_c, y, z)]$$

$$+ \underbrace{D_{KL}[Q(z_c) \parallel P_{\mathcal{Z}_c}(z_c)]}_{R_1} + \underbrace{D_{KL}[Q(y,z) \parallel P_{\mathcal{Y}\mathcal{Z}}(y,z)]}_{R_2},$$

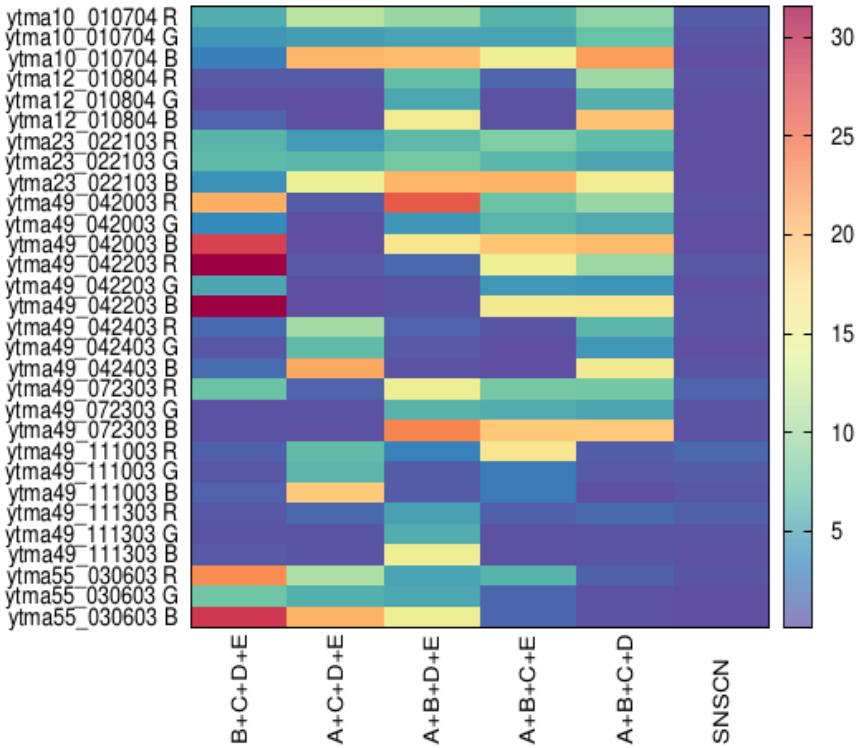
Regularizer

$$l_{SSIM} = 1 - SSIM[x, \mathcal{G}(\mathcal{E}_c(x), \mathcal{F}_\phi(x), \mathcal{E}_\omega(x))]$$

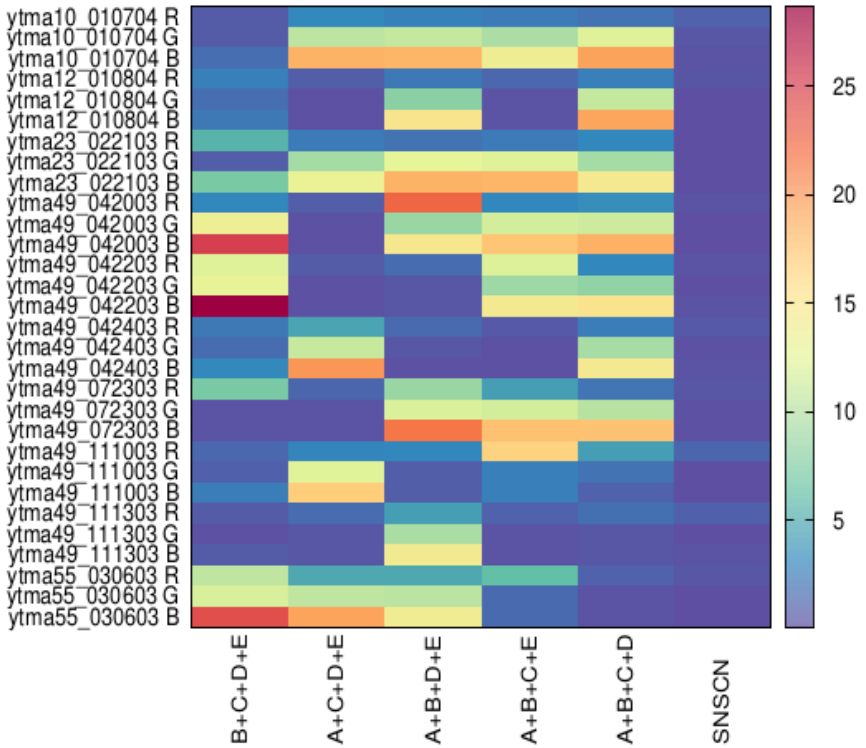
Block Diagram: SNSCN



Ablation Study: Stain estimation

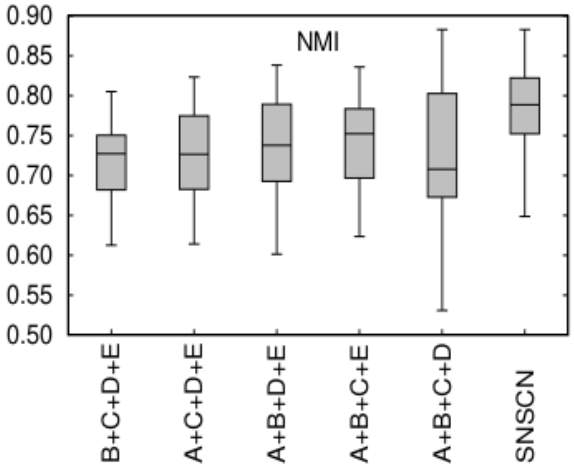


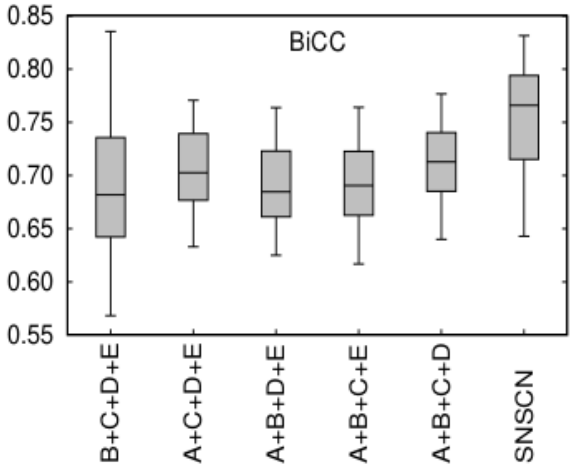
(a) Hematoxylin

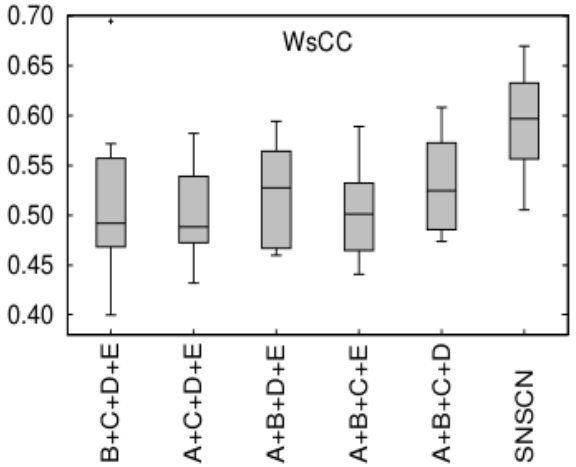


(b) Eosin

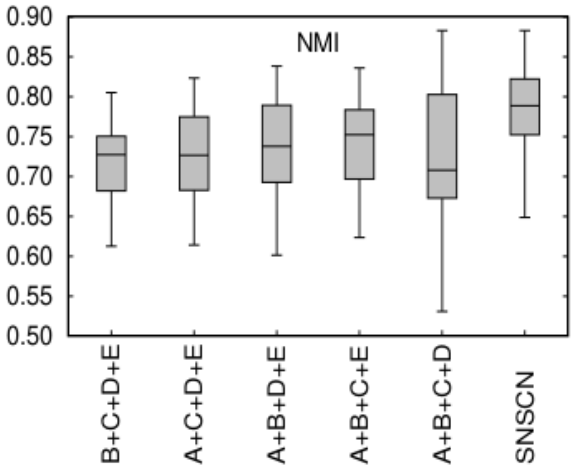
Ablation Study: Color normalization

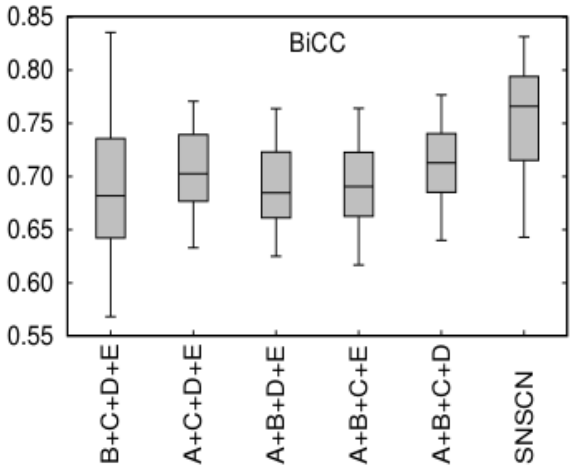


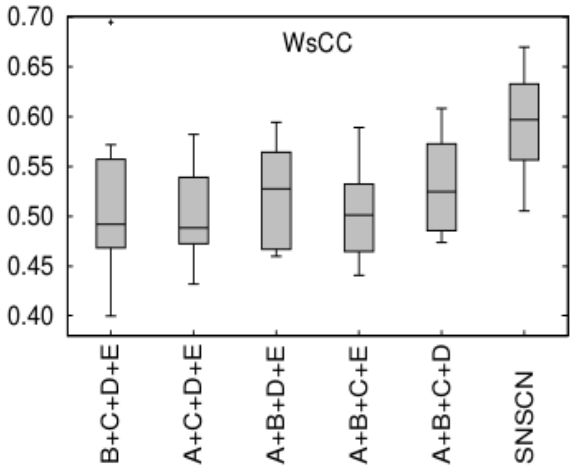




Ablation Study: Color normalization

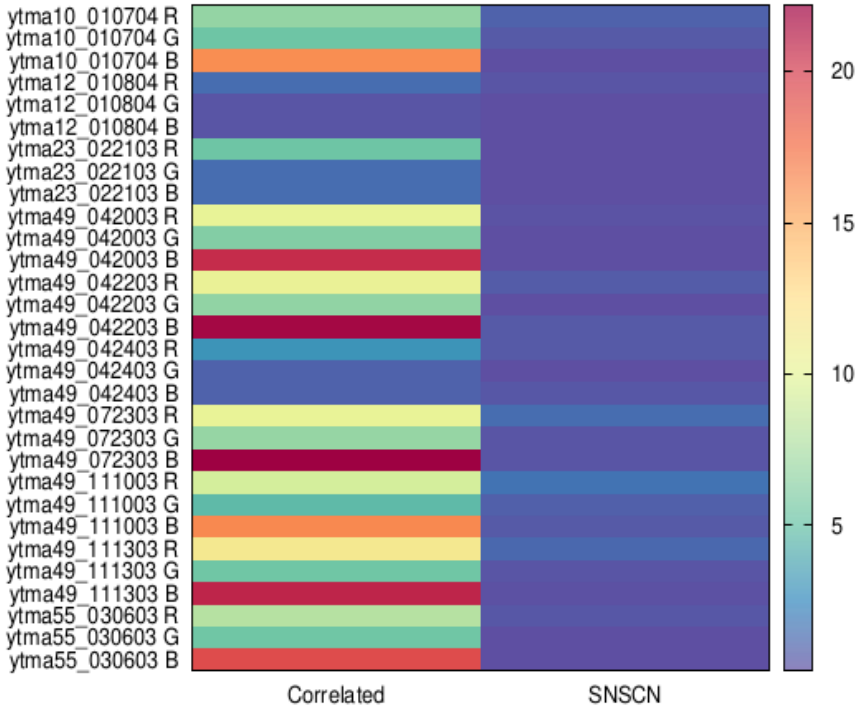


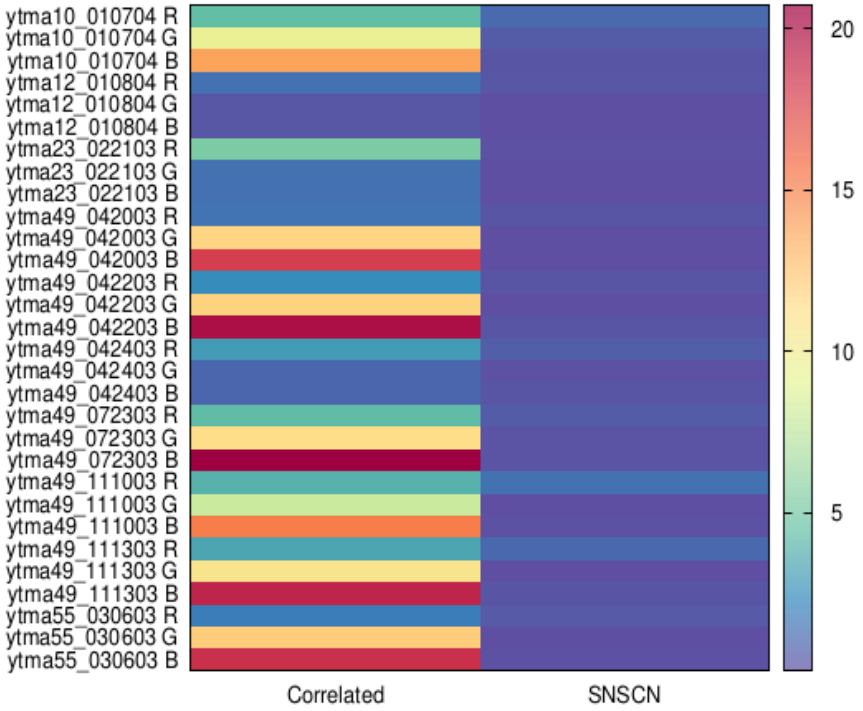




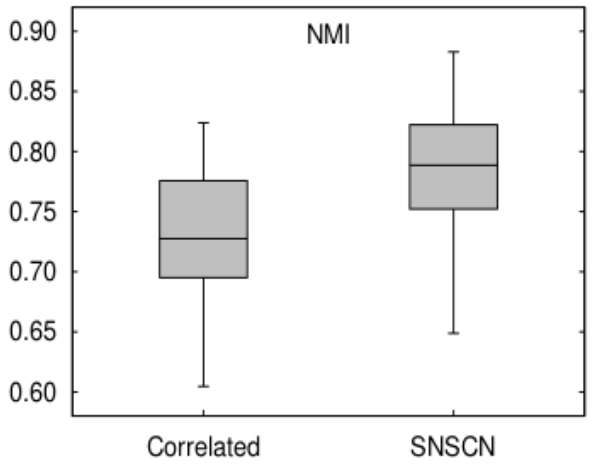
outperforms all combinations as per color consistency after normalization is concerned

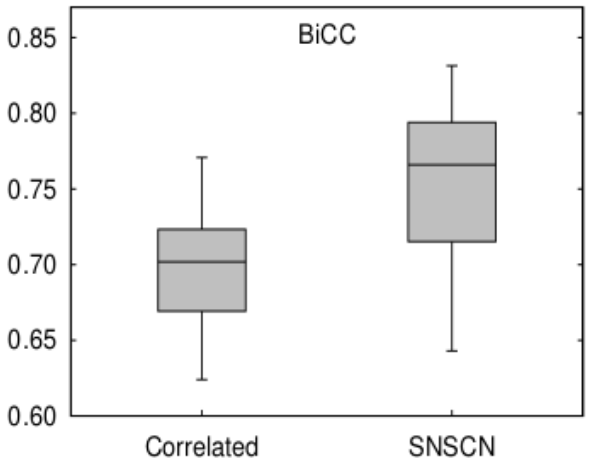
Correlation between color appearance, and segmentation and embedding map

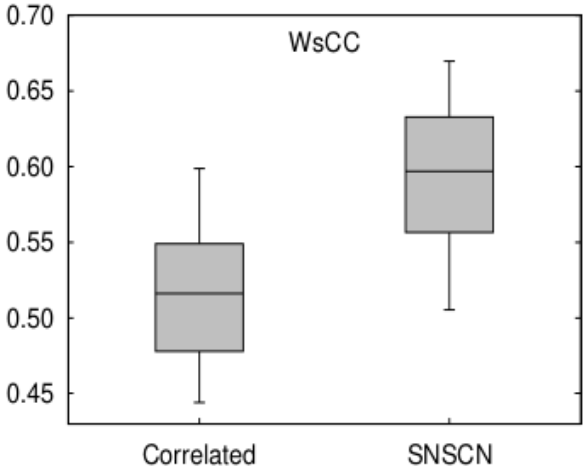




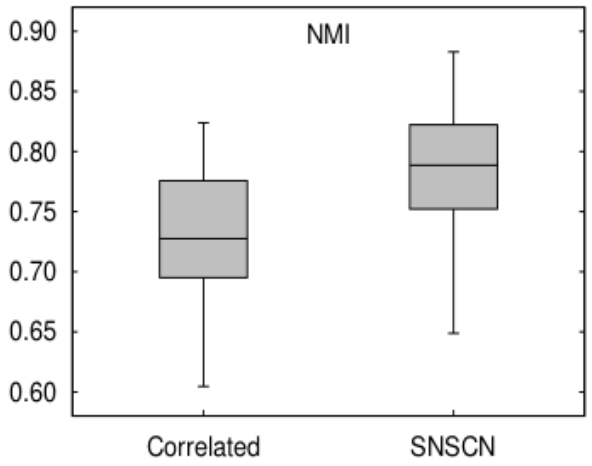
Correlation between color appearance, and segmentation and embedding map

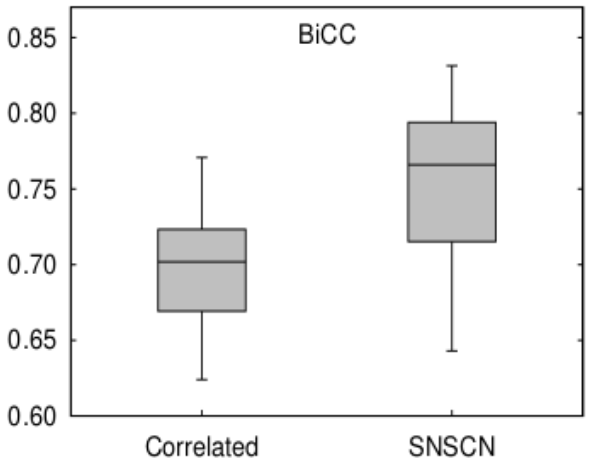


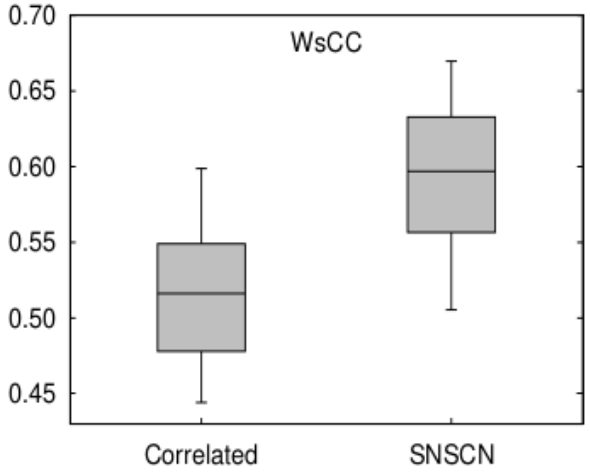




Correlation between color appearance, and segmentation and embedding map

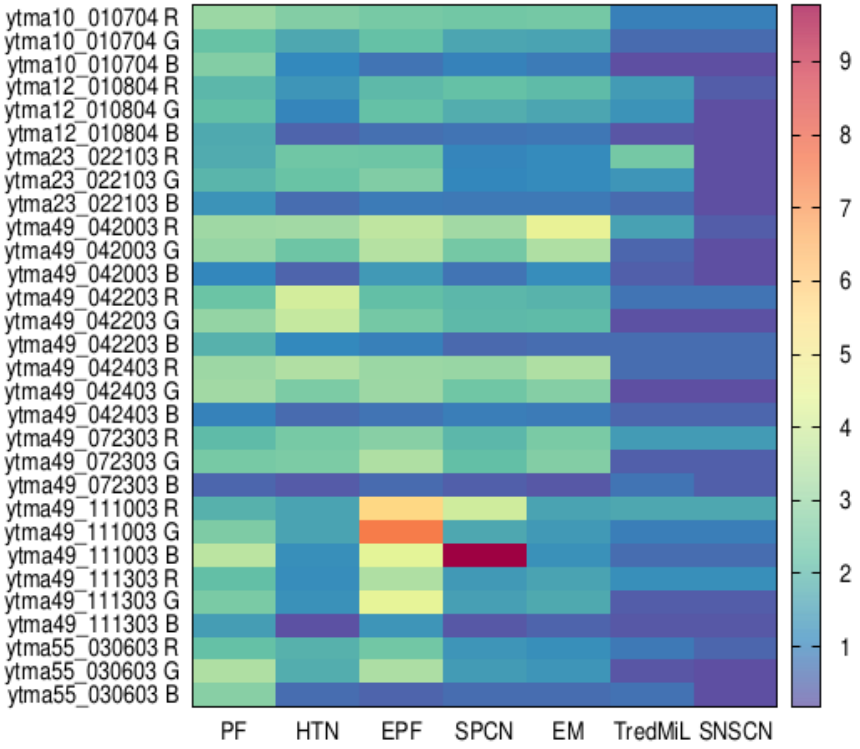


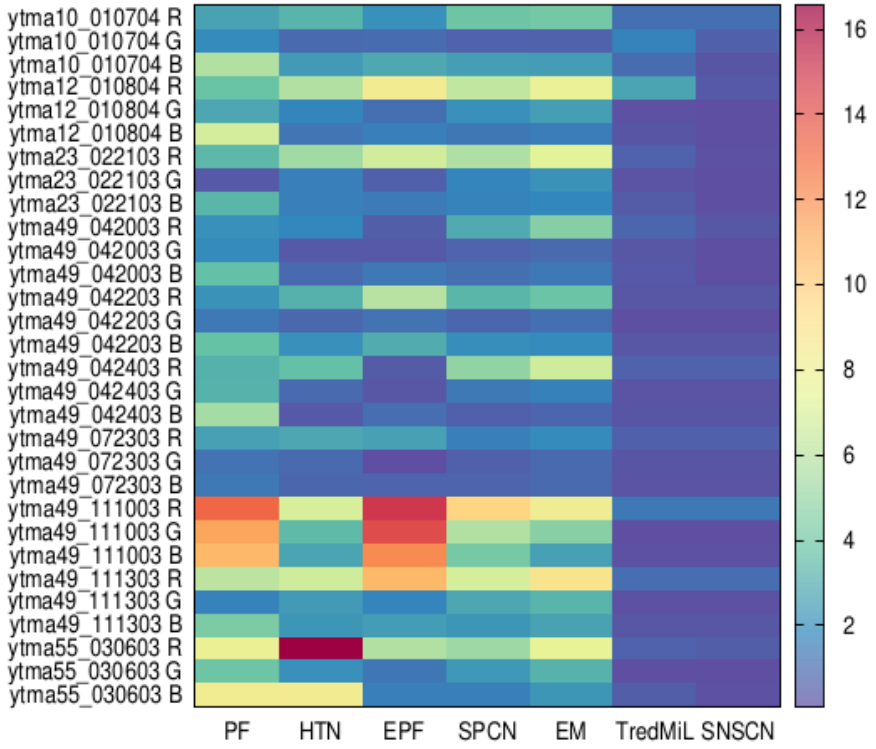




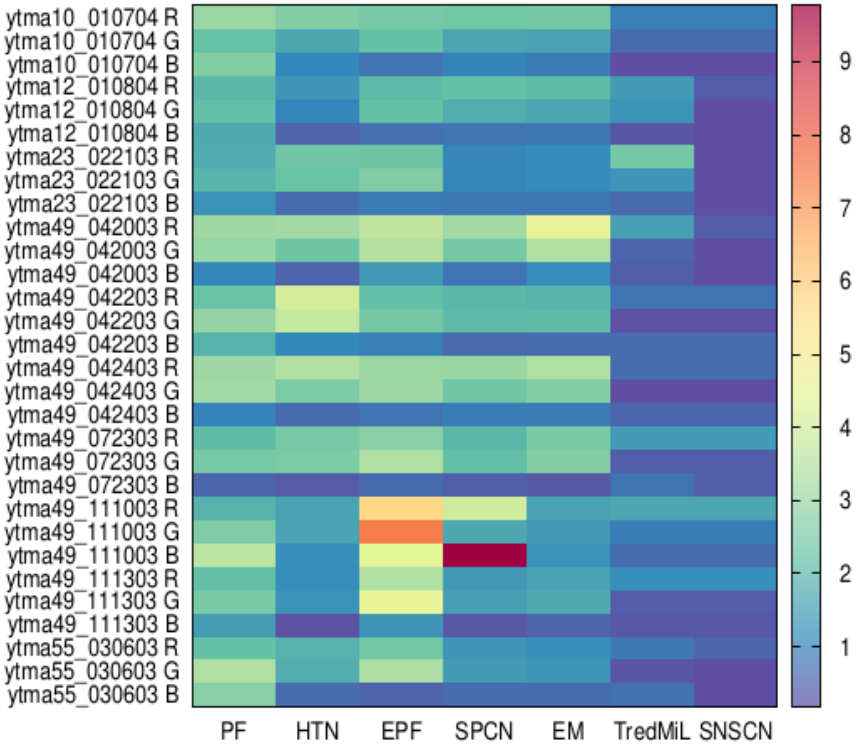
outperforms correlated counterpart as per color consistency after normalization is concerned

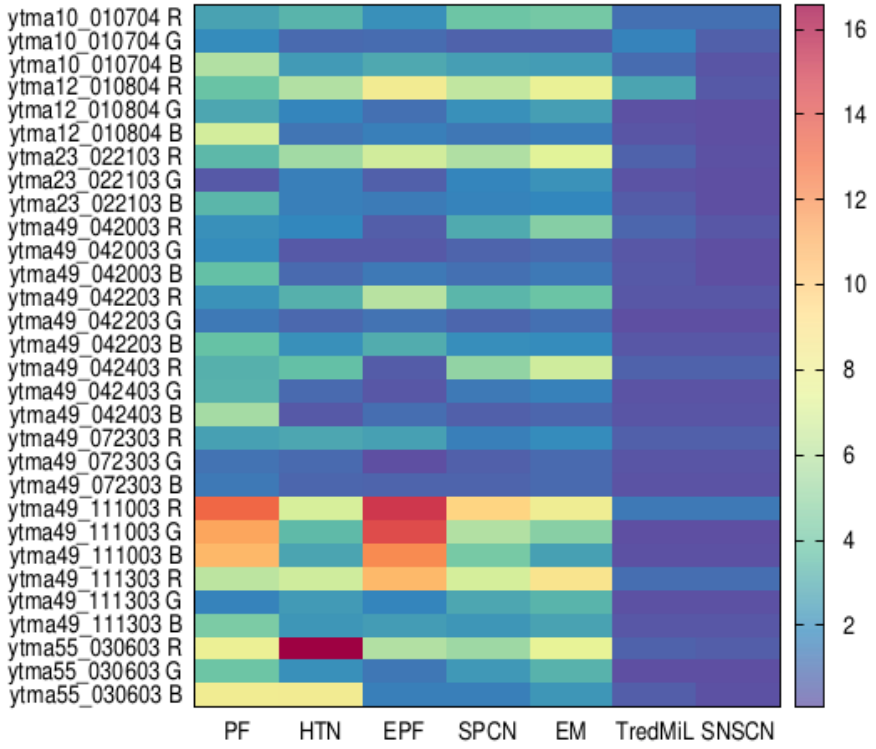
Stain Estimation: vs Existing Methods





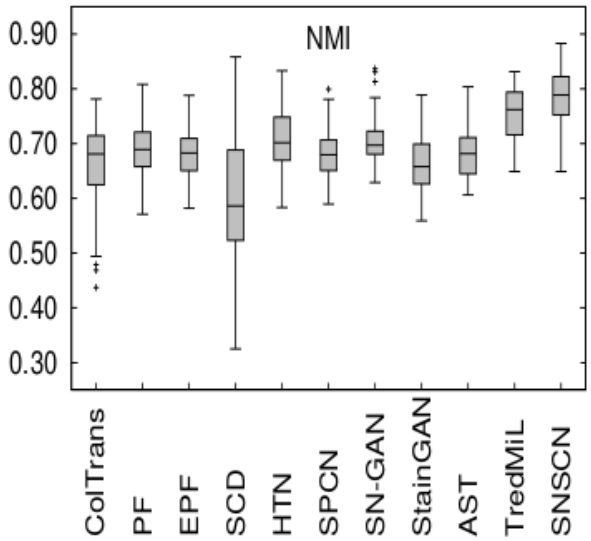
Stain Estimation: vs Existing Methods

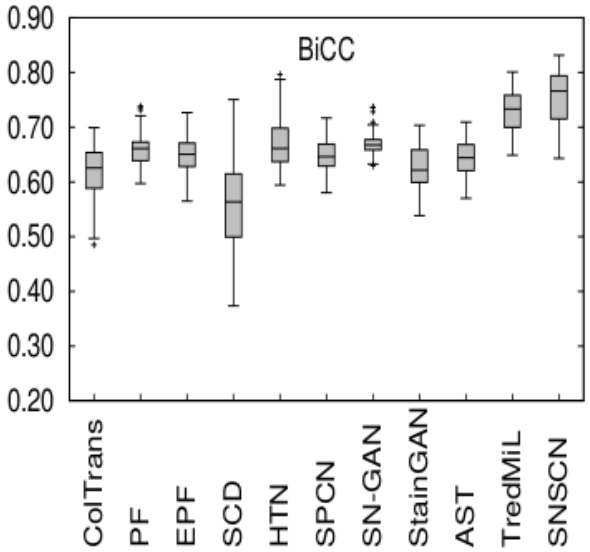


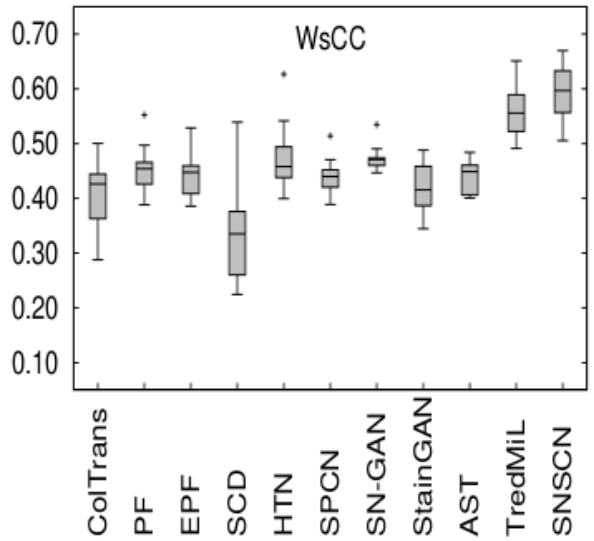


outperforms state-of-the-art methods in stain vector estimation

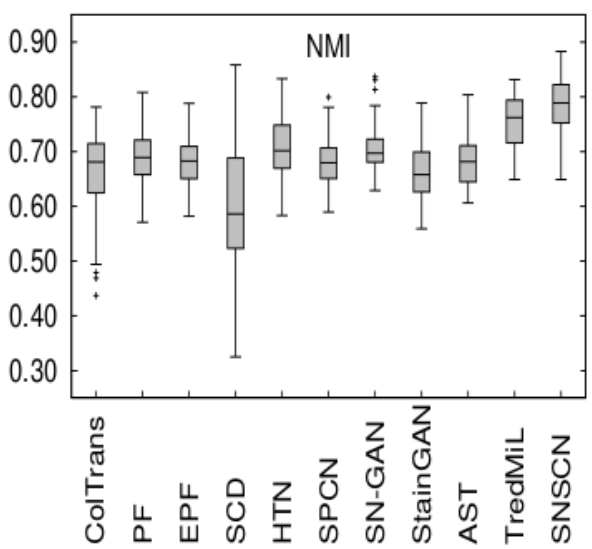
Color Normalization: vs Existing Methods

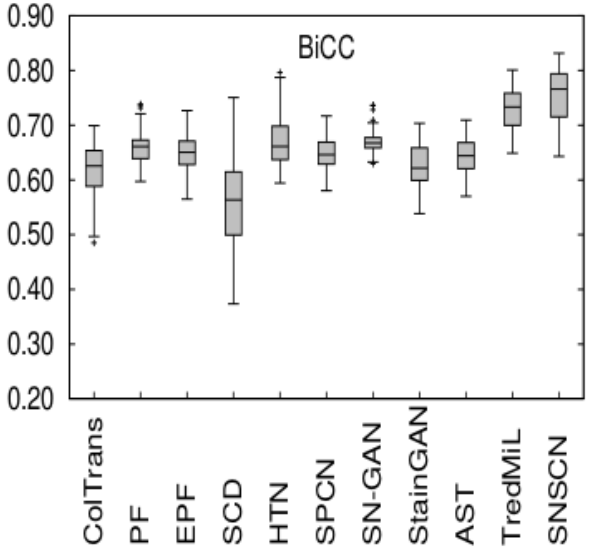


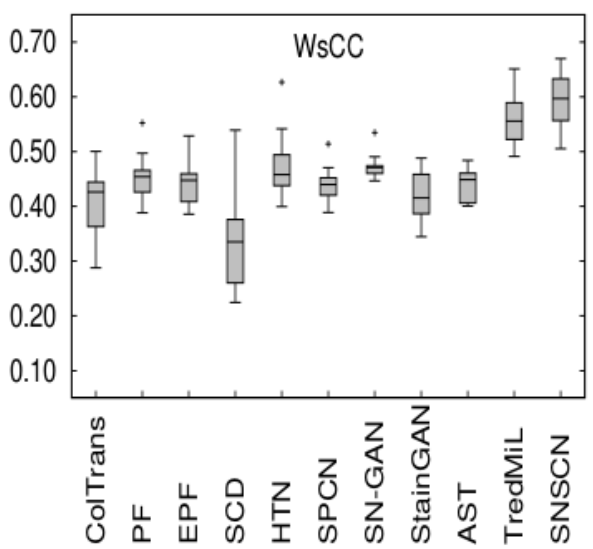




Color Normalization: vs Existing Methods







outperforms state-of-the-art methods as per color consistency after normalization is concerned

Color Normalization: Statistical significance

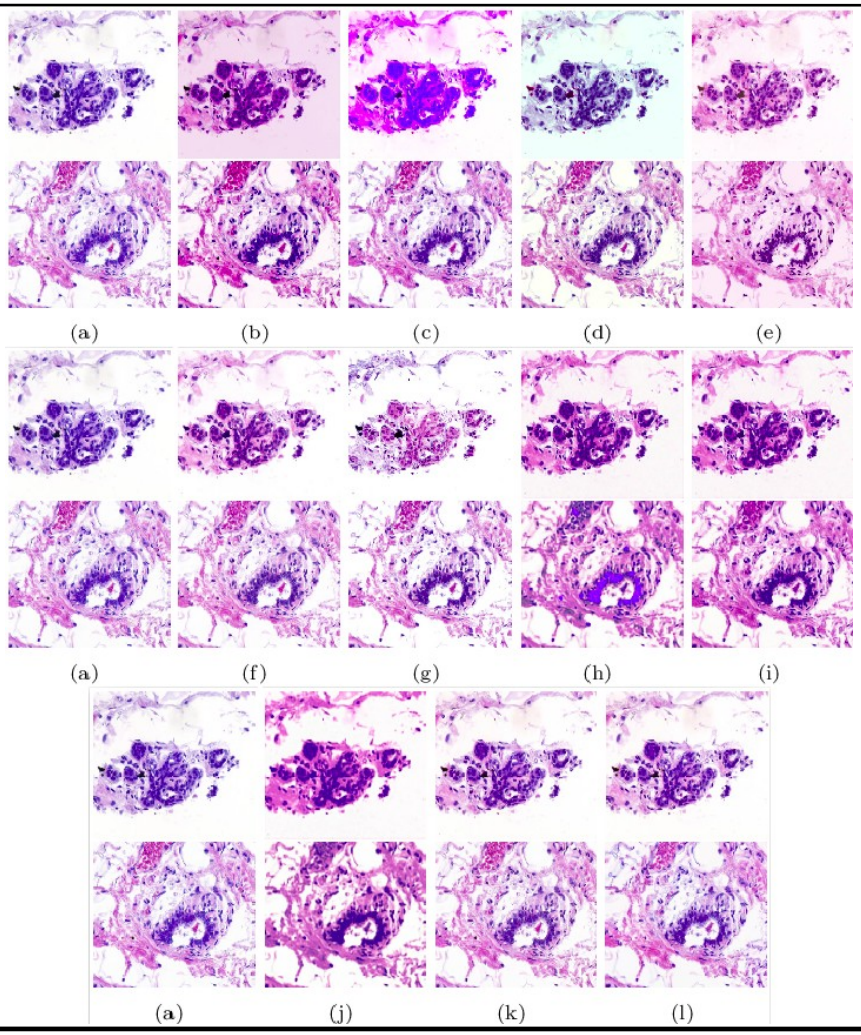
Different Methods	NMI		BiCC		WsCC	
	Wilcoxon	Paired-t	Wilcoxon	Paired-t	Wilcoxon	Paired-t
B+C+D+E	2.57E-11	4.98E-17	1.58E-07	4.44E-09	4.67E-03	9.19E-04
A+C+D+E	1.75E-11	2.40E-14	4.24E-11	7.55E-16	2.53E-03	4.34E-07
A+B+D+E	1.20E-09	5.63E-11	1.85E-11	3.52E-19	2.53E-03	7.52E-06
A+B+C+E	3.77E-11	2.28E-10	1.85E-11	2.31E-20	2.53E-03	5.85E-06
A+B+C+D	2.63E-08	2.91E-10	2.40E-11	6.78E-19	2.53E-03	1.01E-07
Correlated	4.02E-11	4.07E-12	1.75E-11	9.88E-19	2.53E-03	1.47E-05
ColTrans	1.75E-11	9.23E-23	1.75E-11	8.62E-30	2.53E-03	9.81E-10
PF	2.53E-11	3.57E-21	1.75E-11	1.50E-24	2.53E-03	4.87E-08
EPF	1.85E-11	7.73E-23	1.75E-11	8.49E-25	2.53E-03	1.92E-08
SCD	7.43E-11	2.34E-16	1.95E-11	2.32E-23	2.53E-03	4.39E-05
HTN	7.76E-09	2.81E-11	1.17E-10	1.23E-15	3.46E-03	2.38E-04
SPCN	1.75E-11	1.80E-23	1.75E-11	1.45E-26	2.53E-03	9.45E-08
SN-GAN	5.67E-10	7.60E-15	1.85E-11	7.89E-23	2.53E-03	2.03E-06
StainGAN	1.75E-11	5.60E-25	1.75E-11	1.98E-30	2.53E-03	6.90E-09
AST	1.85E-11	2.36E-19	1.75E-11	3.51E-25	2.53E-03	7.96E-07
TredMiL	2.69E-07	3.16E-06	4.30E-09	4.26E-11	2.53E-03	1.71E-04

Color Normalization: Statistical significance

Different Methods	NMI		BiCC		WsCC	
	Wilcoxon	Paired-t	Wilcoxon	Paired-t	Wilcoxon	Paired-t
B+C+D+E	2.57E-11	4.98E-17	1.58E-07	4.44E-09	4.67E-03	9.19E-04
A+C+D+E	1.75E-11	2.40E-14	4.24E-11	7.55E-16	2.53E-03	4.34E-07
A+B+D+E	1.20E-09	5.63E-11	1.85E-11	3.52E-19	2.53E-03	7.52E-06
A+B+C+E	3.77E-11	2.28E-10	1.85E-11	2.31E-20	2.53E-03	5.85E-06
A+B+C+D	2.63E-08	2.91E-10	2.40E-11	6.78E-19	2.53E-03	1.01E-07
Correlated	4.02E-11	4.07E-12	1.75E-11	9.88E-19	2.53E-03	1.47E-05
ColTrans	1.75E-11	9.23E-23	1.75E-11	8.62E-30	2.53E-03	9.81E-10
PF	2.53E-11	3.57E-21	1.75E-11	1.50E-24	2.53E-03	4.87E-08
EPF	1.85E-11	7.73E-23	1.75E-11	8.49E-25	2.53E-03	1.92E-08
SCD	7.43E-11	2.34E-16	1.95E-11	2.32E-23	2.53E-03	4.39E-05
HTN	7.76E-09	2.81E-11	1.17E-10	1.23E-15	3.46E-03	2.38E-04
SPCN	1.75E-11	1.80E-23	1.75E-11	1.45E-26	2.53E-03	9.45E-08
SN-GAN	5.67E-10	7.60E-15	1.85E-11	7.89E-23	2.53E-03	2.03E-06
StainGAN	1.75E-11	5.60E-25	1.75E-11	1.98E-30	2.53E-03	6.90E-09
AST	1.85E-11	2.36E-19	1.75E-11	3.51E-25	2.53E-03	7.96E-07
TredMiL	2.69E-07	3.16E-06	4.30E-09	4.26E-11	2.53E-03	1.71E-04

Performs significantly better in all 96 cases

Color Normalization: vs Existing Methods (Qualitative)



Qualitative performance analysis of different color normalization methods: (a) original, (b) ColTrans, (c) PF, (d) EPF, (e) SCD, (f) HTN, (g) SPCN, (h) SN-GAN, (i) StainGAN, (j) AST, (k) TredMiL and (l) SNSCN

Performance in Nuclei Segmentation: TCGA Data

Methods	Dice	Jaccard	Precision	Recall
SNSCN	**0.788345**	**0.653957**	**0.826117**	**0.786249**
U-Net	0.645650	0.446128	0.624558	0.668216
Mask-R-CNN	0.747086	0.585659	0.799975	0.700757
U-Net++	0.773155	0.620294	0.796708	0.750955
HoVer-Net	0.744516	0.586780	0.811804	0.687529
MoNS	0.755509	0.614706	0.748012	0.763157
Stardist	0.743228	0.585713	0.811579	0.685495
WNSeg	0.773406	0.625322	0.813470	0.737104
Swin-MIL	0.749044	0.593266	0.801989	0.702656
BoNuS	0.784740	0.639496	0.806351	0.764257
Ostrich	0.788035	0.641520	0.813523	0.764096

Performance in Nuclei Segmentation: TCGA Data

Methods	Dice	Jaccard	Precision	Recall
SNSCN	**0.788345**	**0.653957**	**0.826117**	**0.786249**
U-Net	0.645650	0.446128	0.624558	0.668216
Mask-R-CNN	0.747086	0.585659	0.799975	0.700757
U-Net++	0.773155	0.620294	0.796708	0.750955
HoVer-Net	0.744516	0.586780	0.811804	0.687529
MoNS	0.755509	0.614706	0.748012	0.763157
Stardist	0.743228	0.585713	0.811579	0.685495
WNSeg	0.773406	0.625322	0.813470	0.737104
Swin-MIL	0.749044	0.593266	0.801989	0.702656
BoNuS	0.784740	0.639496	0.806351	0.764257
Ostrich	0.788035	0.641520	0.813523	0.764096

outperforms state-of-the-art methods in nuclei segmentation

Performance in Nuclei Segmentation: TCGA Data

paired-*t* test

Methods	Dice	Jaccard	Precision	Recall
U-Net	3.89E-47	4.37E-49	1.14E-15	3.77E-51
Mask-R-CNN	3.44E-31	1.01E-37	8.13E-81	1.83E-08
U-Net++	8.79E-40	7.05E-41	4.70E-25	4.24E-26
HoVer-Net	2.41E-52	5.58E-57	2.52E-12	3.10E-67
MoNS	8.16E-28	2.12E-29	1.26E-60	1.93E-01
Stardist	5.45E-34	1.63E-36	1.15E-04	7.20E-42
WNSeg	1.16E-48	1.17E-49	4.20E-16	4.21E-63
Swin-MIL	4.42E-51	2.95E-57	1.29E-16	5.34E-67
BoNuS	3.84E-17	4.03E-18	9.68E-28	7.56E-26
Ostrich	7.54E-20	1.46E-19	1.95E-24	4.12E-28

Performance in Nuclei Segmentation: TCGA Data

paired-*t* test

Methods	Dice	Jaccard	Precision	Recall
U-Net	3.89E-47	4.37E-49	1.14E-15	3.77E-51
Mask-R-CNN	3.44E-31	1.01E-37	8.13E-81	1.83E-08
U-Net++	8.79E-40	7.05E-41	4.70E-25	4.24E-26
HoVer-Net	2.41E-52	5.58E-57	2.52E-12	3.10E-67
MoNS	8.16E-28	2.12E-29	1.26E-60	1.93E-01
Stardist	5.45E-34	1.63E-36	1.15E-04	7.20E-42
WNSeg	1.16E-48	1.17E-49	4.20E-16	4.21E-63
Swin-MIL	4.42E-51	2.95E-57	1.29E-16	5.34E-67
BoNuS	3.84E-17	4.03E-18	9.68E-28	7.56E-26
Ostrich	7.54E-20	1.46E-19	1.95E-24	4.12E-28

performs significantly better than state-of-the-art methods in nuclei segmentation

Performance in Nuclei Segmentation: TCGA Data

Wilcoxon signed-rank test

Methods	Dice	Jaccard	Precision	Recall
U-Net	7.85E-32	8.61E-32	2.38E-14	6.25E-32
Mask-R-CNN	1.30E-32	1.19E-32	1.86E-33	1.71E-02
U-Net++	2.70E-29	2.44E-29	1.68E-25	1.42E-21
HoVer-Net	3.22E-33	3.22E-33	5.00E-11	1.49E-33
MoNS	7.62E-24	3.46E-24	1.47E-33	1.36E-01
Stardist	7.12E-28	6.64E-28	1.14E-05	4.17E-30
WNSeg	6.44E-32	6.34E-32	7.51E-15	1.62E-33
Swin-MIL	1.92E-33	1.89E-33	1.84E-18	1.47E-33
BoNuS	4.16E-16	1.98E-16	4.03E-24	7.74E-23
Ostrich	3.07E-21	3.07E-21	1.48E-22	3.36E-24

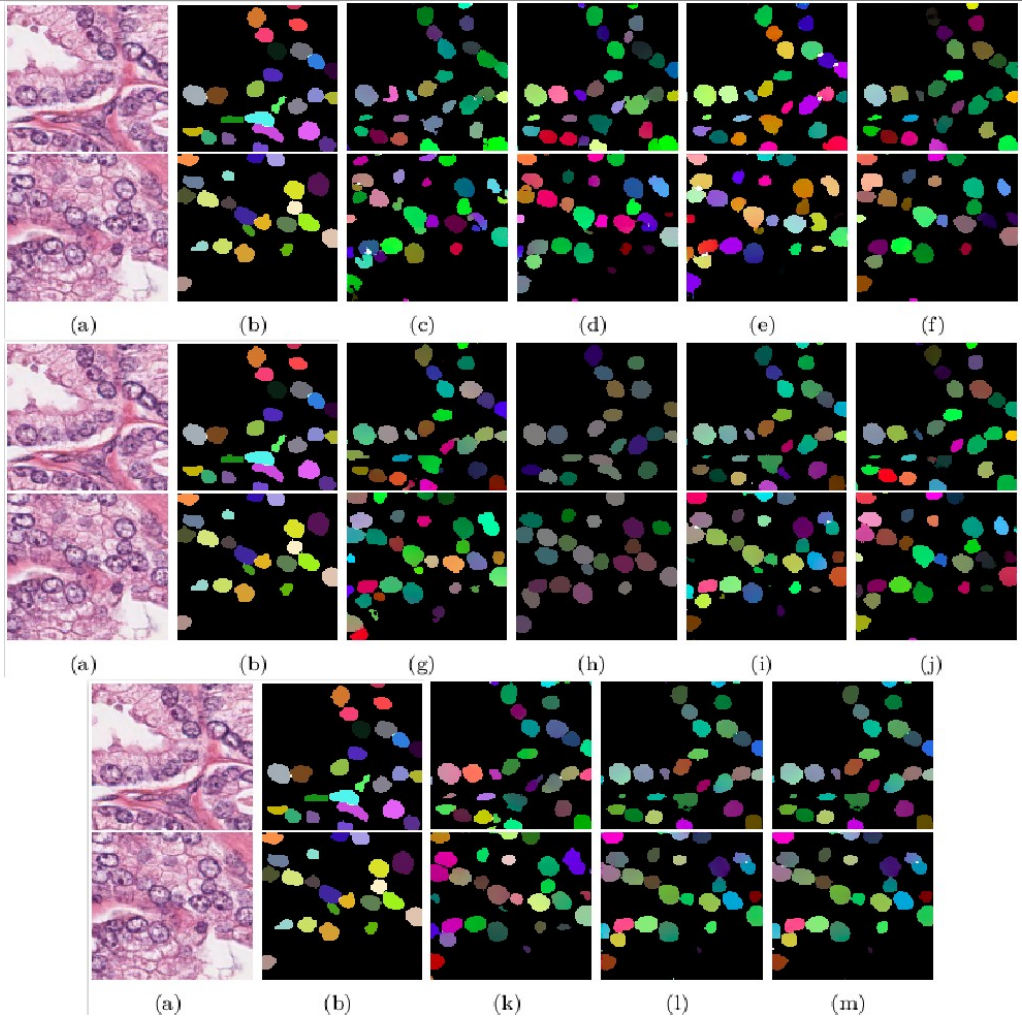
Performance in Nuclei Segmentation: TCGA Data

Wilcoxon signed-rank test

Methods	Dice	Jaccard	Precision	Recall
U-Net	7.85E-32	8.61E-32	2.38E-14	6.25E-32
Mask-R-CNN	1.30E-32	1.19E-32	1.86E-33	1.71E-02
U-Net++	2.70E-29	2.44E-29	1.68E-25	1.42E-21
HoVer-Net	3.22E-33	3.22E-33	5.00E-11	1.49E-33
MoNS	7.62E-24	3.46E-24	1.47E-33	1.36E-01
Stardist	7.12E-28	6.64E-28	1.14E-05	4.17E-30
WNSeg	6.44E-32	6.34E-32	7.51E-15	1.62E-33
Swin-MIL	1.92E-33	1.89E-33	1.84E-18	1.47E-33
BoNuS	4.16E-16	1.98E-16	4.03E-24	7.74E-23
Ostrich	3.07E-21	3.07E-21	1.48E-22	3.36E-24

performs significantly better than state-of-the-art methods in nuclei segmentation

Nuclei Segmentation: vs Existing Methods (Qualitative)



Qualitative performance analysis in nuclei instance segmentation : (a) Original image, (b) Ground-truth; Segmentation performance of (c) U-Net, (d) Mask-R-CNN, (e) U-Net++, (f) HoVer-Net, (g) MoNS, (h) Stardist, (i) WNSeg, (j) Swin-MIL, (k) BoNuS , (l) Ostrich, (m) SNSCN

Conclusion - Major Contributions

Work 1: Development of Rough-Fuzzy Circular clustering.
deals with the incompleteness and vagueness in class definition, overlapping nature of histochemical stains.

Conclusion - Major Contributions

Work 1: Development of Rough-Fuzzy Circular clustering.
deals with the incompleteness and vagueness in class definition, overlapping nature of histochemical stains.

Work 2: A new dissimilarity measure is introduced.
captures intrinsic data distribution and concentration of hue around mean.

Conclusion - Major Contributions

Work 1: Development of Rough-Fuzzy Circular clustering.
deals with the incompleteness and vagueness in class definition, overlapping nature of histochemical stains.

Work 2: A new dissimilarity measure is introduced.
captures intrinsic data distribution and concentration of hue around mean.

Work 3: Truncated normal mixture prior based deep latent model is introduced.
captures disentangled color appearance and stain bound information
enhances generalizability and adaptability of the model.

Conclusion - Major Contributions

Work 1: Development of Rough-Fuzzy Circular clustering.
deals with the incompleteness and vagueness in class definition, overlapping nature of histochemical stains.

Work 2: A new dissimilarity measure is introduced.
captures intrinsic data distribution and concentration of hue around mean.

Work 3: Truncated normal mixture prior based deep latent model is introduced.
captures disentangled color appearance and stain bound information
enhances generalizability and adaptability of the model.

Work 4: Optimal transport based I2I translation network is introduced.
reduces information-disparity between information-rich histological image space and information-poor segmentation map domain applicable to segmentation tasks with different target domain image representations.

Conclusion - Major Contributions

Work 1: Development of Rough-Fuzzy Circular clustering.
deals with the incompleteness and vagueness in class definition, overlapping nature of histochemical stains.

Work 2: A new dissimilarity measure is introduced.
captures intrinsic data distribution and concentration of hue around mean.

Work 3: Truncated normal mixture prior based deep latent model is introduced.
captures disentangled color appearance and stain bound information
enhances generalizability and adaptability of the model.

Work 4: Optimal transport based I2I translation network is introduced.
reduces information-disparity between information-rich histological image space and information-poor segmentation map domain applicable to segmentation tasks with different target domain image representations.

Work 5: Simultaneous Nuclei Segmentation and color normalization model is introduced to perform intertwined tasks.

Future Directions

- Device generalized algorithms for all types of staining including immunohistochemical stains : PAS, Trichrome etc.
- Understanding the utilization of deep generative models in other medical imaging modalities.
- Exploration of geometric deep learning in biomedical image analysis.
- Integration of imaging and non-imaging modalities for accurately predicting and diagnosing underlying diseases.

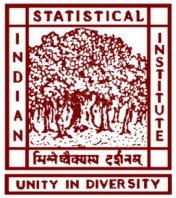
Related Publications

J1. **S. Mahapatra** and P. Maji, "Optimal Transport Driven Asymmetric Image-to-Image Translation for Nuclei Segmentation of Histological Images", ***IEEE Transactions on Artificial Intelligence (under review)***, pp. 1-12, Manuscript ID: TAI-2024-Nov-A-01785.

J2. **S. Mahapatra** and P. Maji, "Truncated Normal Mixture Prior Based Deep Latent Model for Color Normalization of Histological Images", ***IEEE Transactions on Medical Imaging***, vol. 42, no. 6, pp. 1746-1757, 2023.

J3. P. Maji and **S. Mahapatra**, "Circular Clustering in Fuzzy Approximation Spaces for Color Normalization of Histological Images", ***IEEE Transactions on Medical Imaging***, vol. 39, no. 5, pp. 1735-1745, 2020.

J4. P. Maji and **S. Mahapatra**, "Rough-Fuzzy Circular Clustering for Color Normalization of Histological Images", ***Fundamenta Informaticae***, vol. 164, no. 1, pp. 103-117, 2019.



Thank you